

Functionalization of Mechanochemically Passivated Germanium Nanoparticles via “Click” Chemistry


AN ABSTRACT
SUBMITTED ON FIFTEENTH DAY OF AUGUST, 2012

TO THE DEPARTMENT OF CHEMISTRY
IN PARTIAL FULFILMENT OF THE REQUIRMENTS
OF THE SCHOOL OF SCIENCE AND ENGINEERING
OF TULANE UNIVERSITY
FOR THE DEGREE OF
DOCTOR OF PHILOSOPHY

BY



TAPAS KUMAR PURKAIT

APPROVED


MARK J. FINK, Ph.D, Dissertation Advisor


RUSSELL H. SCHMEHL, Ph.D


JAMES P. DONAHUE, Ph.D


SCOTT MICHAEL GRAYSON, Ph.D


BRIAN S. MITCHELL, Ph.D

ABSTRACT

Germanium nanoparticles (Ge NPs) may be fascinating for their electronic and optoelectronic properties, as the band gap of Ge NPs can be tuned from the infrared into the visible range of solar spectrum. Further functionalization of those nanoparticles may potentially lead to numerous applications ranging from surface attachment, bioimaging, drug delivery and nanoparticles based devices. Blue luminescent germanium nanoparticles were synthesized from a novel top-down mechanochemical process using high energy ball milling (HEBM) of bulk germanium. Various reactive organic molecules (such as, alkynes, nitriles, azides) were used in this process to react with fresh surface and passivate the surface through Ge-C or Ge-N bond.

Various purification process, such as gel permeation chromatography (GPC), Soxhlet dialysis etc. were introduced to purify nanoparticles from molecular impurities. A size separation technique was developed using GPC. The size separated Ge NPs were characterized by TEM, small angle X-ray scattering (SAXS), UV-vis absorption and photoluminescence (PL) emission spectroscopy to investigate their size selective properties.

Germanium nanoparticles with alkyne terminal group were prepared by HEBM of germanium with a mixture of n-alkynes and α, ω -diynes. Additional functionalization of those nanoparticles was achieved by copper(I) catalyzed azide-alkyne "click" reaction. A variety of organic and organometallic azides including biologically important glucals have

been reacted in this manner resulting in nanoparticles adorned with ferrocenyl, trimethylsilyl, and glucal groups.

Additional functionalization of those nanoparticles was achieved by reactions with various azides via a Cu(I) catalyzed azide-alkyne "click" reaction. Various azides, including PEG derivatives and cyclodextrin moiety, were grafted to the initially formed surface. Globular nanoparticle arrays were formed through interparticle linking via "click" chemistry or "host-guest" chemistry.

Copper(I) catalyzed "click" chemistry also can be explored with azido-terminated Ge NPs which were synthesized by azidation of chloro-terminated Ge NPs. Water soluble PEGylated Ge NPs were synthesized by "click" reaction for biological application. PEGylated Ge NP clusters were prepared using α , ω -bis alkyno or bis-azido polyethylene glycol (PEG) derivatives by copper catalyzed "click" reaction via inter-particle linking.

These nanoparticles were further functionalized by azido β -cyclodextrin (β -CD) and azido adamantane via alkyne-azide "click" reactions. Nanoparticle clusters were made from the functionalized Ge NPs by "host-guest" chemistry of β -CD functionalized Ge NPs either with adamantane functionalized Ge NPs or fullerene, C₆₀.

Functionalization of Mechanochemically Passivated Germanium Nanoparticles via “Click” Chemistry

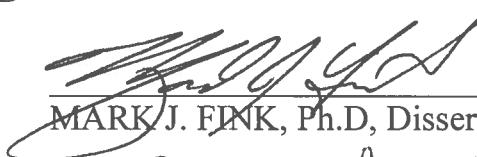
A DISSERTATION
SUBMITTED ON FIFTEENTH DAY OF AUGUST, 2012

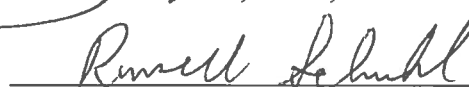
TO THE DEPARTMENT OF CHEMISTRY
IN PARTIAL FULFILMENT OF THE REQUIRMENTS
OF THE SCHOOL OF SCIENCE AND ENGINEERING
OF TULANE UNIVERSITY
FOR THE DEGREE OF
DOCTOR OF PHILOSOPHY

BY


TAPAS KUMAR PURKAIT

APPROVED


MARK J. FINK, Ph.D, Dissertation Advisor


RUSSELL H. SCHMEHL, Ph.D


JAMES P. DONAHUE, Ph.D


SCOTT MICHAEL GRAYSON, Ph.D


BRIAN S. MITCHELL, Ph.D

DEDICATED TO MY PARENTS AND MY WIFE

© Copyright by Tapas Kumar Purkait, 2012
All Rights Reserved

ACKNOWLEDGEMENTS

Foremost, I would like to sincerely thank my advisor Prof. Mark J Fink for his stimulating attitude, constant encouragement and guidance throughout my graduate studies. I greatly appreciate his persistent support and endless patience, which helped me to grow as a chemist and also an independent thinker. I also want to thank Prof. Fink for his financial support during my graduate study.

I would like to thank Prof. Brian S Mitchell for his guidance as co-advisor. His knowledge in mechanochemistry and chemical engineering; which helped me immensely in my work not only as a chemist but also as a chemical engineer. I would like to thank the members of my dissertation committee, Prof. Russel H Schmehl, Prof. James P. Donahue and Prof. Scott Michel Grayson for their valuable time, ideas and advices towards this thesis.

I would like to thank Prof. Joel T Mague for resolving crystal structure. I am also thankful to Prof. Grayson and Prof. Janarthanan Jayawickramarajah for their collaboration and support. I would like to thank Dr. Jibao He for teaching me the TEM instrument and helping me in resolving many problems. I would also like to thank the J. Bennett Johnston, Sr. Center for Advanced Microstructure and Devices (CAMD), Baton Rouge, USA for SAXS and XANES experiments.

I want to thank my previous lab mates Ram, Dan and Dauglas for their support and I am grateful to work with my current lab mates Li, Ted, Zejing and Yuxi. I am also thankful to Dr. James Bolinger for his help in gas chromatography. I would like to thank

Dr. Alina Alb for her support in GPC and DLS characterization. I sincerely thank other members of the faculty and staffs of the chemistry department for their support throughout my graduate studies.

This thesis could not be completed without the support of my parents, my wife, Subhra, and other family members. I could not forget the support of all of my good friends especially Steffen, Upul, Chandru, Ravi, Bala and Pom.

Table of Contents

Acknowledgement.....	ii
Chapter 1 Introduction and background	6
1.1 INTRODUCTION	6
1.2 Semiconductor nanoparticles	7
1.3 Optical absorption and Photoluminescence	10
1.4 Application of Germanium Nanoparticles	15
1.4.1 Photovoltaic application	15
1.4.2 Biological application	16
1.5 Synthesis of Germanium Nanoparticles.....	17
1.5.1 Metathesis of Zintl salts	17
1.5.2 Reduction of halogermanes	18
1.5.3 Plasma synthesis of germanium nanoparticles.....	19
1.5.4 Reduction in inverse micelles.....	19
1.5.5 Synthesis of germanium nanoparticles in supercritical fluids	20
1.5.6 Top-down Approaches:.....	21
1.6 Passivation and Functionalization.....	21
1.6.1 Hydrogermylation	22
1.6.2 Alkylation of chloro-terminated surface.....	23
1.6.3 Direct in-situ Functionalization	24
1.7 Motivation.....	27
1.8 References	29
Chapter 2	35
2 Mechanochemically Synthesis of Passivated Germanium Nanoparticles	35
2.1 Mechanochemical Synthesis.....	35
2.1.1 Introduction	35
2.1.2 Structure and reactivity of germanium surfaces	35
2.1.3 Mechanochemical Synthesis.....	37
2.2 Results and Discussion: TMSA-Passivated Ge Nanoparticles.....	39
2.2.1 Characterization of crude TMSA-passivated Ge nanoparticles.....	41

2.2.2	Size Separation by GPC	44
2.2.3	Confirmation of alkenyl-passivation of Ge surfaces by comparing deuterated-alkenyl-passivated surfaces.	47
2.2.4	Optical Properties of TMSA-Passivated Ge NPs.....	49
2.3	Amine-terminated Germanium Nanoparticles	59
2.3.1	Characterization	59
2.3.2	Water Soluble Ge Nanoparticles.....	65
2.4	Molecular Impurities Formed during Ball-milling	68
2.4.1	Impurities from TMSA-milled products.	68
2.4.2	Impurities formed during ball-milling with phenyl acetylene.	71
2.4.3	Impurities formed during ball-milling with amino-propyne.	73
2.5	Germanium Nanoparticless with other Passivating Reagents.....	75
2.5.1	Nitrile-passivated Ge NPs.....	75
2.6	Conclusion.....	79
2.7	Experimental	80
2.7.1	Method and Materials.	80
2.7.2	Production of TMSA-Passivated Ge Nanoparticles:.....	80
2.7.3	Gel-permeation Chromatography Separation of Ge NPs:	81
2.7.4	Synthesis of TMSA-d ₁ :	81
2.7.5	Synthesis of D-TMSA-passivated Ge NPs:	82
2.7.6	Control Experiment: Milling of Pure TMSA without Ge.....	83
2.7.7	Production of dimethylamino propyne-passivatedGe NPs.....	83
2.7.8	Separation of Ge NPs by Soxhlet dialysis:	83
2.7.9	Synthesis of Nitrile-passivated Ge NPs	85
2.8	Analytical Methods	86
2.8.1	Infrared spectroscopy.	86
2.8.2	Nuclear magnetic resonance spectroscopy.	86
2.8.3	Transmission electron microscopy.	86
2.8.4	UV-vis Absorption and Photoluminescence spectroscopy.	87
2.8.5	GS-MS.....	87
2.8.6	Estimation of quantum yield (QY):.....	87
2.8.7	Small Angle X-ray Scattering experiment.....	88

2.8.8	Powder X-ray diffraction.	89
2.9	APPENDIX	90
	References	92
	Chapter 3	97
3	Application of "Click" Chemistry for Functionalization of Passivated Germanium Nanoparticles.....	97
3.1	Introduction.	97
	Results and Discussion	100
3.2	Alkyne-terminated Germanium Nanoparticles.....	100
3.3	The Grafting of Organic and Organometallic Molecules to the Alkyne-Terminated Ge Nanoparticles using "click" Chemistry	107
3.3.1	Benzyl azide – grafted germanium nanoparticles.....	109
3.3.2	Ester moiety grafted Ge NPs.....	111
3.3.3	Ferrocene grafted Ge NPs.....	113
3.3.4	Glucal-grafted Ge NPs.....	117
3.3.5	Optical properties of functionalized Ge NPs.....	121
3.4	Conclusion.....	124
3.5	Experimental:	124
3.5.1	Method and Materials	124
3.5.2	Synthesis of ω -alkynyloctenyl(20%)-Germanium Nanoparticles:.....	124
3.5.3	The copper (I) catalyzed "Click" Reaction on ω -alkynyloctenyl(20%)-Ge nanoparticle with azides: 125	
3.5.4	TMS-azide grafted Ge NPs.	126
3.5.5	Benzyl-azide grafted Ge NPs.	126
	Benzyl azide was synthesized from benzyl bromide by an azidation reaction. ³⁷ Benzyl bromide (1.2 ml, 10 mmol) was added to 0.5 M solution of NaN_3 in 22 ml DMSO and the mixture was stirred for overnight. The product was separated by ether (100 ml) extraction after washing three times with brine (100 ml). Yield: 98% (1.3 g). ^1H NMR (300 MHz, CD_2Cl_2): δ 7.38 (m, 5H), 4.36 (m, 2H) ppm.	126
3.5.6	Ethyl 2-azidoacetate grafted Ge NPs.	127
3.5.7	4-azido benzoic acid grafted Ge NPs.....	127
3.5.8	Synthesis of ferrocenylpropylene bromide.....	128
3.5.9	Synthesis of ferrocenylpropylene azide.....	129

3.5.10	.Glucal moiety grafted Ge nanoparrticles.....	130
3.6	Analytical Method.....	131
3.6.1	Infrared spectroscopy.	131
3.6.2	Nuclear magnetic resonance spectroscopy.	131
3.6.3	Transmission electron microscopy.	131
3.6.4	UV-vis Absorption and Photoluminscence spectroscopy.	132
3.6.5	GS-MS.....	132
3.7	APPENDIX: TEM images	133
3.8	References	139
CHAPTER 4	143
4	Synthesis of PEGylated Germanium Nanoparticles and Nanoparticle Arrays for Biological Application.....	143
4.1	Introduction	143
4.2	PEGylated germanium nanoparticles and their aggregates from alkyne terminated Ge NPs 145	
4.2.1	PEGylated Ge NP Clusters by "click" reactions using diazido-TEG.....	148
4.2.2	PEGylated Ge NP Clusters by a "click" reaction using diazido-PEG (2Kda).	151
4.3	PEGylated Ge NPs and their aggregates from azido terminated germanium nanoparticles 153	
4.3.1	Synthesis of ω -chloropentenyl Ge NPs	153
4.3.2	PEGylated water soluble germanium nanoparticles.....	155
4.3.3	PEGylated Ge NP Clusters by a "click" reaction using bis-alkynyl PEG	160
4.3.4	Ge NP Clusters using conjugated spacer.....	163
4.4	Nanoparticle Assembly by "Host-Guest" Chemistry	165
4.4.1	-Cyclodextrin-grafted germanium nanoparticles.....	166
4.4.2	Adamantane-grafted Ge nanoparticles	169
4.4.3	Ge-C ₆₀ -Ge Nanoparticle Assembly	171
4.4.4	Ge-Si Nanocluster by assembly of Ge and Si NPs using host-guest interaction	173
4.5	Experimental	176
4.5.1	Method and materials.....	176
4.5.2	Synthesis of ω -alkynyloctenyl-Ge NPs.	176
4.5.3	Synthesis of 1,11-diazido-3,6,9-trioxaundecane (diazido-TEG)	177

4.5.4	Synthesis of Ge NP clusters using ω -alkynyloctenyl(15%)-Ge NPs and diazido TEG by "Click" Reaction:.....	178
4.5.5	Synthesis of Ge NP cluster using ω -alkynyloctenyl(15%)-Ge NPs and diazido PEG by "Click" Reaction: 178	
4.5.6	Synthesis of ω -PEGyloctenyl(20%) Ge NPs from ω -alkynyloctenyl(20%)-Ge NPs	179
4.5.7	Synthesis of ω -chloropentenyl Ge NPs by HEBM.	180
4.5.8	Synthesis of ω -azidopentenyl (50%) Ge NPs.....	180
4.5.9	Synthesis of ω -PEGylpentenyl Ge NPs from ω -azidopentenyl Ge NPs.	181
4.5.10	Synthesis of PEGylated Ge NP clusters using bisazido PEG.	182
4.5.11	Synthesis of 1,4-Diazidobenzene from p-phenylenediamine	183
4.5.12	Synthesis of Ge NP arrays using 1,4-diazidibenzene as a spacer via "click" reaction.....	183
4.5.13	Synthesis of mono-6-O-(p-tolylsulfonyl)- β -cyclodextrin.....	184
4.5.14	Synthesis of β -CD grafted Ge NPs	185
4.5.15	Synthesis of ω -adamantanyloctenyl(20%)-Ge NPs from ω -alkynyloctenyl(20%)-Ge NPs	185
4.5.16	Synthesis of Ge-C ₆₀ -Ge Assembly by host-guest interaction	186
4.6	Analytical Methods	186
4.6.1	Infrared spectroscopy.	186
4.6.2	Nuclear magnetic resonance spectroscopy.	187
4.6.3	Transmission electron microscopy.	187
4.6.4	UV-vis Absorption and Photoluminescence spectroscopy.	187
4.7	References	189
Chapter 5	193
5	Conclusion and Future Direction	193

Chapter 1 Introduction and background

1.1 INTRODUCTION

Group IV semiconductor materials play a crucial role in modern technology particularly in the field of microelectronics and photovoltaics. When the size of a semiconductor material scales down to the order of a nanometer, they exhibit new optical and electronic properties distinct from their bulk materials.¹ Among group IV semiconductor nanoparticles, silicon nanoparticles have received most attention due to their efficient and tunable light emission² starting from the discovery of visible luminescence from porous silicon.³ However, germanium nanoparticles (Ge NPs) may be useful for electronic and optoelectronic applications including photovoltaics, as the band gap of Ge NPs can be tuned from the infrared into the visible range of solar spectrum.^{4, 5} Because of their stronger quantum confinement effects and better light absorption characteristics compared to silicon, Ge nanoparticles may be more attractive for device applications that require small band gap materials.⁶ Thus, there is a growing interest for synthesis, functionalization and characterization of these nanoparticles.

This thesis describes the synthesis and passivation of Ge NPs by a novel mechanochemical process, followed by further functionalization of their surfaces by alkyne-azide "click" chemistry. Various organic, organometallic and biomolecular compounds were grafted to Ge NPs using copper(I) catalyzed alkyne-azide "click"

chemistry to achieve useful properties including water solubility and biocompatibility. Furthermore, globular nanoparticle arrays can be made through interparticle linking using the "click" chemistry.

1.2 Semiconductor nanoparticles

The band gap of a semiconductor nanoparticle increases when the size of the nanoparticle is reduced. This size effect results from the confinement of the charge carrier to nanoparticle physical dimension that approaches the critical characteristic length of a Bohr radius for an electrostatically bound electron-hole pair or exciton. This phenomena is called quantum confinement and the particles that exhibit are called quantum dot (QDs).¹ The size effect can be explained quantum mechanically using a simple “particle in a box” model; which leads to the conclusion that

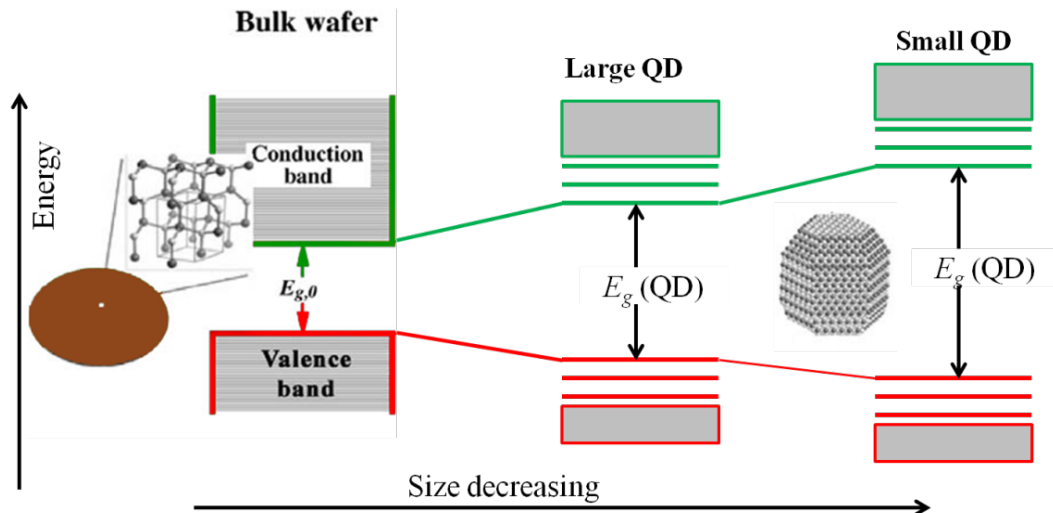


Figure 1-1: Bulk semiconductors have continuous valence band and conduction band separated by a relatively small band gap; where as in nanoparticles, valence and conduction bands split into discrete energy levels, with the energy gap (E_g) increasing with decreasing particle size.

the energy gap is simply proportional to $1/r^2$, where r is the radius of a spherical QD. In addition to increasing energy gap, quantum confinement leads to a transformation of the continuous energy bands of the bulk material into discrete energy levels; which leads to confinement of an exciton in the small potential well (Figure 1)⁷ and introduces uncertainty into the momentum of the exciton according to the uncertainty principle

In recent years, there has been immense progress in the synthesis and characterization of compound semiconductor QDs (such as CdSe, CdS, InP ect.) as they exhibit well known size, shape and surface chemistry.⁸⁻¹⁰ They have the ability to tune emission efficiently by changing their size primarily due to strong quantum confinement in direct band gap materials. For instance, larger quantum dots have a greater spectrum-shift towards the red compared to smaller dots, and exhibit less pronounced quantum properties. Conversely, the smaller particles allow one to take advantage of more subtle quantum confinement effects.

Narrow “size-tunable light emission” of these QDs can be used as multi-color fluorescent labeling¹¹ or light emitting diodes¹² by changing QD size.^{13, 14} Semiconductor NPs or QDs have outstanding photostability over organic dyes and have the capability of absorbing high energy without damage the particles (Figure 2).¹⁴ Other potential application of these nanoparticles include use in single electron transistors¹⁵, liquid crystals¹⁶ and solar cells.^{6, 17} However, compound semiconductors are not suitable for biological applications as they are electrochemically active and they generate reactive oxygen species (ROS) in the cell which have been found to be toxic.¹⁸

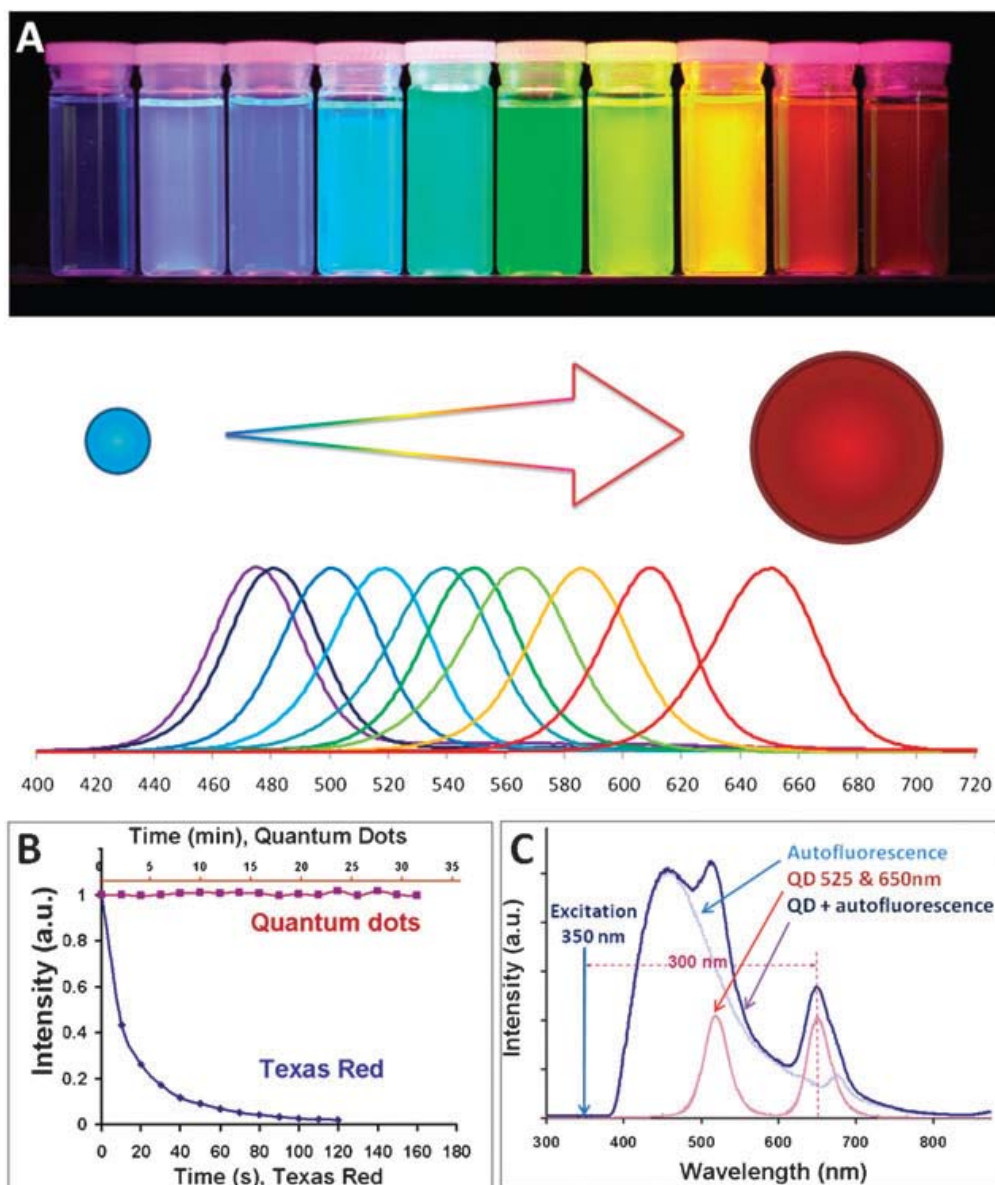


Figure 1-2: Photophysical properties of QD probes. (A) Narrow size-tunable light emission QD probes provides fluorescent color control by changing QD size. (B) Outstanding photo-stability of QDs compared to efficient photo-bleaching of organic dyes. (C) Capability of absorbing high-energy (UV-blue) light and emitting fluorescence with a large Stokes shift without damage.¹⁴

1.3 Optical absorption and Photoluminescence

The direct and indirect gap semiconductors are distinguished by the relative positions of the conduction band minimum and the valence band maximum in the wave vector, k , space. In a direct gap material, both the conduction band minimum and the valence band maximum occur at the zone center where $k = 0$; whereas, in an indirect gap material, such as Si and Ge etc., the conduction band minimum does not occur at $k = 0$.¹⁹ Bulk Ge has an indirect band gap of 0.66 eV and according to the band structure of Ge, the absorption coefficient of bulk Ge has distinct peaks at 550 nm (2.1 eV) and 280 nm (4.3 eV) associated with direct band transitions at L and X, respectively. The germanium band diagram is shown in the **Figure 1-3**.

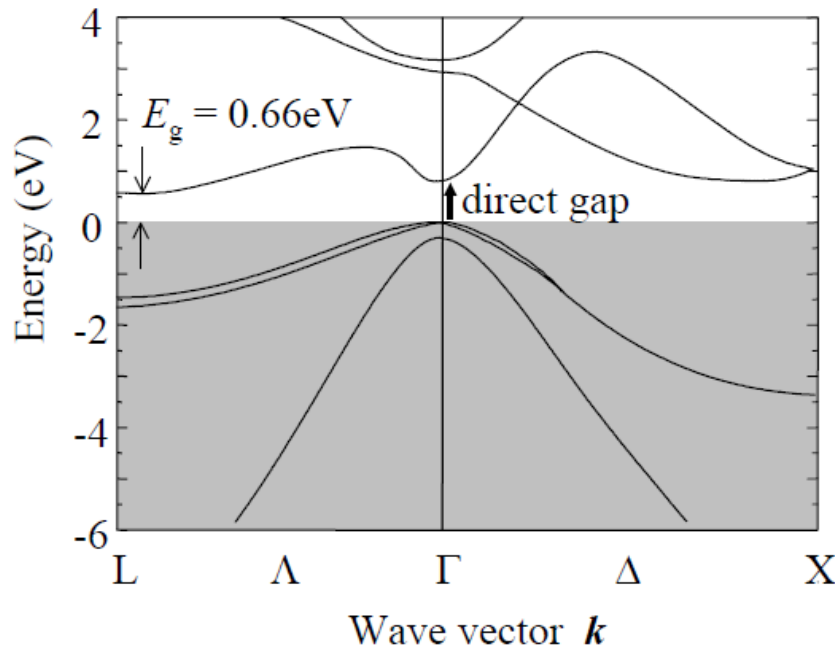


Figure 1-3:Electronic band structure of bulk germanium which has an indirect gap of 0.66 eV.¹⁹

During photon absorption in indirect band gap semiconductors, conservation of momentum implies that the photon absorption process must be assisted by either absorbing or emitting a phonon (a quantum of lattice vibration), which supplies the missing crystal momentum. The band gap of a semiconductor material can be estimated from their optical absorption. The optical absorption coefficients of bulk semiconductors are mostly described by the following two expressions

$$\alpha(h\nu) \propto (h\nu - E_g)^{1/2} \text{ for direct band gap semiconductors... (1)}$$

$$\alpha(h\nu) \propto (h\nu - E_g \pm E_p)^2 \text{ for indirect band gap semiconductors... (2);}$$

where $h\nu$, E_g , and E_p are the photon energy, bandgap, and phonon energies, respectively.¹⁹ However, for germanium nanoparticles some have claimed a good fit to (2),^{20, 21} in most cases, the absorption spectra of the Ge nanocrystals do not follow any of the above equations. There are several factors which are responsible for this complication- firstly, polydispersed sample consisting of various size particles (which consist various energy gap between valence and conduction band); secondly, light scattering which can affect the transmission spectrum (which is directly measure of optical spectra); and more importantly, phonon assisted absorption at higher temperatures.²²

After the photon absorption, the excited electron and hole will relax very rapidly by emitting phonons. When the electron reaches at the bottom of the conduction band (on the other hand, the hole reaches top of the valence band), the electron-hole pair (exciton) can recombine radiatively with the emission of a photon (luminescence), or nonradiatively by transferring the electron's energy to the lattice. This process is made more efficient by impurities or defects in the material or by dangling bonds at the surface.

The electron-hole recombination in a direct band gap material does not involve any phonons since there is no need for momentum change for the electron. Hence, PL process for direct band gap material is the first order process with shorter radiative lifetime (10^{-9} - 10^{-8} s). In contrast, in an indirect gap material, the excited electron located in the conduction band needs to undergo a change in momentum state before it can recombine with a hole in the valence band; therefore, the electron-hole recombination must be accompanied by the emission of a phonon. The PL process for indirect gap material is therefore a 2nd order process with longer radiative lifetime ($\sim 10^{-5}$ - 10^{-3} s) and the PL efficiency is small as there is competition with nonradiative combination.²³

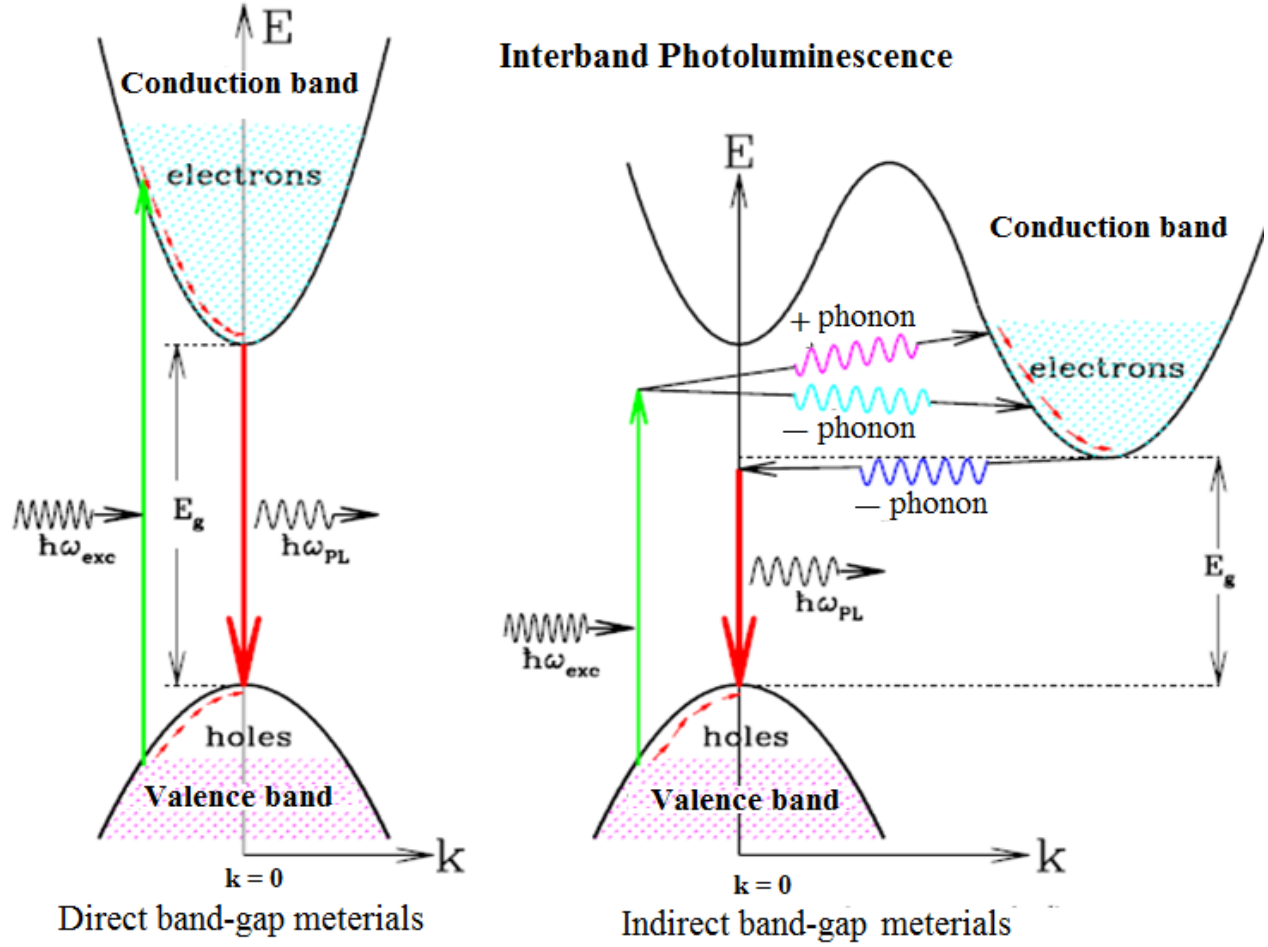


Figure 1-4: Schematic band diagrams for the photoluminescence processes in a direct gap material (left) and an indirect gap material (right). The shaded states at the bottom of the conduction band and the empty states at the top of the valence band respectively represent the electrons and holes created by the absorption of photons with energy $\hbar\omega > E_g$. The cascade of transitions within the conduction and valence bands represents the rapid thermalization of the excited electrons and holes through phonon emission.²³

For sub-100 nm size particles of an indirect band gap semiconductor, there are several factors that play a role to improve radiative recombination. When the particle size decreases and approaches the Bohr exciton radius (for Ge it is 11.5 nm), confinement of charge carriers leads to an increase of the band gap and also to an increased overlap of

electron and hole wave function through a dipole operator. Therefore, these particles might have a direct or quasi-direct band gap which allows non-phonon recombination.²⁴⁻

²⁶ In mean time, uncertainty of momentum space relaxes the momentum conservation rule and allows the transition.

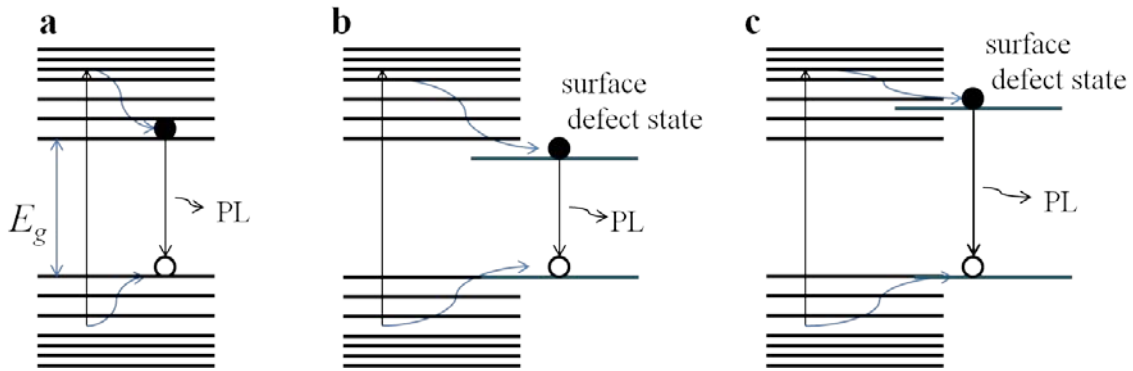


Figure 1-5: Schematic energy diagram of a NP showing PL mechanism a) without surface defect states, where PL is exclusively due to quantum confinement, b) with surface defect state which reduces the energy gap resulting in red emission, c) with surface defect state which increase the energy gap resulting blue emission.

In addition to quantum confinement there are two other factors which can influence the PL: surface related phenomena (surface defects) and phase transition (crystal defects). If the surface of Ge NPs is not fully passivated, surface dangling bonds can act as traps which increase the nonradiative recombination and quench the PL. Possible PL mechanism of Ge NPs or Si NPs was shown in the Figure 5. Most of the studies claimed that surface defect states act as traps which decrease the effective band gap and lead to a red shift of the PL peak (red emission)²⁷⁻²⁹ and PL in the near infrared and infrared probably involves a deep trap in the gap of the Ge nanoparticles. However, surface defect states could increase the gap causing a blue shift of the PL (blue emission).³⁰⁻³²

1.4 Application of Germanium Nanoparticles

1.4.1 Photovoltaic application

Germanium is important semiconductor in optical and optoelectronic device applications including photovoltaic, photodetector and image sensors as it has high absorption coefficient, high charge-carrier mobility and a low energy band gap.³³⁻³⁵ For photovoltaic applications, the size-tunable bandgap of the Ge NPs is of particular interest as the band gap of the Ge NPs can be tuned between 0.66 eV to above 2 eV by changing the particle size.^{4, 6} Efficiency of photoconversions can be improved greatly if these quantum confinement particles produce multiple excitons by absorbing single photon; which is called multiple exciton generation (MEG).³⁶

Thin films of Ge NPs for photovoltaic applications can be made by dip-coating or spin coating. However, the organic ligands attached to these NP films make them resistive. Conductivity of these films can be improved by thermal annealing. Previously Kortshagen *et al* demonstrated annealed Si and Ge NPs film based solar cells.⁶ Low performance of these solar cells is due to non-uniform morphology of NP film. Recently, Swihart and coworkers achieved highly conductive ligand-free Si/ Ge alloy NP inks, made by laser pyrolysis of silane and germane, for low cost photovoltaic devices.³⁷

1.4.2 Biological application

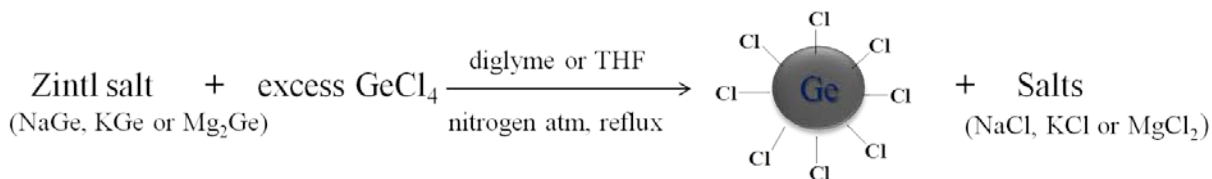
Like silicon, germanium is an electronically stable and bioinert material. Cytotoxicity or biocompatibility of Ge NPs was studied when these particles were used *in vivo*. There are several recent application of Ge NPs in bioimaging. Water soluble dinitrophenyl-functionalized Ge NPs (3-5 nm) were labeled with dye as they have weak fluorescence and these particles were cross lined to immunoglobulin E antibodies on the surface of mast cells RBL-2H3.³⁸ Amine-terminated blue luminescent Ge NPs (4.0–5.5 nm) were synthesized by hydride reduction of germanium tetrachloride in the inverse micelles followed by hydrogermylation with allylamine. Their use in biological imaging is demonstrated by use of HepG2 cells. These Ge NPs show very low cytotoxicity according to the mitochondrial activity of the cells.³⁹ However, another amine-terminated water soluble Ge NPs, synthesized from inverse micelle method followed by hydrogermylation with allylamine, showed high toxicity to cell. These amine terminated cationic surface might increase both the intracellular calcium level and the concentration reactive oxygen species (ROS) causing cytotoxicity.⁴⁰

1.5 Synthesis of Germanium Nanoparticles

Various synthetic methods have been used to prepare colloidal suspensions of Ge nanoparticles. As the reactivity and structure of Ge are similar Si, most synthetic methods, useful for Si, can be applied to the synthesis of germanium nanoparticles. The synthesis of Ge NPs can be categorized into two general approaches: bottom-up, where molecular precursors (such as halogermanes) are used to prepare Ge NPs and top-down, where bulk Ge is commutated to form Ge NPs.

1.5.1 Metathesis of Zintl salts

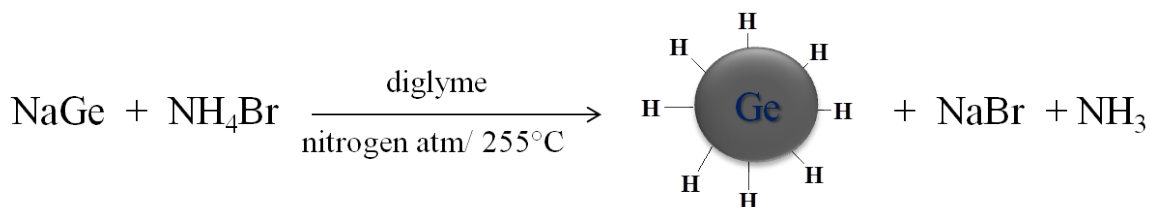
Germanium Zintl salts are polyanions of germanium with cations of alkali metals (Na, K or Mg). Germanium nanoparticles may be synthesized from the metathesis of Zintl salt and tetrachlorogermane (GeCl_4).^{41, 42} Chloride-terminated germanium nanoparticles may be synthesized from the reaction of suspension of the Zintl salt (such as NaGe, KGe, or Mg_2Ge) in glyme with an excess of GeCl_4 under inert atmosphere with reflux conditions. These Cl-terminated Ge NPs may be terminated with alkyl groups by the reaction with alkyl lithium or Grignard reagents. The particles are crystalline and have a narrow size distribution.



Scheme 1-1: Ge NPs synthesis from metathesis of Zintl salt

Hydrogen-terminated germanium nanoparticles were synthesized by reaction of Zintl salt (NaGe) with NH_4Br by Kauzlarich et al.⁴³ These Ge nanoparticles could be

prepared as amorphous or crystalline nanoparticles in quantitative yields and with a narrow size distribution.

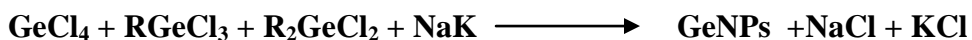


Scheme 1-2: Ge NPs synthesis from the reaction between Zintl salt and NH_4Br .

This hydrogen-terminated surface was reacted with alkenes to obtain alkyl passivation via thermally initiated hydrogermylation.

1.5.2 Reduction of halogermanes

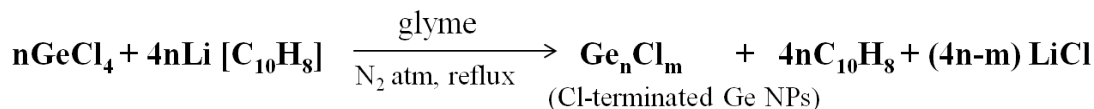
Germanium nanoparticles may also be synthesized from reduction of alkylchlorogermanes by NaK alloy under an inert atmosphere.^{44, 45} This reduction is performed at high temperature (275°C) and high pressure (200 atm). There is a very little selectivity over size, shape and surface termination and the products tend to be mixture of germanium nanowires and germanium nanoparticles with a low yield of Ge NPs.⁴⁵



Scheme 1-3: Reduction of halogermanes

Reduction of germanium tetrachloride by lithium naphthalenide (LiNp) produces colloidal Ge NPs with narrow size distribution (6-10 nm) at 60°C and

atmospheric pressure.⁴⁶ The particles initially produced are amorphous, requiring annealing with a ruby laser light to become crystalline.



Scheme 1-4: Reduction of halogermanes by lithium naphthalanide.

1.5.3 Plasma synthesis of germanium nanoparticles

A nonthermal plasma technique was used to produce germanium nanoparticles using a flow through nonthermal plasma reactor which consists of a quartz tube through which precursor gases are passed.^{4, 47} Germanium tetrachloride (GeCl₄) and argon (Ar) (with ratio of 5:95) used as gas precursor are passed through the reactor at 200 kPa. Hydrogen and additional Ar are also added to the gas flow entering the reactor; H₂ serves to scavenge chlorine produced in the dissociation of GeCl₄, while Ar acts as a background gas in the plasma and can be adjusted to alter the total gas flow rate. In this process it is difficult to control size of the particles. However, Kortshagen *et al* reported size control crystalline germanium nanoparticles with this synthetic method.⁴ Initially synthesized hydrogen-terminated germanium nanoparticles are passivated by hydrogermylation using alkynes.

1.5.4 Reduction in inverse micelles

Germanium nanoparticles with narrow size distribution can be achieved by the inverse micelle method.⁴⁸⁻⁵⁰ Inverse micelles were formed with dodecyl pentaethylene glycol ether ($C_{12}E_5$), a non-ionic surfactant in a hydrophobic solvent (e.g. hexane). Germanium halides are reduced in the inverse micelle by various reducing agents such as $LiAlH_4$ or $NaBH_4$ to form Ge NPs. The partial separation of the halide salt and reductant into hydrophilic and hydrophobic regions of the inverse micelles permits some control over size distribution. The micelle controls the size of the particles in the following ways: they might act as cavities which limit the size; and micelle might slow down the reaction rate followed by preventing NP growth. However, surface chemistry of these nanoparticles is not clear as it might form mixture of H-terminated and $C_{12}E_5$ capped the surface. The H-terminated surface can be further passivated by hydrogermylation.

1.5.5 Synthesis of germanium nanoparticles in supercritical fluids

Korgel *et al* reported the synthesis of germanium nanoparticles in supercritical fluids at high temperatures (~ 400 - 550°C) and high pressures (20.7 MPa).⁵¹ Diphenylgermane (DPG) and tetraethylgermane (TEG) were used as precursors, which undergo thermolysis to crystalline Ge NPs in supercritical hexane and octanol. Octanol is added to control particle growth and passivate germanium surface through an alkoxide linkage. Though the supercritical fluid can produce highly crystalline and tunable size nanoparticles, the yield of this process is very low. This is one of the examples of direct passivation other than hydrogermylation of hydrogen-terminated surface or organometallic route to passivate Cl-terminated Ge surfaces. However, there is less

control over further functionalization. In another thermal decomposition method, tetraethylgermane (TEG), a germanium precursor, was decomposed at 430 °C in a high pressure reactor to form Ge NPs.^{52, 53}

1.5.6 Top-down Approaches:

Porous nanocrystalline luminescent Ge film and Ge NPs with average size 3-4 nm prepared by etching of Ge surface using HF/ H₃PO₄/ H₂O₂ solution to form H-terminated surface.⁵⁴ Oxide coated Ge NPs were also prepared by ball-milling using Ge powder in ethanol.⁵⁵ These nanoparticles were rapidly photooxidized in air by irradiating monochromatic (IR to UV) light, above their band-gap energy, and size-selectively etched in an aqueous solution; which induced a decrease in core size.

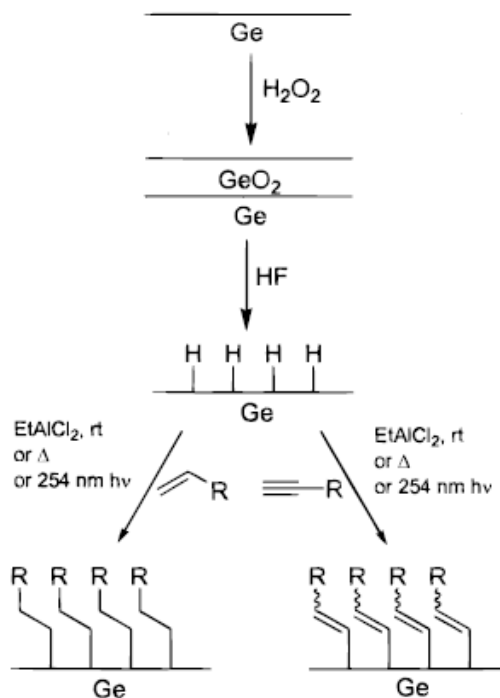
1.6 Passivation and Functionalization

Surface atoms of nanoparticles may play an important role in the optoelectronic properties compared to their bulk atoms due to their enormous surface area-to-volume ratios.⁵⁶ Passivations of these surfaces are required to protect the surface dangling bonds and electronic surface states (which protect against surface defect states); which might increase nonradiative recombination in Ge NPs. Moreover, it also protects against chemical oxidation, as well as inter-particle aggregation and prevents Ostwald ripening. Further functionalization of those materials will not only provide intriguing properties

like, water solubility or biocompatibility, but it also may lead to numerous applications ranging from bioimaging, drug delivery to electronic devices.

1.6.1 Hydrogermylation

Most of the solution based synthesis of germanium nanoparticles involves unstable surfaces such as H-terminated or Cl-terminated surfaces. H-terminated surface may be functionalized via hydrogermylation with alkenes or alkynes;^{43, 57} which is a similar to the chemically hydrosilylation reaction.⁵⁸ Hydrogermylation can be initiated either thermally, photochemically or by help of Lewis acid catalysis. Thermally induced hydrogermylation can be achieved by heating nanoparticle solution in alkene or alkyne at 200-220 °C.⁵⁹ UV photoinduced hydrogermylation can be achieved by irradiating H-terminated Ge NPs in 1-alkene or alkyne using 254 nm or 365 nm light. A solution of EtAlCl₂ is used as a catalyst for the hydrogermylation of alkene or alkyne.



Scheme 1-5: Hydrogermylation reactions on H-terminated surface.⁵⁷

Water soluble Ge NPs terminated with NH_2 were produced by hydrogermylation of H-terminated Ge NPs, synthesized by inverse micelle, with allyl amine.⁵⁰ However, *in-situ* functionalization via hydrogermylation was reported from the thermal reduction of germanium halides in 1-octadecene.⁶⁰ Ge NPs synthesized by nonthermal plasma method were also functionalized *in-situ* by hydrogermylation.

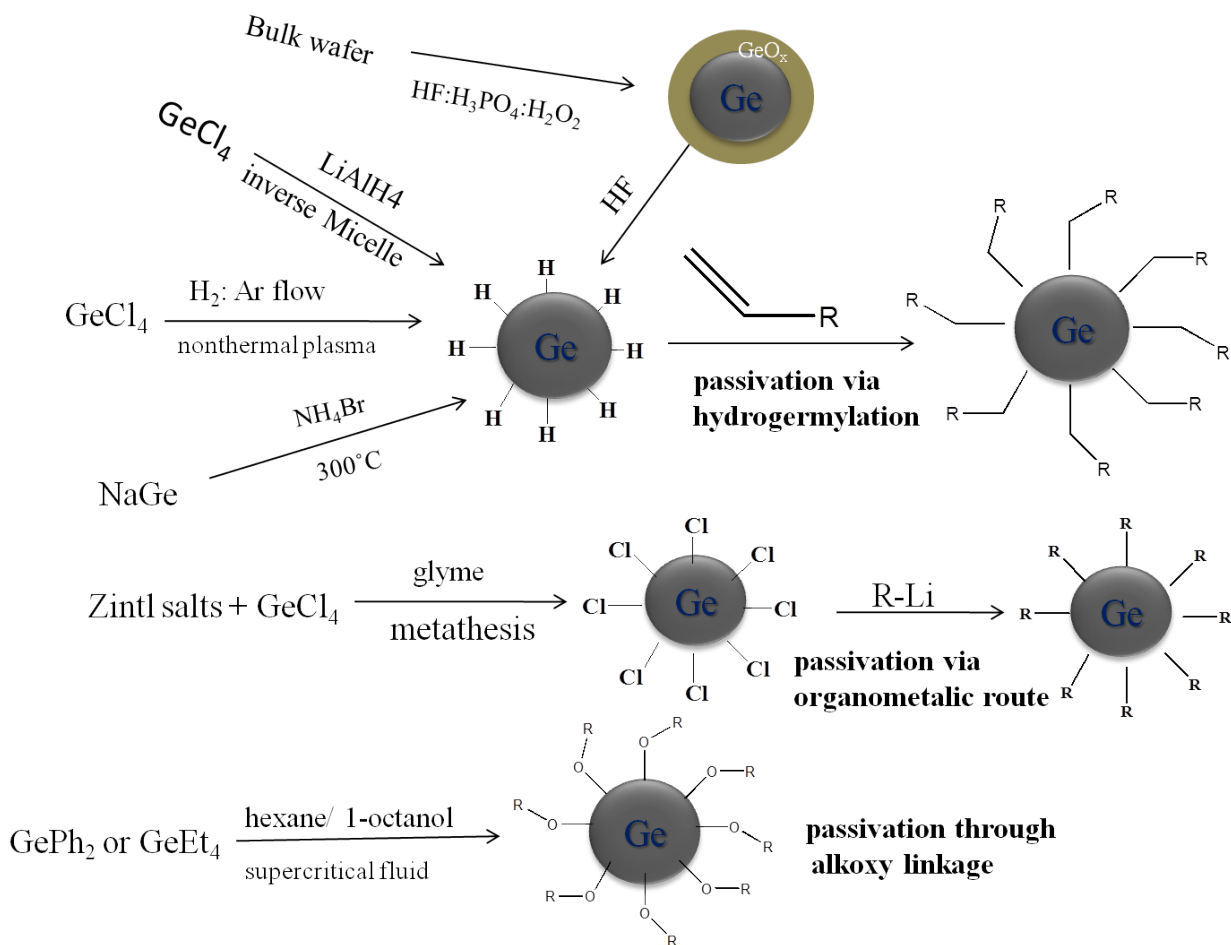
1.6.2 Alkylation of chloro-terminated surface

Organometallic routes to functionalized halogen-terminated Ge surface have been explored. Chloro-terminated Ge NPs can be prepared from the metathesis of Zintl salts or from the reduction of chlorogermanes. Alkylation of chloro-terminated Ge NPs can be

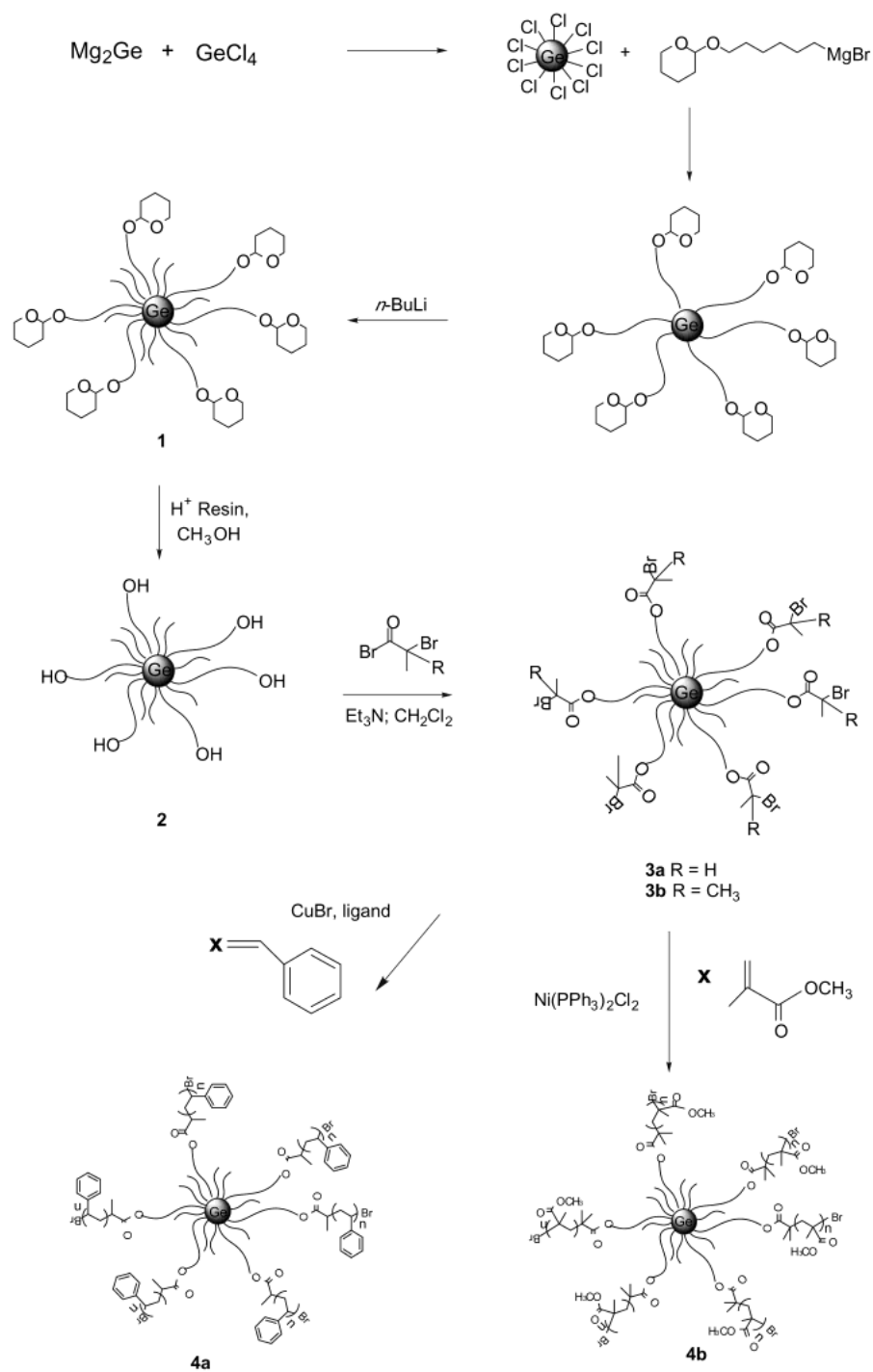
effected by either alkyl lithium (RLi) or an alkyl Grignard (RMgBr) reagent. Kauzlarich *et al* showed various functionalization of Ge NPs by alkylation of chloro-terminated surface. Acetyl-, hydroxyl-, and Br-terminated Ge NPs were synthesized from Cl-terminated Ge NPs by treating with Grignard reagent containing acetal group followed by hydrolysis and reaction with acid bromide.⁶¹ However, organometallic routes are very hazardous as it involves very reactive reagents.

1.6.3 Direct in-situ Functionalization

Alkyl-passivated Ge NPs were prepared by thermal reduction of GeI₄/ GeI₂ mixture by BuLi in 1-octadecene.⁶⁰ The size of the nanoparticles were tuned by controlling Ge(IV)/ Ge(II) ratio and reaction temperature. Initially H-terminated Ge NPs were capped by 1-octadecene via hydrogermylation. This is an example of *in-situ* alkyl passivation or functionalization. Other *in-situ* functionalization of Ge NPs includes alkoxy linkage (Ge-O-R) formed during synthesis in supercritical fluids.⁵¹ During Ge NPs synthesis in supercritical hexane and 1-octanol mixture, the later acts as a capping ligand to passivate the Ge surface through alkoxy linkage.



Scheme 1-6: Various routes for synthesizing functionalized Ge NPs.



Scheme 1-7: Scheme for preparing surface-functionalized Ge NPs by organometallic routes.⁶¹

1.7 Motivation

Based on the background review, it is obvious that present solution synthesis techniques of free standing Ge NPs are multi step processes which involve modification of unstable H-terminated or Cl-terminated surfaces. In addition, they may require either high temperature or highly reactive reagents. Further functionalization may not be possible on a moderate scale. An ideal synthetic procedure would deal with synthesis, passivation and functionalization of germanium nanoparticles in a direct efficient way under mild reaction conditions.

This work was motivated by a novel mechanochemical synthesis of Si NPs by high energy ball-milling (HEBM).⁶² This method is a facile and efficient method for the synthesis and simultaneous passivation (or functionalization) of silicon nanoparticles. In HEBM a Si wafer is fractured and the newly formed new reactive Si surfaces react with 1-alkene or 1-alkynes during ball-milling. However, Ge NPs were previously prepared by ball-milling of Ge powder in ethanol. These Ge NPs were coated with oxide surface and further steps were introduced to clean and functionalized Ge NPs. Moreover, ultra high vacuum study revealed that clean reconstructed Ge surfaces undergo reaction with reactive organic molecules (such as 1-alkene, 1-alkynes etc.) to form organic passivation of Ge surfaces with strong covalent Ge-C bond.

Therefore, passivated germanium nanoparticles were synthesized by a direct top-down mechanochemical approach using HEBM, followed by various functionalization of those nanoparticles by various azides using “click” reaction. Chapter 2 of this thesis illustrates synthesis of Ge NPs with various surface passivation and their surface and optical characterization. Mechanochemically synthesized Si NPs were

passivated previously by various aliphatic n-alkynes including 1-octyne. Here we use various functionalize alkynes such as, trimethylsilylacetylene (TMSA), 3-dimethylamino-1-propyne, 1,7-octadiyne, 5-chloro-1-pentyne etc. The simple alkyne, TMSA, was used to prove the organic functionality by its TMS group using spectroscopic techniques. The idea of using a bi-functional organic compound as a coreactant during HEBM is to passivate nanoparticles with one reactive group, while the other is used for further reaction chemistry. The aminopropyne was used to amine-functionalized alkenyl-passivated Ge NPs which would be soluble in alcohol or water. Other bifunctional alkynes such as, 1,7-octadiyne and 5-chloro-1-pentyne will form alkyne and chloro-terminated alkenyl-passivated Ge NPs.

Further functionalization can be achieved using peripheral alkyne or chloro-groups to make water soluble, biocompatible Ge NPs. Chapter 3 of this thesis presents a novel functionalization approach by grafting organic, organometallic and biomolecule via alkyne azide “click” chemistry. Chapter 4 illustrates synthesis of PEGylated Ge NPs and synthesis of Ge NPs arrays through inter-particle linking either via “click” chemistry or “host-guest” chemistry.

1.8 References

1. Alivisatos, A. P., Semiconductor clusters, nanocrystals, and quantum dots. *Science (Washington, D. C.)* **1996**, 271, (5251), 933-7.
2. Nayfeh, M. H.; L. Mitas, V. K., Silicon nanoparticles: New photonic and electronic material at the transition between solid and molecule. In *Nanosililicon*, Nayfeh, M. H., Ed. Elsevir: 2007; p 1.
3. Canham, L. T., Silicon quantum wire array fabrication by electrochemical and chemical dissolution of wafers. *Appl. Phys. Lett.* **1990**, 57, (10), 1046-8.
4. Gresback, R.; Holman, Z.; Kortshagen, U., Nonthermal plasma synthesis of size-controlled, monodisperse, freestanding germanium nanocrystals. *Appl. Phys. Lett.* **2007**, 91, (9), 093119.
5. Wilcoxon, J. P.; Provencio, P. P.; Samara, G. A., Synthesis and optical properties of colloidal germanium nanocrystals. *Phys. Rev. B* **2001**, 64, (3), 035417.
6. Kortshagen, U.; Anthony, R.; Gresback, R.; Holman, Z.; Ligman, R.; Liu, C.-Y.; Mangolini, L.; Campbell, S. A., Plasma synthesis of group IV quantum dots for luminescence and photovoltaic applications. *Pure Appl. Chem.* **2008**, 80, 1901-1908.
7. Jennifer, H.; Victor, K., "Soft" Chemical Synthesis and Manipulation of Semiconductor Nanocrystals. In *Nanocrystal Quantum Dots, Second Edition*, Victor, K., Ed. CRC Press: 2010; pp 1-61.
8. Dabbousi, B. O.; Rodriguez-Viejo, J.; Mikulec, F. V.; Heine, J. R.; Mattoussi, H.; Ober, R.; Jensen, K. F.; Bawendi, M. G., (CdSe)ZnS Core-Shell Quantum Dots: Synthesis and Optical and Structural Characterization of a Size Series of Highly Luminescent Materials. *J. Phys. Chem. B* **1997**, 101, (46), 9463-9475.
9. Manna, L.; Scher, E. C.; Alivisatos, A. P., Synthesis of Soluble and Processable Rod-, Arrow-, Teardrop-, and Tetrapod-Shaped CdSe Nanocrystals. *J. Am. Chem. Soc.* **2000**, 122, (51), 12700-12706.
10. Yoffe, A. D., Semiconductor quantum dots and related systems: electronic, optical, luminescence, and related properties of low-dimensional systems. *Adv. Phys.* **2001**, 50, (1), 1-208.
11. Dubertret, B.; Skourides, P.; Norris, D. J.; Noireaux, V.; Brivanlou, A. H.; Libchaber, A., In vivo imaging of quantum dots encapsulated in phospholipid micelles. *Science (Washington, DC, U. S.)* **2002**, 298, (5599), 1759-1762.

12. Schlamp, M. C.; Peng, X.; Alivisatos, A. P., Improved efficiencies in light emitting diodes made with CdSe(CdS) core/shell type nanocrystals and a semiconducting polymer. *J. Appl. Phys.* **1997**, 82, (11), 5837-5842.
13. Gao, X.; Yang, L.; Petros, J. A.; Marshall, F. F.; Simons, J. W.; Nie, S., In vivo molecular and cellular imaging with quantum dots. *Curr. Opin. Biotechnol.* **2005**, 16, (1), 63-72.
14. Zrazhevskiy, P.; Sena, M.; Gao, X., Designing multifunctional quantum dots for bioimaging, detection, and drug delivery. *Chem. Soc. Rev.* **2010**, 39, (11), 4326-4354.
15. Klein, D. L.; Roth, R.; Lim, A. K. L.; Alivisatos, A. P.; McEuen, P. L., A single-electron transistor made from a cadmium selenide nanocrystal. *Nature (London)* **1997**, 389, (6652), 699-701.
16. Li, L.-S.; Alivisatos, A. P., Semiconductor nanorod liquid crystals and their assembly on a substrate. *Adv. Mater. (Weinheim, Ger.)* **2003**, 15, (5), 408-411.
17. Huynh, W. U.; Dittmer, J. J.; Alivisatos, A. P., Hybrid nanorod-polymer solar cells. *Science (Washington, DC, U. S.)* **2002**, 295, (5564), 2425-2427.
18. Bottrill, M.; Green, M., Some aspects of quantum dot toxicity. *Chem. Commun. (Cambridge, U. K.)* **2011**, 47, (25), 7039-7050.
19. Fox, M., *Optical Properties of Solids*. Oxford Univ. Press: New York, 2001.
20. Dowd, A.; Elliman, R. G.; Luther-Davies, B., Linear optical properties of Ge nanocrystals in silica. *Appl. Phys. Lett.* **2001**, 79, (15), 2327-2329.
21. Han, M.; Gong, Y.; Ma, J.; Liu, F.; Wang, G., Optical properties of germanium cluster-based nanostructured film. *Jpn. J. Appl. Phys., Part 1* **1995**, 34, (Suppl. 34-1), 49-52.
22. Nozaki, S.; Morisaki, H.; Sato, S., Germanium nanocrystals. In *Encyclopedia of Nanoscience and Nanotechnology*, American Scientific Publishers: 2004; Vol. 3, pp 805-820.
23. Li, A., Interaction of nanoparticles with radiation. *Astron. Soc. Pac. Conf. Ser.* **2004**, 309, 417-452.
24. Nayfeh, M. H.; Rigakis, N.; Yamani, Z., Photoexcitation of Si-Si surface states in nanocrystallites. *Phys. Rev. B: Condens. Matter* **1997**, 56, (4), 2079-2084.
25. Takagahara, T.; Takeda, K., Theory of the quantum confinement effect on excitons in quantum dots of indirect-gap materials. *Phys. Rev. B: Condens. Matter* **1992**, 46, (23), 15578-81.

26. Meier, C.; Luettjohann, S.; Offer, M.; Wiggers, H.; Lorke, A., Silicon nanoparticles: excitonic fine structure and oscillator strength. *Adv. Solid State Phys.* **2009**, 48, 79-90.
27. Fan, J.; Chu, P. K., Group IV Nanoparticles: synthesis, Properties, and Biological Applications. *Small* **2010**, 6, (19), 2080-2098.
28. Wolkin, M. V.; Jorne, J.; Fauchet, P. M.; Allan, G.; Delerue, C., Electronic States and Luminescence in Porous Silicon Quantum Dots: The Role of Oxygen. *Physical Review Letters* **1999**, 82, (1), 197-200.
29. Godefroo, S.; Hayne, M.; Jivanescu, M.; Stesmans, A.; Zacharias, M.; Lebedev, O. I.; Van Tendeloo, G.; Moshchalkov, V. V., Classification and control of the origin of photoluminescence from Si nanocrystals. *Nature Nanotechnology* **2008**, 3, (3), 174-178.
30. Zhao, Y.; Li, D.; Sang, W.; Yang, D.; Jiang, M., The influence of microstructure on optical properties of porous silicon. *Solid-State Electronics* **2007**, 51, (5), 678-682.
31. Niquet, Y. M.; Allan, G.; Delerue, C.; Lannoo, M., Quantum confinement in germanium nanocrystals. *Appl. Phys. Lett.* **2000**, 77, (8), 1182-1184.
32. Weissker, H. C.; Furthmuller, J.; Bechstedt, F., Optical properties of Ge and Si nanocrystallites from ab initio calculations. I. Embedded nanocrystallites. *Phys. Rev. B: Condens. Matter Mater. Phys.* **2002**, 65, (15), 155327/1-155327/9.
33. Guter, W.; Schoene, J.; Philipps, S. P.; Steiner, M.; Siefer, G.; Wekkeli, A.; Welser, E.; Oliva, E.; Bett, A. W.; Dimroth, F., Current-matched triple-junction solar cell reaching 41.1% conversion efficiency under concentrated sunlight. *Appl. Phys. Lett.* **2009**, 94, (22), 223504/1-223504/3.
34. Kaufmann, R.; Isella, G.; Sanchez-Amores, A.; Neukom, S.; Neels, A.; Neumann, L.; Brenzikofer, A.; Dommann, A.; Urban, C.; von, K. H., Near infrared image sensor with integrated germanium photodiodes. *J. Appl. Phys.* **2011**, 110, (2), 023107/1-023107/6.
35. Tang, L.; Kocabas, S. E.; Latif, S.; Okyay, A. K.; Ly-Gagnon, D.-S.; Saraswat, K. C.; Miller, D. A. B., Nanometre-scale germanium photodetector enhanced by a near-infrared dipole antenna. *Nat. Photonics* **2008**, 2, (4), 226-229.
36. Beard, M. C.; Knutsen, K. P.; Yu, P.; Luther, J. M.; Song, Q.; Metzger, W. K.; Ellingson, R. J.; Nozik, A. J., Multiple Exciton Generation in Colloidal Silicon Nanocrystals. *Nano Lett.* **2007**, 7, (8), 2506-2512.
37. Erogbogbo, F.; Liu, T.; Ramadurai, N.; Tuccarione, P.; Lai, L.; Swihart, M. T.; Prasad, P. N., Creating Ligand-Free Silicon Germanium Alloy Nanocrystal Inks. *ACS Nano* **2011**, 5, (10), 7950-7959.

38. Lambert, T. N.; Andrews, N. L.; Gerung, H.; Boyle, T. J.; Oliver, J. M.; Wilson, B. S.; Han, S. M., Water-soluble germanium(0) nanocrystals: cell recognition and near-infrared photothermal conversion properties. *Small* **2007**, 3, (4), 691-699.
39. Prabakar, S.; Shiohara, A.; Hanada, S.; Fujioka, K.; Yamamoto, K.; Tilley, R. D., Size Controlled Synthesis of Germanium Nanocrystals by Hydride Reducing Agents and Their Biological Applications. *Chem. Mater.* 22, (2), 482-486.
40. Ma, Y.-H.; Huang, C.-P.; Tsai, J.-S.; Shen, M.-Y.; Li, Y.-K.; Lin, L.-Y., Water-soluble germanium nanoparticles cause necrotic cell death and the damage can be attenuated by blocking the transduction of necrotic signaling pathway. *Toxicol. Lett.* **2011**, 207, (3), 258-269.
41. Taylor, B. R.; Kauzlarich, S. M.; Lee, H. W. H.; Delgado, G. R., Solution Synthesis of Germanium Nanocrystals Demonstrating Quantum Confinement. *Chem. Mater.* **1998**, 10, (1), 22-24.
42. Taylor, B. R.; Kauzlarich, S. M.; Delgado, G. R.; Lee, H. W. H., Solution Synthesis and Characterization of Quantum Confined Ge Nanoparticles. *Chem. Mater.* **1999**, 11, (9), 2493-2500.
43. Ma, X.; Wu, F.; Kauzlarich, S. M., Alkyl-terminated crystalline Ge nanoparticles prepared from NaGe: Synthesis, functionalization and optical properties. *J. Solid State Chem.* **2008**, 181, (7), 1628-1633.
44. Heath, J. R.; Shiang, J. J.; Alivisatos, A. P., Germanium quantum dots: optical properties and synthesis. *J. Chem. Phys.* **1994**, 101, (2), 1607-15.
45. Heath, J. R.; LeGoues, F. K., A liquid solution synthesis of single crystal germanium quantum wires. *Chem. Phys. Lett.* **1993**, 208, (3-4), 263-8.
46. Kornowski, A.; Giersig, M.; Vogel, R.; Chemseddine, A.; Weller, H., Nanometer-sized colloidal germanium particles: wet-chemical synthesis, laser-induced crystallization and particle growth. *Adv. Mater. (Weinheim, Fed. Repub. Ger.)* **1993**, 5, (9), 634-6.
47. Cernetti, P.; Gresback, R.; Campbell, S. A.; Kortshagen, U., Nonthermal plasma synthesis of faceted germanium nanocrystals. *Chem. Vap. Deposition* **2007**, 13, (6-7), 345-350.
48. Wang, W.; Poudel, B.; Huang, J. Y.; Wang, D. Z.; Kunwar, S.; Ren, Z. F., Synthesis of gram-scale germanium nanocrystals by a low-temperature inverse micelle solvothermal route. *Nanotechnology* **2005**, 16, (8), 1126-1129.
49. Wang, W.; Huang, J.; Ren, Z., Synthesis of Germanium Nanocubes by a Low-Temperature Inverse Micelle Solvothermal Technique. *Langmuir* **2005**, 21, (2), 751-754.

50. Prabakar, S.; Shiohara, A.; Hanada, S.; Fujioka, K.; Yamamoto, K.; Tilley, R. D., Size Controlled Synthesis of Germanium Nanocrystals by Hydride Reducing Agents and Their Biological Applications. *Chem. Mater.* **2010**, 22, (2), 482-486.
51. Lu, X.; Ziegler, K. J.; Ghezelbash, A.; Johnston, K. P.; Korgel, B. A., Synthesis of Germanium Nanocrystals in High Temperature Supercritical Fluid Solvents. *Nano Lett.* **2004**, 4, (5), 969-974.
52. Gerung, H.; Boyle, T. J.; Tribby, L. J.; Bunge, S. D.; Brinker, C. J.; Han, S. M., Solution Synthesis of Germanium Nanowires Using a Ge²⁺ Alkoxide Precursor. *J. Am. Chem. Soc.* **2006**, 128, (15), 5244-5250.
53. Gerion, D.; Zaitseva, N.; Saw, C.; Casula, M. F.; Fakra, S.; Van, B. T.; Galli, G., Solution Synthesis of Germanium Nanocrystals: Success and Open Challenges. *Nano Lett.* **2004**, 4, (4), 597-602.
54. Kartopu, G.; Sapelkin, A. V.; Karavanskii, V. A.; Serincan, U.; Turan, R., Structural and optical properties of porous nanocrystalline Ge. *J. Appl. Phys.* **2008**, 103, (11), 113518/1-113518/7.
55. Sato, S.; Ikeda, T.; Hamada, K.; Kimura, K., Size regulation by bandgap-controlled etching: Application to germanium nanoparticles. *Solid State Commun.* **2009**, 149, (21-22), 862-865.
56. Veinot, J., Surface Passivation and Functionalization of Si Nanocrystals. In *Silicon Nanocrystals*, Wiley-VCH Verlag GmbH & Co. KGaA: 2010; pp 155-172.
57. Choi, K.; Buriak, J. M., Hydrogermylation of Alkenes and Alkynes on Hydride-Terminated Ge(100) Surfaces. *Langmuir* **2000**, 16, (20), 7737-7741.
58. Buriak, J. M., Organometallic Chemistry on Silicon and Germanium Surfaces. *Chem. Rev. (Washington, D. C.)* **2002**, 102, (5), 1271-1308.
59. Fok, E.; Shih, M.; Meldrum, A.; Veinot, J. G. C., Preparation of alkyl-surface functionalized germanium quantum dots via thermally initiated hydrogermylation. *Chem. Commun. (Cambridge, U. K.)* **2004**, (4), 386-387.
60. Lee, D. C.; Pietryga, J. M.; Robel, I.; Werder, D. J.; Schaller, R. D.; Klimov, V. I., Colloidal Synthesis of Infrared-Emitting Germanium Nanocrystals. *J. Am. Chem. Soc.* **2009**, 131, (10), 3436-3437.
61. Tanke, R. S.; Kauzlarich, S. M.; Patten, T. E.; Pettigrew, K. A.; Murphy, D. L.; Thompson, M. E.; Lee, H. W. H., Synthesis of Germanium Nanoclusters with Irreversibly Attached Functional Groups: Acetals, Alcohols, Esters, and Polymers. *Chem. Mater.* **2003**, 15, (8), 1682-1689.

62. Heintz, A. S.; Fink, M. J.; Mitchell, B. S., Mechanochemical Synthesis of Blue Luminescent Alkyl/Alkenyl-Passivated Silicon Nanoparticles. *Adv. Mater.* **2007**, 19, (22), 3984-3988.

Chapter 2

2 Mechanochemically Synthesis of Passivated Germanium Nanoparticles

2.1 Mechanochemical Synthesis

2.1.1 Introduction

Germanium nanoparticles have been prepared by a variety of methods including the etching of bulk germanium,¹ nonthermal plasma techniques,² metathesis of a Ge zintl salt,^{3,4} the reduction of halogermanes⁵ and thermal decomposition of organogermanes^{6,7} in super critical fluids.⁸ Most of these approaches requires high temperature, the use of highly reactive or corrosive chemicals, and often requires the modification of unstable hydrogen or halogen terminated surfaces. However, Heintz *et al* first reported synthesis of passivated silicon nanoparticles in large scale by a direct top-down approach using high energy ball-milling.⁹ The alkyl/alkenyl-passivated silicon surface is obtained through milling in a reactive organic liquid like alkenes or alkynes under inert atmosphere. As the surface and reactivity of germanium are very similar to silicon, a mechanochemical approach should be applied to the synthesis of germanium nanoparticles.¹⁰

2.1.2 Structure and reactivity of germanium surfaces

Similar to silicon and carbon (diamond), germanium forms a diamond cubic lattice structure in its most stable crystalline state (Figure 2.1). The crystallographic planes of in the fractured Ge are Ge(100) and Ge(111).¹⁰ The surface dangling bonds of

Ge makes the surface very reactive. In air, these surfaces react with oxygen to form a germanium oxide layer on top of the surface. However, unlike silicon oxide, germanium oxide is not stable and can be dissolved in water causing electronic defects.¹⁰

Under high vacuum conditions, both Ge(100) and Ge(111) surfaces undergo extensive reconstructions to minimize the surface energy. The Ge(100) surface reconstructs to form germanium dimers, thereby reducing the number of dangling bonds per surface Ge atom from two to one. The surface structure of reconstructed Ge(100) is similar to that of Si(100)-2×1; *e.g.*, both exhibit dimer rows with similar geometrical spacing. These dimers are somewhat similar to a double bond, i.e., containing Ge-Ge σ bond and a very weak π bond (even weaker than that of Si dimer). Unlike a true double bond, the dimers are zwitterionic in nature containing the up Ge atom which is nucleophilic and the down Ge atom which is more electrophilic.¹¹

The zwitterionic nature of the (100) surface allows it to undergo (2+2) cycloaddition reaction with alkenes and alkynes.^{10, 12-14} The Ge(111) surface is radical in nature containing one dangling bond per atom and each dangling bond can react with an alkene or an alkyne via radical reaction.¹⁰ However, these surfaces also can react with other functional groups or molecules such as S₈, Cl₂ or H₂.¹⁰

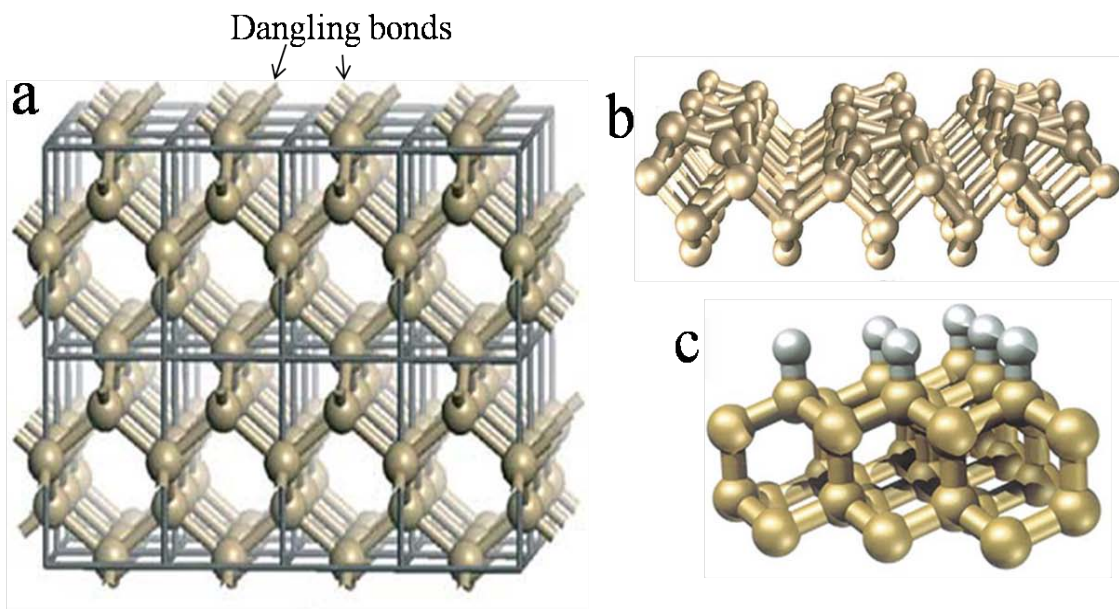


Figure 2.1. (a) Bulk diamond structure of crystalline germanium. Each atom is tetrahedrally bonded to four nearest neighbors. (b) The dimer rows of the Ge (1 0 0)-2 × 1 surface reconstruction. (c) Radical nature of Ge(111) surfaces.

2.1.3 Mechanochemical Synthesis

In order to synthesize alkenyl-passivated germanium nanoparticles, we have followed a direct mechanochemical approach, involving the mechanical fracture of germanium in the presence of reactive organic reagents, using high energy ball-milling (HEBM).⁹ A milling vial is loaded under inert atmosphere with millimeter sized pieces of semiconductor grade germanium and various alkynes such as, trimethylsilylacetylene (TMSA), 1-octyne, and 3-dimethylamino-1-propyne. Stainless steel milling balls are added to the milling vial, which is then sealed and placed in the Spex 8000D mixer/ mill. In this top-down mechanochemical method, we have produced Ge nanoparticles simultaneously and have tailored the surface by organic passivation by alkyl/alkenyl groups covalently linked through strong Ge–C bonds. In ultra high vacuum studies, the direct reaction of

small alkenes/ alkynes on Ge surface have been reported^{10, 12-14} and in the case of mechanical scribing, it has been proposed that such reaction occurs through reactive dimer, Ge=Ge, and surface radical sites.^{15, 16} Here, alkynes react with new reactive sites to passivate Ge-surface through strong Ge-C covalent bond. In **Figure 2.2** a schematic of mechanochemical synthesis illustrates formation of fresh surfaces (Ge dimer and Ge radical surfaces) and a reduced particle size from oxide coated Ge chunk, and the reaction of fresh surfaces with reactive alkynes to form alkenyl-passivated Ge NPs.

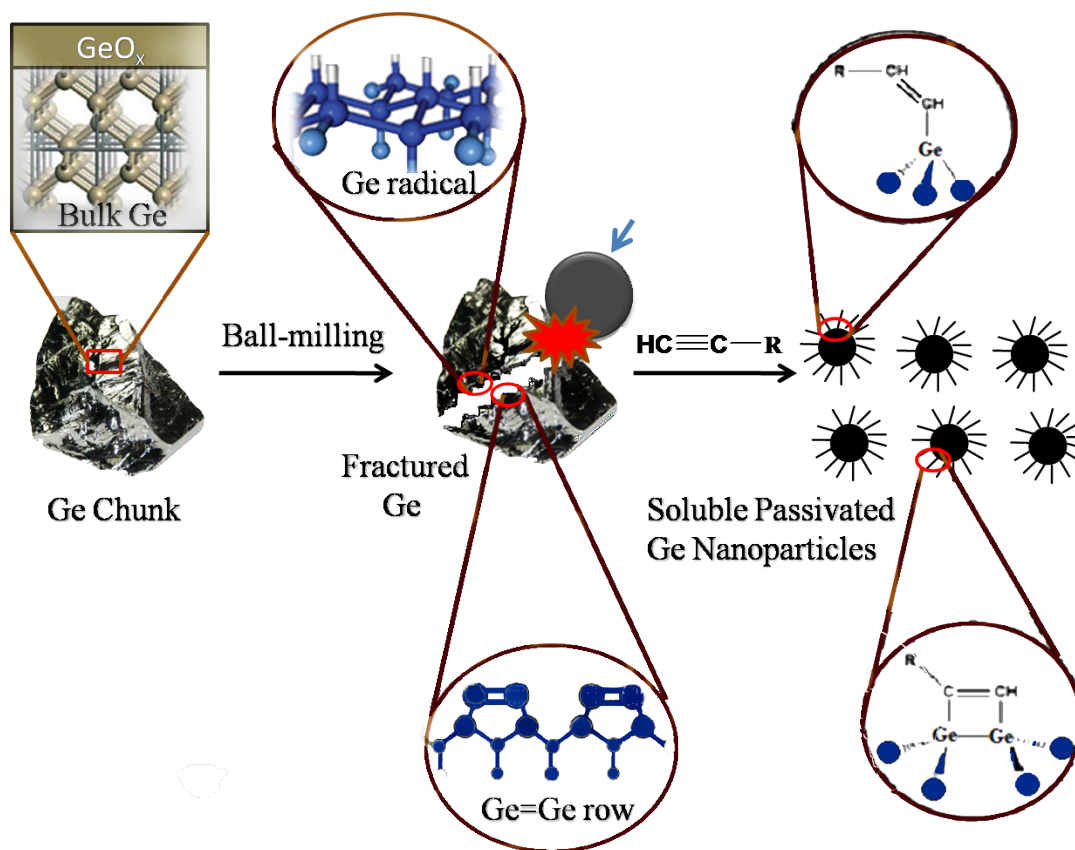
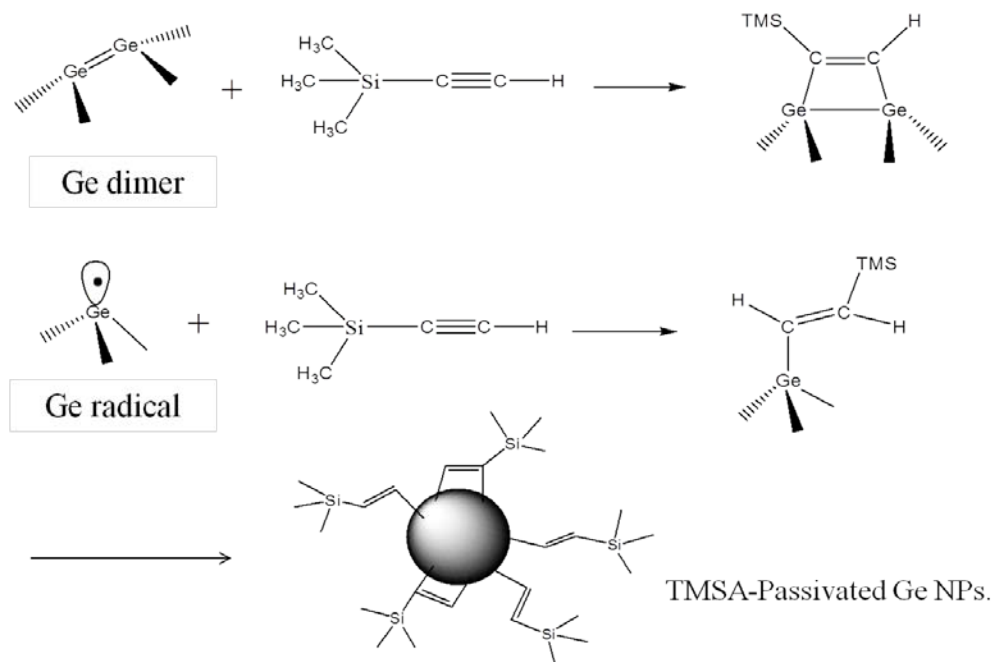


Figure 2.2. Schematic illustration of the mechanochemical synthesis of passivated Ge nanoparticles.

2.2 Results and Discussion: TMSA-Passivated Ge Nanoparticles

The interaction of Ge nanoparticle surfaces with alkynes may be similar to adducts from previous ultra high vacuum studies of Ge surfaces, although differences may exist.¹⁰ Some possible bonding modes with trimethylsilylacetylene (TMSA) are shown by the representation in **Scheme 2.2**.



Scheme 2.2: Possible bonding modes with TMSA and the representation of the TMSA-passivated Ge NPs with different bonding modes (below).

After 24 hours of high energy ball-milling (HEBM), TMSA-passivated Ge nanoparticles (Ge-TMSA NPs) in TMSA were separated from larger insoluble particles by centrifugation. These larger particles were also passivated by TMSA. From XRD data (in Figure 2.5) it was found that the residue after centrifugation was indeed crystalline.

The crystallite size (D) can be estimated using the full width at half-maximum (FWHM, B) of the XRD peak at 2θ from the Scherrer equation:

$$B(2\theta) = \frac{K\lambda}{D \cos \theta} \quad (1).$$

where λ is the X-ray wavelength (0.154 nm for Cu K radiation) and K is the proportionality constant ($K=0.89$).¹⁷ The estimated average crystallite size was ~30 nm.

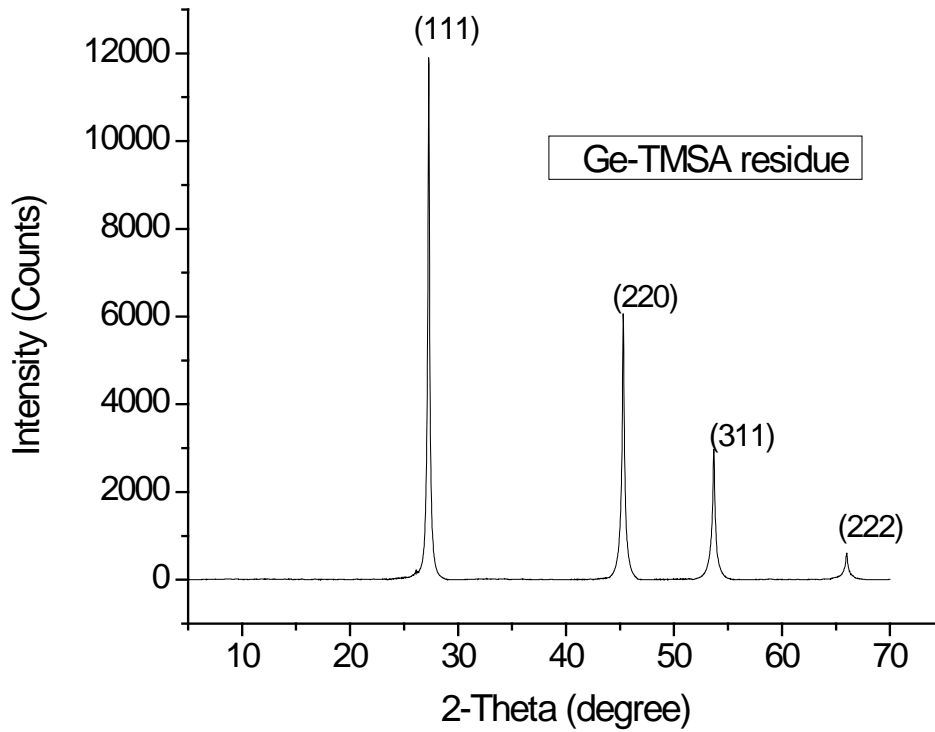


Figure 2.5: XRD of GeTMSA residue after centrifugation

2.2.1 Characterization of crude TMSA-passivated Ge nanoparticles

The crude GeTMSA NPs contain a very small amount of aromatic impurities. The ^1H NMR and ^{13}C NMR spectra (Figure 2.6) of the crude product show sharp aromatic peaks along with broad nanoparticle peaks at 0.8 to 1.5 ppm. In the ^1H NMR spectra, the peaks for these aromatic impurities appear around 7.4-8 ppm, whereas vinylic protons from the nanoparticles appear around 6-7 ppm. As they are near to germanium surface, these vinylic peaks become very broad and weak. Identification and characterization of the aromatic impurities will be discussed in the next section.

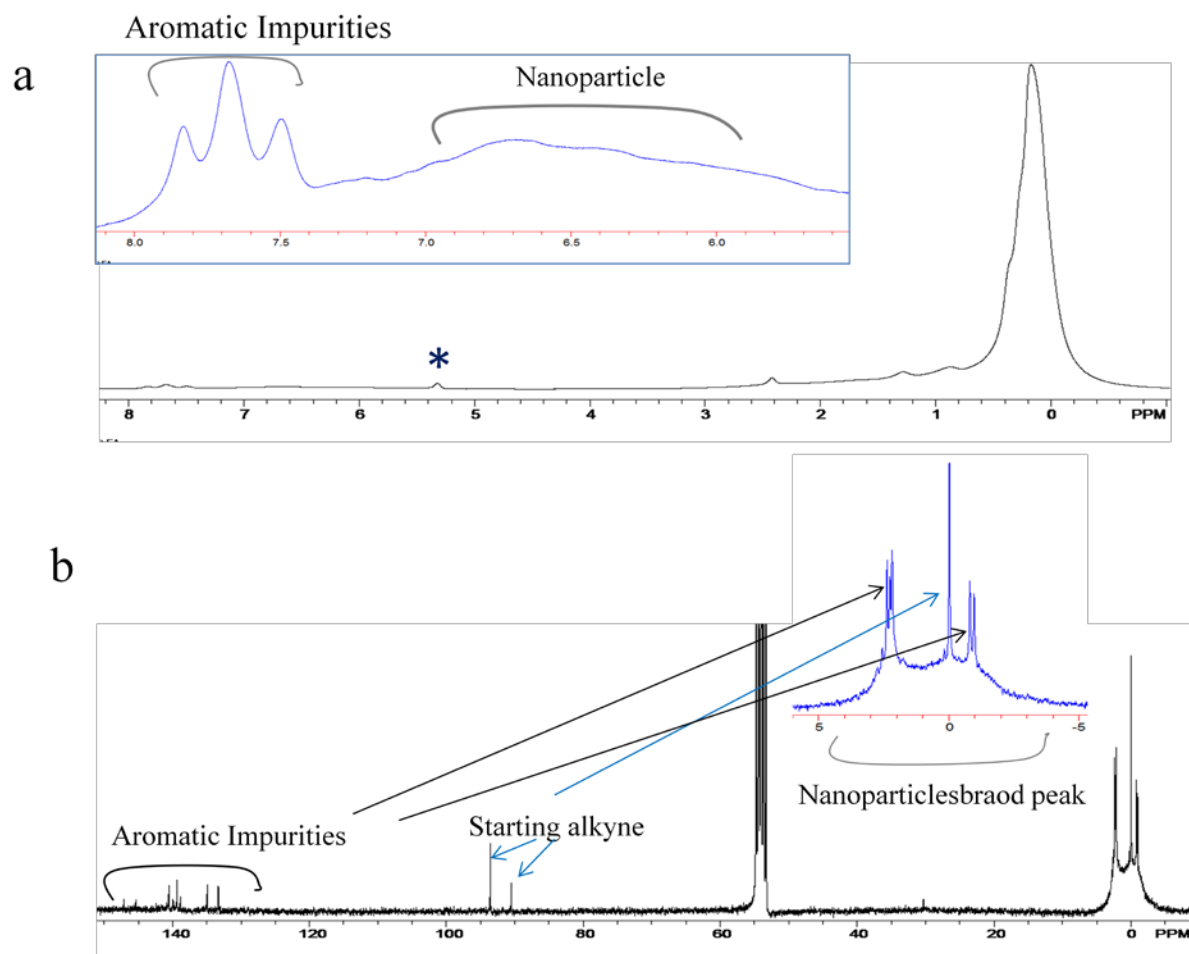


Figure 2.6: ^1H NMR (a) and ^{13}C NMR (b) spectra of the crude nanoparticle product in CD_2Cl_2 after 24 hours ball-milling.

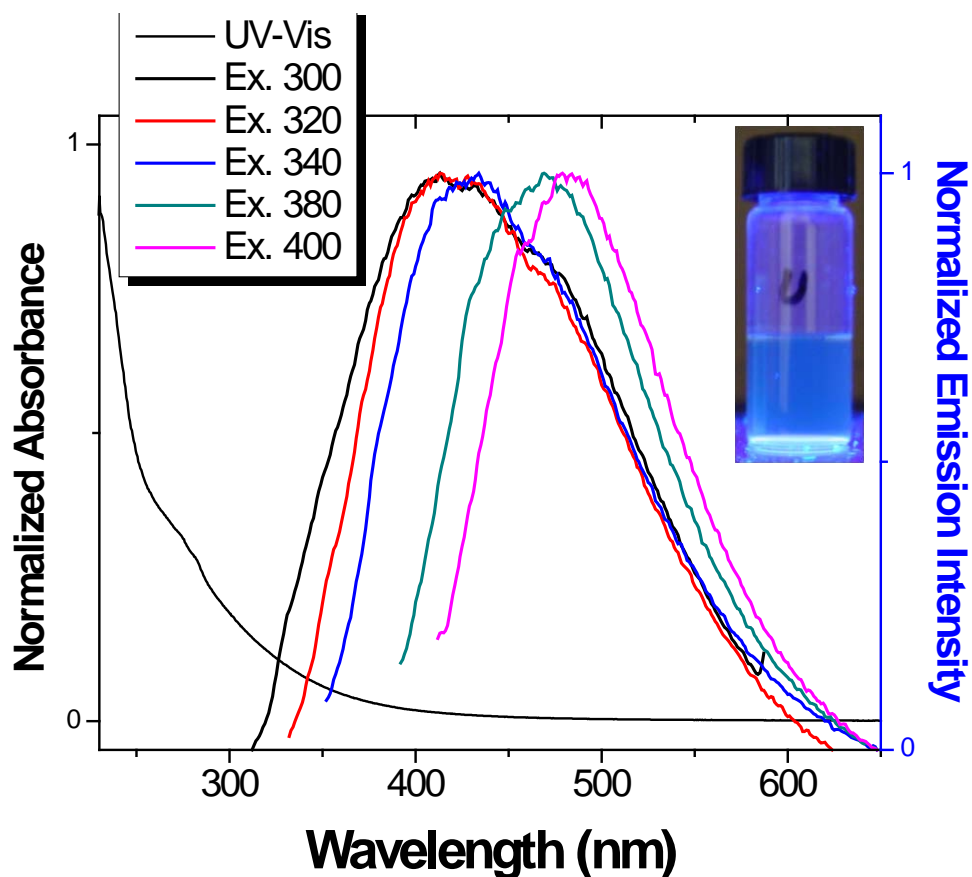


Figure 2.7: UV-vis spectra and PL emission spectra of TMSA passivated Genanoparticle before GPC separation. The inset showing a blue luminescence the Ge NPs under UV light.

The photoluminescence (PL) mechanism of an indirect band-gap material at nanometer regime was discussed in Chapter 1.3. The Ge NPs, synthesized via various solution routes, emit light in the visible range and more often in blue light.^{3, 18, 19} However, some infrared-emitting Ge NPs have been reported.²⁰ TMSA-passivated polydispersed Ge NPs show a blue luminescence under UV radiation.

Figure 2.7 shows UV-Vis spectra and PL emission spectra of TMSA passivated Ge nanoparticles before size separation. The UV-Vis spectrum shows a single absorption with a tail up to 500 nm. The aromatic impurities result in a shoulder around 280 nm. The

broad PL emission spectra obtained under various excitation wavelengths ranging from 300 nm to 420 nm. With increasing excitation wavelength, the PL emission maxima were found to shift to longer wavelength. Although the origin of photoluminescence is a matter of debate,²¹ it can originate either from the decay of quantum confinement excitons or can be attributed to surface defect state.^{22, 23} The broad PL spectra indicate that we have various sizes nanoparticles in the solution and the red –shift in emission wavelengths is consistent with the excitation of population of increasingly larger nanoparticles.

TEM images (Figure 2.8) of the unseparated nanoparticles show various sizes of particles ranging from few nanometers to 25 nanometers, which is consistent of PL results. It was found from the size distribution that most of the nanoparticles are smaller in size and average size was 4-5 nm. The shape of some larger nanoparticles was found to be non-spherical. This is likely due to strain induced in those particles during high energy ball-milling.^{24, 25}

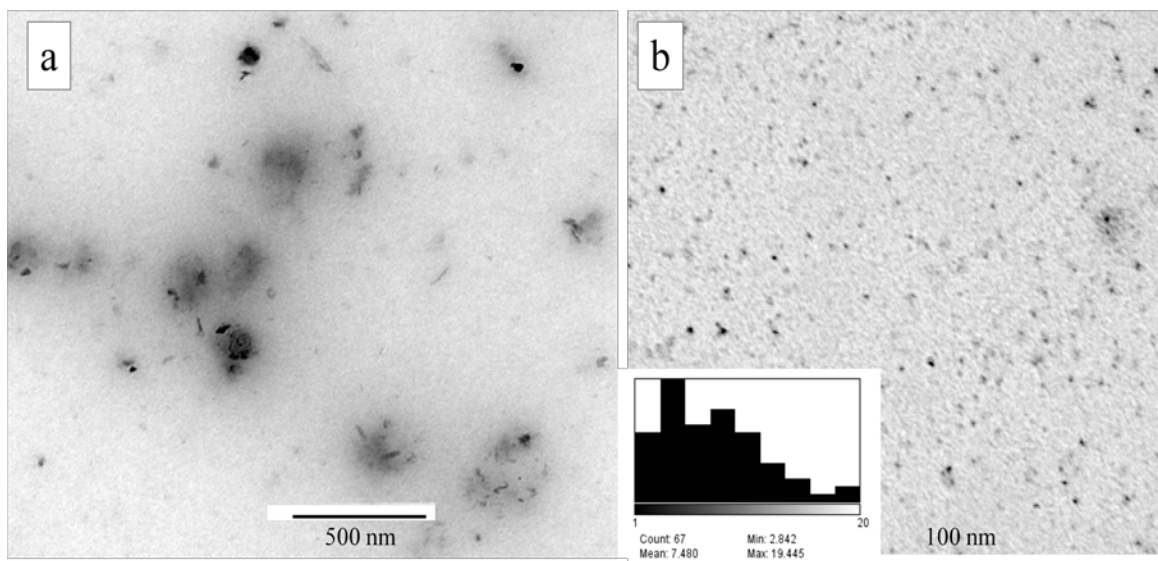


Figure 2.8: TEM images of TMSA passivated Ge NPs. before size separation.

2.2.2 Size Separation by GPC

The TMSA passivated nanoparticles were fractionated by gel permeation chromatography (GPC) using Bio-beads S-X1 beads. With GPC, larger sized nanoparticles, greater than the molecular exclusion limit, pass through the column unhindered, whereas small sized particles will be retained in the column. The small particles permeate the pores of the bio-beads and thus take longer time to pass through the column. Methylene chloride is used as an elution solvent. Fractions are collected in 1.5 ml increment in separate vials for further characterization. Molecular impurities were separated from the nanoparticle solution and appeared in the later fraction (fraction 12 and fraction 13).

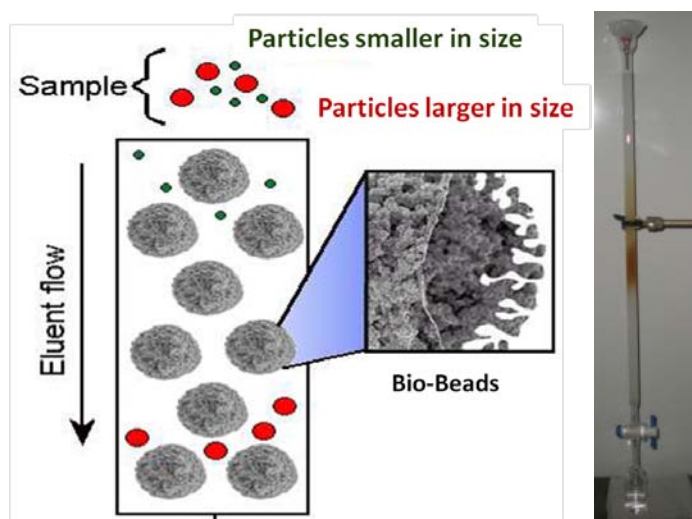


Figure 2.10: a) Schematic representation of Size separation of Ge NPs using Bio-beads; b) GPC column used to fractionate nanoparticles.

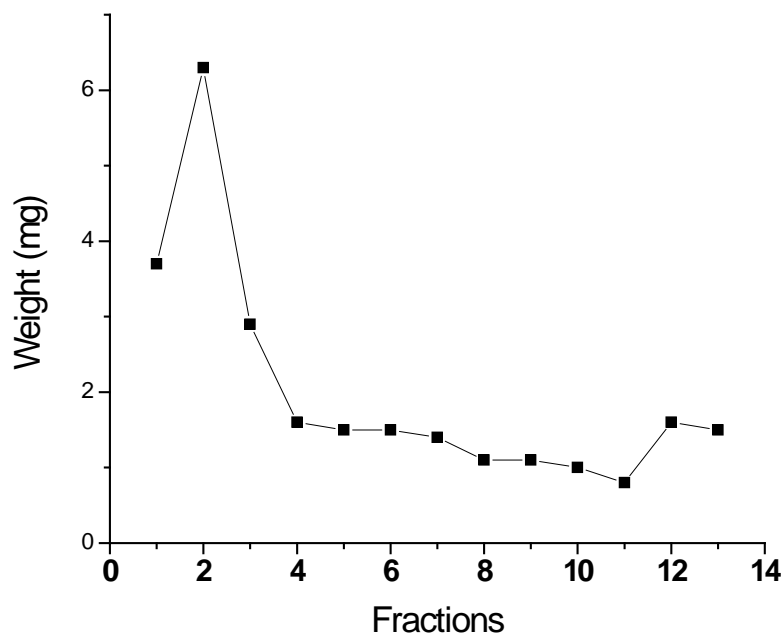


Figure 2.11. Weight distribution of various GPC separated Fractions.



Figure 2.12: GPC separated various fractions. Number 1 represents elution volume (0-1.5)ml of the first fraction taken.

Figure 2.13 shows the ^1H NMR spectra of the TMSA passivated germanium nanoparticles after separation of aromatic impurities. In the ^1H NMR spectra, a broad intense peak around 0-1 ppm indicates TMS-protons and very broad peak around 5-6 ppm indicates vinyl-protons which are very close to the surface. The broadening of peak may be due to several reasons; one of which is the various bonding modes which are possible.

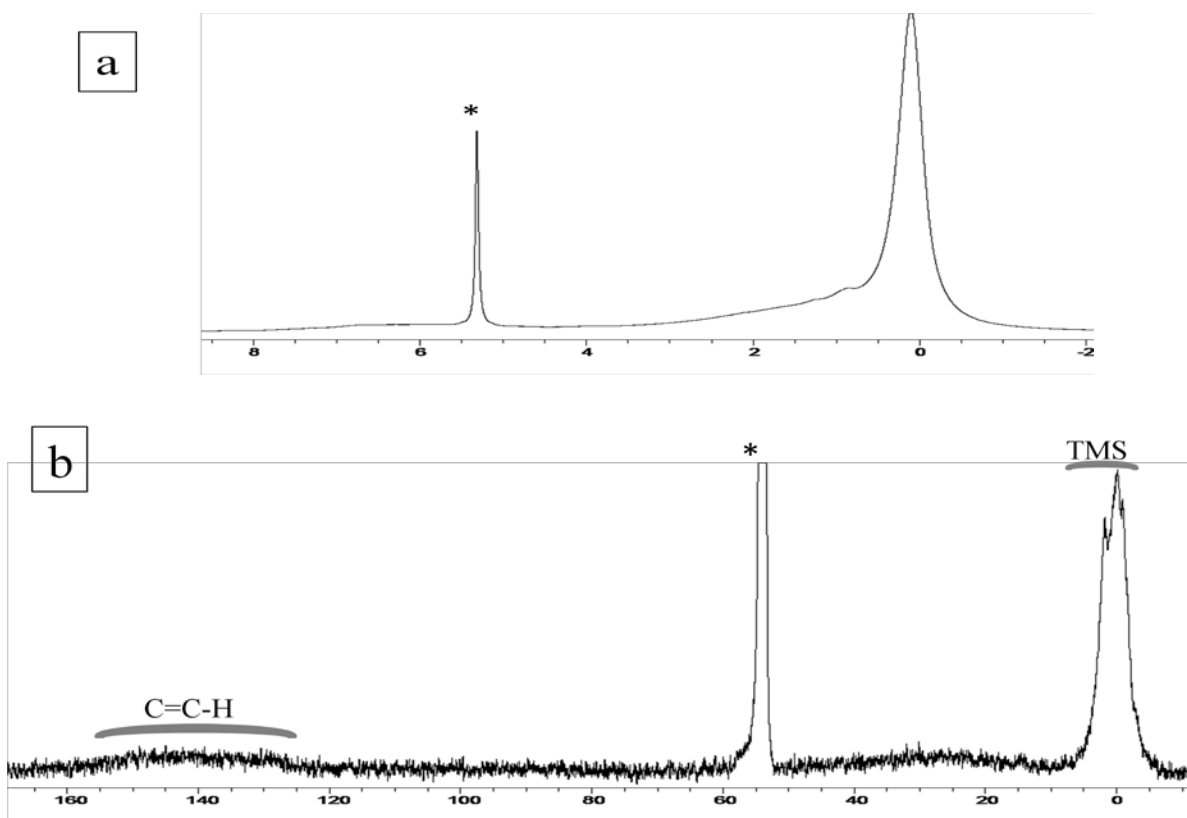


Figure 2.13: ^1H NMR (a) and ^{13}C NMR (b) spectra of the TMSA passivated Ge nanoparticle after separation of impurities.

Figure 2.14 shows a Fourier transform infrared (FT-IR) spectrum of TMSA passivated germanium nanoparticle. The infrared spectrum shows clear evidence of TMSA passivation. The strong band between $2820\text{--}2990\text{ cm}^{-1}$ indicates C-H stretching vibration and the peaks at 1465 and 1376 cm^{-1} indicate C-H bending vibrations. A weak broad peak around 1580 cm^{-1} is due to C=C stretching. Previously reported $\nu(\text{C}=\text{C})$ stretching for 1-dodecyl and 1-pentenyl passivated Ge surface was 1594 cm^{-1} .²⁶ Prominent Si-C stretching peaks at 1250 cm^{-1} and 840 cm^{-1} indicate TMSA passivated to germanium nanoparticle surface. The Ge-C stretch is typically seen at 830 cm^{-1} .^{22, 23} However, Klimov *et al* reported Ge-C stretch peak $\sim 700\text{ cm}^{-1}$ from their IR-emitting Ge

NCS.²⁰ A sharp peak $\sim 750\text{ cm}^{-1}$ is consistent with Ge-C stretching. The Ge-O stretch is typically seen at $870\text{-}910\text{ cm}^{-1}$. It should be broad and intense as FT-IR is more sensitive to Ge-O stretches than Ge-C stretching. A broad band at $1100\text{-}930\text{ cm}^{-1}$ has been seen in the FT-IR spectra, which is in the Si-O region. However, Ge-O stretching can also be seen (as Ge-O-C or other mode) in this region.²⁰

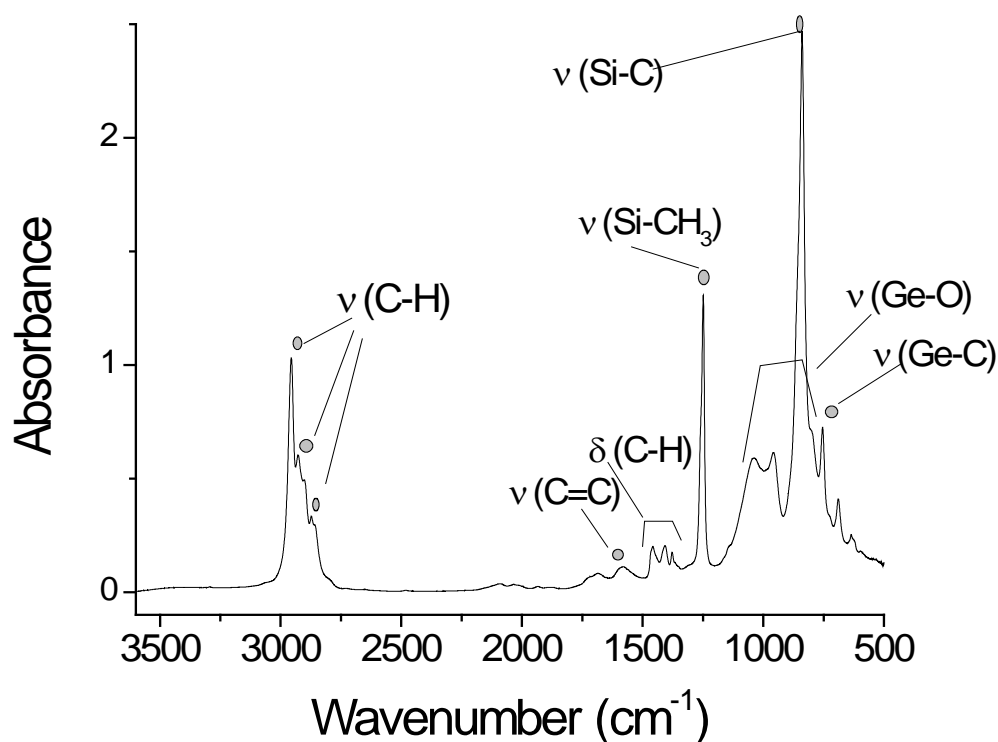


Figure 2.14: FT-IR spectra of TMSA passivatedGe nanoparticle.

2.2.3 Confirmation of alkenyl-passivation of Ge surfaces by comparing deuterated-alkenyl-passivated surfaces.

TMSA-*d*₁ passivated Ge NPs were synthesized by high energy ball-milling (HEBM) of Ge pieces and trimethylsilyl acetylene-*d*₁. ¹H NMR spectrum of crude TMSA-*d*₁-passivated Ge NPs (**Figure 2.15**) shows TMS resonances from both aromatic

impurities (0.3- 0.4 ppm) and nanoparticles (0- 0.4 ppm). The broad peaks which were seen in the ^1H NMR of Ge-TMSA NPs for the vinylic protons, are absent in the ^1H NMR of Ge-TMSA- d_1 NPs and that confirms alkenyl group formation from a reaction of an alkyne on Ge surface. The ^1H NMR spectrum of the crude Ge-TMSA- d_1 NPs does not show peaks from impurities in the aromatic regions.

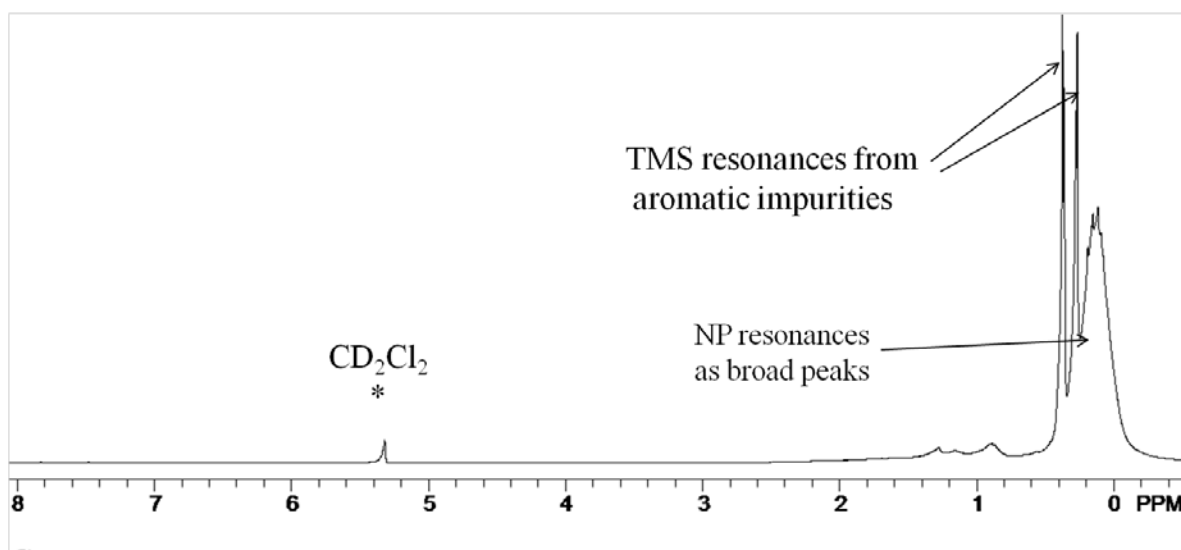


Figure 2.15: ^1H NMR spectra of Ge-TMSA- d_1 NPs in CD_2Cl_2 .

The FT-IR spectrum (**Figure 2.16**) of purified TMSA- d_1 -passivated Ge NPs shows a peak at 2120 cm^{-1} which is more prominent than that of the fully protio-Ge-TMSA NPs. This peak may be due to $\nu(\text{=C-D})$ from the alkenyl surface. A $\nu(\text{=C-H})$ from the alkenyl surface would be so weak and not be seen in the FT-IR spectra of Ge-TMSA NPs.

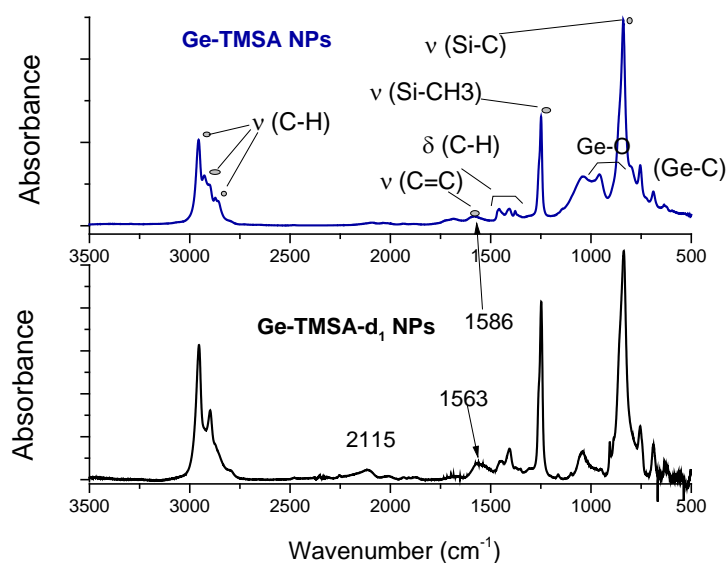


Figure 2.16: FT-IR spectra of Ge-TMSA, Ge-TMSA- d_1 nanoparticles.

2.2.4 Optical Properties of TMSA-Passivated Ge NPs

Optical properties of Ge nanocrystals have been studied both theoretically^{27, 28} and experimentally.^{4-7, 19, 20, 22, 27, 29-40} There are several reports which claim that photoluminescence from Ge NPs results from size dependent properties.^{2-4, 8} Wilcoxon et al. observed a size dependent PL emission. They claimed that Ge NPs with 2 nm in size show PL emission peak at 500 nm; whereas a 4 nm Ge NP emits at 650 nm.³⁷ Shoak et al reported Ge NPs with 5 nm in size emits light at 352 nm (in blue region).³¹ Takeoka et al observed a size dependent PL from their Ge nanocrystals, embedded in SiO₂ matrices, with average size range from 0.9 nm to 5.3 nm in the near infrared region.⁴⁰

The optical properties of various fractions of GPC separated nanoparticles have been studied by UV-vis absorption spectroscopy and photoluminescence (PL) in order to further assess their size separation. A representative absorption coefficient vs. energy plot of various fractions shows spectra of later fractions move to higher in energy (**Figure**

2.17a). Optical band-gaps of various fractions were calculated from the x-intercept of the linear fit of square root of absorption coefficient vs. energy plot (**Figure 2.18**) and optical band-gaps were found to be from 2.49 eV (for fraction 2) to 2.78 eV (for fraction 10). PL emission spectra of various fractions at excitation wavelengths 280 nm, 320 nm and 380 nm are shown in the **Figure 2.17b, 2.17c** and **2.17d** respectively. For excitation wavelength 280 nm, the emission maxima moved from 391 nm (for fraction 10) to 479 nm (for fraction 2) with increasing size. The PL spectra at longer excitation wavelength (*e.g.* 400 nm) shows relatively narrow peak separation for various fractions (**Figure 2.17d**) and that is due to only larger size particles emitting at that excitation wavelength. The broader spectra and bimodal distribution may either due to presence of a separate emission from the surface defect which is more likely to be seen in larger particles or due to inefficiency of GPC separation at high molecular weight region (as the molecular exclusion limit of Bio-beads SX1 is 14,000 Da).

Most of the reported emission quantum yield (QY) of Ge NPs are in the range of ~1-2%. The maximum QY reported from Ge NPs is 8%.^{20, 41} For Ge-TMSA NPs, QY of GPC separated fractions were found to range from 0.51% (for fraction 2) to 2.5% (for fraction 10), which increases with decreasing size (**Figure 2.19**). Very low QY for earlier fractions is due to increase of larger particles which usually do not contribute to the PL, and thus leads to the decrease of quantum efficiency.

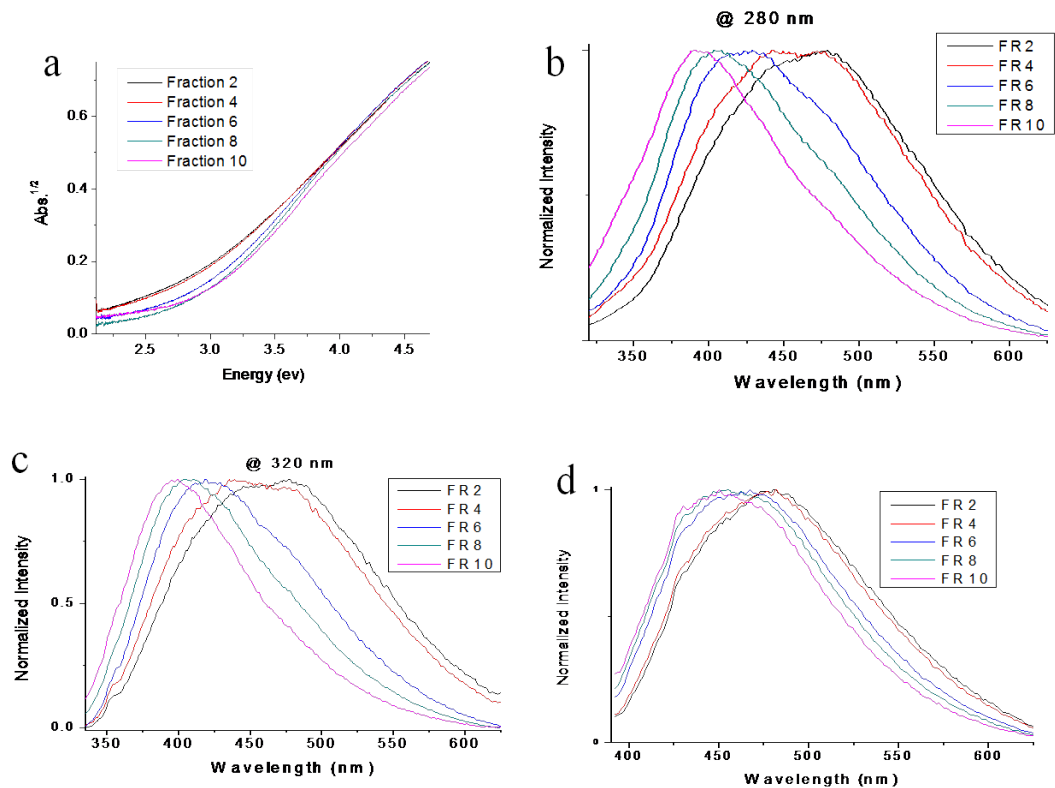


Figure 2.17: UV-vis spectra of various size separated fractions (a); PL emission spectra of that at excitation wavelength 280 nm (b), 320 nm (c), and 380nm (d).

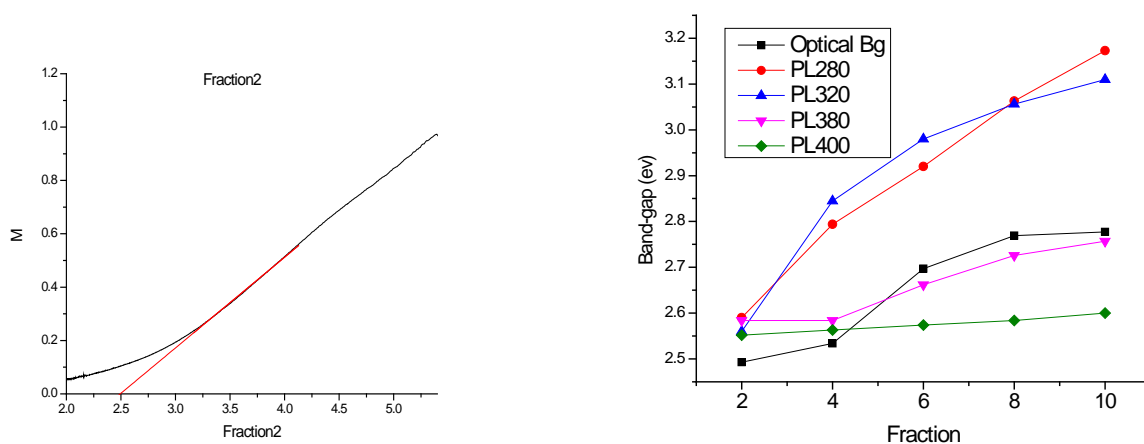


Figure 2.18. Optical band gap calculation (left) and optical band gap and PL emission max.vs. various fraction plot (right).

Figure 2.20 shows the TEM images of an intermediate fraction (i.e. fraction 6). From the histogram (**Figure 2. 20b**), the average size of fraction 6 was found to be 3.8 (± 0.7) nm. The lattice fringes observed in the high resolution TEM (HRTEM) images (**Figure 2.20c**) shows that the nanoparticles are indeed single-crystal. Energy dispersive X-ray spectroscopy (EDS) spectrum (**Figure 2.21**) obtained on the nanoparticles exhibits three pronounced peak at 1.2 keV (for GeL α), 9.9 keV (for GeK α), 11keV (for GeK β) due to germanium and a pronounced peak at 1.8 keV (for SiK α) due to silicon from the surface ligand of the germanium nanoparticles. The copper peaks appear in the EDS spectrum, which came from the Cu-grid.

Size separation of the nanoparticles was further confirmed by the size distributions obtained by small angle X-ray scattering transmission (SAXS). We did not see any characteristic feature or peak in the scattering intensity vs. scattering vector (q) plot (supporting information). From the scattering intensity vs scattering vector (q) plot, size distribution of various fractions was calculated using maximum entropy (MaxEnt) method considering particles are spherical. In **Figure 2.23**, size distribution of various fractions indicates average particle size decreases, as it moves from earlier to later fraction. Mean particle size was found to range from 3.68 nm (for fraction 2) to 2.74 nm (for fraction 8). We did not get good data for fraction 10, because we could not deposit enough solid sample on the Kapton tape. Mean particle diameter of fraction was found 3.14 nm from SAXS size distribution, whereas the same was 3.8 (± 0.7) nm from TEM histogram. Though, size distribution from SAXS differs from that of TEM, SAXS is an established technique for studying pore morphologies and nanoparticles. It is difficult to see the smaller particles by TEM and aggregation could lead a wrong size distribution.

Moreover, as the sampling size of SAXS is much larger than that of TEM, size distribution is statistically more reliable for SAXS than the latter.

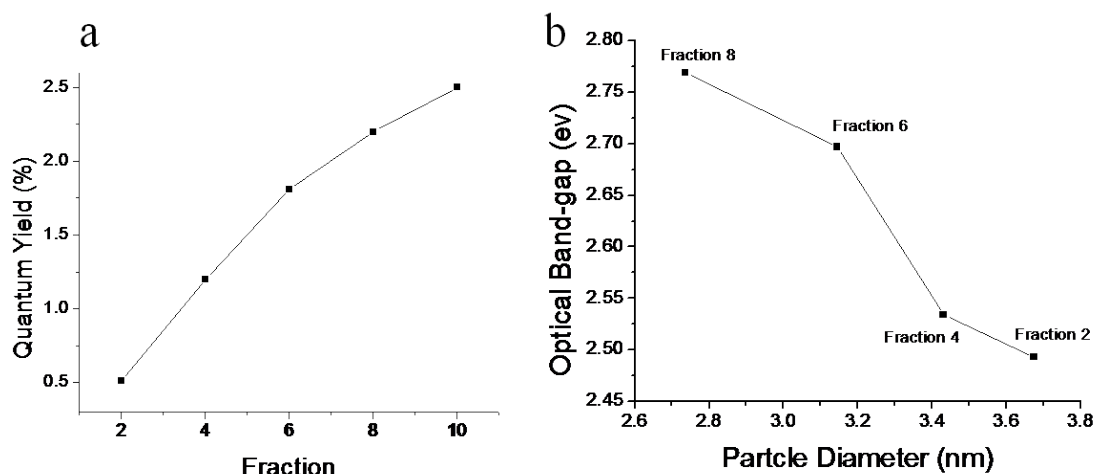


Figure 2.19: Quantum Yield (%) vs. various fraction plot (a); Optical band-gap vs. particle diameter obtained from SAXS size distribution plot (b).

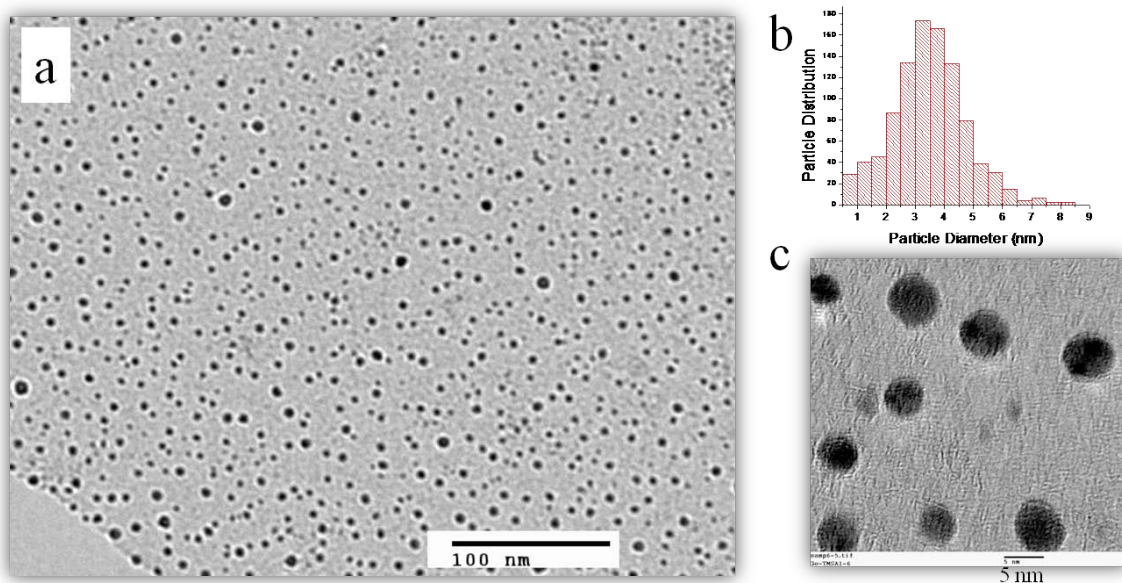


Figure 2.20. TEM microgram of Fraction 6 of TMSA passivated Ge nanoparticle

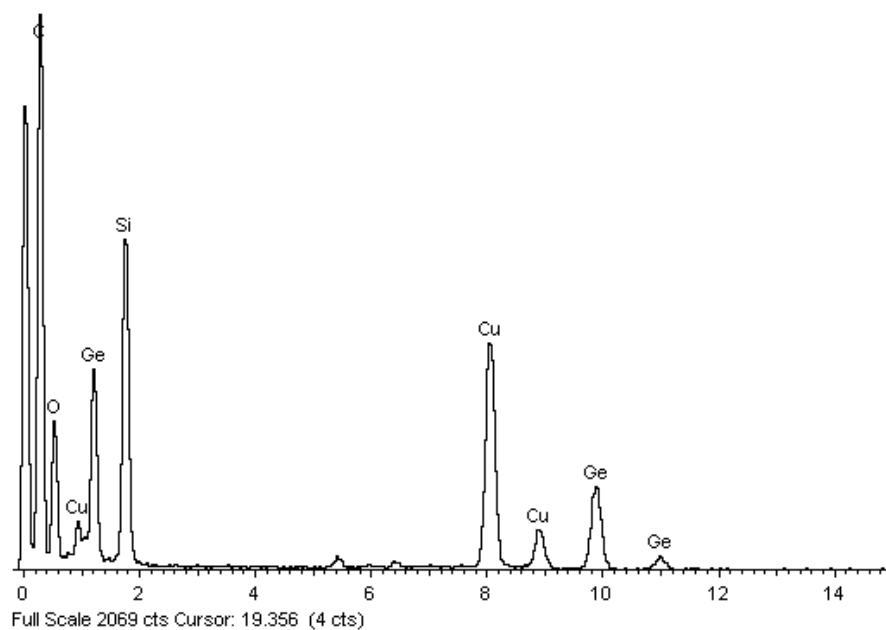


Figure 2.21: Energy-dispersive X-ray spectra (EDX) of TMSA-passivated Ge NPs.

Table 1: Optical data for various GPC separated fraction

Fraction	Mean Diameter from SAXS(A)	Optical Bandgap (ev)	PL Bandgap @excitation λ 320 nm (ev)	PL Bandgap @excitation λ 380 nm (ev)	Quantum Yield (%)
2	36.75 (± 0.003)	2.493(± 0.0028)	2.56(± 0.005)	2.584(± 0.005)	0.51 (± 0.19)
4	34.31 (± 0.003)	2.534(± 0.0029)	2.845(± 0.006)	2.584(± 0.006)	1.2 (± 0.15)
6	31.44 (± 0.003)	2.697(± 0.0028)	2.98 (± 0.006)	2.662(± 0.005)	1.8 (± 0.23)
8	27.36 (± 0.003)	2.769(± 0.0032)	3.056(± 0.006)	2.726(± 0.006)	2.2 (± 0.03)
10	-----	2.777(± 0.0041)	3.11 (± 0.006)	2.757(± 0.006)	2.5 (± 0.15)

Figure 2.19b and **Table 1** show that the relationship between optical band gap and particle size. The blue PL (above 2.5 eV) of various sizes of Ge NPs can be compared to previously reported blue PL from Ge NPs synthesized by various methods. The origin of blue PL can be explained from the theoretical calculation of electronic structure of Ge NPs using sp^3 tight-binding description. The origin of blue PL of Ge NPs comes from the defects in the oxide or other surface defects. However, size dependent blue PL was observed from TMSA-passivated Ge NPs; which can be explained by the schematic diagram in **Figure 2.22**. A surface defect state is fixed in energy and it remains higher in energy compared to the lowest level of conduction band (specially for larger NPs). The observed size dependence of the blue PL of TMSA-passivated Ge NPs is due to the recombination of an electron from the defect state with a hole from the valence band whose energy is size dependent.

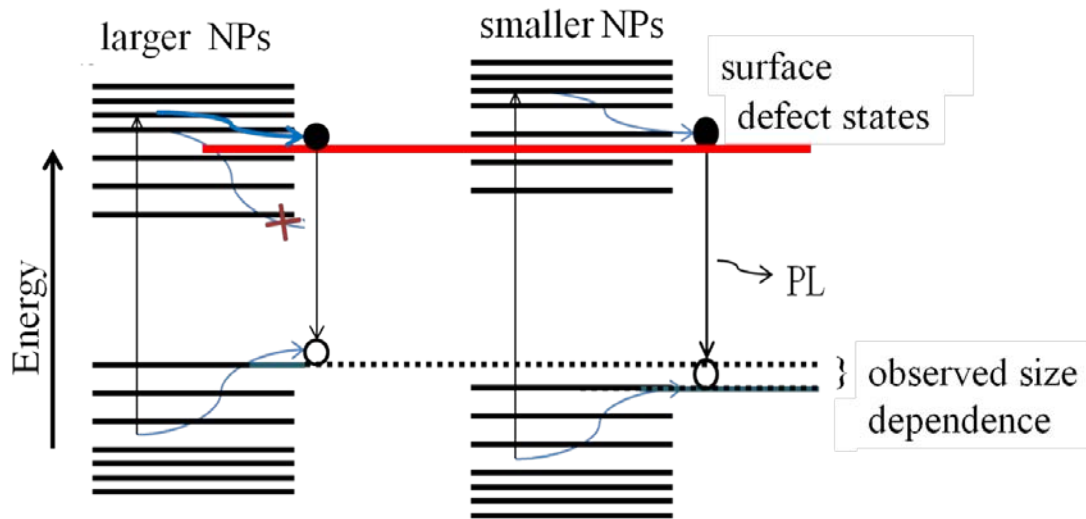


Figure 2.22: Schematic diagram of energy levels of larger and smaller NPs with fixed energy surface defect state. The observed size dependent PL is due to change in energy of valence bands.

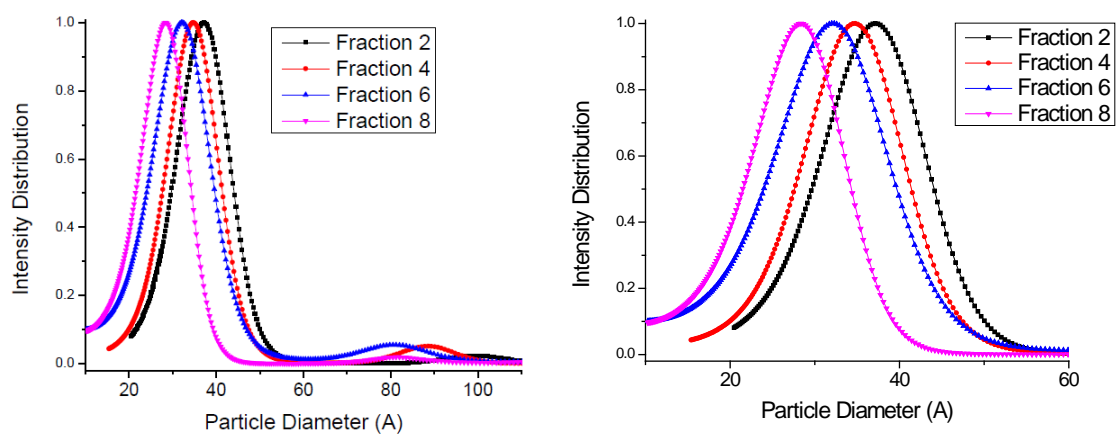


Figure 2.23: Size distribution of various GPC separated fractions, calculated from scattering plot.

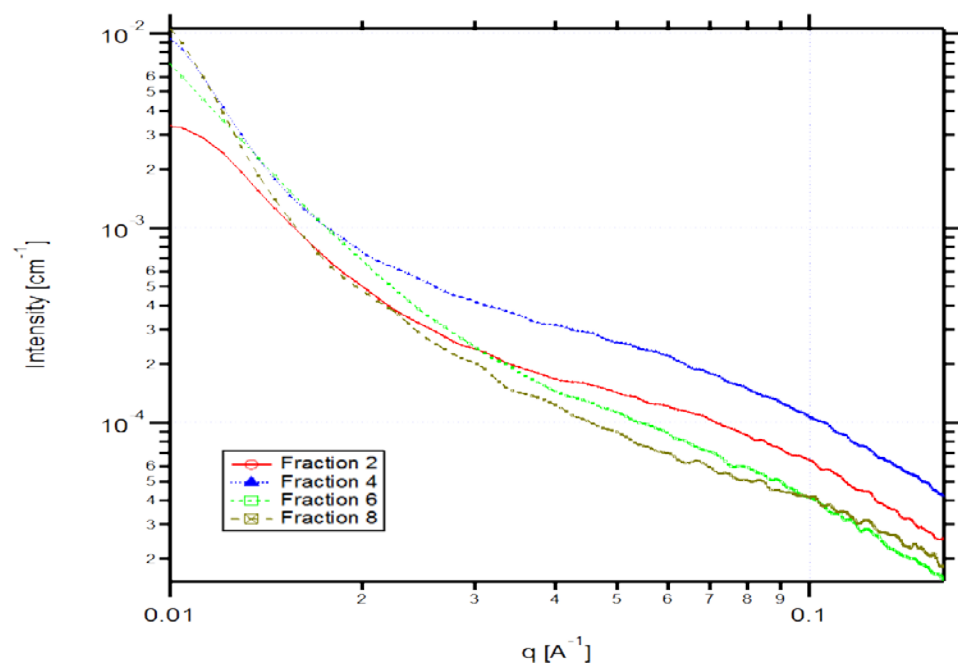


Figure 2.24. Scattering intensity vs. scattering vector (q) plot for various size separated fractions.

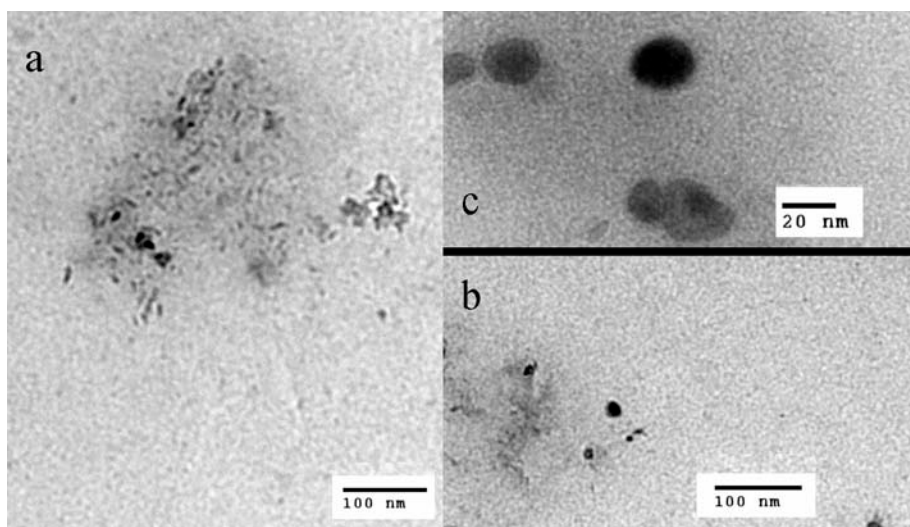


Figure 2.25. TEM microgram of Fraction1 of TMSA passivated Ge nanoparticles.

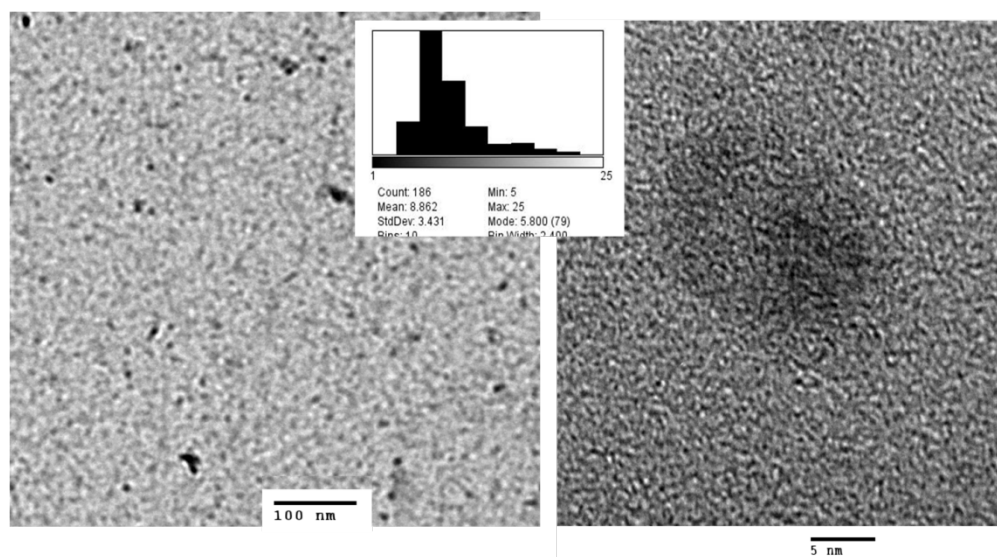


Figure 2.26. TEM microgram of Fraction3 of TMSA passivated Ge nanoparticles.

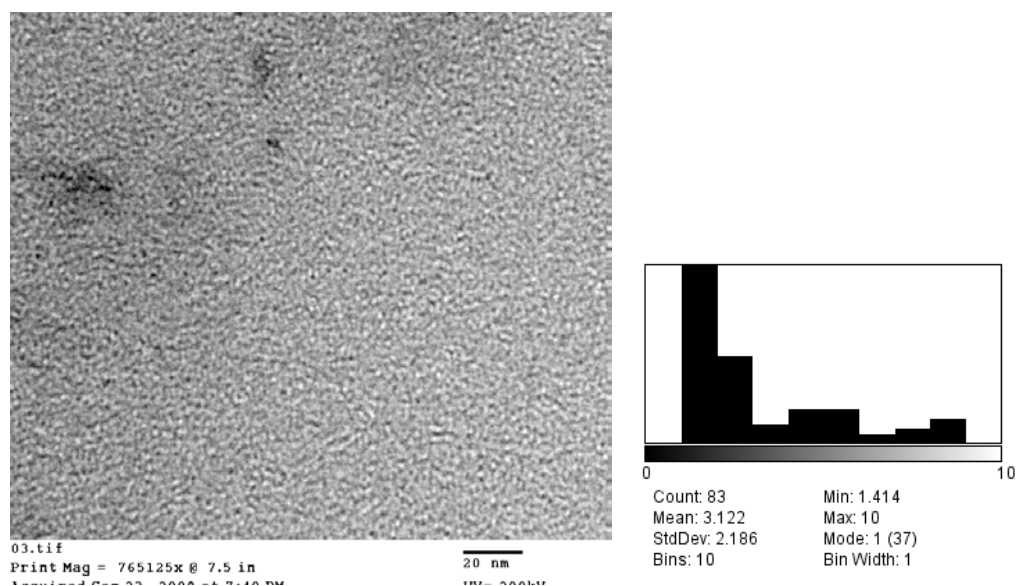


Figure 2.27: TEM of Fraction 9 of GPC separated Ge-TMSA NPs.

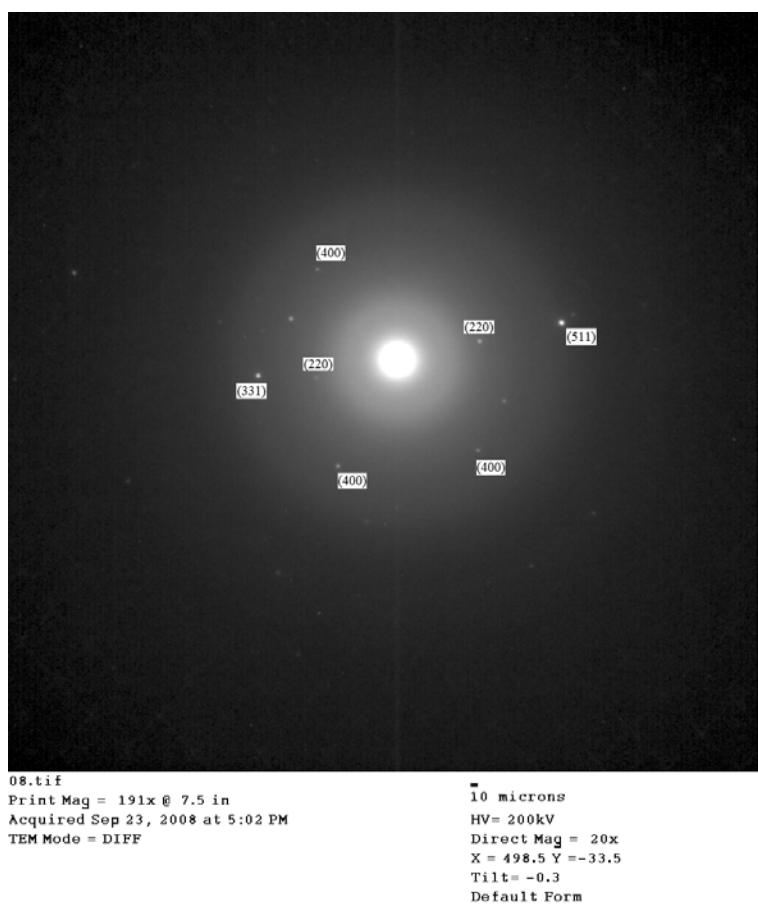
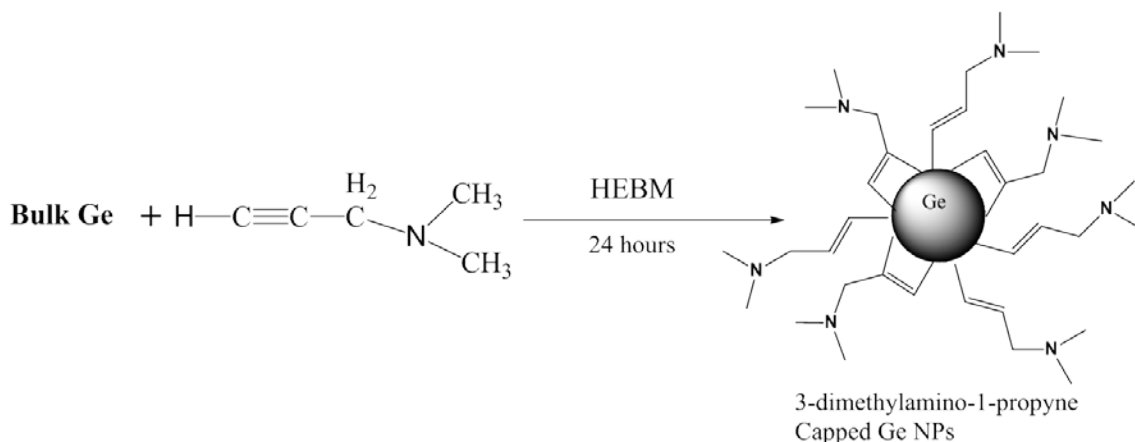


Figure 2.28. Selected Area Electron Diffraction (SAED) pattern of the TMSA-passivated Ge NPs.

2.3 Amine-terminated Germanium Nanoparticles

Water soluble NH_2 -terminated Ge NPs were previously synthesized by catalytic hydrogermylation of H-terminated surface using allylamine or other alkene amine.^{39, 42, 43} As primary amine might react with fresh germanium surfaces during ball-milling, dimethyl amino-1-propyne was used to produce Ge NPs by mechanochemical synthesis. Here, the alkyne of aminopropyne reacts during reactive ball-milling with Ge surfaces forming strong Ge-C bond while leaving dimethylamino on the periphery.



Scheme2.2: A representation of germanium nanoparticle passivated by 3-dimethylamino-1-propyne in different bonding modes.

2.3.1 Characterization

Blue luminescent dimethylamine terminated Ge NPs were synthesized by reactive ball-milling with germanium chips and 24 ml 3-dimethylamino-1-propyne. Crude products contain a large amount of molecular impurities which can be removed by dialysis. As we have found normal dialysis is a very slow process to remove all molecular impurities, we have initiated a semi-continuous-flow dialysis set up using Soxhlet dialysis

(SD), (i.e. dialysis in a Soxhlet apparatus), to separate side products from the nanoparticle solution.⁴⁴ The dialysis membrane that was used is a Spectra/Por[®] regenerated cellulose membrane (MWCO =1000 Da), which is stable in most organic solvents including methanol. The MWCO of the membrane was chosen in such a way that only small molecular side products can pass the membrane but the nanoparticles.

Dimethylaminopropenyl capped Ge (Ge-DMAP) NPs purified by Soxhlet dialysis can be redispersed in methanol, ethanol or aqueous alcohol. **Figure 2.29** shows UV-vis absorption spectra of Ge NPs and molecular impurities separated by Soxhlet dialysis. A peak at 300 nm in the impurities' absorption spectra is due to aromatic impurities. On the other hand, absorption spectra of Ge NPs show a shoulder at 315 nm; which was not seen in TMSA-passivated Ge NPs. However, previously reported Ge NPs shows some peak or shoulder at ~350 nm.

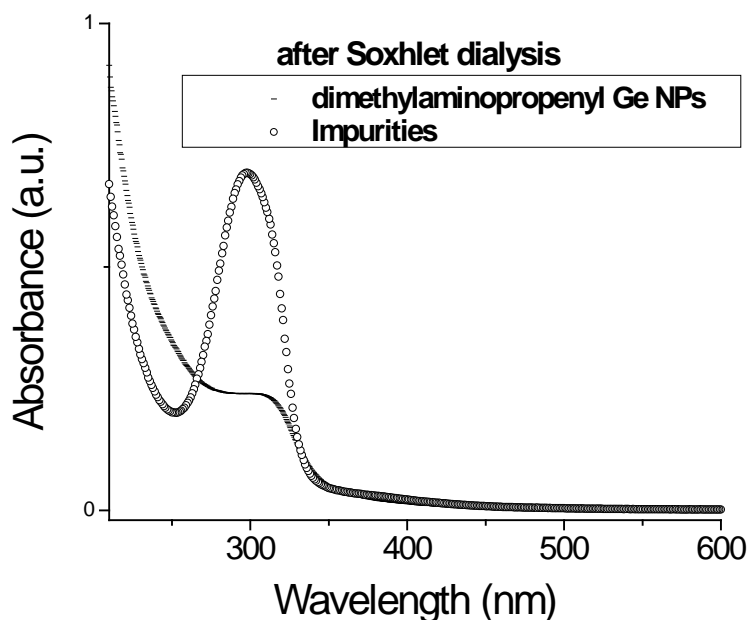


Figure 2.29: UV-Vis absorption spectra of Ge nanoparticles and Impurities separated by Soxhlet-Dialysis.

Broad PL emission spectra ranging from 350 nm to 650 nm were obtained under various excitation wavelengths (**Figure 2.30**). The PL maxima were observed a shift to longer wavelength upon increasing excitation wavelength. A bimodal distribution consisting two peaks at 447nm and 483 nm were observed for excitation wavelength 300 nm and 320. The emission peaks move to higher wavelength from 455 nm, 465 nm, 481 nm to 506 nm for excitation wavelengths 360, 380, 400 and 440 nm. The PL of Ge-DMAP NPs is a bit red shifted (~50 nm) compared to Ge-TMSA NPs. However, Zuilhof *et als.* observed a red shifted PL from their water soluble amine-terminated Si NPs compared to alkyl-terminated Si NPs.⁴⁵

In the FTIR spectra (**Figure 2.31**), the peaks in the range of 2750-2950 cm^{-1} are due to C-H stretching vibrations. A peak at 2770 cm^{-1} occurs in the C-H stretching region due to C-H connected to N which has a lone pair. A tiny peak was seen at ~ 2050 cm^{-1} due to $\nu(\text{Ge-H})$ and a broad peak at ~3400 cm^{-1} is due to O-H stretching. This O-H stretching, might have formed from absorbed water in the sample or Ge-OH from the surface. An intense and broad peak was seen at Ge-O region from 750-950 cm^{-1} is due to $\nu(\text{Ge-O})$ and this Ge-O is mostly from Ge-OH. A distinct Ge-C stretching vibration was not seen at ~750 cm^{-1} due to the overlap of Ge-O. Stretching of C=C vibration usually appeared ~1600 cm^{-1} . Broadening of peak in this region might due to $\delta(\text{O-H})$. A C-H bending was seen at 1460-1375 cm^{-1} . A sharp peak at 1220 cm^{-1} was observed due to $\nu(\text{C-N})$.

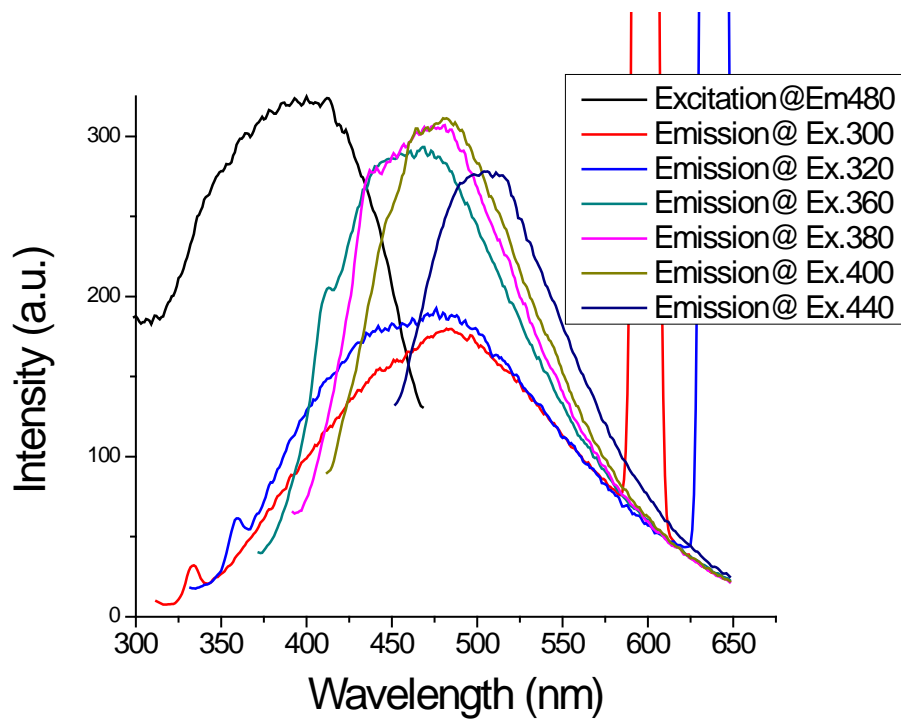


Figure 2.30: PL emission and excitation spectra of Ge-DMAP nanoparticles separated by Soxhlet-Dialysis.

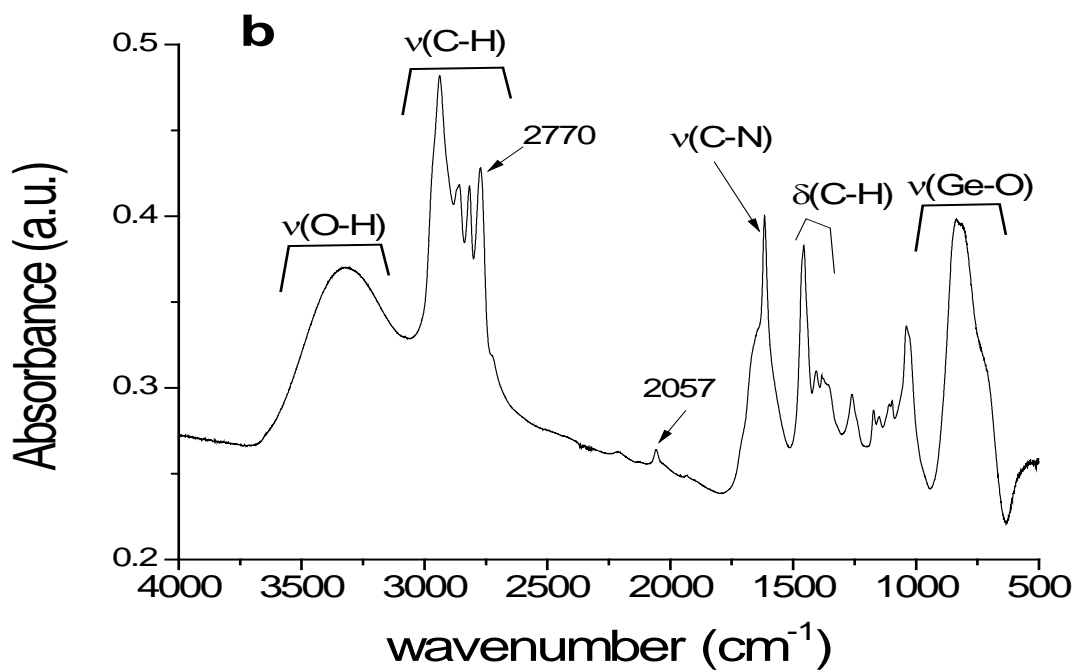


Figure 2.31: FT-IR spectrum of dimethylamino propenyl Ge NPs

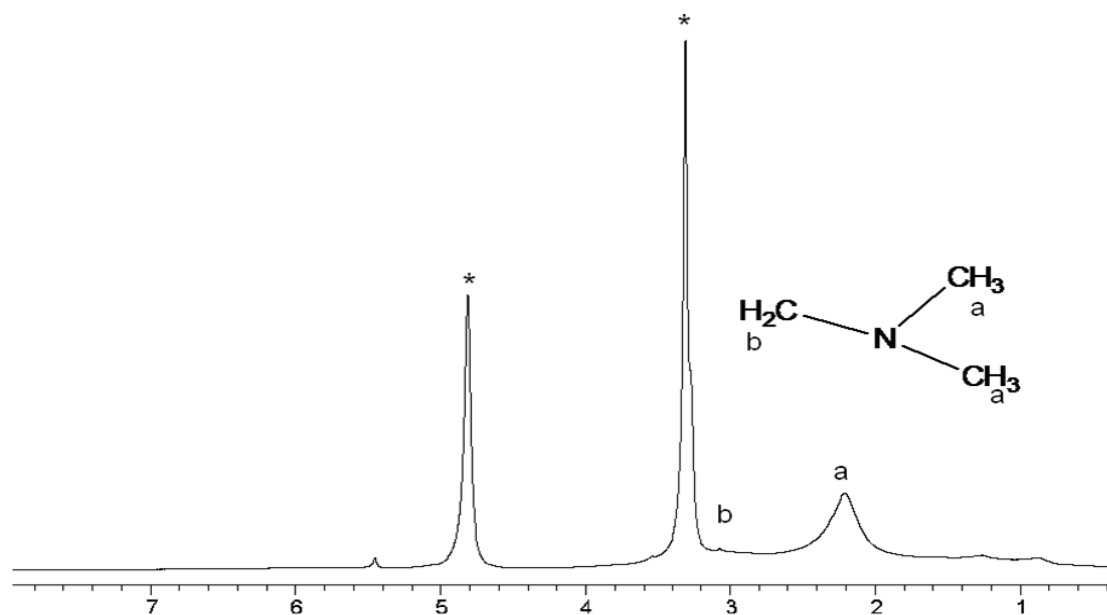


Figure 2.32 a: ^1H NMR spectra of Ge nanoparticles separated by Soxhlet-Dialysis in CD_3OD .

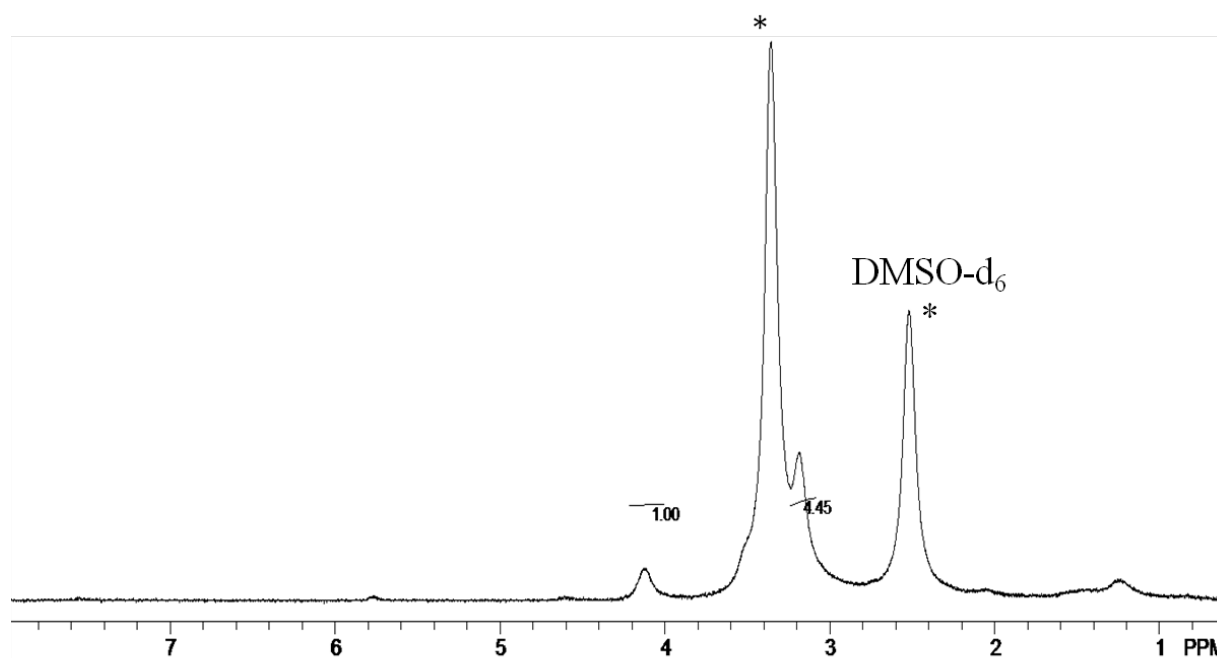


Figure 2.32 b: ^1H NMR spectra of Ge nanoparticles separated by Soxhlet-Dialysis in $\text{DMSO}-d_6$.

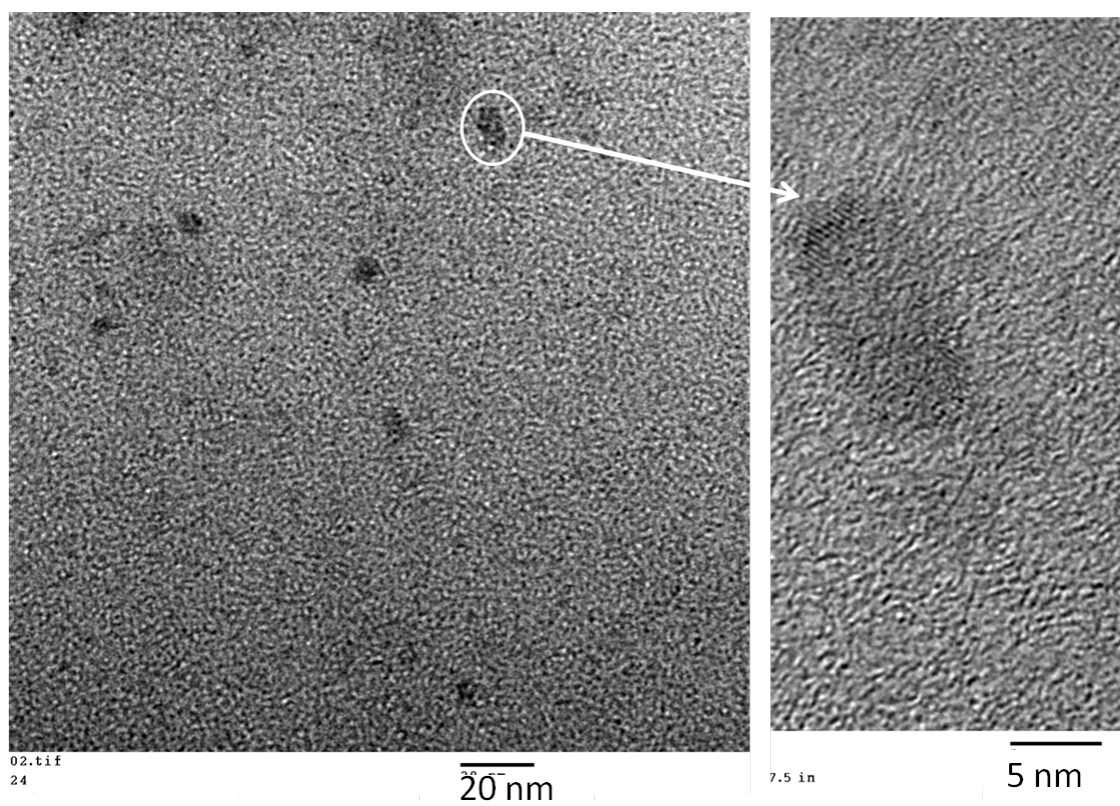
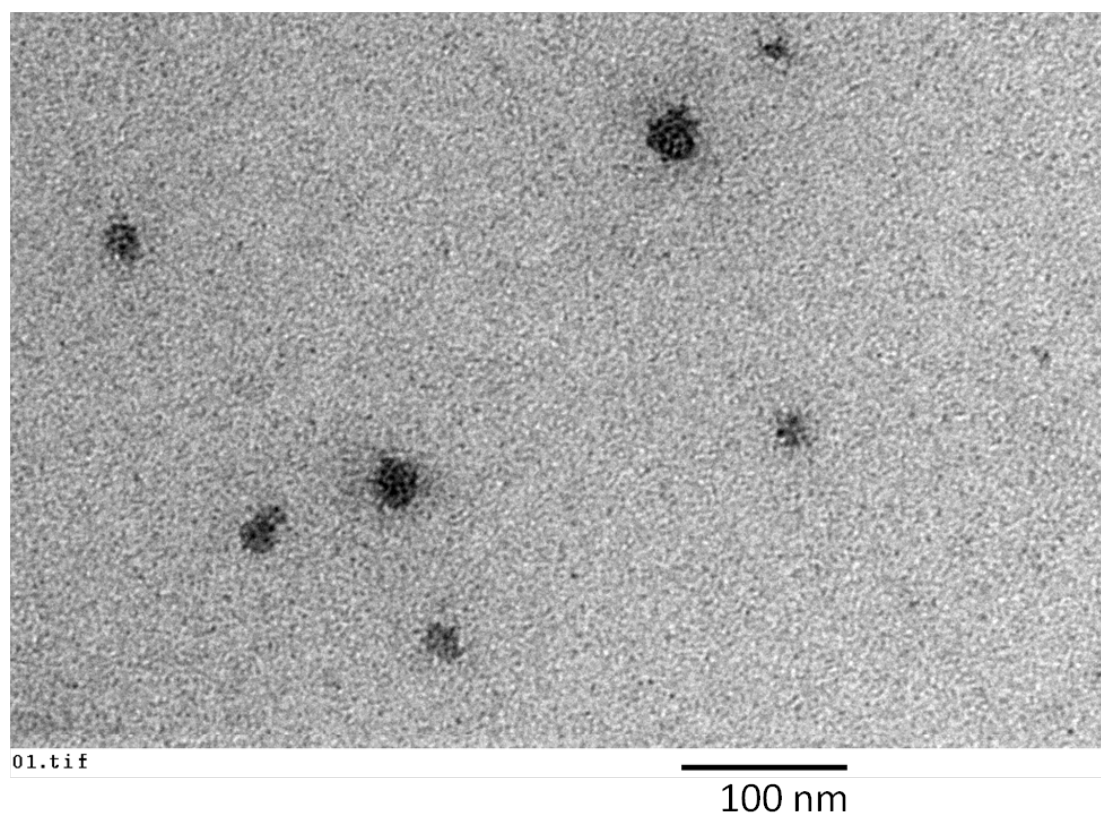
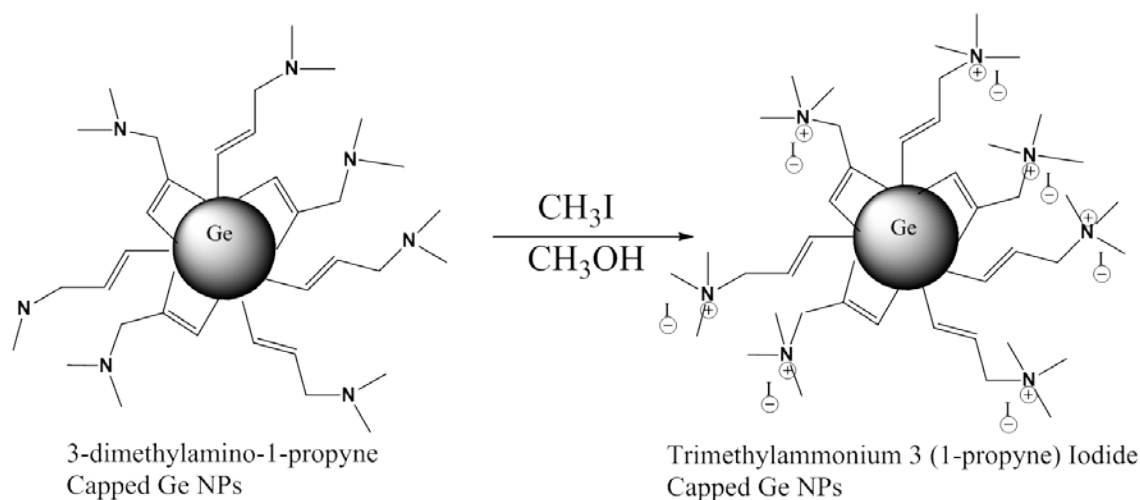


Figure 2.33: TEM and HRTEM images of Ge-DMAP NPs.

2.3.2 Water Soluble Ge Nanoparticles

Water soluble Ge NPs were synthesized by N-methylation of the dimethylamine terminated Ge NPs. Methyl iodide was added to the Ge NPs solution to form trimethyl ammonium iodide-terminated Ge NPs. This quaternary ammonium salt makes the nanoparticles water soluble. This steric quaternary salt gave extra stability to the nanoparticle surface.



Scheme 2.4: Synthesis of water soluble Ge NPs by N-methylation.

The FT-IR spectrum of trimethylammonium-1-propenyl Ge NPs (**Figure 2.34**) shows peaks for $\nu(\text{C-H})$ and $\delta(\text{C-H})$ at $2950\text{--}2850\text{ cm}^{-1}$ and $1465\text{--}1375\text{ cm}^{-1}$ respectively. Disappearance of a $\nu(\text{C-H})$ peak at $\sim 2700\text{ cm}^{-1}$ indicates that lone pair of N is absent due to formation of quaternary ammonium salt by methylation. A broad peak at $\sim 3400\text{ cm}^{-1}$ and a sharp peak at $\sim 1600\text{ cm}^{-1}$ may be due to $\nu(\text{O-H})$ and $\delta(\text{O-H})$ from absorbed water in the sample. A sharp peak at 1220 cm^{-1} was observed due to $\nu(\text{C-N})$.

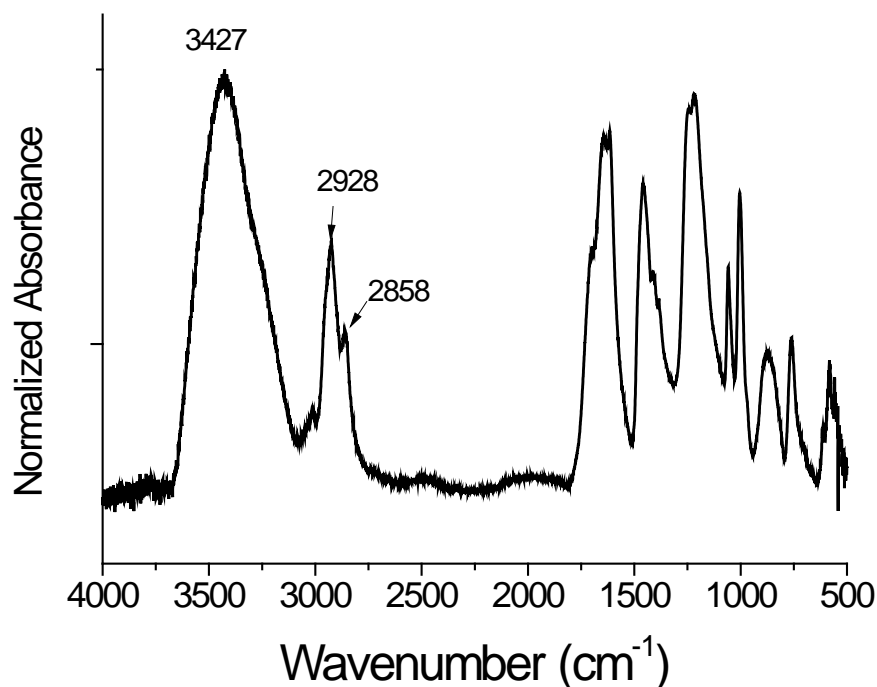


Figure 2.34: FT-IR spectrum of trimethylammonium-propenyl capped Ge NP.

UV visible absorption spectrum of water soluble Ge NPs shows a similar absorption spectrum compared to the starting dimethylamine terminated Ge NPs. PL emission spectra of the trimethylammonium-propenyl capped Ge NPs at various excitation wavelengths, from 300 to 420 nm, are shown in the **Figure 2.35**. These water soluble NPs display an intense emission in the 350-650 nm range. The emission peaks move to higher wavelength (red-shift) upon increasing excitation wavelength from 300 nm to 420 nm. The red-shift in emission wavelengths is consistent with the excitation of population of increasingly larger nanoparticles.

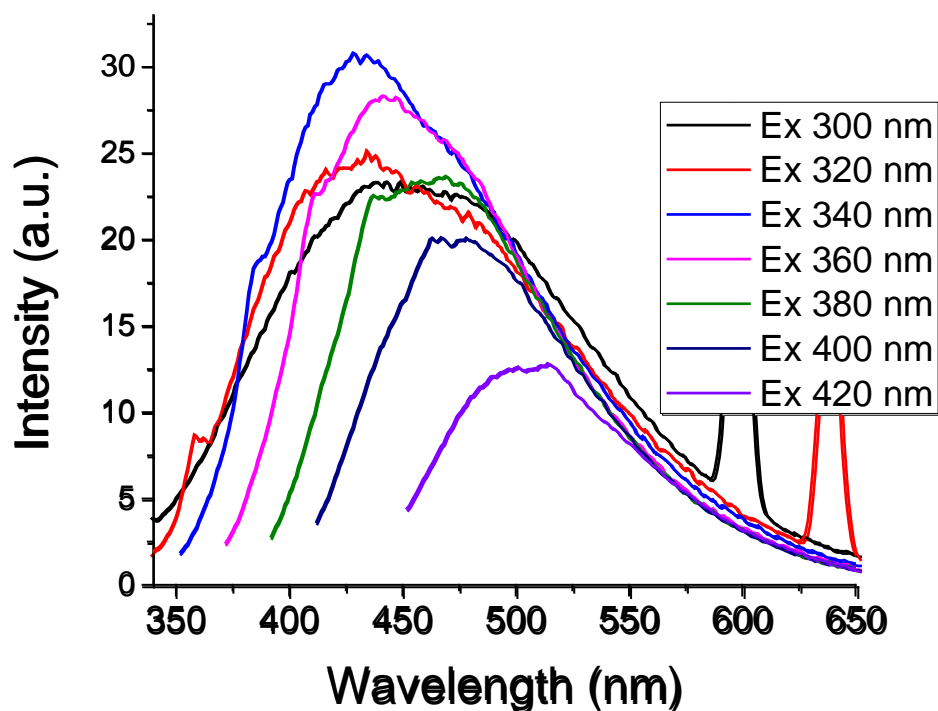
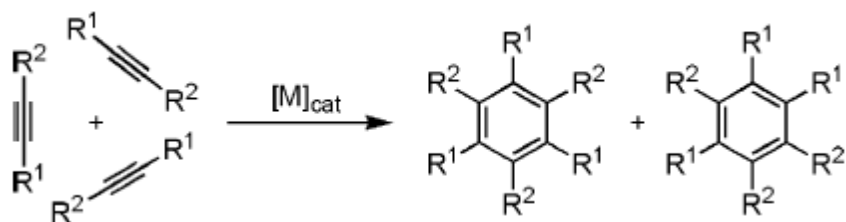


Figure 2.35: PL emission spectra of trimethylammonium-propenyl capped Ge NP

Cytotoxicity study of trimethylammonium propenyl Ge NPs was performed on various cells, including human colonic adenocarcinoma Caco-2 and rat alveolar macrophage NR8383 cells.⁴⁶ Similar to other cationic surface nanoparticles, these Ge NPs show some cytotoxicity. The proposed mechanism of the cytotoxicity is due to the formation of reactive oxygen species in the mitochondrion of a cell. However, compared to other amine-terminated cationic Si and Ge nanoparticles, these particles show very low cytotoxicity due to steric hindered positive charge by three bulky methyl group on the N.

2.4 Molecular Impurities Formed during Ball-milling

In the previous sections, we discussed about the formation of molecular impurities during the milling process. Various approaches, such as gel permeation chromatography (GPC), dialysis or Soxhlet dialysis etc., were used to separate the molecular aromatic impurities from Ge NPs. Alkynes undergo (2+2+2) cyclotrimerization, a well known organic reaction, to form these aromatic impurities during milling process inside stainless steel vial. Transition-metal-catalyzed [2 + 2 + 2] cyclotrimerization of alkynes was reported and it is used as a general method to make arene rings (Scheme 1).⁴⁷⁻⁵¹

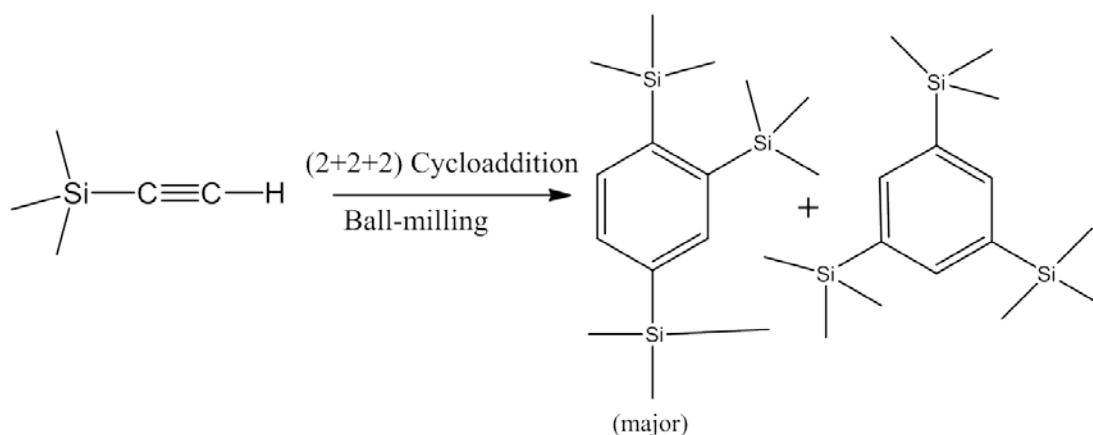


Scheme 2.5: Transition-metal-catalyzed [2 + 2 + 2] cyclotrimerization of alkynes.

2.4.1 Impurities from TMSA-milled products.

Aromatic impurities were separated from TMSA-passivated Ge NPs by GPC. The aromatic compounds collected as molecular impurities in the later fraction during GPC separation are 1,2,4-tris-(trimethylsilyl)-benzene and 1,3,5-tris-(trimethylsilyl)-benzene. 1H NMR (**Figure 2.36**), ^{13}C NMR spectra (**Figure 2.37**) and GCMS spectra (**Figure 2.38** and **2.39**) confirmed that the aromatic impurities are two geometrical isomers, 1,2,4-tris-(trimethylsilyl)-benzene and 1,3,5-tris-(trimethylsilyl)-benzene (10:1). They formed about 10% in mass of the total crude nanoparticles. 1,2,4-

tris-(trimethylsilyl)-benzene has peaks in ^1H NMR are at 0.257(s), 0.351(s), 0.364 (s), 7.47(d), 7.632(d), 7.816(s) ppm and 1,3,5-tris-(trimethylsilyl)-benzene has peaks in ^1H NMR are at 0.269(s), 7.667(s) ppm, which are confirmed by reported synthesized products of trimerization of TMSA using transition metal catalysts.^{37,51}



Scheme 2.6: Cyclotrimerization reaction of TMSA to form aromatic impurities during ball-milling

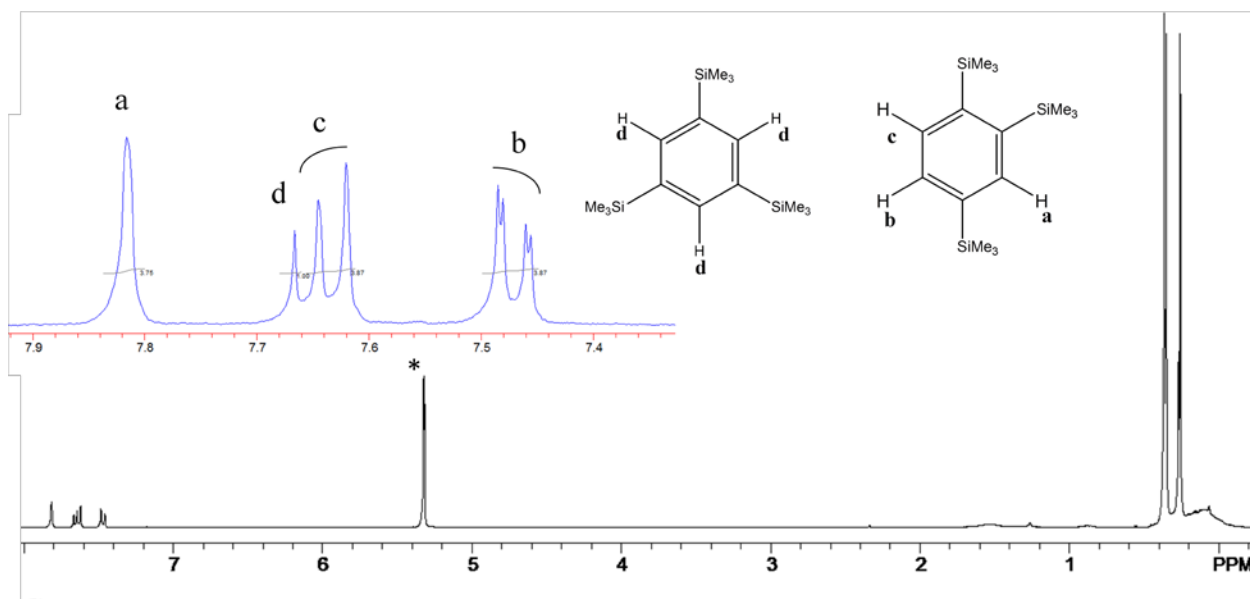


Figure 2.36: ^1H NMR spectra of fraction 12 which contains mostly aromatic impurities.

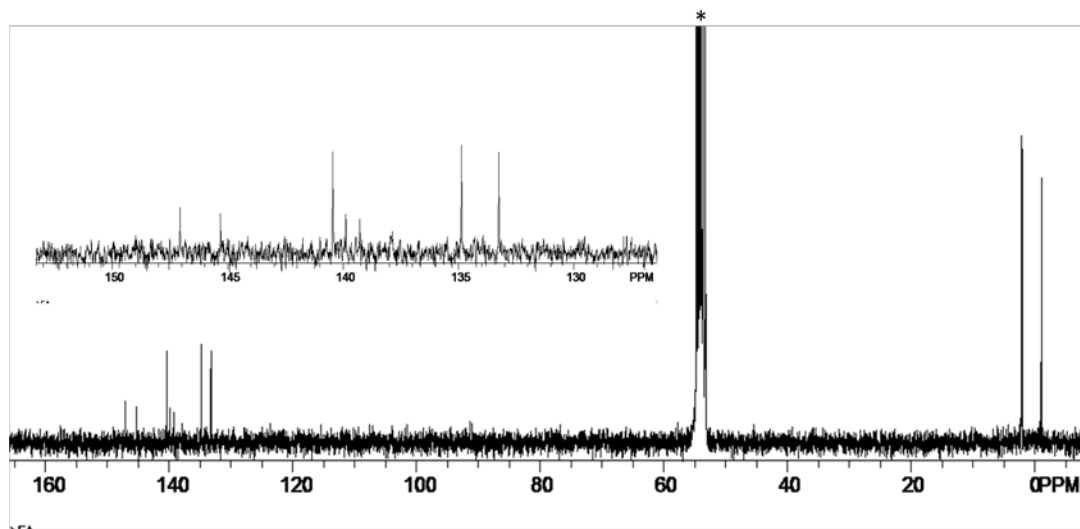


Figure 2.37. ^{13}C $\{^1\text{H}\}$ NMR spectra (in CD_2Cl_2) of fraction 12 which contains mostly aromatic impurities.

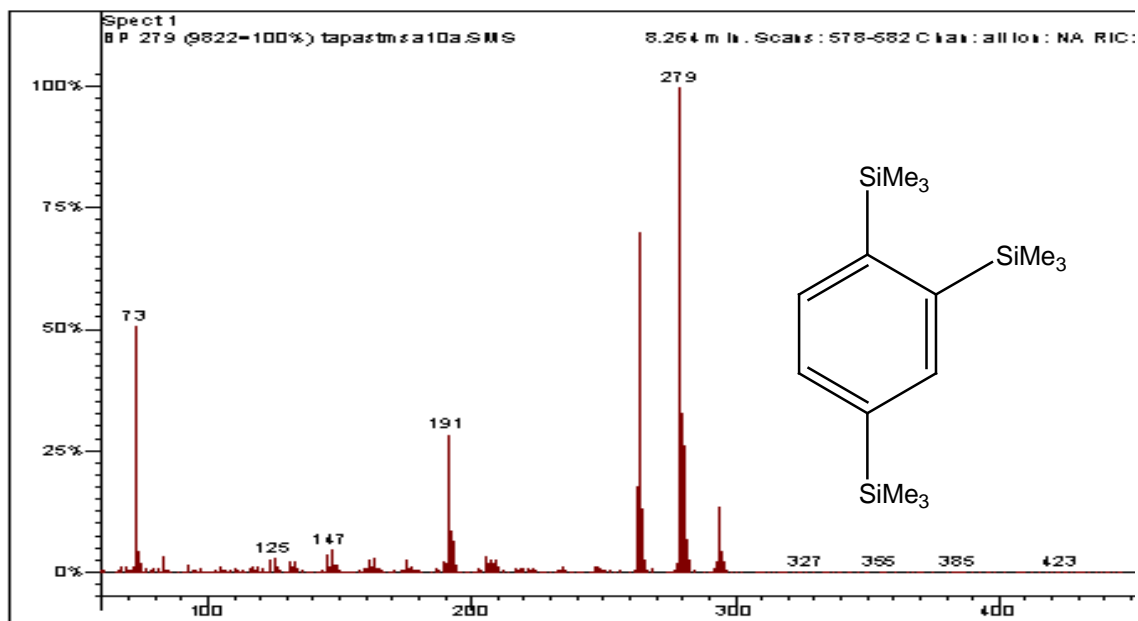


Figure 2.38. GCMS Spectra of major aromatic impurities found in fraction 12.

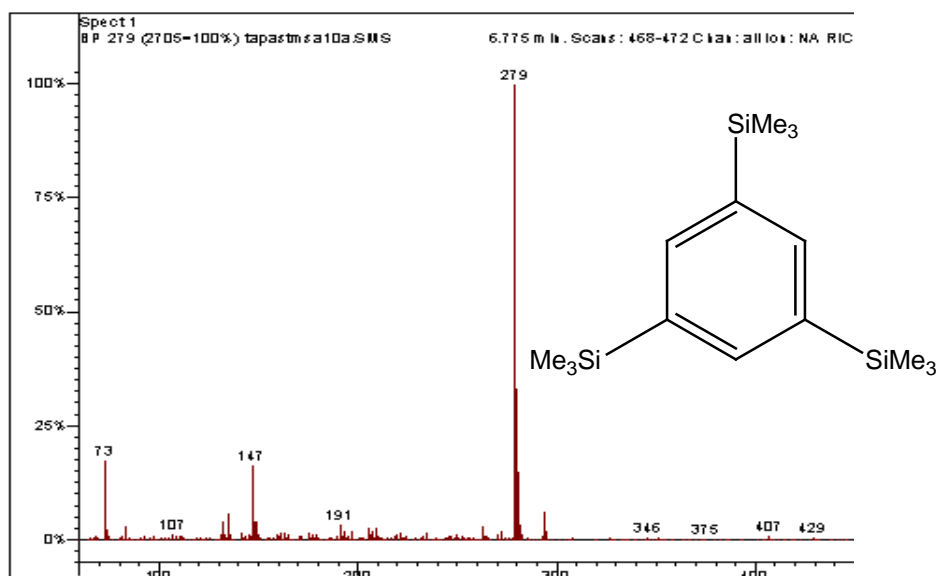
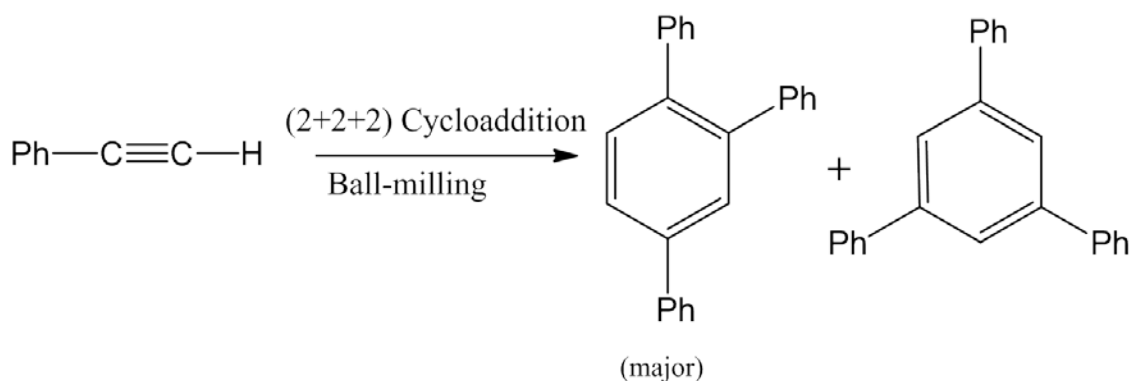


Figure 2.39. GCMS spectra of minor aromatic impurities found in fraction 12.

In order to confirm impurities and surface structure on Ge NPs, high energy ball-milling (HEBM) of pure TMSA without Ge, as a control experiment, was performed. NMR, FT-IR spectra and GCMS of the TMSA milled product support the aromatic impurities formation during HEBM.

2.4.2 Impurities formed during ball-milling with phenyl acetylene.

Phenylacetylene is very reactive and undergoes self-polymerization (*i.e.* cyclotrimerization and or further polymerization) yielding 0.52 g of crude product from HEBM of germanium (1 g). Phenylacetylene undergoes a cyclotrimerization reaction to form 1,2,4-triphenyl benzene, as a major isomer, and 1,3,5-triphenyl benzene as the minor isomer.^{48, 49} The major isomer was confirmed from the crystal structure (**Figure 2.40**); which was crystallized at low temperature from the crude products



Scheme 2.7: Cyclotrimerization reaction of phenylacetylene to form aromatic impurities during ball-milling

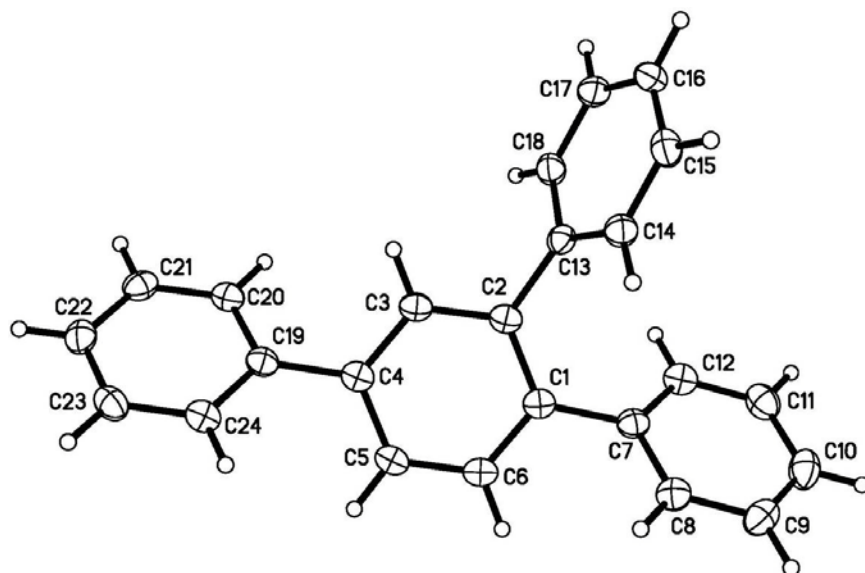


Figure 2.40: ORTEP diagram of crystal structure of 1,2,4-triphenylbenzene.

In the ^1H NMR, all aromatic proton peaks appear at 7-8 ppm; however in the $^{13}\text{C}\{^1\text{H}\}$ NMR spectra (**Figure 2.41**), peaks from phenyl ring appear at 123-132 ppm and at 140-144 ppm. Two control experiments were performed: ball-milling of pure phenylacetylene with or without ethylenediamine. Obviously, and in both cases no germanium was present. The purpose of using ethylenediamine is that ethylenediamine

would form chelating complexes with transition metal ions and remove any ions from solution; which might induces the cyclotrimerization reaction. However in both cases, there is no change in mass or in the NMR spectra, and it was difficult to separate Ge NPs from the huge impurities. This implies that even the zero valence transition metals, which cannot be removed by ethylenediamine, may catalyze the (2+2+2) cyclotrimerization reaction.

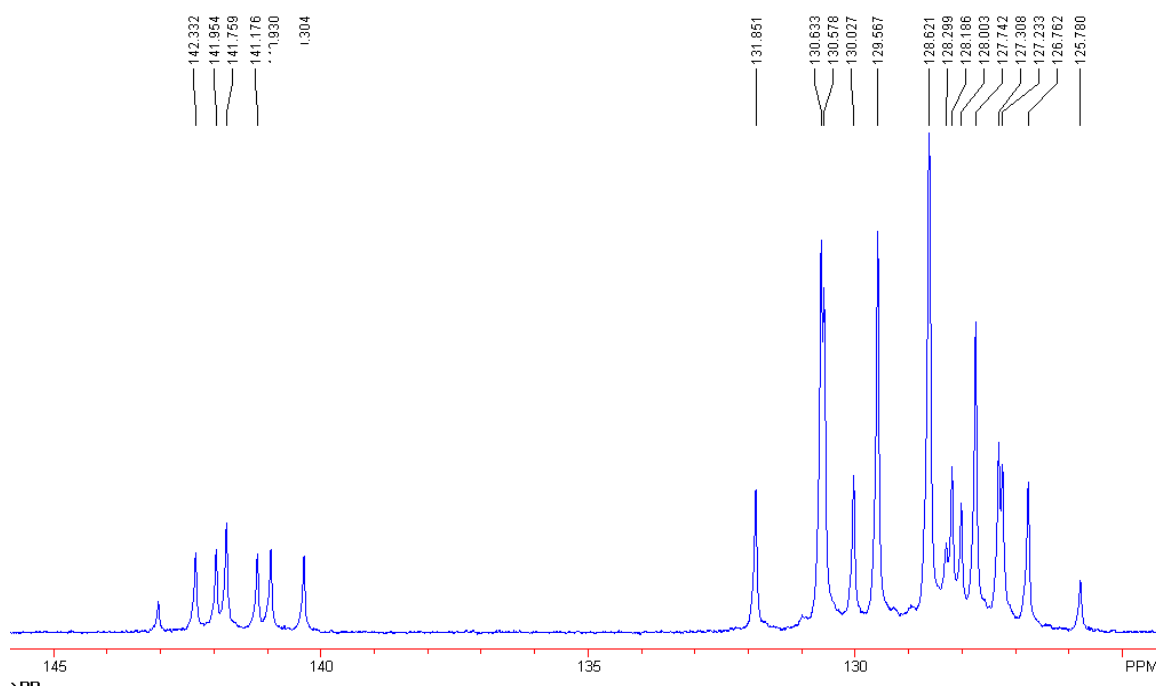


Figure 2.41: $^{13}\text{C}\{^1\text{H}\}$ NMR spectrum of phenylacetylene and Ge milled crude products in CD_2Cl_2 .

2.4.3 Impurities formed during ball-milling with amino-propyne.

Figure 2.42 shows ^1H NMR and $^{13}\text{C}\{^1\text{H}\}$ NMR of crude products in D_2O . In ^1H NMR spectra peaks between 7.4 to 8 ppm due to aromatic impurities formed during HEBM through cyclotrimerization of alkynes (*i.e.* 3-dimethylamino-1-propyne). Those

aromatic impurities are 1,2,4-tris (dimethylamino)-ethyl benzene and 1,3,5-tris (dimethylamino)-ethyl benzene. Aromatic impurities peaks were prominent in the ^{13}C NMR spectra; which were seen between 130-140 ppm.

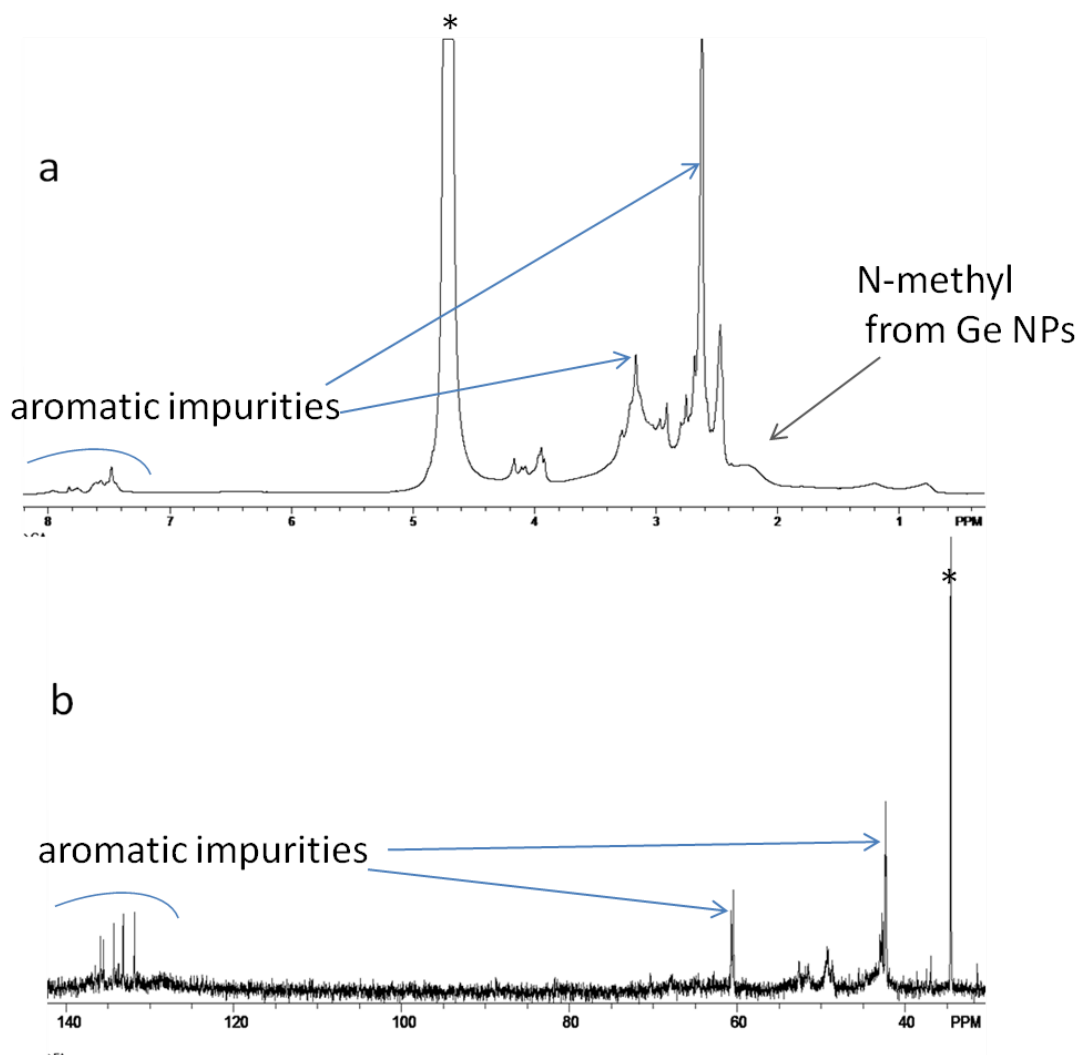


Figure 2.42: ^1H NMR (a) and ^{13}C NMR(b) spectra of crude Ge nanoparticles in D_2O .

2.5 Germanium Nanoparticles with other Passivating Reagents

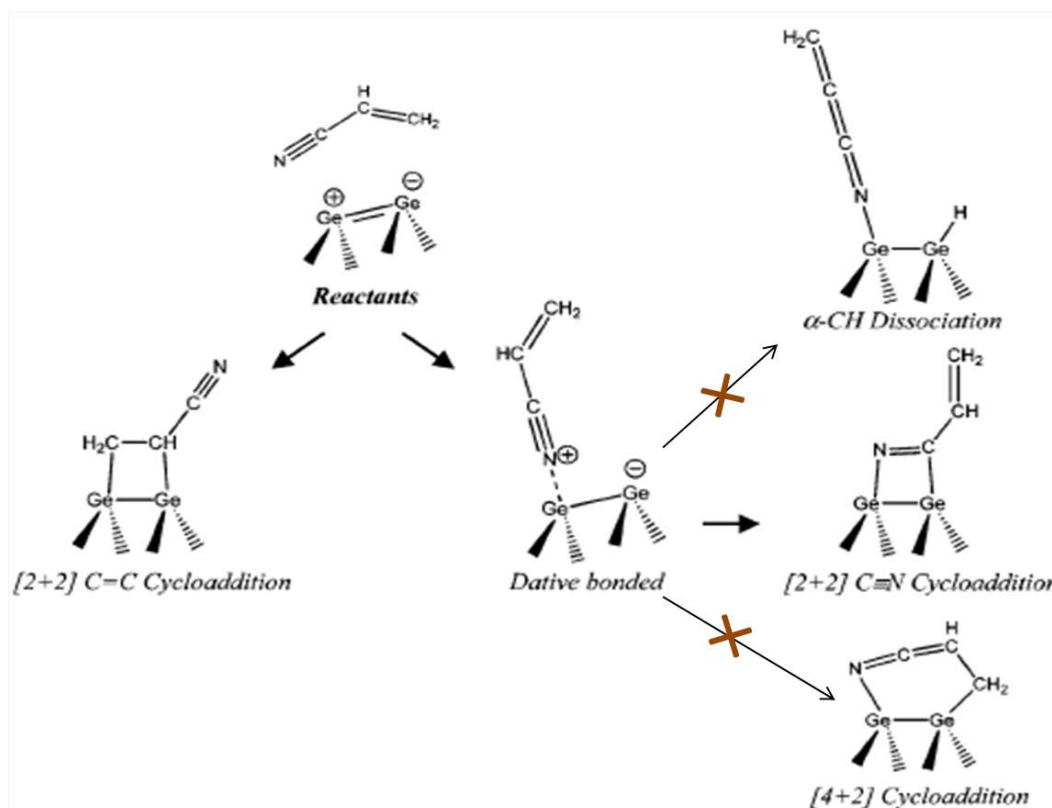
The reactivity of various unsaturated heteronuclear compounds, including ketones, nitrile etc. has been studied on freshly prepared Ge surfaces.^{10, 52-54} Previously, Heinz *et al* has prepared passivated Si NPs by various heteronuclear organic including alcohol, aldehyde and ketones by high energy ball-milling.⁹ There is no report of Si or Ge NPs synthesis by nitrile passivation.

2.5.1 Nitrile-passivated Ge NPs

Nitriles are found to be less reactive through (2+2) cycloaddition of CN on Ge surfaces compare to Si surface, as the Ge-N bond is weaker than the Si-N bond. Various nitriles including acetonitrile, acrylonitrile (2-propenenitrile) and butyronitrile were ball-milled with Ge pieces (1g) for 24 hours. Soluble nanoparticles were separated by centrifugation. After centrifugation, colorless solution does not have any luminescence under UV-light and no mass was collected from acetonitrile and Ge milled products. So, it confirms the previous reported argument that acetonitrile does not undergoes any reaction on Ge surface. However, about 10 mg and 50 mg yellow-red NPs were collected after centrifugation from butyronitrile and acrylonitrile milling, respectively.

Conjugated nitriles such as acrylonitrile (2-propenenitrile) react with silicon surfaces to form both a (4+2) cycloaddition product through the conjugated π system and a (2+2) cycloaddition product through C=C (**Scheme 2.8**).^{53, 54} The ketene amine functionality should show a strong peak around 1950-2100 cm^{-1} for $\nu(\text{C}=\text{C}=\text{N})$ in the FTIR spectra.⁵³ Absence of a peak in this region in FT-IR spectra (**Figure 2.43**) of acrylonitrile -passivated Ge NPs argues against the formation of a (4+2) cycloaddition

product; which was observed previously in the adsorption study on Ge surface. A sharp peak at 2246 cm^{-1} and a tiny peak at 2218 cm^{-1} appear due to asymmetric and symmetric stretching of $\nu(\text{C}\equiv\text{N})$ respectively; which supports the formation of a (2+2) cycloaddition product. A (2+2) $\text{C}\equiv\text{N}$ cycloaddition would lead to the formation of a $\text{C}=\text{N}$ on the surface and $\text{C}=\text{C}$ on the periphery from the reaction of acrylonitrile and Ge surface. A tiny peak at 3085 and a strong peak $\sim 1650\text{ cm}^{-1}$ are due to $\nu(\text{C}=\text{H})$ and $\nu(\text{C}=\text{N})$, respectively.⁵² The peripheral $\nu(\text{C}=\text{C})$ appear at $\sim 1600\text{ cm}^{-1}$.



Scheme 2.8: Possible bonding modes from the reaction of acrylonitrile with Ge surfaces during ball-milling

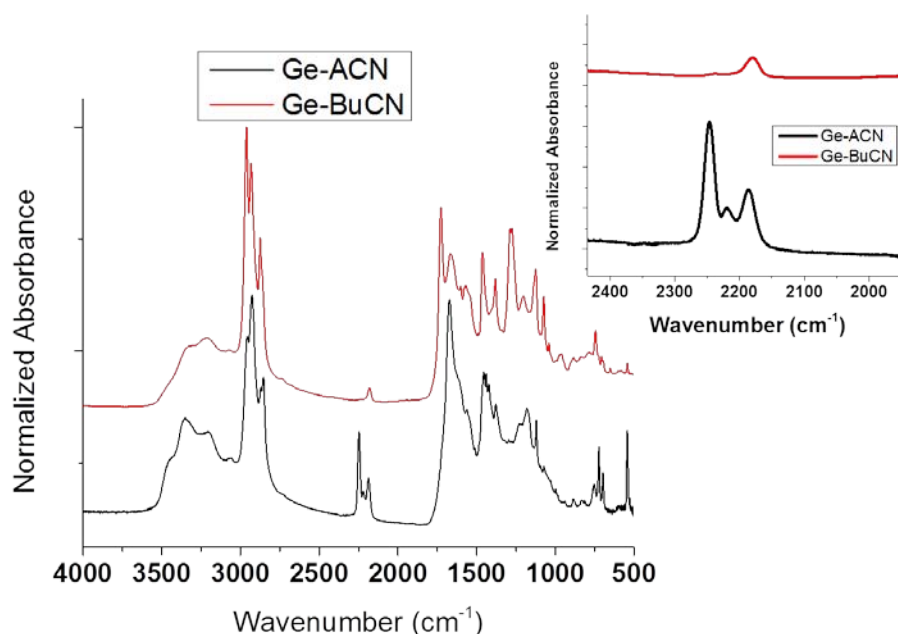


Figure 2.43: FT-IR spectra of acrylonitrile and butyronitrile-capped Ge NPs.

On the other hand, butyronitrile capped Ge NPs formed only (2+2) $\text{C}=\text{N}$ cycloaddition product which was confirmed by FT-IR spectrum (**Figure 2.43**).⁵³ A strong peak at $\sim 1650 \text{ cm}^{-1}$ in the FT-IR spectrum is due to $\nu(\text{C}=\text{N})$. However, FT-IR spectra of both acrylonitrile- and butyronitrile-passivated Ge NPs show a peak at 2185 cm^{-1} ; which may due to Ge-N dative bond formation which gives a weaker $\nu(\text{C}=\text{N})$ and a couple of broad peaks from $3200\text{--}3300 \text{ cm}^{-1}$ are due to N-H stretching; which might occurred from hydrolysis of weak Ge-N bond.

Photoluminescence (PL) spectra (**Figure 2.44**) of acrylonitrile-capped Ge NPs show an intense broad emission from 350 nm to 650 nm with red-shift of emission peak compared to alkyl/ alkenyl-passivated Ge NPs synthesized by ball-milling. Emission peaks move to longer wavelengths upon increasing the excitation wavelengths. Emission

intensity is almost 20 times stronger than the alkenyl-passivated Ge NPs synthesized by ball-milling.

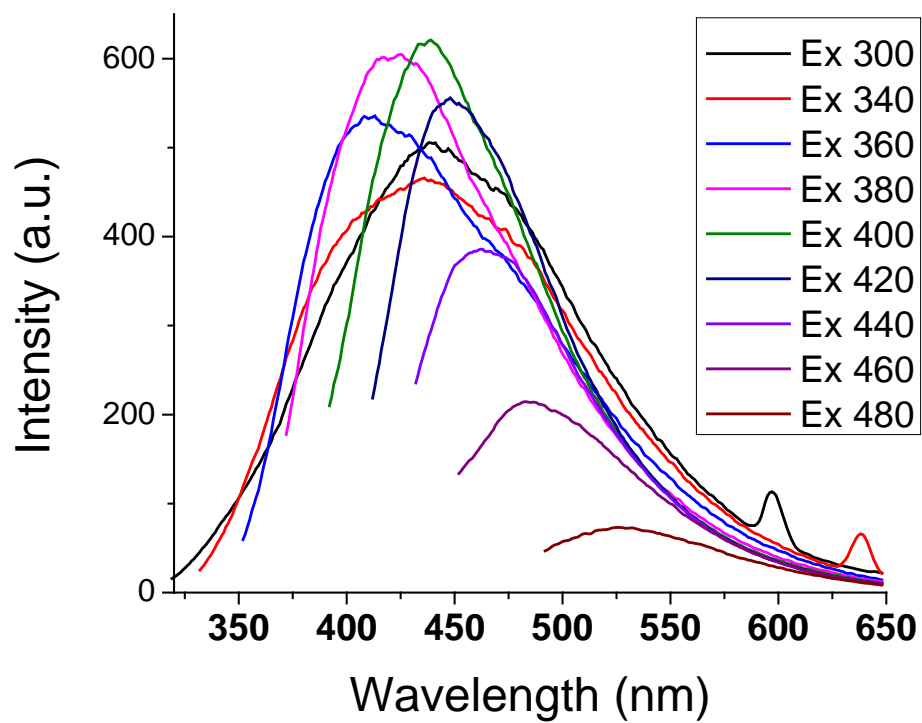


Figure 2.44: PL emission spectra of acrylonitrile-passivated Ge NPs in dichromethane.

2.6 Conclusion

In conclusion, a novel top-down method has been demonstrated for the synthesis of alkenyl-passivated germanium nanoparticles using high-energy ball-milling. This green process does not use corrosive solvents and the starting materials can be recycled. Alkynes may undergo trimerization to form substituted benzene during HEBM. We have purified synthesized nanoparticles and at the same time size separated by gel permeation chromatography (GPC). Since polydispersed nanoparticles by HEBM, we have developed novel size separation by GPC. Though the origin of PL of indirect band-gap semiconductor is in debate, a size dependent PL was observed. For a GPC separated fraction, SAXS size distribution shows a smaller particle size compared to TEM size distribution. As SAXS is a better technique for pore morphology materials and nanoparticles, it gave better size distribution of size separated Ge NPs. The efficiency of the size separation can be perhaps improved by using HPLC with a preparative column.

2.7 Experimental

2.7.1 *Method and Materials.*

Germanium (~2mm pieces), 99.999% purity, was purchased from Sigma-Aldrich and trimethylsilylacetylene (TMSA) was purchased from Gelest and used without further purification. 3-N,N-dimethyl-1-propyne (DMP 98%) and 1-octyne (98%) were purchased from Alfa-Aesar and used after distillation under nitrogen. Bio-beads S-X1 Beads, 200 mesh, were purchased from Bio-Rad. The dialysis membrane, Spectra/ Por 7 (MWCO 1 kDa) with regenerate cellulose (RC), was purchased from Spectrum.

2.7.2 *Production of TMSA-Passivated Ge Nanoparticles:*

Germanium pieces (0.75 g) were placed in a stainless steel milling vial along with stainless steel milling balls, each with a diameter of 1.2 cm and weighing approximately 8.1 g. In a nitrogen filled glovebox, the milling vial was filled with 25ml of reactive alkyne (i.e. TMSA) and then tightly sealed. The milling vial was placed in a SPEX 8000-D Dual Mixer/Mill, and high energy ball-milling was performed for 24 hours.

After 24 hours of milling, the reaction mixture is centrifuged to remove larger particles. The solution contains passivated germanium nanoparticles which are soluble. The solvents are removed by rotary-evaporation to yield a dry nanoparticle product. This nanoparticle product can be redispersed in organic solvents like methyl chloride, hexane etc. Crude Yield: 140-150 mg.

2.7.3 *Gel-permeation Chromatography Separation of Ge NPs:*

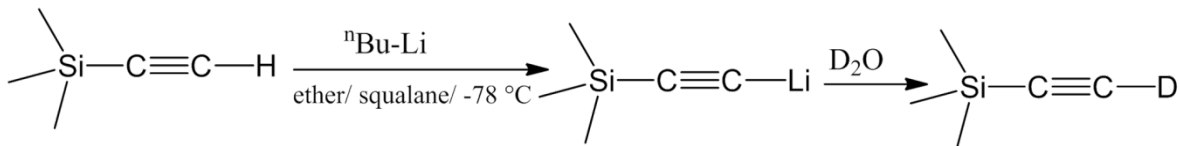
The size separation of nanoparticle is done by gel permeation chromatography (GPC). Bio-bead S-X1 beads were swelled for overnight in a swelling solvent (THF) and pack in a column (40 cm \times 1.3 cm). Dichloromethane was used as an elution solvent. Concentrated nanoparticle solution (50 mg Ge TMSA NPs in 1 ml DCM) was added and fractionated into 14 fractions. Fractions were collected in 1.5 ml increment in separate vials for further characterization. The first fraction was collected when the first color band was seen to elute. Later fractions (fraction 12, 13 and 14) contain mostly impurities.

Yield of GeTMSA NPs after GPC separation: 40 mg (80%). and yield of impurities: 8 mg (16%). **^1H NMR** (300 MHz, CD_2Cl_2): δ 0-1 (broad, 9 H); 5-6 ppm (very broad and weak, 1H.) **$^{13}\text{C}\{^1\text{H}\}$ NMR** (500 MHz, CD_2Cl_2): δ 0.0 ppm and 130-150 ppm. **UV-vis Absorption** (in dichloromethane): Single absorption with a tail up to 500 nm. **PL emission** (in dichloromethane): 350-600 nm with emission peak 400-490 nm by changing ex. wavelengths. **FT-IR** (thin film on KBr): 2820-2990 ($\nu(\text{C-H})$); 1580 ($\nu(\text{C=C})$); 1465-1376 ($\delta(\text{C-H})$); 1250 ($\nu(\text{Si-CH}_3)$); 1100-850 ($\nu(\text{Ge-O})$); 830 ($\nu(\text{Si-C})$); 750 cm^{-1} ($\nu(\text{Ge-C})$).

2.7.4 *Synthesis of TMSA- d_1 :*

Squalane (10 ml) was added in a 250 ml two-neck flask equipped with a stir bar and a graduated addition funnel. The squalane was degassed for 30 minutes at 50 $^\circ\text{C}$ under vacuum. The flask was back filled with nitrogen and cooled down to -78 $^\circ\text{C}$. Distilled and degassed trimethylsilyl acetylene (16 ml, 100 mmol) and 100 ml diethylether were added under nitrogen flow. $^n\text{Butyllithium}$ (2.5 M in hexane, 40 ml, 100

mmol) was added through cannula slowly by addition funnel under nitrogen. After 30 minutes the solution was warmed to room temperature.



Scheme 2.9: Synthesis of TMSA- d_1 .

The resulting solution was concentrated by vacuum and D_2O (1.8 ml, 100 mmol) was added. TMSA- d_1 was distilled out as colorless liquid at 52 °C under nitrogen with a short-path distillation apparatus connected with three-way distillation adapter. Yield: 12 ml (75%). **^1H NMR** (300 MHz, CD_2Cl_2): δ 0.2 (s, 9 H). **FT-IR** (thin film on KBr): 2820-2990; 2570; 1910; 1453; 1372; 1255; 855; 762; 652 cm^{-1} .

2.7.5 Synthesis of D-TMSA-passivated Ge NPs:

TMSA- d_1 -passivated Ge NPs were prepared using same procedure as Ge-TMSA NPs made. A milling vial was loaded with 20 ml of TMSA- d_1 and Ge pieces (0.75 g) in a nitrogen filled glove box and ball-milled for 24 hours using Spex 8000D dual mixer. Dark red color NP solution was separated by centrifugation and purified by GPC using Bio-beads S-X1. Yield: 140 mg. **^1H NMR** (300 MHz, CD_2Cl_2): δ 0.8-1.4 (broad) ppm. **FT-IR** (thin film on KBr): 2820-2990; 1580; 1465-1376; 1250; 1100-850; 830; 750 cm^{-1} .

2.7.6 Control Experiment: Milling of Pure TMSA without Ge

A milling vial was filled with TMSA (25 ml) in a glove box and ball-milled for 24 hours using SPEX 8000-D Dual Mixer. Yield: 15 -20 mg. ^1H NMR (300 MHz, CH_2Cl_2): δ 0.257 (s), 0.351 (s), 0.269 (s), 0.364 (s). 7.47 (d, $J=7.4$ Hz), 7.632 (d, $J=7.4$ Hz), 7.816 (s), 7.667 (s) ppm.

2.7.7 Production of dimethylamino propyne-passivatedGe NPs.

Germanium (0.75 g of millimeter sized pieces) was placed in a stainless steel milling vial along with two stainless steel milling balls, each with a diameter of 1.2 cm and weighing approximately 8.1 g. In a glove box under nitrogen atmosphere, the vial was loaded, filled with approximately 20 ml of 3-dimethylamino-1-propyne (98%) and then tightly sealed. After charging and sealing, the milling vial was placed in a SPEX 8000-D Dual Mixer/Mill, and HEBM was performed over various lengths of time.

After 24 hours of milling, the reaction mixture was centrifuged to remove larger particles. The solution contains dimethylamino-1-propyne passivated germanium nanoparticles which were soluble. Approximately 20 ml of water was added to the vial to solublize more particles from the residue. All of the solvent was removed to get a dry nanoparticle product by rotary evaporation. This nanoparticle product is soluble in methanol or other polar solvents and it is weakly soluble in water.

2.7.8 Separation of Ge NPs by Soxhlet dialysis:

A Soxhlet dialysis set up was used to separate side products from the nanoparticle solution (Figure 2.3).⁴⁴ A Spectra/ Por[®] regenerated cellulose dialysis membrane (MWCO =1000 Da), which is stable in most organic solvents like methanol

was used. Methanol (100 ml) was added to a 250 ml three necked flask which was connected with a 50 ml capacity Soxhlet Apparatus. A 5 ml solution of crude Ge nanoparticles (130 mg crude nanoparticle soluble in 5 ml methanol) was placed in 25 cm length dialysis bag (Spectra/Por, 1kDa MWCO) and the dialysis bag was sealed at both ends with cotton string. A stir bar was placed inside the bag for weight. A thermocouple was attached to the one neck of the flask. The solution was refluxed at 60-62° C. Every After 2 hours every 20 ml of fresh methanol was added. After 12 hours the experiment was stopped. After Soxhlet-dialysis, nanoparticles were collected from the inside of the bag, dried by vacuum and the lyophilized.

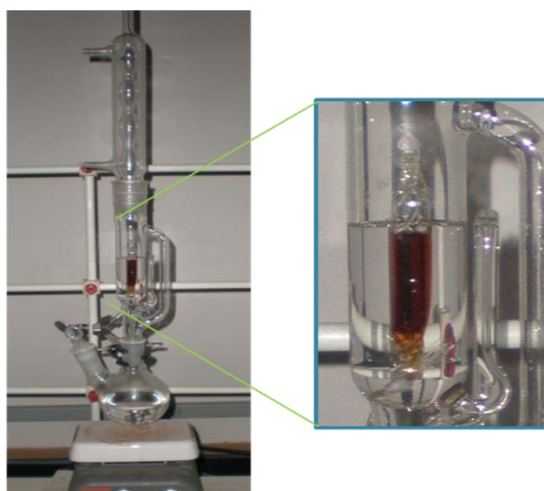


Figure2.43: Soxhlet-Dialysis experiment set up.

^1H NMR (300 MHz, CD_3OD): δ 2.2 (s, 2H); 3.1 (broad, 2H) ppm. **FT-IR** (thin film on KBr): $\sim 3500\text{ cm}^{-1}$ (broad, O-H stretching); $2750\text{--}2950\text{ cm}^{-1}$ (C-H stretching); 2770 cm^{-1} ($^1\text{C-H}$ stretching); 2055 cm^{-1} (Ge-H); 1615 cm^{-1} (C-N and C=C stretching); $\sim 1375\text{--}1460\text{ cm}^{-1}$ (C-H bending); $1000\text{--}1150\text{ cm}^{-1}$ (Ge-O stretching). **UV-vis Absorption** (in methanol): Single absorption with a shoulder at 310 nm. **PL emission** (in methanol):

Broad emission from 350-650 nm (emission peak change from 430-550 by changing excitation wavelength).

The crude nanoparticle solution was also separated by gel permeation chromatography (GPC). Bio-Gel P10, purchased from Bio-Rad, was swelled for overnight in water and packed in a column (45 cm in height and 1.35 cm in width). Water is used as an elution solvent. Fractions are collected in 2ml increment in separate vials for further characterization. The first fraction is collected when first color solution is eluting.

2.7.9 Synthesis of Nitrile-passivated Ge NPs

A stainless steel milling vial, charged with stainless steel milling balls, each with a diameter of 1.2 cm and weighing approximately 8.1 g, was loaded with germanium pieces (0.75 g, 99.999%) and 25 ml nitriles (i.e. acetonitrile, acrylonitrile and butyronitrile) in a nitrogen filled glove. The milling vial was placed in a SPEX 8000-D Dual Mixer/Mill, and high energy ball-milling was performed for 24 hours. After 24 hours of milling, the reaction mixture is centrifuged to remove larger particles. The solution contains passivated germanium nanoparticles which are soluble. The solvents were removed by rotaryevaporation to yield a dry nanoparticle product. This nanoparticle product can be redispersed in organic solvents- methyl chloride, hexane etc.

Yield of acetonitrile Ge-milled products: 0 mg,

Yield of butyronitrile-capped Ge NPs: 10 mg. **FT-IR** (thin film on KBr): 3350-3200 (broad); 3000-2850; 2185; 1650; 1460-1370; 1280; 750.

yield of acrylonitrile-capped Ge NPs: 50 mg. **FT-IR** (thin film on KBr): 3350-3200 (broad); 3085 (weak); 3000-2850; 2246; 2218 (weak); 2185; 1650; 1460-1370; 1124; 750.

2.8 Analytical Methods

2.8.1 *Infrared spectroscopy.*

Fourier Transformed Infrared (FT-IR) Spectroscopy was performed using a Thermo Nicolet NEXUS 670 FT-IR. Samples were prepared as a thin film of functionalized Ge NPs prepared by depositing dichloromethane solution of Ge NPs on KBr plate. FT-IR sample chamber was purged with dry nitrogen before collecting any data. FT-IR spectra were recorded after 512 scan with 1 cm^{-1} resolution.

2.8.2 *Nuclear magnetic resonance spectroscopy.*

Nuclear magnetic resonance spectra were obtained using a Bruker Avance 300 MHz high resolution NMR spectrometer. Ge NPs were dissolved in nmr solvents, such as, in chloroform-*d*, methylene chloride-*d*₂ and benzene-*d*₆ and the solution was transferred into a clean NMR tube.

2.8.3 *Transmission electron microscopy.*

Transmission electron microscopy (TEM) images were taken with a JOEL 2011 TEM using an accelerating voltage of 200 kV. A droplet of diluted nanoparticle solution in toluene was deposited on the carbon coated copper grid placed on a filter paper. The filter paper soaked up the excess solution before inserting in grid in the TEM sample

holder. Energy dispersive spectroscopic (EDS) data were obtained in the TEM using an Oxford Inca attachment with a 3 nm beam spot on a copper grid.

2.8.4 *UV-vis Absorption and Photoluminescence spectroscopy.*

UV-Vis absorbance spectra were obtained with a Cary 50 spectrophotometer in dichloromethane. Maximum absorbance was kept below 0.5. The photoluminescence emission characteristics from the Ge nanoparticles in dichloromethane were acquired using a Varian Cary Eclipse spectrofluorimeter. The emission spectra were recorded with excitation wavelengths between 300 nm to 450 nm with slow scanning speed (120 nm/min) using a 1 cm quartz cuvette. UV-vis absorption and PL emission spectra of amine-terminated Ge NPs were recorded either in methanol or in deionized water.

2.8.5 *GS-MS.*

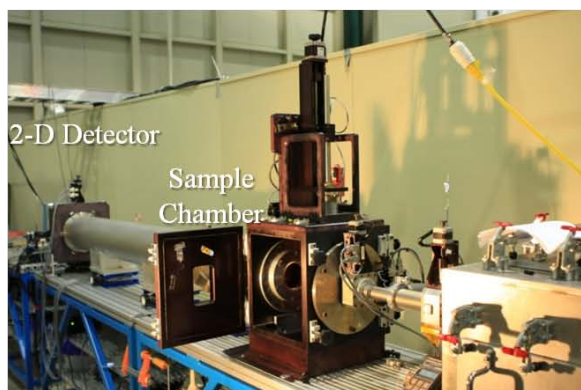
Molecular impurities were confirmed by GC-MS (Varian 450 GC, Varian 300 MS) with VF5-MS capillary column.

2.8.6 *Estimation of quantum yield (QY):*

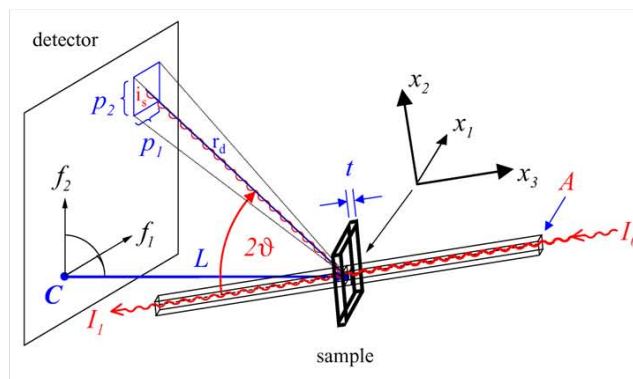
Background subtracted UV-vis absorption spectra and solvent corrected PL emission spectra of various dilutions of GPC separated fractions in hexanes were collected at excitation wavelength 300 nm. The integrated intensities were calculated from the solvent corrected PL spectra and plotted against respective absorbance at 300 nm. From the linear fitting connecting the (0,0) point, slope was calculated for each plot. Similarly, the slope was calculated for various dilution of standard 9,10-dimethylanthracene at 300 nm in the same solvent. QY was calculated from multiplying slope ratio of sample and standard with standard QY which is 93%.¹

2.8.7 *Small Angle X-ray Scattering experiment*

Small Angle X-ray Scattering (SAXS) experiments were performed on the SAXS beam line at the J. Bennett Johnston, Sr. Center for Advanced Microstructure and Devices (CAMD), Baton Rouge, USA. The SAXS beam line is equipped with the LNLS double crystal monochromator allows photon energies to be selected from roughly 3 to 14 keV. A 2D X-Ray detector was used to record the scattering intensity, $I(q)$, as a function of the modulus of scattering vector (q), $q=(4\pi/\lambda)\sin \theta$, θ being half the scattering angle.⁵⁵ Wide angle scattering can be performed with the Phosphor Imager SI image plate and scanner. A segmented flight path allows SAXS q -ranges from .0015 to .44 \AA^{-1} and WAXS to 2.5 \AA^{-1} . Size separated solid nanoparticles samples were either deposited on kapton tape or made self supporting thin film before putting in to the sample chamber. The path length of nanoparticles' film was less than 0.5 mm. Maintaining 1 million counts, scattered intensities were recorded during about 30 minutes exposure. The data were processed and converted from 2D scattering images into 1D diagrams of scattering intensities vs scattering vector q by FIT2D program. From the background corrected intensity vs. scattering vector q plot, size distribution of the size separated samples were calculated using maximum entropy method (MaxEnt) assuming hard sphere model using the software IGOR Pro 6.12A with Irena 2.38 macro.



SAXS beam line



Scattering geometry

Figure 2.44: SAXS beam line at CAMD, Baton Rouge (left) and schematic drawing of scattering geometry (right).

2.8.8 Powder X-ray diffraction.

Powder X-ray diffraction (XRD) data were collected on Scintag XDS 2000X-ray diffractometer using Cu K α radiation (8.047 KeV energy) using Si(Li) Peltier (Thermo Electron Corp.) cooled detector.

2.9 APPENDIX

Calculation of Surface coverage and total number of Ge atoms of Ge NPs

Similar to Si, Ge forms a diamond cubic lattice and its fcc cubic unit cell, with cell dimension of 0.566, consists of 8 Ge atoms. Now, the ratio of the surface sites to total number of Ge atoms in a Ge nanoparticle with certain size was calculated following a method that calculated for Si NPs.⁵⁶ Assuming spherical shape of Ge NPs, volume of a nanoparticle sphere can be approximated to mean volume of inner and outer cubes that fit inside and outside of the sphere (Figure 2.44 b). The calculation for the Ge NPs of size between 1 to 10 nm are shown in the table.

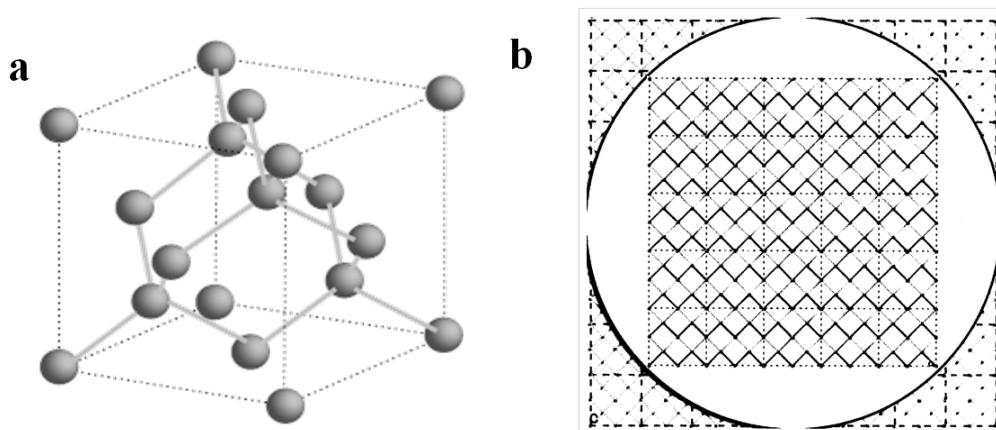


Figure 2.44: a) Unit cell of bulk crystalline germanium, b) A geometric 2D representation of a box inside of another box representing the sphere in between them. The approximate size of the sphere = (inner box + outer box)/2

The reconstructed Ge surfaces would react with alkenes or alkynes to form (2+2) adduct and radical site adduct. An alkene or alkyne molecule would react with two Ge atoms to form a (2+2) adduct; whereas radical sites require an alkene/ alkyne per a Ge atom. If we assume 1:1 ratio of two adducts, three organic ligands are required to passivate two Ge surface atoms.

Table2: Calculation surface coverage of organic ligands per 100 Ge atoms in a Ge NP.

Particle Diameter (nm)	Total number of Ge atoms	Number of surface atoms	Number of organic ligands (R)	Ge _x R X=	% Surface coverage
1	54	31	20	2.7	37.03
2	432	146	97	4.5	22.45
3	1239	301	200	6.2	16.14
4	2720	514	343	7.9	12.61
5	3985	675	450	8.9	11.29
6	7633	1067	711	10.7	9.31
7	11890	1441	961	12.5	8.08
8	17761	1873	1248	14.2	7.27
9	26773	2494	1663	16.1	6.21
10	36324	3053	2035	17.8	5.60

References

1. Kartopu, G.; Sapelkin, A. V.; Karavanskii, V. A.; Serincan, U.; Turan, R., Structural and optical properties of porous nanocrystalline Ge. *J. Appl. Phys.* **2008**, 103, (11), 113518-7.
2. Gresback, R.; Holman, Z.; Kortshagen, U., Nonthermal plasma synthesis of size-controlled, monodisperse, freestanding germanium nanocrystals. *Appl. Phys. Lett.* **2007**, 91, (9), 093119.
3. Taylor, B. R.; Kauzlarich, S. M.; Delgado, G. R.; Lee, H. W. H., Solution Synthesis and Characterization of Quantum Confined Ge Nanoparticles. *Chem. Mater.* **1999**, 11, (9), 2493-2500.
4. Taylor, B. R.; Kauzlarich, S. M.; Lee, H. W. H.; Delgado, G. R., Solution Synthesis of Germanium Nanocrystals Demonstrating Quantum Confinement. *Chem. Mater.* **1998**, 10, (1), 22-24.
5. Heath, J. R.; Shiang, J. J.; Alivisatos, A. P., Germanium quantum dots: Optical properties and synthesis. *J. Chem. Phys.* **1994**, 101, (2), 1607-1615.
6. Gerion, D.; Zaitseva, N.; Saw, C.; Casula, M. F.; Fakra, S.; Van Buuren, T.; Galli, G., Solution Synthesis of Germanium Nanocrystals: Success and Open Challenges. *Nano Lett.* **2004**, 4, (4), 597-602.
7. Gerung, H.; Boyle, T. J.; Tribby, L. J.; Bunge, S. D.; Brinker, C. J.; Han, S. M., Solution Synthesis of Germanium Nanowires Using a Ge²⁺ Alkoxide Precursor. *J. Am. Chem. Soc.* **2006**, 128, (15), 5244-5250.
8. Lu, X.; Fanfair, D. D.; Johnston, K. P.; Korgel, B. A., High Yield Solution[^]Liquid[^]Solid Synthesis of Germanium Nanowires. *J. Am. Chem. Soc.* **2005**, 127, (45), 15718-15719.
9. Heintz, A. S.; Fink, M. J.; Mitchell, B. S., Mechanochemical Synthesis of Blue Luminescent Alkyl/Alkenyl-Passivated Silicon Nanoparticles. *Adv. Mater.* **2007**, 19, (22), 3984-3988.
10. Bent, S. F., Reactivity of the Germanium Surfaces: Chemical Passivation and Functionalization. *Annu. Rev. Phys. Chem.* **2006**, 56, 467-95.
11. Duke, C. B., ChemInform Abstract: Semiconductor Surface Reconstruction: The Structural Chemistry of Two- Dimensional Surface Compounds. *ChemInform* **1996**, 27, (41), no-no.

12. Fink, A.; Huber, R.; Widdra, W., Ethylene adsorption on Ge(100)-(2 x 1): A combined angle-resolved photoemission and thermal desorption spectroscopy study. *J. Chem. Phys.* **2001**, 115, (6), 2768-2775.
13. Kim, A.; Choi, D. S.; Lee, J. Y.; Kim, S., Adsorption and Thermal Stability of Ethylene on Ge(100). *J. Phys. Chem. B* **2004**, 108, (10), 3256-3261.
14. Lal, P.; Teplyakov, A. V.; Noah, Y.; Kong, M. J.; Wang, G. T.; Bent, S. F., Adsorption of ethylene on the Ge(100)-2 x 1 surface: Coverage and time-dependent behavior. *J. Chem. Phys.* **1999**, 110, (21), 10545-10553.
15. Jiang, G.; Niederhauser, T. L.; Fleming, S. A.; Asplund, M. C.; Linford, M. R., Evidence for a Radical Mechanism in Monolayer Formation on Silicon Ground (or Scribed) in the Presence of Alkyl Halides. *Langmuir* **2004**, 20, (5), 1772-1774.
16. Niederhauser, T. L.; Lua, Y.-Y.; Sun, Y.; Jiang, G.; Strossman, G. S.; Pianetta, P.; Linford, M. R., Formation of (Functionalized) Monolayers and Simultaneous Surface Patterning by Scribing Silicon in the Presence of Alkyl Halides. *Chem. Mater.* **2001**, 14, (1), 27-29.
17. Langford, J. I.; Wilson, A. J. C., Scherrer after sixty years: A survey and some new results in the determination of crystallite size. In *Journal of Applied Crystallography*, 1978; Vol. 11, pp 102-113.
18. Fan, J.; Chu, P. K., Group IV Nanoparticles: synthesis, Properties, and Biological Applications. *Small* **2010**, 6, (19), 2080-2098.
19. Lu, X.; Ziegler, K. J.; Ghezelbash, A.; Johnston, K. P.; Korgel, B. A., Synthesis of Germanium Nanocrystals in High Temperature Supercritical Fluid Solvents. *Nano Lett.* **2004**, 4, (5), 969-974.
20. Lee, D. C.; Pietryga, J. M.; Robel, I.; Werder, D. J.; Schaller, R. D.; Klimov, V. I., Colloidal Synthesis of Infrared-Emitting Germanium Nanocrystals. *J. Am. Chem. Soc.* **2009**, 131, (10), 3436-3437.
21. Nayfeh, N. R., E.; Mitas, L., *Synthesis, Functionalization, and Surface Treatment of Nanoparticles*. American Scientific Publishers, Stevenson Ranch: CA: 2001; Vol. Ch. 10.
22. Ma, X.; Wu, F.; Kauzlarich, S. M., Alkyl-terminated crystalline Ge nanoparticles prepared from NaGe: Synthesis, functionalization and optical properties. *J. Solid State Chem.* **2008**, 181, (7), 1628-1633.
23. Taylor, B. R.; Fox, G. A.; Hope-Weeks, L. J.; Maxwell, R. S.; Kauzlarich, S. M.; Lee, H. W. H., Solution preparation of Ge nanoparticles with chemically tailored surfaces. *Materials Science and Engineering B* **2002**, 96, (2), 90-93.

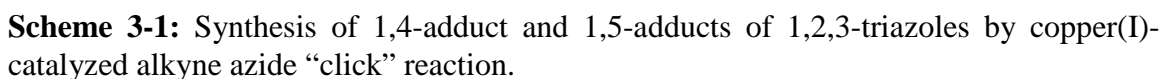
24. Gaffet, E., Phase transition induced by ball milling in germanium. *Materials Science and Engineering: A* **1991**, 136, 161-169.
25. Kumari, S.; Singh, D. K.; Giri, P. K., Strain Anisotropy in Freestanding Germanium Nanoparticles Synthesized by Ball Milling. *J. Nanosci. Nanotechnol.* **2009**, 9, 5231-5236.
26. Choi, K.; Buriak, J. M., Hydrogermylation of Alkenes and Alkynes on Hydride-Terminated Ge(100) Surfaces. *Langmuir* **2000**, 16, (20), 7737-7741.
27. Niquet, Y. M.; Allan, G.; Delerue, C.; Lannoo, M., Quantum confinement in germanium nanocrystals. *Appl. Phys. Lett.* **2000**, 77, (8), 1182-1184.
28. Weissker, H. C.; Furthmuller, J.; Bechstedt, F., Optical properties of Ge and Si nanocrystallites from ab initio calculations. I. Embedded nanocrystallites. *Phys. Rev. B: Condens. Matter Mater. Phys.* **2002**, 65, (15), 155327/1-155327/9.
29. Prabakar, S.; Shiohara, A.; Hanada, S.; Fujioka, K.; Yamamoto, K.; Tilley, R. D., Size Controlled Synthesis of Germanium Nanocrystals by Hydride Reducing Agents and Their Biological Applications. *Chem. Mater.* **2009**.
30. Timothy, J. B.; Louis, J. T.; Leigh Anna, M. O.; Sang, M. H., Synthesis and Characterization of Germanium Coordination Compounds for Production of Germanium Nanomaterials. *Eur. J. Inorg. Chem.* **2009**, 2009, (36), 5550-5560.
31. Chou, N. H.; Oyler, K. D.; Motl, N. E.; Schaak, R. E., Colloidal synthesis of germanium nanocrystals using room-temperature benchtop chemistry. *Chem. Mater.* **2009**, 21, (18), 4105-4107.
32. Zaitseva, N.; Dai, Z. R.; Grant, C. D.; Harper, J.; Saw, C., Germanium Nanocrystals Synthesized in High-Boiling-Point Organic Solvents. *Chem. Mater.* **2007**, 19, (21), 5174-5178.
33. Chiu, H. W.; Kauzlarich, S. M., Investigation of Reaction Conditions for Optimal Germanium Nanoparticle Production by a Simple Reduction Route. *Chem. Mater.* **2006**, 18, (4), 1023-1028.
34. Fok, E.; Shih, M.; Meldrum, A.; Veinot, J. G. C., Preparation of alkyl-surface functionalized germanium quantum dots via thermally initiated hydrogermylation. *Chem. Commun.* **2004**, (4), 386-387.
35. Stoldt, C. R.; Haag, M. A.; Larsen, B. A., Preparation of freestanding germanium nanocrystals by ultrasonic aerosol pyrolysis. *Appl. Phys. Lett.* **2008**, 93, (4), 043125.
36. Warner, J. H.; Tilley, R. D., Synthesis of water-soluble photoluminescent germanium nanocrystals. *Nanotechnology* **2006**, 17, (15), 3745.

37. Wilcoxon, J. P.; Provencio, P. P.; Samara, G. A., Synthesis and optical properties of colloidal germanium nanocrystals. *Phys. Rev. B* **2001**, 64, (3), 035417.
38. Wilcoxon, J. P.; Provencio, P. P.; Samara, G. A., Synthesis and optical properties of colloidal germanium nanocrystals. *Phys. Rev. B: Condens. Matter Mater. Phys.* **2001**, 64, (3), 035417/1-035417/9.
39. Prabakar, S.; Shiohara, A.; Hanada, S.; Fujioka, K.; Yamamoto, K.; Tilley, R. D., Size Controlled Synthesis of Germanium Nanocrystals by Hydride Reducing Agents and Their Biological Applications. *Chem. Mater.* **2010**, 22, (2), 482-486.
40. Takeoka, S.; Fujii, M.; Hayashi, S.; Yamamoto, K., Size-dependent near-infrared photoluminescence from Ge nanocrystals embedded in SiO₂ matrixes. *Phys. Rev. B: Condens. Matter Mater. Phys.* **1998**, 58, (12), 7921-7925.
41. Sun, B.; Zou, G.; Shen, X.; Zhang, X., Exciton dissociation and photovoltaic effect in germanium nanocrystals and poly(3-hexylthiophene) composites. *Appl. Phys. Lett.* **2009**, 94, (23), 233504/1-233504/3.
42. Lambert, T. N.; Andrews, N. L.; Gerung, H.; Boyle, T. J.; Oliver, J. M.; Wilson, B. S.; Han, S. M., Water-soluble germanium(0) nanocrystals: cell recognition and near-infrared photothermal conversion properties. *Small* **2007**, 3, (4), 691-699.
43. Ma, Y.-H.; Huang, C.-P.; Tsai, J.-S.; Shen, M.-Y.; Li, Y.-K.; Lin, L.-Y., Water-soluble germanium nanoparticles cause necrotic cell death and the damage can be attenuated by blocking the transduction of necrotic signaling pathway. *Toxicol. Lett.* **2011**, 207, (3), 258-269.
44. Anyanwu, U. K.; Venkataraman, D., Soxhlet-dialysis: a method to recover soluble polymer supported catalysts. *Green Chemistry* **2005**, 7, (6), 424-425.
45. Rosso-Vasic, M.; Spruijt, E.; Popovic, Z.; Overgaag, K.; van, L. B.; Grandidier, B.; Vanmaekelbergh, D.; Dominguez-Gutierrez, D.; De, C. L.; Zuilhof, H., Amine-terminated silicon nanoparticles: synthesis, optical properties and their use in bioimaging. *J. Mater. Chem.* **2009**, 19, (33), 5926-5933.
46. Bhattacharjee, S.; Rietjens, I.; Alink, G.; Antonius, M.; Purkait, T. K.; Xu, Z.; Singh, M.; Atkins, T.; Regli, S.; Clark, R.; Shukaliak, A.; Mitchell, B.; Fink, M. J.; Veinot, J. G.; Kauzlarich, S.; Zuilhof, H., Cytotoxicity of Surface-functionalized Silicon and Germanium Nanoparticles: The Dominant Role of Surface Charges. *Particle and Fibre Toxicology* **2012**, submitted.
47. Cadierno, V.; Garc a-Garrido, S. E.; Gimeno, J., Efficient Intermolecular [2 + 2 + 2] Alkyne Cyclotrimerization in Aqueous Medium Using a Ruthenium(IV) Precatalyst. *Journal of the American Chemical Society* **2006**, 128, (47), 15094-15095.

48. Xu, B.-H.; Wu, D.-H.; Li, Y.-Z.; Yan, H., Reactivity of CpCo 16e Half-Sandwich Complexes Containing a Chelating 1,2-Dicarba-closo-dodecaborane-1,2-dichalcogenolate Ligand toward Phenylacetylene. *Organometallics* **2007**, 26, (17), 4344-4349.
49. Hilt, G.; Hess, W.; Vogler, T.; Hengst, C., Ligand and solvent effects on cobalt(I)-catalyzed reactions: Alkyne dimerization versus [2+2+2]-cyclootrimerization versus Diels-Alder reaction versus [4+2+2]-cycloaddition. *J. Organomet. Chem.* **2005**, 690, (23), 5170-5181.
50. Zhu, Z.; Wang, C.; Xiang, X.; Pi, C.; Zhou, X., DyI₂ initiated mild and highly selective silyl radical-catalyzed cyclootrimerization of terminal alkynes and polymerization of MMA. *Chem. Commun. (Cambridge, U. K.)* **2006**, (19), 2066-2068.
51. Zhu, Z.; Wang, J.; Zhang, Z.; Xiang, X.; Zhou, X., Metallic Dysprosium Induced Silyl Radical Reactions: Intermolecular Cyclization and Reduction of Alkynes and Imines. *Organometallics* **2007**, 26, (10), 2499-2500.
52. Wong, K. T.; Bent, S. F., Pericyclic Reactions of Organic Molecules at Semiconductor Surfaces. In *Functionalization of Semiconductor Surfaces*, John Wiley & Sons, Inc.: 2012; pp 51-88.
53. Filler, M. A.; Mui, C.; Musgrave, C. B.; Bent, S. F., Competition and Selectivity in the Reaction of Nitriles on on Ge(100)-2.1. *Journal of the American Chemical Society* **2003**, 125, (16), 4928-4936.
54. Mui, C.; Filler, M. A.; Bent, S. F.; Musgrave, C. B., Reactions of Nitriles at Semiconductor Surfaces. *The Journal of Physical Chemistry B* **2003**, 107, (44), 12256-12267.
55. Glatter, O.; Kratky, O.; Editors, *Small Angle X-ray Scattering*. Academic Press: 1982; p 515 pp.
56. Pettigrew, K. A. Solution synthesis and characterization of silicon and silicon/germanium nanoparticles. Copyright (C) 2012 American Chemical Society (ACS). All Rights Reserved., 2004.

3 Application of “Click” Chemistry for Functionalization of Passivated Germanium Nanoparticles.

Surface atoms may play an important role compared to their bulk atoms in the optoelectronic properties of nanoparticles due to their enormous surface area-to-volume ratios.¹ Passivation of these surfaces are required to protect against chemical oxidation, as well as interparticle aggregation and Ostwald ripening. Further functionalization of those materials will not only provide intriguing properties like solubility or biocompatibility, but also may lead to numerous applications ranging from bioimaging, drug delivery and electronic devices.² In order to add additional functionality to the nanoparticles, alkyne-azide “click” chemistry could prove to be an efficient method for connecting various functional molecules to the passivated Ge NP surfaces.

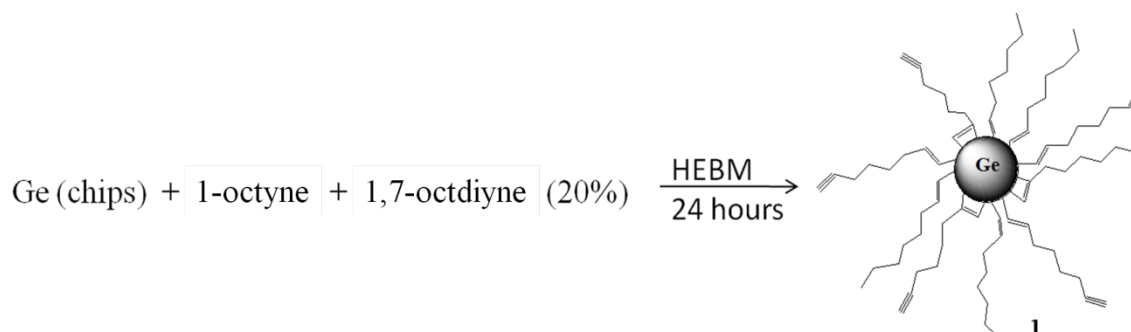


According to the concept of “click” reaction, the copper(I)-catalyzed alkyne-azide cycloaddition is the most efficient “click” reaction because of its selectivity and acceptance to mild and non-demanding reaction conditions.^{3, 4} The non-catalyzed alkyne-azide cycloaddition, the so called Huisgen 1, 3-dipolar cycloaddition, is a very slow non-selective reaction, and produces both 1,4 and 1,5-isomers of the 1,2,3-triazole; whereas the copper(I)-catalyzed alkyne-azide “click” reaction, a very fast chemoselective reaction, produces only the 1,4-isomer (Scheme 3.1) and it has a wide applications ranging from drug discovery to material sciences.⁵⁻¹⁰ Previously, alkyne-azide “click” chemistry has been used to functionalize gold nanoparticles,^{11, 12} metal oxide nanoparticles,^{13, 14} silica nanoparticles¹⁵ and silicon surfaces¹⁶⁻¹⁸. Most often silicon nanoparticles were passivated and functionalized via the hydrosilylation route.^{1, 19, 20} Kauzlarich and co-workers reported various functionalization of germanium nanoparticles using a variety routes.²¹ To date, an insignificant amount of work has been reported on functionalized germanium nanoparticles. Synthesis of those nanoparticles are more challenging as it requires high temperature, highly reactive reagents, and may require modification of hydrogen terminated surfaces. Further functionalization may not be possible on a moderate scale.

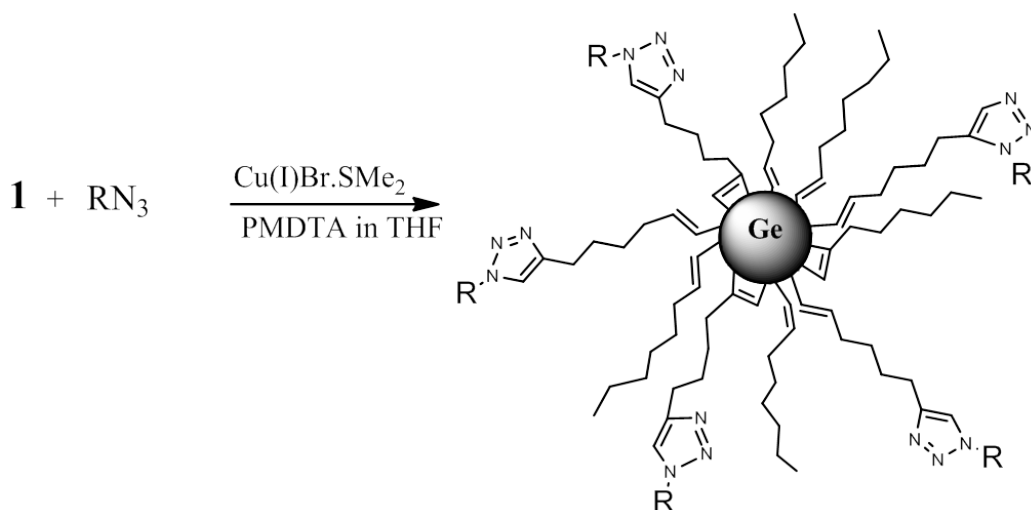
An ideal synthetic procedure would deal with synthesis, passivation and functionalization of germanium nanoparticles in a direct and efficient way under mild reaction conditions. We have synthesized passivated germanium nanoparticles by a direct top-down mechanochemical approach using high energy ball-milling (HEBM)²², followed by functionalization of those nanoparticles by various azides using the “click” reaction. In this chapter, we report an one pot production of alkenyl-passivated Ge

nanoparticles with terminal alkyne groups from bulk germanium and 1-octyne and 1,7-octadiyne by HEBM (**Scheme 3.2**). During this mechanochemical process, alkynes react with the fractured and fresh Ge surfaces to passivate them. In case of α, ω -bis-alkyne (i.e. 1,7-octadiyne), one carbon-carbon triple bond reacts with the surface and other remains on the periphery for further reactions. The purpose of using 1-octyne as a spacer ligand is to eliminate cross-linking between particles and to prevent "hair-pinning" of the 1,7-octadiyne.

Scheme 3.2: Passivation of Ge nanoparticles with 1-octyne and 1,7-octadiyne



Scheme 3.3: "Click" reaction of passivated Ge nanoparticles with various azides



Results and Discussion

3.2 Alkyne-terminated Germanium Nanoparticles

Alkyne-terminated Ge NPs (such as **1**) were synthesized using n-alkynes and α,ω -diynes (**Scheme 3.2**) from reactive ball-milling. Various surface coverage of terminal alkyne groups was achieved by changing diyne to n-alkyne ratios during ball-milling. Since the reagents, 1-octyne and 1,7-octadiyne, react at the Ge surfaces with nearly identical rates, and that the surrounding media is in excess relative to the surface, the surface coverage of the germanium reflects the composition of the alkynes in the solution. 20% alkyne-terminated (ω -alkynyloctenyl(20%)) Ge NPs may be prepared from a mixture whose mole fraction is 20% 1,7-octadiyne and 80% 1-octyne. To get higher coverages, such as like ω -alkynyloctenyl(50%) Ge NPs, we use shorter chain n-alkynes, e.g. 1-hexyne (50%) and 1,7-octadiyne.

Mechanochemically synthesized alkyne-terminated Ge NPs contain some aromatic impurities formed during high energy ball-milling via cyclotrimerization of alkynes which is discussed in detail in chapter 2. These molecular impurities may be removed by GPC using Bio-beads S-X1 as stationary phase and methylene chloride as an eluting solvent. Larger size nanoparticles elute earlier leaving molecular impurities which elute later. In addition, the synthesized polydispersed Ge NPs can be size separated and collected into various fractions. Earlier fractions contain larger particles and later fractions contain smaller particles.

The ^1H NMR spectra of ω -alkynyloctenyl(20%) Ge NPs in CD_2Cl_2 is shown in **Figure 3.2**. The peak at 2.2 ppm is assigned to the alkyne proton, the peak at ~ 1.9 ppm is

assigned to the CH₂ adjacent to the alkyne group. A peak at 0.8 ppm is due to methyl protons and broad peaks from 1.1 to 1.6 ppm are due to chain methylene protons. The ratio of the integration of the alkyne proton peak (at 2.2 ppm) and the CH₃ peak (at 0.8 ppm) is 2:11; which shows alkyne termination coverage is about 20-25%. The broadening of the alkyne peak makes the integration imprecise. The ¹³C{¹H} NMR spectrum also confirms the alkyne group showing resonances at 70 ppm and 85 ppm.

FT-IR spectrum (**Figure 3.3**) shows alkyne C-H stretching at 3300 cm⁻¹ and the ν(C≡C) at 2050 cm⁻¹.²³ Peaks from saturated C-H stretching range from 2850-3000 cm⁻¹ and peaks at 1375 and 1475 cm⁻¹ corresponds to C-H bending vibrations.²³ A broad peak from 700-900 cm⁻¹ is due to Ge-O stretching. The Ge-C stretching vibration comes usually ~690-750 cm⁻¹. The Ge-C stretch is typically seen at 830 cm⁻¹.^{24, 25} Klimov *et al* reported Ge-C stretch peak ~700 cm⁻¹ from their IR emitting Ge NCs. A sharp peak ~700 cm⁻¹ overlapping with Ge-O peak is due to Ge-C stretching.²⁶

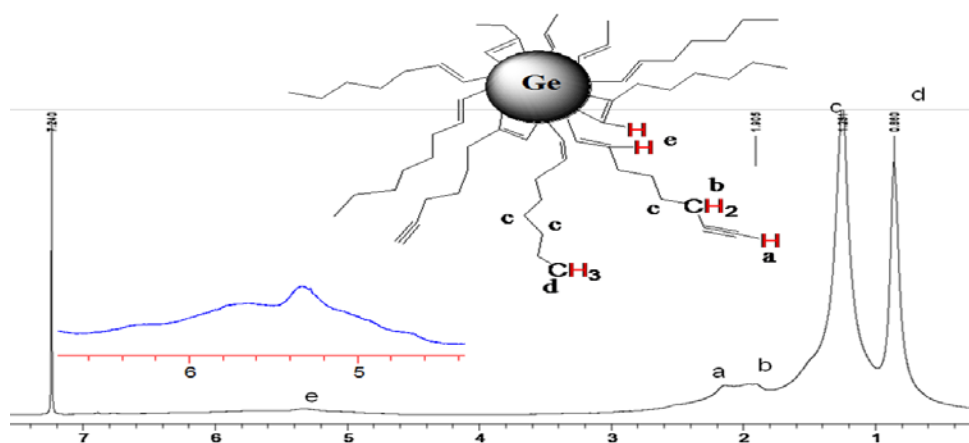


Figure 3.2 a: ¹H NMR spectra of ω-alkynyloctenyl(20%) Ge NPs.in CDCl₃.

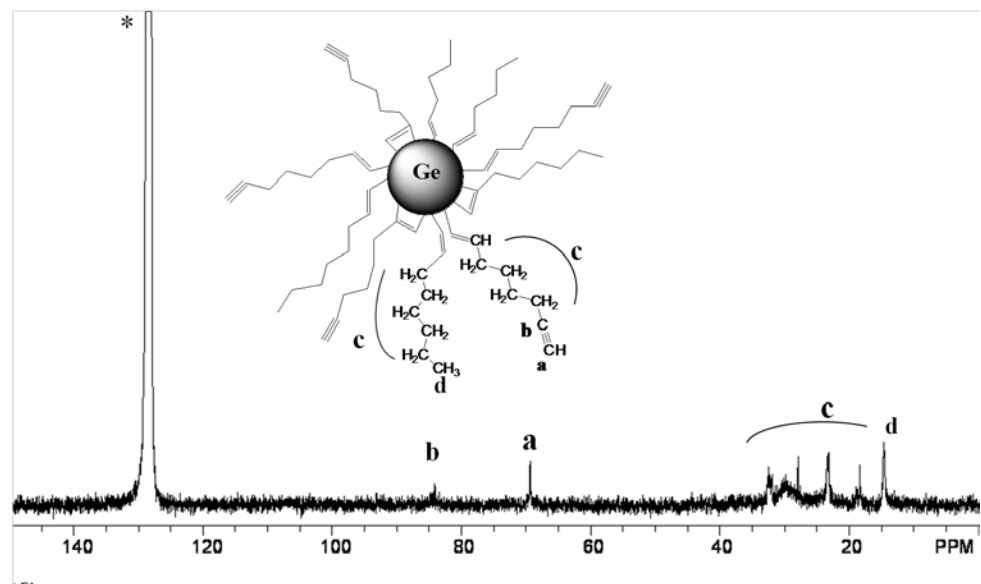


Figure 3.2 b: ^{13}C { ^1H } NMR spectra of ω -alkynyloctenyl(20%) Ge NPs in C_6D_6 .

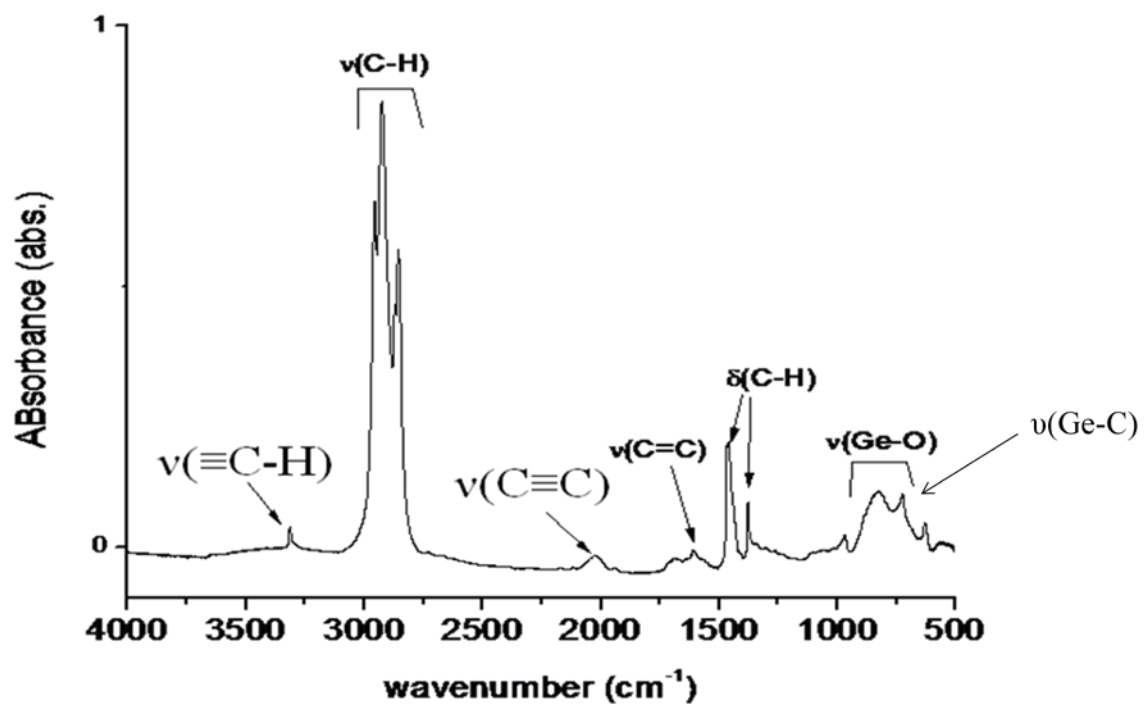


Figure 3.3: FTIR spectra of a thin film of ω -alkynyloctenyl(20%)-Ge NPs on KBr plate.

TEM images (**Figure 3.4**) of these ω -alkynyloctenyl(20%)-Ge NPs shows various particle sizes ranging from a few nanometers to 25 nanometers. Ge NPs were further size separated by GPC to obtain narrow size distribution. The TEM image (in Figure 3.6) of one of the earlier fractions shows larger size particles with narrow size distribution. Most of these particles are spherical, except for some large particles which are assymetric (Figure 3.5). This might be possible as too much strain induced in those particle during high energy ball milling. Lattice fringes from HRTEM images show that these particles are indeed crystalline. From the lattice fringes d-spacing was 3.3 Å which is from the Ge(111). Selected area electron diffraction (SAED) shows various dots from various planes including Ge(111), Ge(211) and Ge(311). Some d-spacing are different than the Ge diamond structure. This may also due to the strain induced during HEBM. EDX spectra show a very sharp peaks at 1.2 keV (for Ge $L\alpha$), two other peak at 9.9 keV (for Ge $K\alpha$) and 11 keV (for Ge $K\beta$), confirming the presence of Ge.

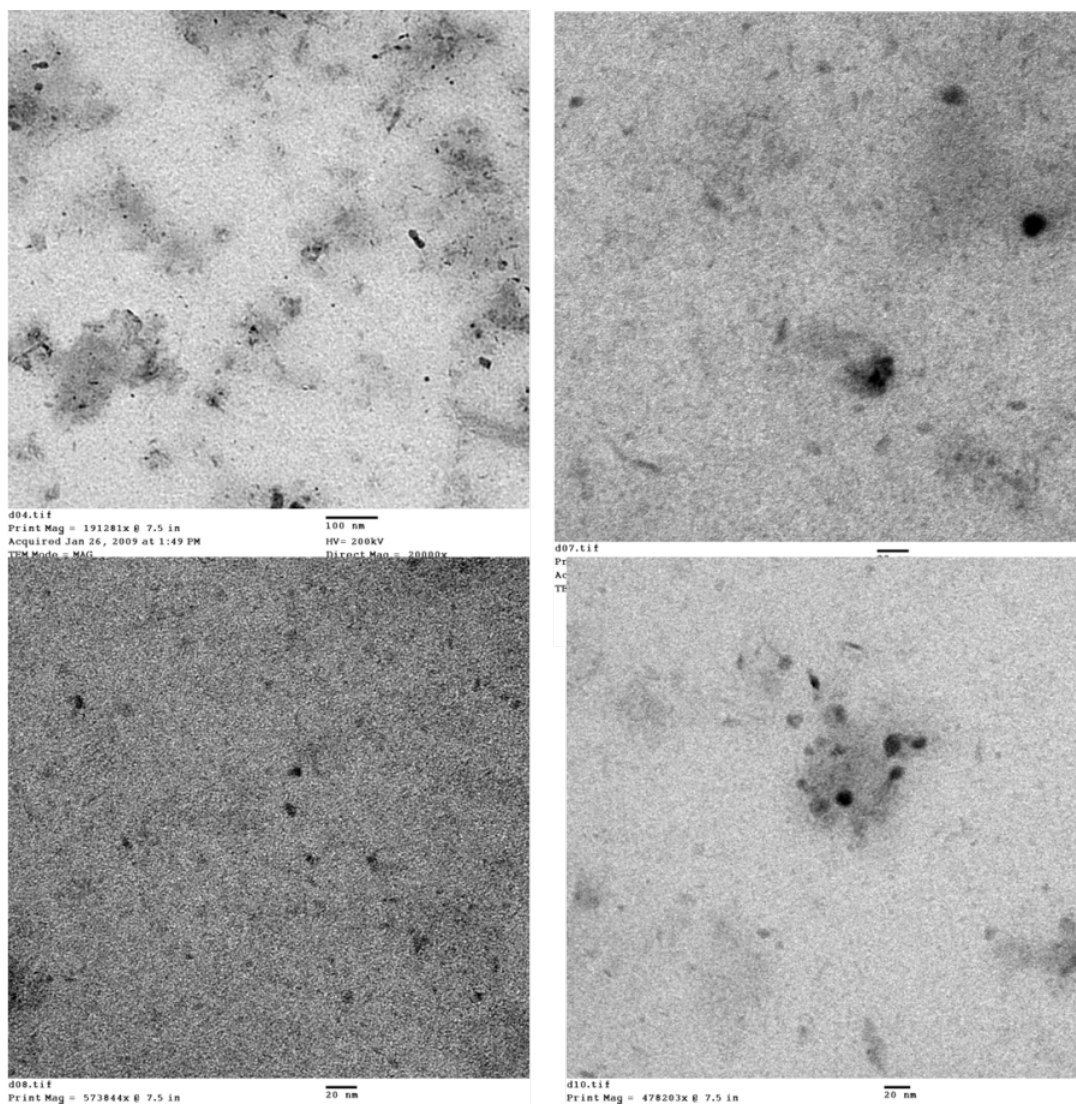


Figure 3.4: TEM images of alkyne-terminated (ω -alkynyloctenyl (20%)) Ge nanoparticles.

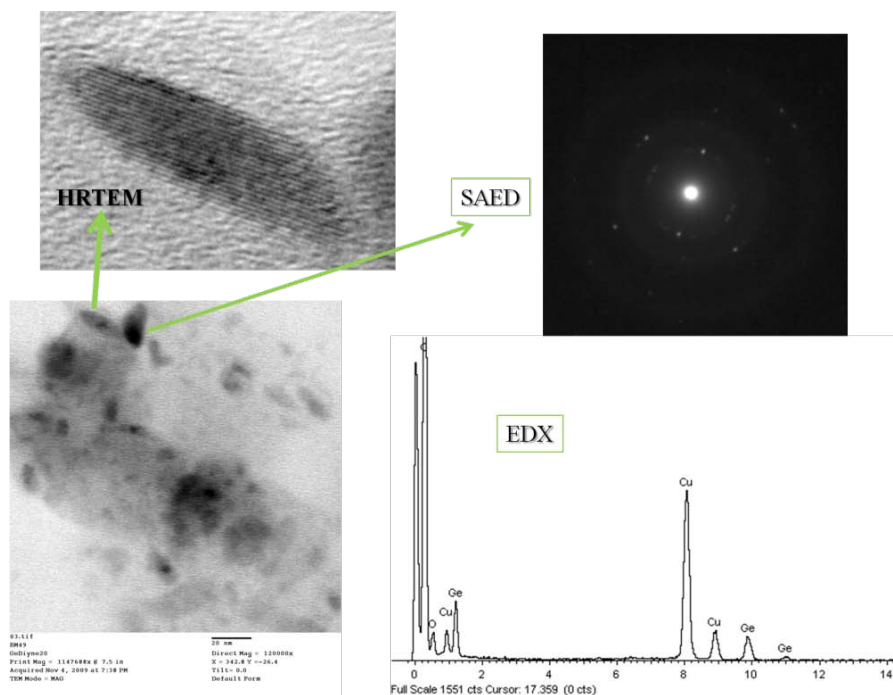


Figure 3.5: HRTEM images, SAED and EDX of non spherical alkyne-terminated (ω -alkynyloctenyl(20%)) Ge nanoparticles.

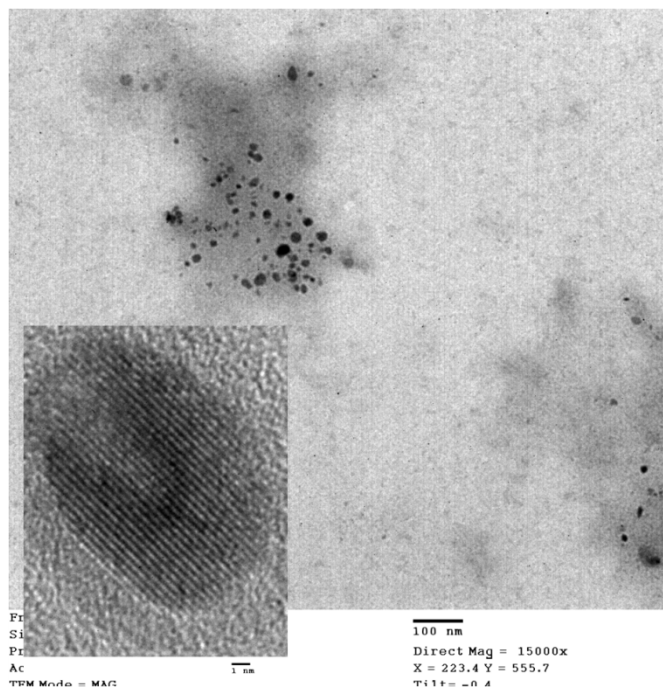


Figure 3.6: TEM images of GPC size separated alkyne-terminated (ω -alkynyloctenyl(20%)) Ge NPs.

The UV-Vis spectrum of ω -alkynyloctenyl(20%) Ge NPs in dichloromethane (**Figure 3.7**) shows a featureless absorbance which decreases with increasing wavelength with a tail which extends up to 500 nm. The shape of the spectrum is consistent to with an indirect band gap semiconductor absorbance. Broad PL emission spectra obtained under various excitation wavelengths ranging from 300 nm to 420 nm. With increasing excitation wavelength, the PL emission maxima were found to shift to longer wavelength. Though the origin of photoluminescence is a matter of debate, it can originate from a quantum confinement effect. The broad PL spectra indicate that we have various sizes nanoparticles in the solution and the red shift in emission wavelengths is consistent with the excitation of population of increasingly larger nanoparticles.

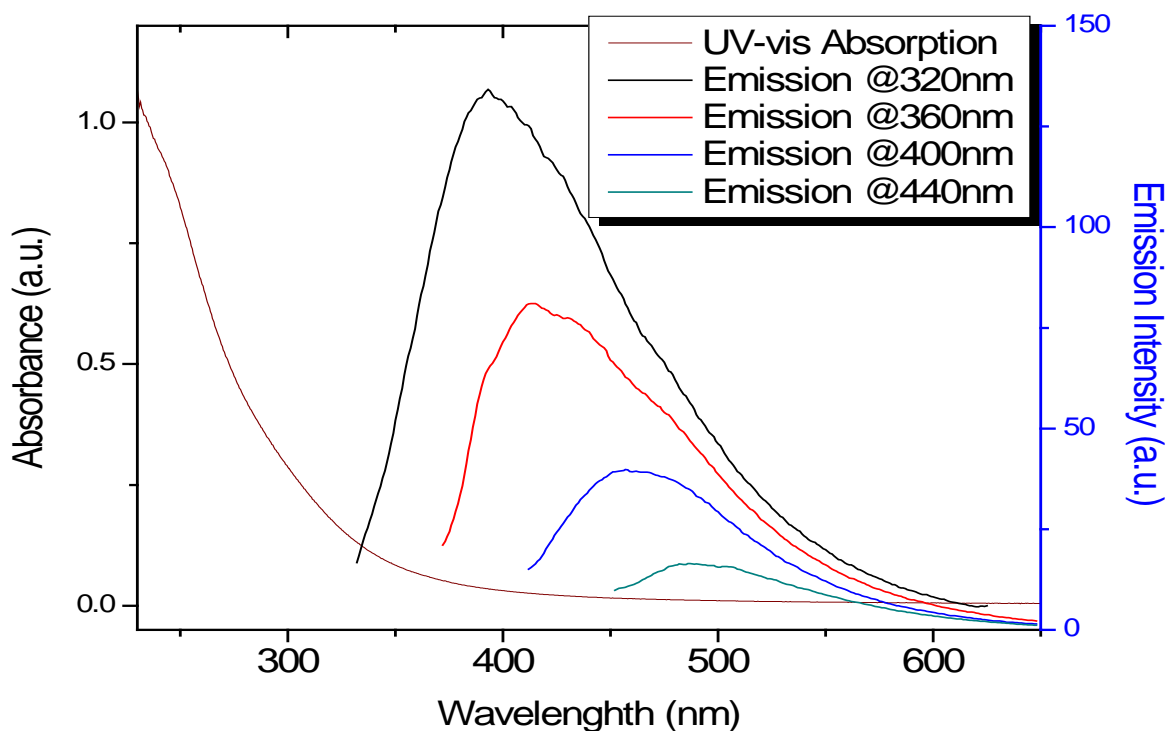


Figure 3.7: UV-Vis absorption spectra and emission spectra of ω -alkynyloctenyl(20%) Ge NPs.

3.3 The Grafting of Organic and Organometallic Molecules to the Alkyne-Terminated Ge Nanoparticles using “click” Chemistry

Mechanochemically synthesized Ge NPs were functionalized by copper(I) catalyzed alkyne azide “click” chemistry using various organic azides (i.e. TMSN₃, 2-ethylazido acetate etc), organometallic azides (i.e. ferrocenylpropylene azide) and biomolecules (i.e. glycosylazides).

The copper catalyzed (2+3) dipolar cycloaddition reaction was applied to alkyne terminated Ge NPs using commercially available small organic azides and trimethylsilyl azide. Alkyne-terminated (ω -alkynyloctenyl (20%)) Ge NPs in THF and TMSN₃ undergo “click” reaction in presence of copper(I) catalyst in room temperature to give TMS-grafted Ge NPs in 70% yield (by weight). **Figure 3.8** shows the ¹H NMR spectrum of TMS-azide grafted Ge NPs by the “click” reaction. A peak ~0.1 ppm is due to TMS-protons and a peak at 2.4 ppm is due to methylene protons connected to the triazole ring. (It is shifted from 1.8 ppm as methylene protons were connected to alkyne group). The disappearance of the alkyne proton at 2.2 ppm was observed. The triazole proton was seen at 7.4 ppm when nmr solvent changed from CDCl₃ to CD₂Cl₂.²⁷ In CD₂Cl₂ spectra other impurities peaks are evident.

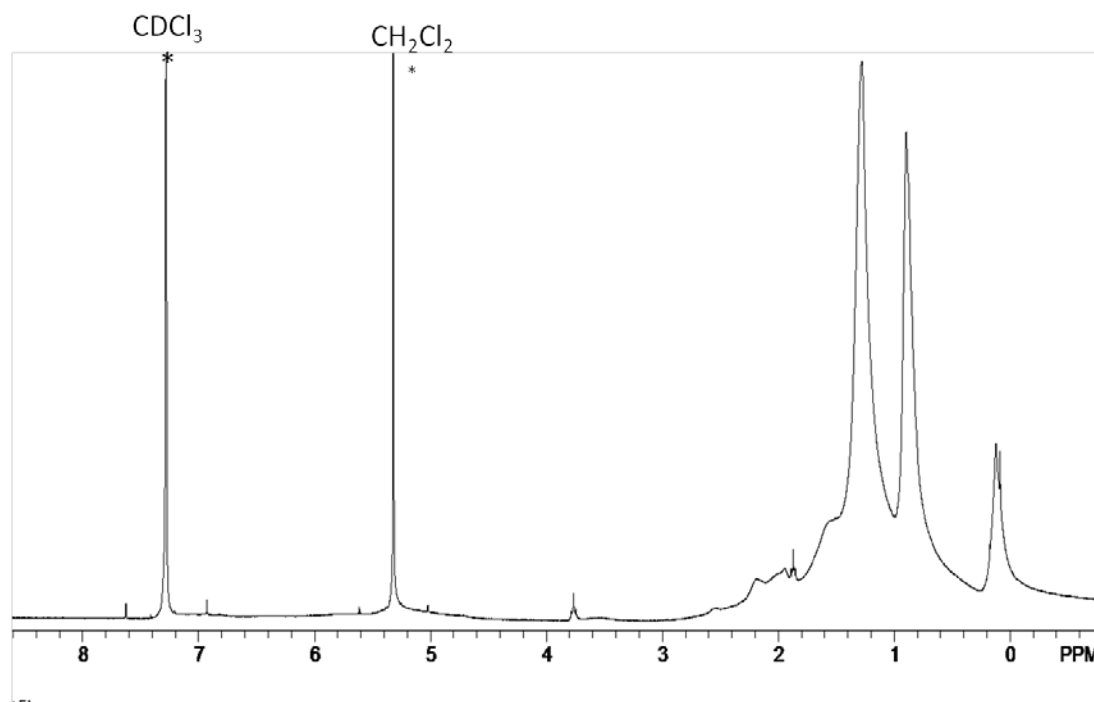


Figure 3.8: 1H NMR spectra of $TMSN_3$ grafted Ge NPs in $CDCl_3$

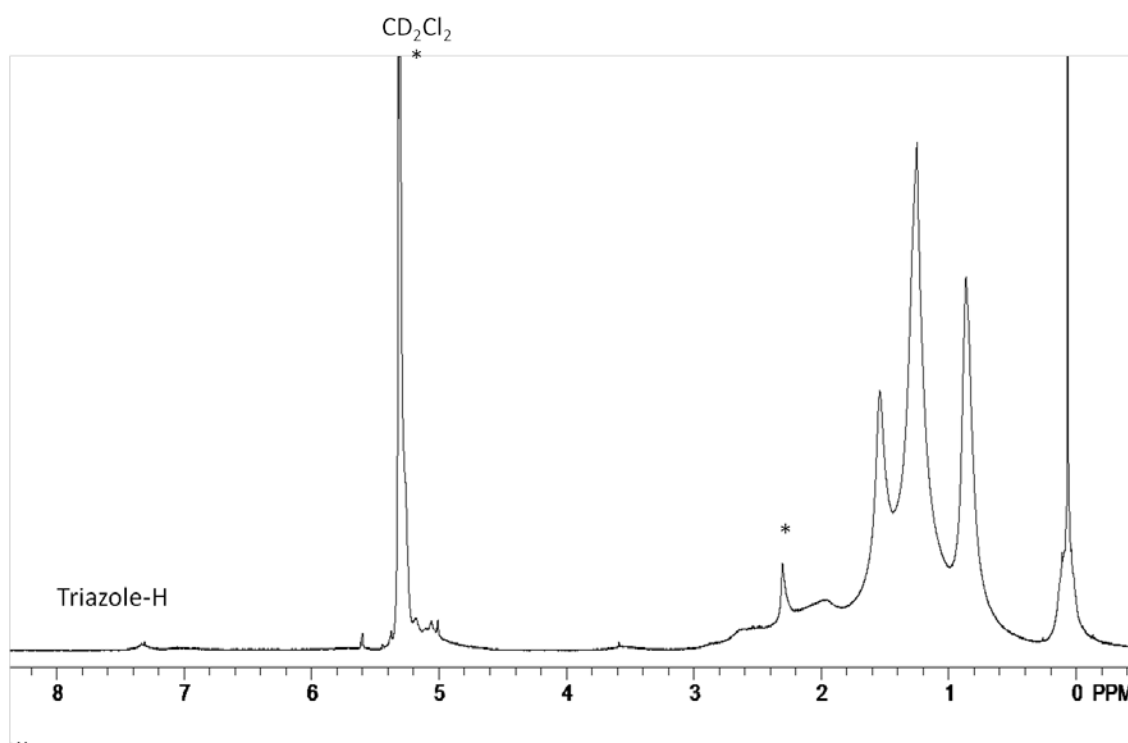


Figure 3.8 b: 1H NMR spectra of $TMSN_3$ grafted Ge NPs in CD_2Cl_2

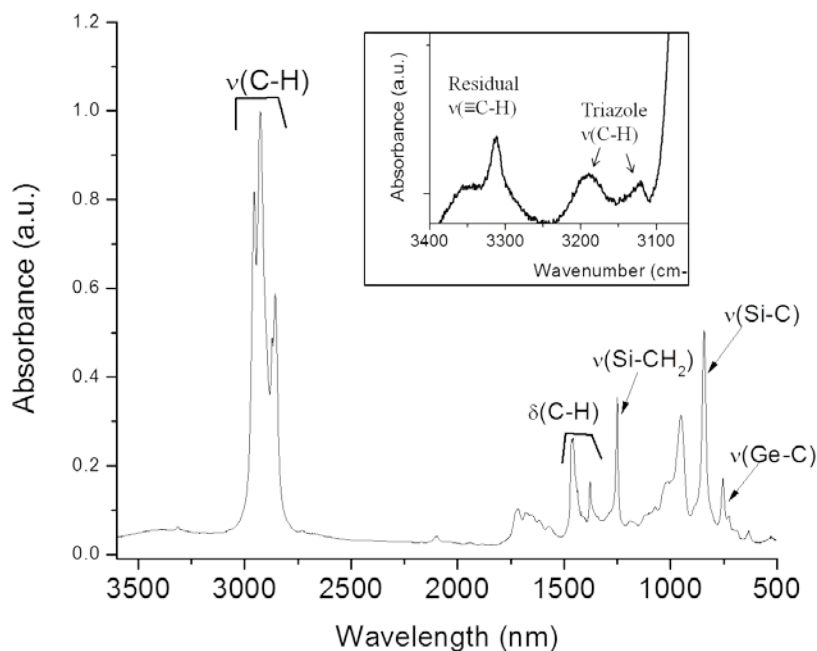


Figure 3.9: FT-IR spectra of TMSN₃ grafted Ge NPs taken on KBr plate.

3.3.1 Benzyl azide – grafted germanium nanoparticles

Benzyl groups were grafted on Ge NPs by the alkyne-azide “click” reaction with benzyl azide and alkyne-terminated Ge-NPs. The aromatic benzyl group was confirmed by ¹H NMR and FT-IR spectra. In the FT-IR spectrum (in figure 3.10) a new tiny peak was seen at 3138 cm⁻¹ due to C-H stretching from the triazole ring, which formed during “click” reaction. Aryl ν(C-H) from the benzyl group appeared at 3068 cm⁻¹. A broad peak at around 1600 cm⁻¹ is due to aromatic ν(C=C). Saturated C-H stretching was seen around 2850-3000 cm⁻¹. Two sharp peaks at 1375 and 1465 cm⁻¹ are observed due to (C-H) bending.

Figure 3.11 shows the ^1H NMR spectrum of the benzyl grafted Ge NPs. A broad peak at 0.8 ppm is due to methyl protons from the chain of the octenyl group on Ge surface. Alkyl chain methylene protons appear in the range of 1.2 to 1.5 ppm. A sharp peak at 1.5 ppm was observed due to residue solvent (H_2O or HOD) peak in the NMR solvent. Aromatic protons in the benzyl group and the triazole peak appear at 7.2-7.4 ppm.

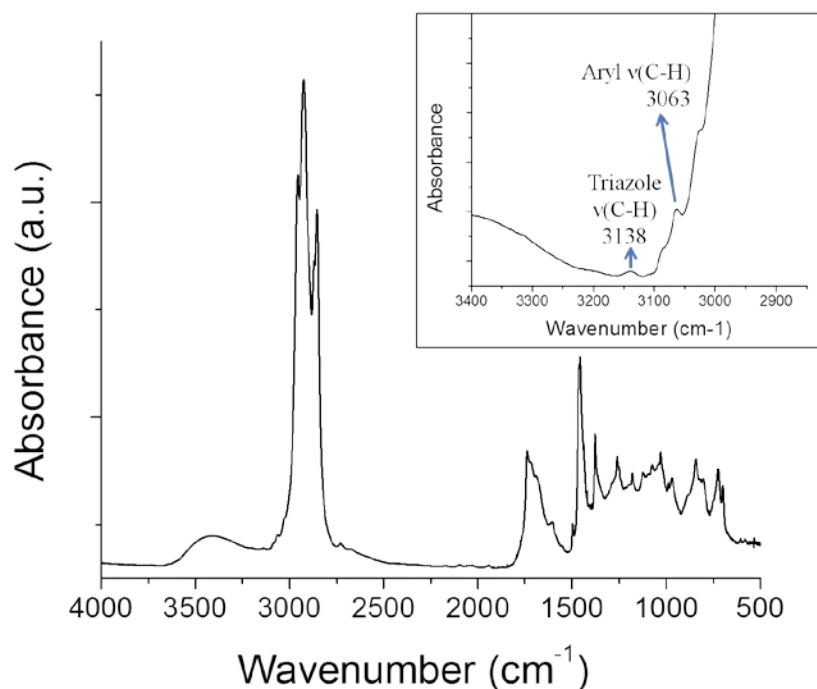


Figure 3.10: FT-IR spectrum of PhCH_2N_3 grafted Ge NPs.

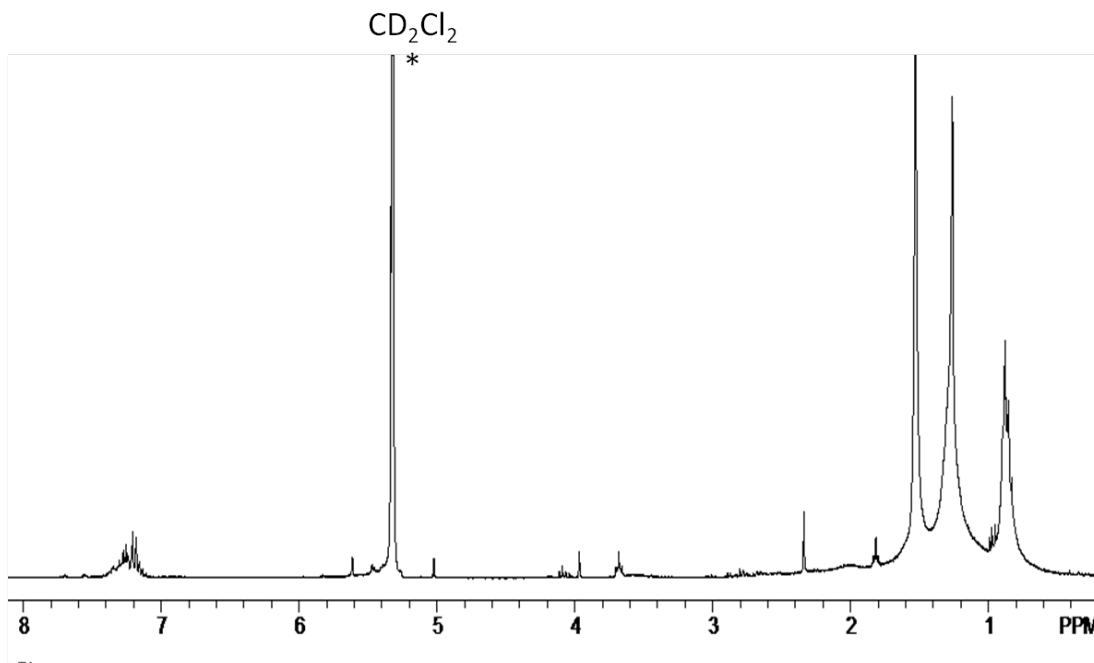


Figure 3.11: ^1H NMR spectra of PhCH_2N_3 grafted Ge NPs in CD_2Cl_2 .

In the FT-IR spectrum (Figure 3.9), the peak at 3300 cm^{-1} is greatly diminished. Typical, a triazole $\nu(\text{C-H})$ can be seen at $3180\text{--}3050\text{ cm}^{-1}$. A small broad peak $\sim 3180\text{ cm}^{-1}$ is due to the triazole C-H stretching. Two new sharp peaks at 1250 cm^{-1} and $\sim 800\text{ cm}^{-1}$ are due to Si- CH_2 stretching and Si-C stretching vibration respectively. After the “click” reaction, the Ge-O peak decreases and the Ge-C peak $\sim 750\text{ cm}^{-1}$ is now prominent.

3.3.2 Ester moiety grafted Ge NPs.

Ester functionalized Ge NPs were prepared by alkyne azide “click” reaction using alkyne terminated Ge NPs and 2-ethylazido acetate. The products were purified by dialysis using a RC dialysis membrane (MWCO 1kDA). The ester moiety on the nanoparticles was confirmed by the FT-IR spectrum (in **Figure 3.13**), which shows a new peak at 1750 cm^{-1} for $\nu(\text{C=O})$ stretching and at 1210 cm^{-1} for $\nu_s(\text{C-CO-O})$ and at $\sim 1100\text{ cm}^{-1}$ for $\nu_s(\text{C-O})$. A new peak at 3150 cm^{-1} is due to triazole proton. The saturated $\nu_s(\text{C-})$

H) was observed from 2850-3000 cm^{-1} and $\delta(\text{C-H})$ bending was seen at 1465 and 1375 cm^{-1} . The $\nu_s(\text{Ge-C})$ was seen at 740 cm^{-1} as prominent peak compare to that of the starting alkyne terminated Ge NPs due to reduction of germanium oxide during reaction.

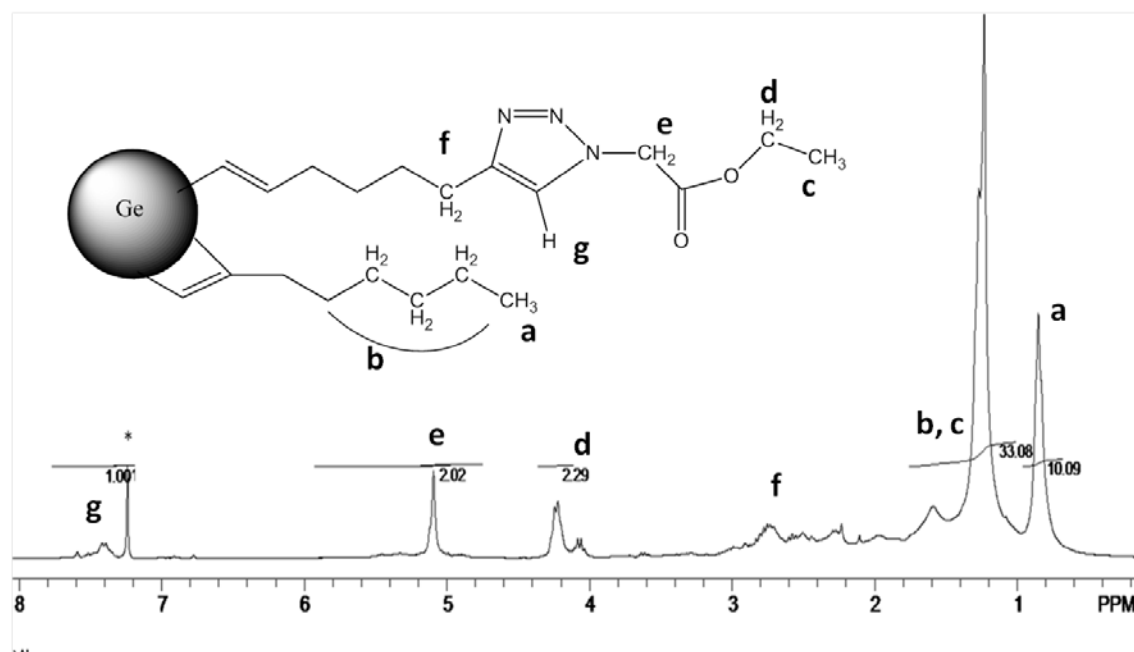


Figure 3.12: ^1H NMR spectra of ethylazido acetate grafted Ge NPs in CDCl_3 .

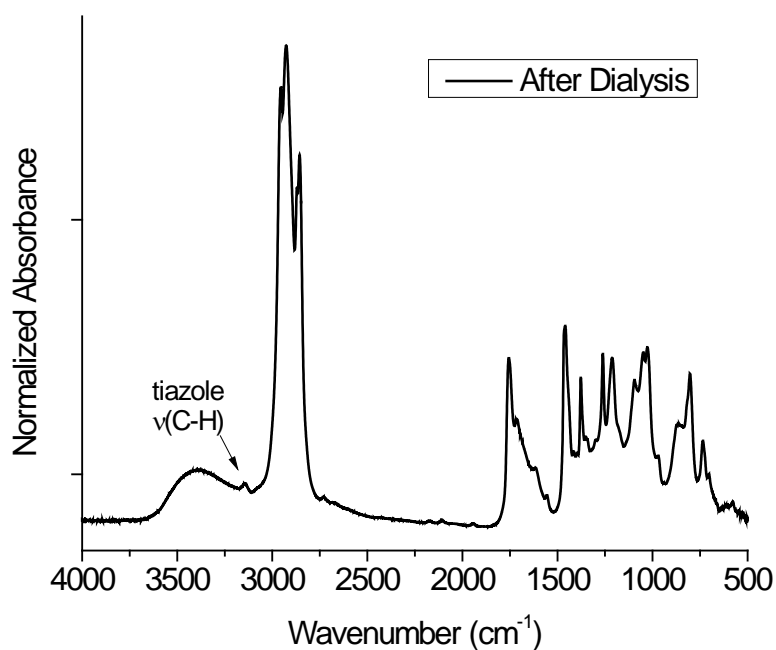


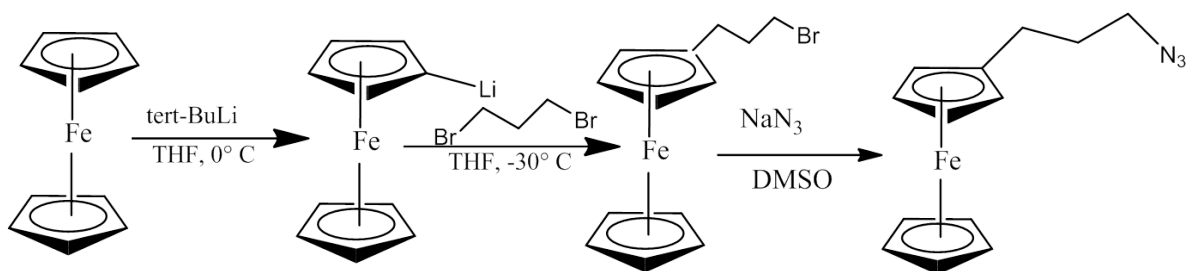
Figure 3.13: FT-IR spectra of 2-ethylazido acetate grafted Ge NPs on KBr plate

The ^1H NMR spectrum (**Figure 3.12**) of the purified product shows a similar broad peak at 0.8 ppm for terminal methyl protons from the alkyl chain and broad and multiplet peaks from 1.2 ppm to 1.4 ppm for alkyl chain methylene protons. Methyl protons from the ester should show a peak ~ 1.2 ppm; which overlapped with the the chain methylene protons peak. A peak at 4.2 ppm is due the methylene protons of ester. A weak and broad peak at 7.4 ppm is due to triazole proton resonance.²⁷ Integration of triazole proton to ester methylene protons and alkyl chain methyle protons was found to be 1:2:11, which shows a ester surface coverage is 21%.

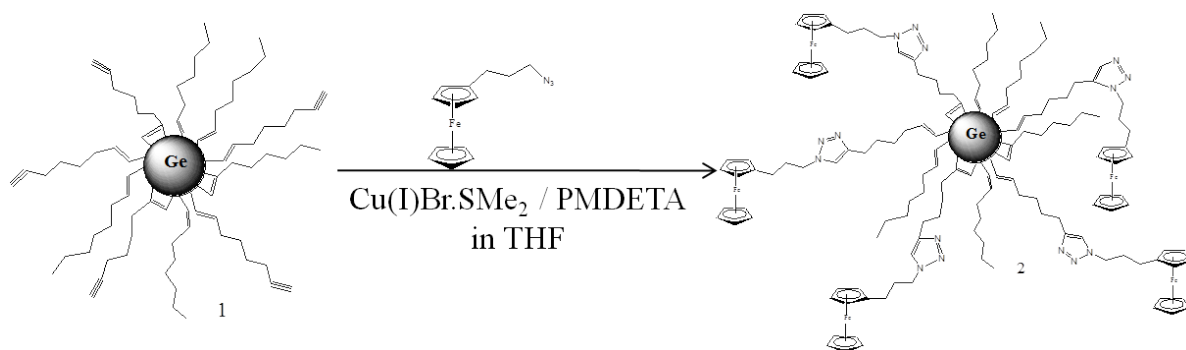
3.3.3 *Ferrocene grafted Ge NPs.*

Growing interest in synthesizing electrochemically active ferrocene-moiety grafted materials is due to their unique redox and catalytic properties, as well as good electrochemical responses.^{28, 29} Previously ferrocene moiety was covalently grafted on Si surfaces and carbon nanofiber by copper(I) catalyzed “click” chemistry^{16, 17, 30, 31}.

The ferrocene moiety was grafted on to the germanium nanoparticle surface by a click reaction between synthesized ferrocenyl propylene azide and alkyne terminated Ge NPs. Ferrocenyl propylene azide was synthesized starting from ferrocene via Scheme 3.3. Ferrocenyl propylene bromide was synthesized from nucleophilic substitution reaction of a monolithiated ferrocene and 1,3-dibromopropane. Ferrocenylpropylene azide was synthesized from its bromo derivative by azidation. Bromo and azido derivatives were fully characterized by GCMS, FT-IR, ^1H NMR and $^{13}\text{C}\{^1\text{H}\}$ NMR spectra.



Scheme 3.3: Synthesis of ferrocenyl propylene azide from ferrocene.



Scheme 3.4: Synthesis of ferrocene-grafted Ge NPs..

The ^1H NMR spectrum of ferrocene grafted Ge NPs is shown in the Figure 3.14. A prominent peak at 4.1 ppm in the NMR spectra of the purified products is due to ferrocene protons and a broad peak ~ 7.3 ppm is due to triazole aromatic proton.²⁷ A peak at 2.4 ppm is due to CH_2 protons neighboring to the ferrocene moiety. Methylene protons connected to the triazole ring were assigned at ~ 3.7 ppm. Similar to starting alkyne terminated Ge NPs peaks at 0.8 ppm and peaks from 1.2 ppm to 1.6 ppm are due to chain methyl and methylene protons respectively. Residual water in the NMR solvent (CD_2Cl_2) comes at 1.5 ppm and overlap with methylene protons' peak.

Although the ^1H NMR spectrum shows two distinct peaks for triazole and ferrocene aromatic protons, both aromatic C-H str can be seen in the range of 3050-3150 cm^{-1} in the FT-IR spectrum (**Figure 3.15**). A peak at 3090 cm^{-1} is due to a ferrocene

aromatic $\nu(\text{C-H})$ stretch and it appears in the same position as the starting ferrocenylazide. Another weak peak was seen at 3035 cm^{-1} due to triazole $\nu(\text{C-H})$. A prominent peak at $\sim 1600\text{ cm}^{-1}$ was seen after the "click" reaction due to the ferrocene $\nu(\text{C}=\text{C})$.

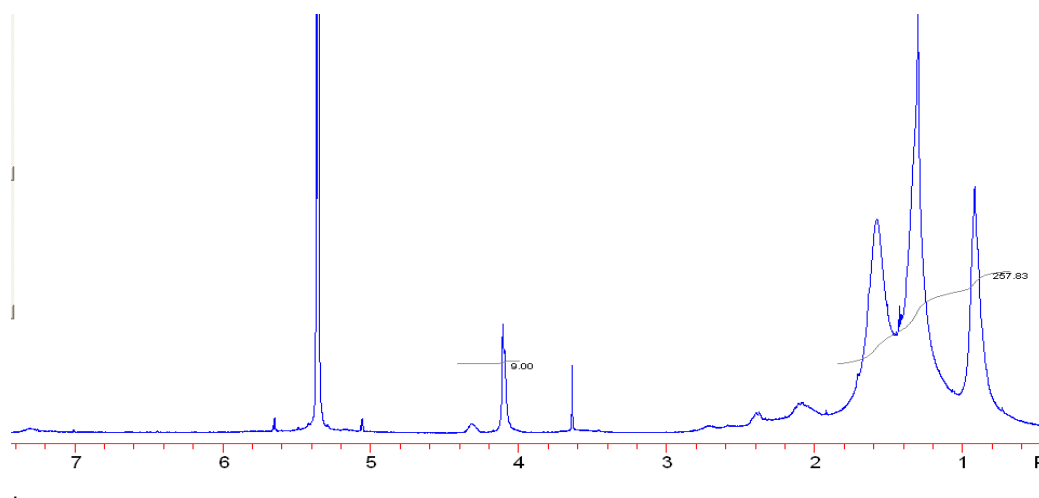


Figure 3.14: ^1H NMR spectra of ferrocene-moiety grafted Ge NPs in CD_2Cl_2 .

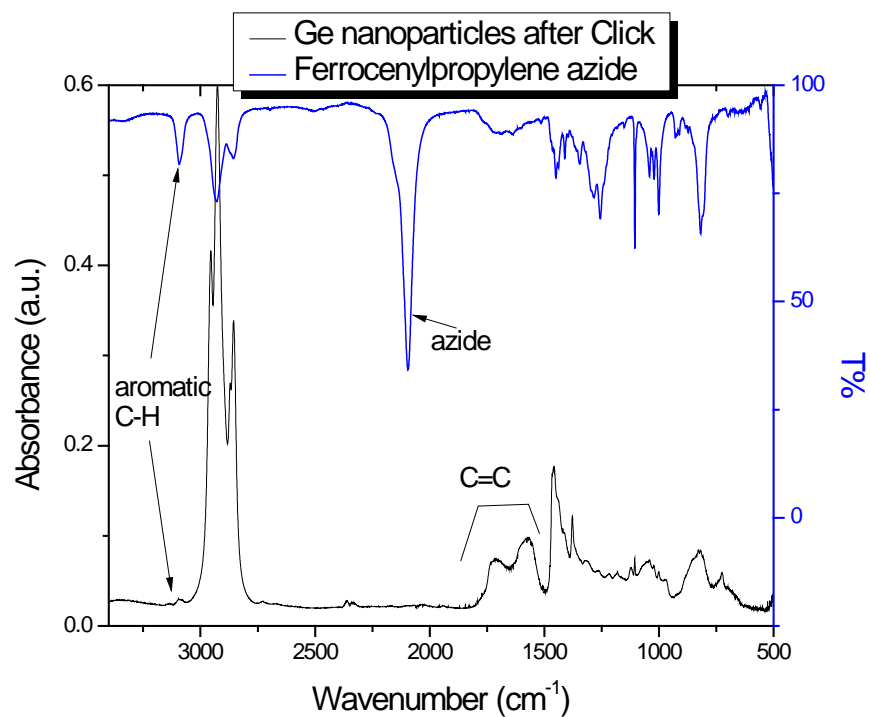


Figure 3.15: FT-IR spectra of ferrocene-moiety grafted Ge NPs.

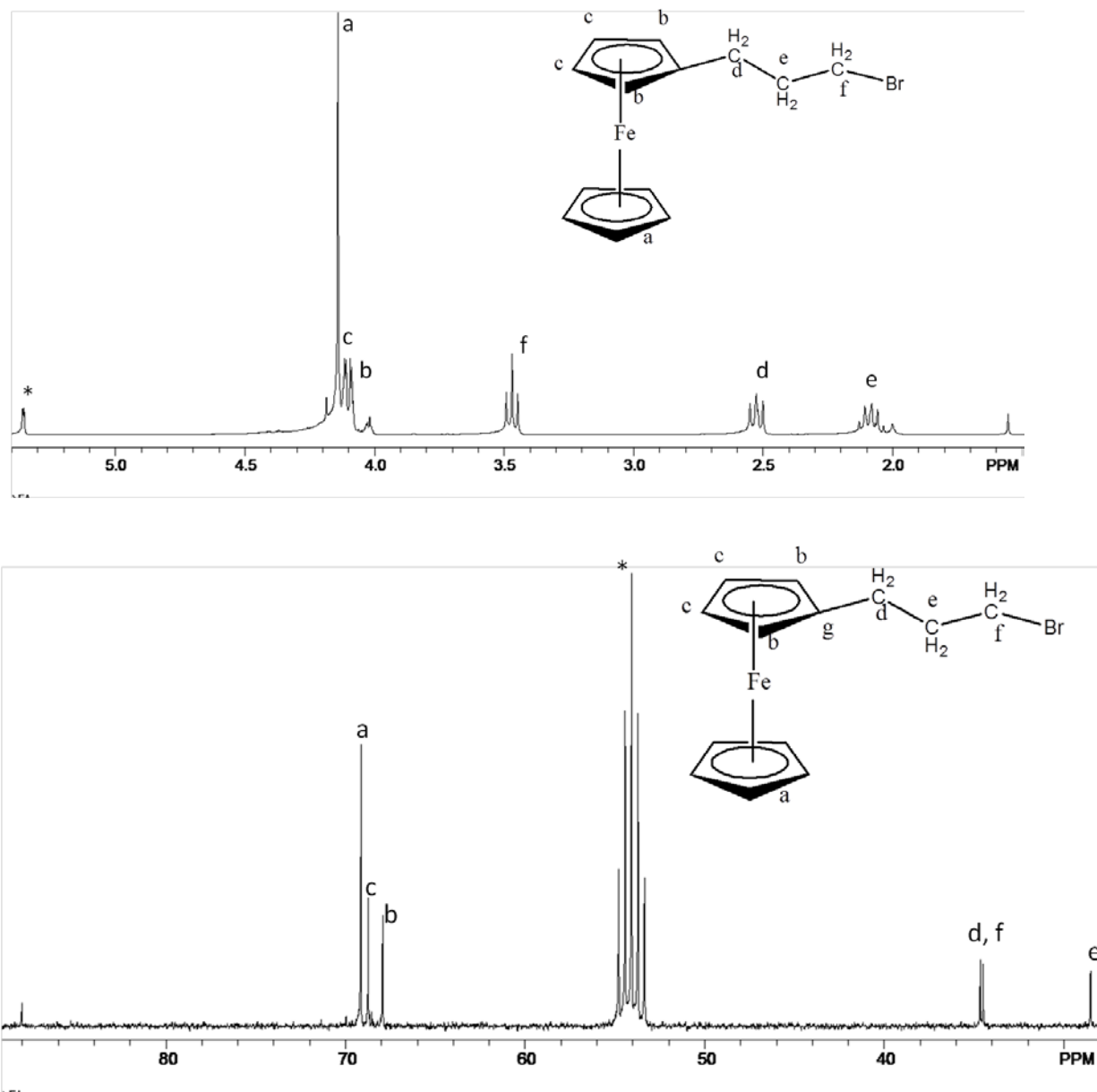
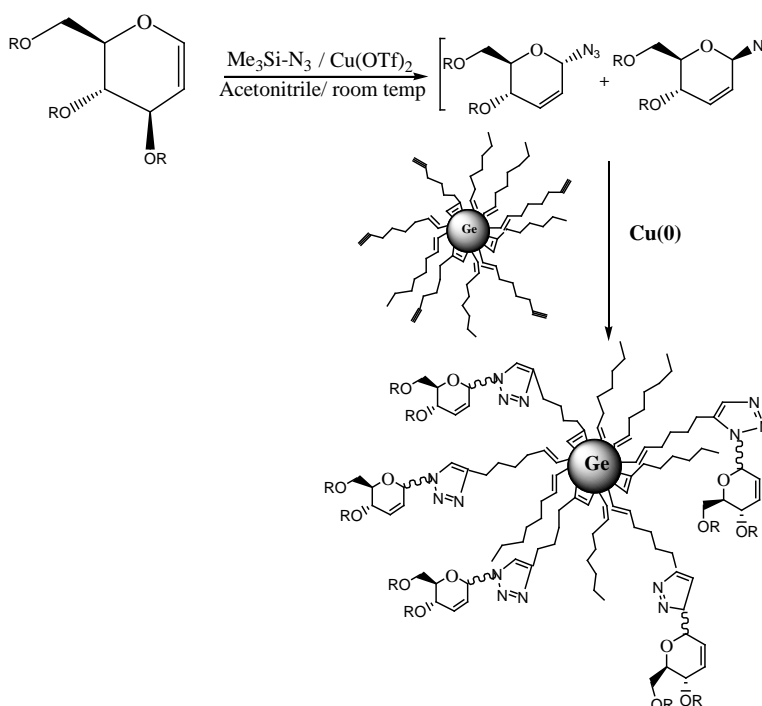


Figure 3.16: ^1H NMR (a) and ^{13}C NMR (b) spectra of ferrocenylpropylene bromide.

3.3.4 Glucal-grafted Ge NPs

Glucals, the glycals formed from sugars, are 1,2-unsaturated derivatives of hexoses; which are very important biomolecules as they exhibit a versatile reactivity due to their cyclic enol ether functionality.^{32, 33} One of the most important chemistries of glycals is the Ferrier rearrangement which involves a nucleophilic substitution followed by an allylic shift to form 2,3-unsaturated glycoside in presence of a Lewis acid-catalyst^{34, 35}.

We use a direct one-pot method, a tandem Ferrier rearrangement and “click” reaction, to graft glucals on the Ge NPs from commercially available D-glucals and TMSN₃.³⁶ Glycosylazides, prepared in situ from glucal derivatives and TMSN₃ via Ferrier rearrangement, followed by an alkyne-azide “click” reaction with alkyne-terminated Ge NPs to have triazole-linked glycoconjugates functionality on the nanoparticles (**Scheme 3.4**).



Scheme 3.5: One pot synthesis of glucal-grafted Ge NPs.

The Ferrier reaction was performed in presence of a Lewis acid catalyst, copper (II) triflate, in acetonitrile with an excess of TMSN_3 . Excess TMSN_3 and CH_3CN were removed by vacuum and nanoparticle solution in THF, followed by excess copper (0) wire added to the crude glycosylazides. $\text{Cu}(0)$ would reduce $\text{Cu}(\text{II})$ in solution to form an active “click” catalyst $\text{Cu}(\text{I})$ in the solution. After the reaction, the glucal grafted Ge NPs were purified by dialysis using a dialysis membrane (MWCO 1kDa). These nanoparticles show enhanced solubility in organic solvents including alcohols.

The ^1H NMR spectrum of tri-O-acetyl glucal grafted Ge NPs is shown in Figure 3.17. The methyl and methylene protons from the alkyl chain were assigned at 0.8 ppm and 1.2-1.4 ppm. Broad peaks at 2 ppm and ~4.2 ppm are due to acetyl methyl protons and sugar C-H backbone protons. A weak peak at ~6.2 ppm is due to glucal's vinyl protons. A triazole resonance was seen at 7.5 ppm as a very weak tiny peak.²⁷ On the other hand, tri-O-benzyl glucal grafted Ge NPs shows a significant broad and intense peak ~7.3 ppm due to benzene ring protons and triazole proton might overlap with the broad benzene ring peak. Methylene protons neighboring to benzene ring were seen at ~2 ppm as a broad peak.

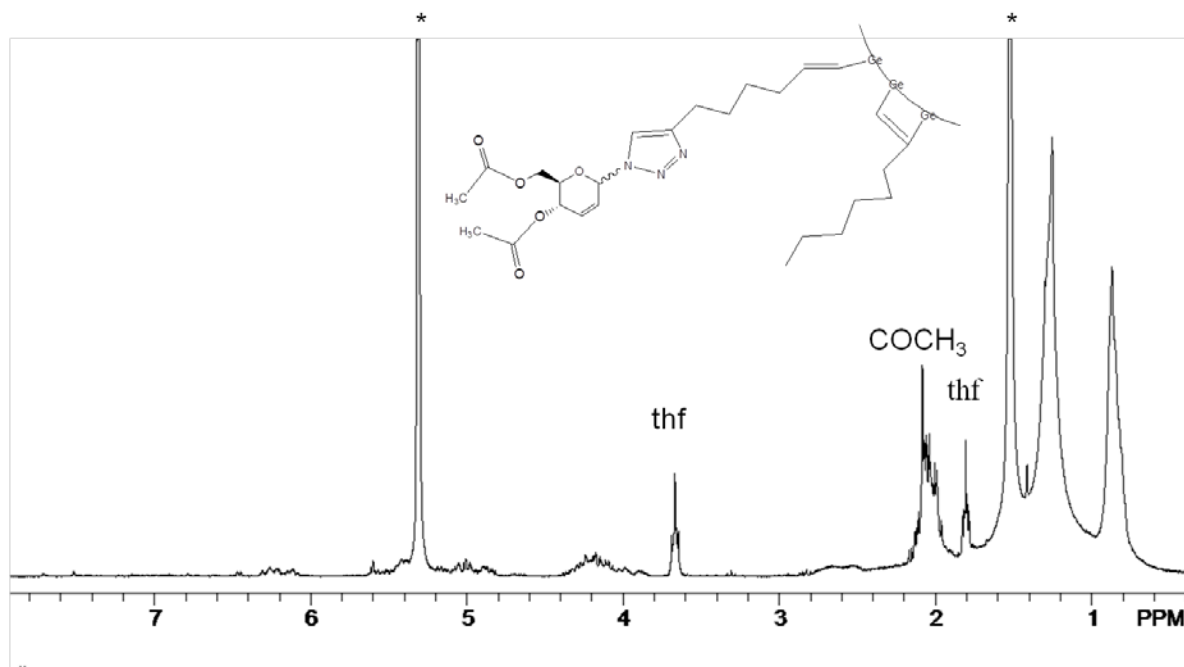


Figure 3.17: ^1H NMR spectra of tri-O-acetyl glucal grafted Ge NPs.

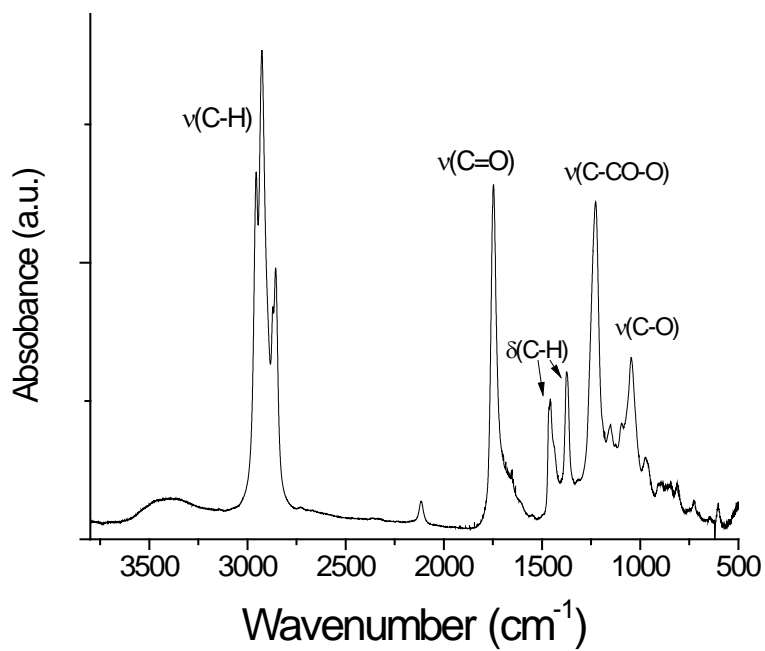


Figure 3.18: FT-IR Spectrum of tri-O-acetyl glucal grafted Ge NPs.

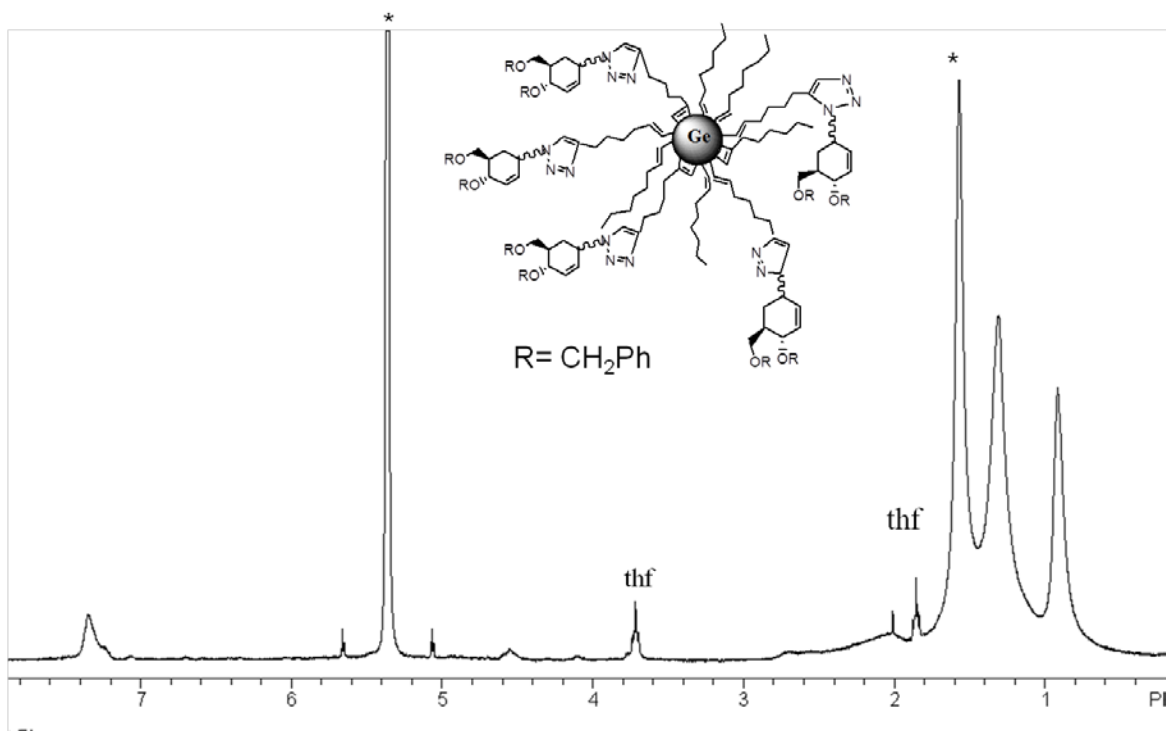


Figure 3.19: ^1H NMR Spectra of tri-O-benzyl glucal grafted Ge NPs.

In the FT-IR spectrum of tri-O-acetyl glucal grafted Ge NPs, the $\nu(\text{C}=\text{O})$ str and $\nu(\text{C}-\text{CO}-\text{O})$ str were seen at 1750 cm^{-1} and 1226 cm^{-1} respectively. A peak at 1045 cm^{-1} is due to $\nu(\text{C}-\text{O})$ str. $\nu(\text{C}-\text{H})$ str and $\delta(\text{C}-\text{H})$ bending were unchanged compare to starting Ge NPs. A residual $\nu(\text{N}_3)$ stretching peak was seen $\sim 2100\text{ cm}^{-1}$, which suggest a small amount of glycosylazide present in the product.

3.3.5 Optical properties of functionalized Ge NPs

Mechanochemically synthesized alkyne-terminated Ge NPs show blue luminescence similar to TMSA-passivized Ge NPs. The optical properties of the functionalized Ge NPs, after “click” reaction do not differ significantly from the optical properties starting alkyne-terminated particles.

Figure 3.20 shows the UV-vis absorption spectra in CH_2Cl_2 of various functionalized particles. The absorption plots are very similar to the starting Ge NPs except for the ester-grafted-Ge NPs. and ferrocene-grafted (Ge-Fc). The ester grafted Ge NPs shows a shoulder at ~ 300 nm in UV-vis absorption spectra. On the other hand the GeFc NPs show some features at lower wavelengths similar to pure ferrocene, though it is not prominent. However, 10%, 20% surface coverage of functional group is not enough to change the optical properties of the Ge NPs.

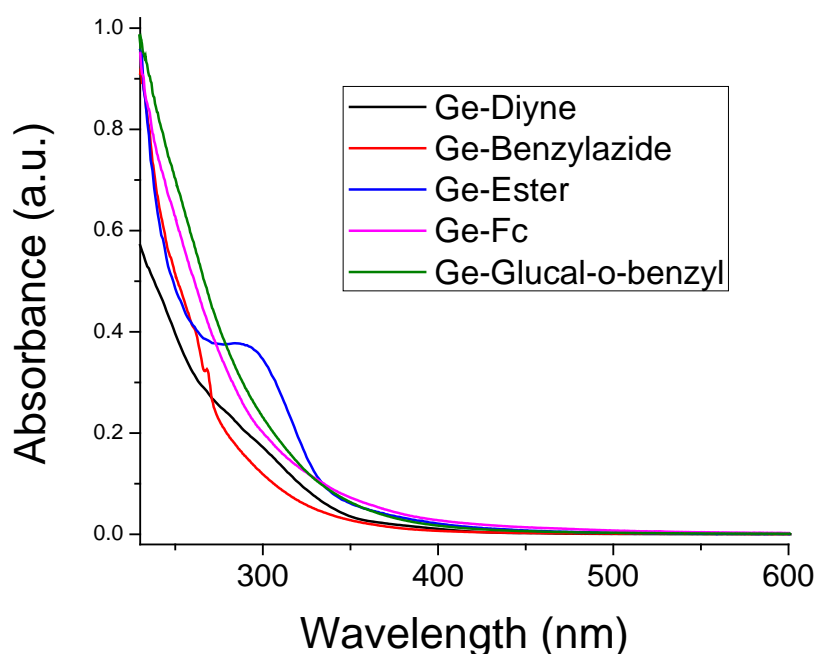


Figure 3.20: UV-vis absorption spectra of the functionalized Ge NPs in CH_2Cl_2 .

PL emission spectra of various functionalized Ge NPs wavelength show a comparison of emission with initial alkyne terminated Ge NPs (Ge alkyne). Emission peaks of most functionalized particles at 300 nm excitation remain unchanged, except for the ferrocene and glucal-grafted Ge NPs. The ferrocene-grafted Ge NPs show a blue shift, while the glucal-grafted Ge NPs show a red shift in the emission spectra at 300 nm excitation wavelength. However, at longer excitation wavelength (380 nm), the emission peaks do not differ much.

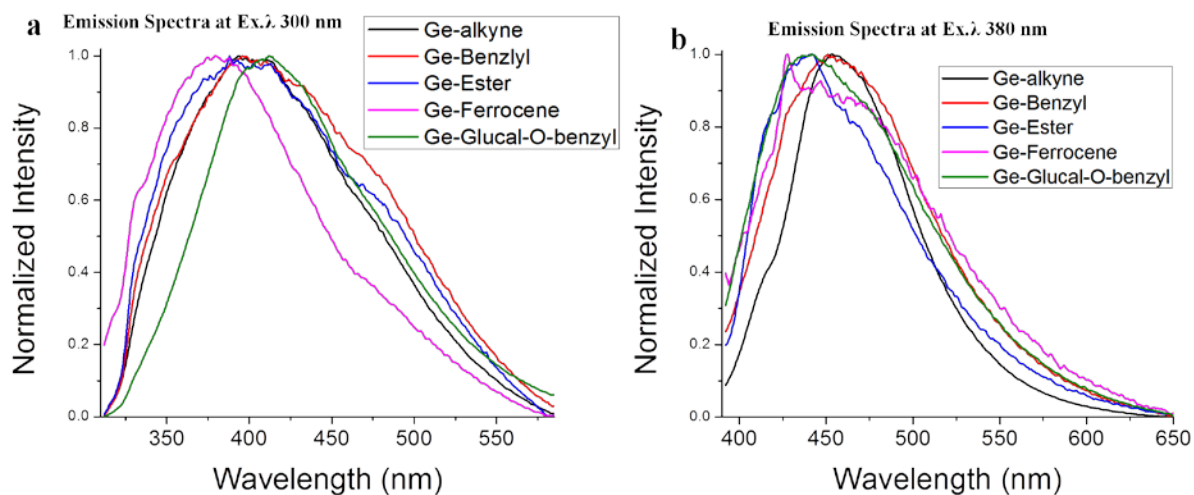


Figure 3.21: PL emission spectra of various functionalized Ge NPs at 300 nm (a) and at 380 nm (b).

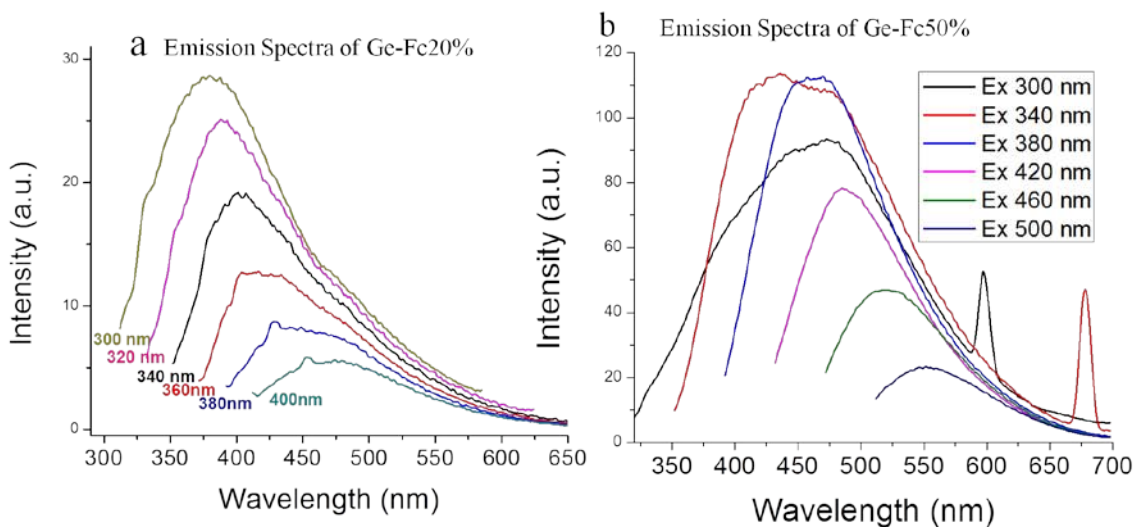


Figure 3.22: PL emission spectra of ferrocene grafted Ge NPs with 20% (a) and 50% (b) surface coverage .

Ge NPs with 50% surface coverage of ferrocene moiety show completely different result, showing a significant red shift in emission spectra (more than 50nm at 300nm excitation). The PL emission spectra of GeFc 50% NPs at various excitation λ is shown in **Figure 3.22**. Emission spectra at lower excitation wavelength are broader. Emissions are extended up to 700 nm from 300nm.

3.4 Conclusion

Various organic, organometallic and biomolecular azide were used to functionalize passivated Ge NPs by “click” chemistry. Further functionalization provides enhanced solubility and stability against air oxidation and nanoparticle aggregation. In this chapter we tried to explore “click” chemistry as an alternative and efficient method compared to hydrogermylation or other organometallic modification of meta-stable Ge surfaces for surface functionalization.

3.5 Experimental:

3.5.1 *Method and Materials*

Germanium (~2mm pieces), 99.999% purity, was purchased from Sigma-Aldrich. 1-octyne (98%) and 1,7-octa-diyne (98%) were purchased from Alfa-Aesar and used without further purification. Trimethylsilyl azide (99%) was purchased from Gelest and used without further purification. N,N,N',N',N''-pentamethyldiethylenetriamine (PMDTA) (99%), benzyl bromide (98%), from 2-ethyl bromo acetate (98%), Ferrocene (98%), tert-butyl lithium (1.7 M solution in pentane), 1,3-dibromopropane (99%) were purchased from Sigma-Aldrich. 1,3-dibromopropane and all solvents including THF were distilled and degassed before use.

3.5.2 *Synthesis of ω -alkynyloctenyl(20%)-Germanium Nanoparticles:*

Germanium (0.75 g) was placed in a stainless steel milling vial along with stainless steel milling balls, each with a diameter of 1.2 cm and weighing 8.1 g. The milling vial was filled with 25ml of the reactive alkyne mixture, 20 ml (80%) of 1-octyne

and 5 ml (20%) of 1,7-octadiyne in a nitrogen filled glove box, and then tightly sealed. The milling vial was placed in a SPEX 8000-D Dual Mixer/Mill, and high energy ball-milling was performed for 24 hours.

After 24 hours of milling, the reaction mixture was centrifuged, and soluble nanoparticles were separated from the residue of larger particles. The crude nanoparticle were dried and the starting alkynes (i.e. 1-octyne and 1,7-octadiyne) were recovered by vacuum distillation. The solid nanoparticles can be redispersed in any organic solvents like methylene chloride, hexane, THF etc. The crude nanoparticles were purified through a gel permeation chromatography (GPC) gravity column (45 cm in length and 1.35 cm in width) using Bio-beads S-X1, as the stationary phase, and dichloromethane, as the elution solvent. **¹H NMR** (300 MHz, CDCl₃): δ 5.4-6 ppm (broad and weak), 2.2(broad), 1.8 (broad), 1.2-1.5 (m), 0.8 (s). **FT-IR** (thin film on KBr plate): 3300, 2850-3000, 2100, ~1600, 1465, 1375, 750-900, 750 cm⁻¹.

3.5.3 The copper (I) catalyzed "Click" Reaction on ω-alkynyloctenyl(20%)-Germanium nanoparticle with azides:

50 mg of ω-alkynyloctenyl (20%) germanium nanoparticles were dissolved in 10 ml of THF in a 100 ml Schlenk flask. azide, The RN₃, (50 mg) and a 0.5 ml of N,N,N',N',N''-pentamethyldiethylenetriamine (PMDTA) were then added to the solution. The solution was degassed three pump-thaw-degas cycles. Copper(I)bromide.-dimethylsulfate (20-30 mg) was added to the degassed mixture under N₂ flow. The solution was stirred overnight under nitrogen to complete the reaction. The reaction mixture then was concentrated by rotary-evaporation and the particles redispersed in 40 ml dichloromethane. The dichloromethane solution was washed three times with 40 ml

brine/ ethylenediamine solution. The nanoparticle solution was dried over anhydrous MgSO_4 , filtered and concentrated by rotary-evaporation. The crude NPs were further purified by gel permeation chromatography (GPC) using Bio-beads S-X1, as a stationary phase, and dichloromethane, as the eluting solvent, to remove any molecular impurities or unreacted azide.

3.5.4 TMS-azide grafted Ge NPs.

Trimethylsilylazide (99%) was used for the copper(I) catalyzed “click” reaction without further purification. Yield : 70% (35 mg by weight). **^1H NMR** (300 MHz, CD_2Cl_2): δ : 0.1 (TMS protons); 0.9 (CH_3 from alkyl chain), 1.2 to 1.7 (broad m, CH_2 from alkyl chain), 7.6 (triazole proton) ppm.. **FT-IR**: 2850-300 ($\nu(\text{C-H})$); 3180 ($\nu(\text{C-H}$ triazole)), 1375, 1475 ($\delta(\text{C-H})$); 1250 ($\nu(\text{Si-CH}_2)$); 800 ($\nu(\text{Si-C})$) and 750 cm^{-1} ($\nu(\text{Ge-C})$).

3.5.5 Benzyl-azide grafted Ge NPs.

Benzyl azide was synthesized from benzyl bromide by an azidation reaction.³⁷ Benzyl bromide (1.2 ml, 10 mmol) was added to 0.5 M solution of NaN_3 in 22 ml DMSO and the mixture was stirred for overnight. The product was separated by ether (100 ml) extraction after washing three times with brine (100 ml). Yield: 98% (1.3 g). **^1H NMR** (300 MHz, CD_2Cl_2): δ 7.38 (m, 5H), 4.36 (m, 2H) ppm.

The benzyl azide (50 mg) and 50 mg alkyne-terminated Ge NPs was used for the “click” reaction. Yield: 74%.(37 mg). The product can be redispersed in organic solvents such as dichloromethane, THF, toluene etc. **^1H NMR** (300 MHz, CD_2Cl_2): 7.2-7.4 (broad, m), 1.56, 1.3, 0.9 ppm. **FT-IR** (thin film on KBr plate): 3138 (weak), 3063 (weak), 2850-300, ~ 1600 , 1465, 1375, 750 cm^{-1} .

3.5.6 Ethyl 2-azidoacetate grafted Ge NPs.

Ethyl 2-azidoacetate was synthesized from 2-ethyl bromo acetate by an azidation reaction³⁸. Ethyl bromo acetate (8.35 g, 50 mmol) and excess sodium azide (0.2 mol) was reacted in 50% acetone and water (300 ml) for overnight. The reaction mixture was concentrated by rotary evaporation and extracted in dichloromethane (100 ml) after washing three times with brine solution. The product was isolated as colorless oil: 100% yield. ¹H NMR(300 MHz, CDCl₃): δ 4.18 (q, J=7.2 Hz, 2H), 3.79 (s, 2H), 1.23 (t, J=7.2, 3H).

The ethyl 2-azidoacetate (50 mg) and 50 mg alkyne-terminated Ge NPs were used for the “click” reaction. Yield: 32 mg (65% by weight). ¹H NMR (300 MHz, CDCl₃): δ 7.4 (weak), 5.1 (s), 4.2, 1.2-1.4 (m), 0.8 (s) ppm. FT-IR (thin film on KBr plate): 3138, 300-2850, 1750, 1210, 1100, 1465, 1375, 740 cm⁻¹.

3.5.7 4-azido benzoic acid grafted Ge NPs.

4-azido benzoic acid was synthesized from 4-amino benzoic acid³⁹. 4-amino benzoic acid (2.057 g, 15 mmol) was dissolved in dry acetonitrile (30 ml) and cooled to 0°C. Tert-butyl nitrite, ^tBuONO, (2.57 g, 25 mmol, 3 ml) followed by TMSN₃ (2.07g, 18 mmol) was added to this stirred reaction mixture and the solution stirred for overnight at room temperature. The reaction mixture was concentrated by rotary evaporation, and the crude product was purified by silica gel chromatography (dichloromethane) to give a yellowish solid.

3.5.8 *Synthesis of ferrocenylpropylene bromide.*

Ferrocenylpropylene bromide was synthesized using a standard Schlenk line technique. *Tert*-butyl lithium ($t\text{BuLi}$) was transferred directly from the reagent bottle using a cannula under positive pressure of N_2 . Ferrocenylpropylene bromide was synthesized using two steps: first monolithiation of ferrocene, followed by nucleophilic substitution of monolithiated ferrocene with dibromopropane. The experimental set-up is shown in the **Figure 3.23**.

Step I: Monolithiation of ferrocene. The monolithiation of ferrocene was completed through a modification of a previously reported method.^{40, 41} Ferrocene (1g, 5.4 mmol) in 15 ml distilled THF was placed in a 100 ml three neck flask equipped with a stir bar attached with a 25 ml measuring addition funnel. *tert*-Butyllithium (3ml pentane, 1.7 M solution), 0.5 mmol, was transferred to the measuring addition funnel through a cannula. The solution was then added to ferrocene solution at 0°C over a period of 10 minutes. After 10 minutes at 0°C , the solution was chilled to -78°C .

Step II: Nucleophilic reaction with dibromopropane. The chilled solution was transferred through cannula to the stirred THF solution of 1,3-dibromopropane (in excess) in a 100 ml Schlenk flask equipped with an addition funnel at -78°C . The reaction was brought to room temperature and allowed to react for a few hours under N_2 . After the reaction, all of the THF and unreacted dibromopropane were removed by vacuum. Additional 25ml hexane was added to the crude dry product and the resulting mixture was separated by filtration. The product was concentrated by rotary evaporation and it was further purified by silica gel column using hexane/ dichloromethane, as an eluent. A pure yellow orange solid product of ferrocenylpropylene bromide was obtained.

Yield of the product is 30% (0.55 g). $^1\text{H NMR}$: 4.15 (s, 5H), 4.11 (m, 4H), 3.45 (t, 2H), 2.5 (t, 2H), 2.1 (quintet, 2H) ppm.

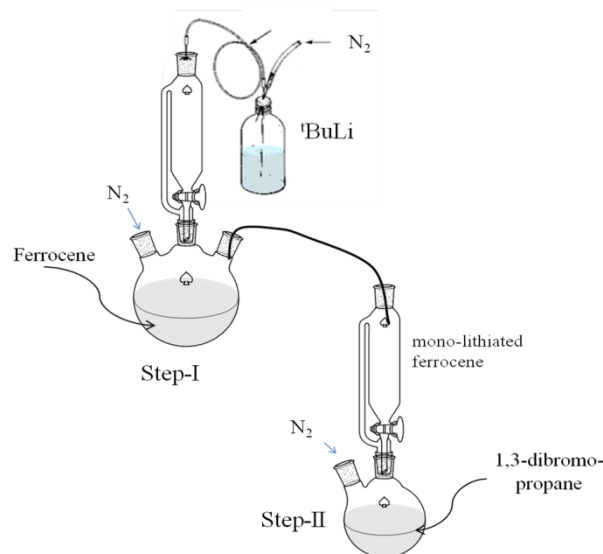


Figure 3.23: Experimental set-up for synthesis of ferrocenylpropylene bromide from ferrocene.

3.5.9 Synthesis of ferrocenylpropylene azide.

Ferrocenylpropylene bromide (0.5 mmol, 167.5 mg) and sodium azide (1.5 mmol, 100 mg) were dissolved in 50 ml acetonitrile and the solution was stirred for overnight at room temperature to form ferrocenylpropylene azide. The reaction mixture was concentrated by rotary evaporation and products were extracted in dichloromethane (40 ml) after washing with brine solution (3× 40 ml). The orange solid product was dried over MgSO_4 , filtered, and concentrated by rotary evaporation. Yield: 135 mg (100%). $^1\text{H NMR}$: 4.11 (s, 5H), 4.06 (m, 4H), 3.28 (t, 2H), 2.4 (t, 2H), 1.8 (quintet, 2H) ppm.

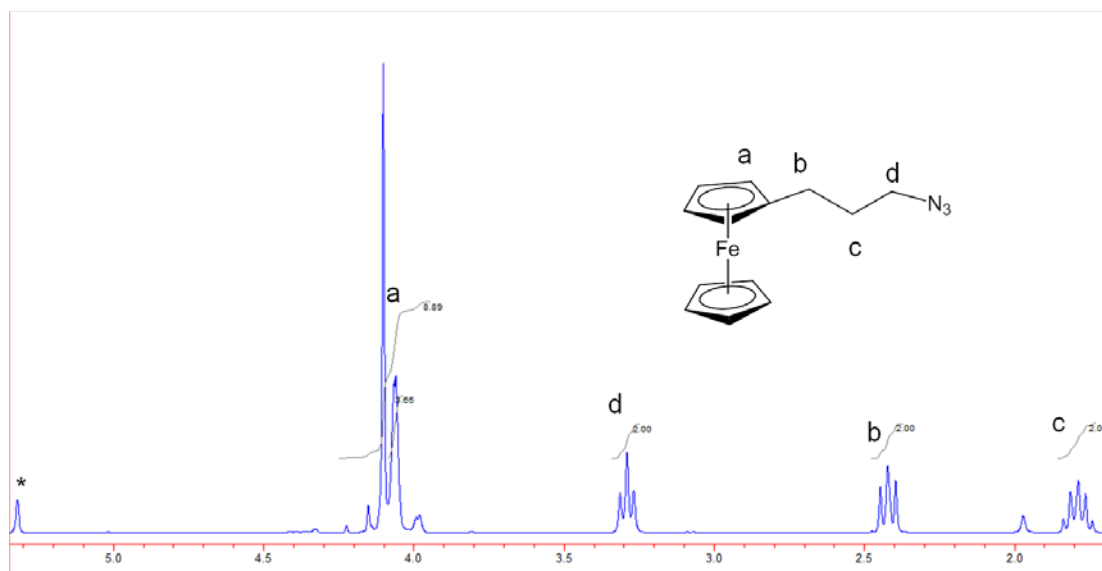


Figure 3.24: ^1H NMR spectra of ferrocenylpropylene azide in CD_2Cl_2 .

3.5.10 .Glucal moiety grafted Ge nanoparrticles.

Glucals were grafted via a tandem Ferrier and click reaction in one pot.³⁶ Tri-O-acetyl-D-glucals (98%) , tri-O-benzyl-D-glucal (97%) and copper triflate ($\text{Cu}(\text{OTf})_2$, 98%) were purchased from Sigma Aldrich. Acetonitrile and THF were used before distillation. In a 50ml reaction flask a mixture of glucal triacetate (0.5 mmol), TMSN_3 (0.7 mmol) and the Lewis acid catalyst $\text{Cu}(\text{OTf})_2$ (5 mol%) in 5ml acetonitrile was stirred for few hours. After the reaction, acetonitrile and unreacted TMSN_3 were removed by vacuum. The 20% alkyne-terminated Ge NPs (50 mg) in 25 ml distilled THF and Cu-wire (10 mg) were added to the flask and stirred for overnight at room temperature. The reaction mixture was concentrated by rotaryevaporation and products were dispersed in 30 ml methylene chloride. Ethylene diamine (1ml) was added and the solution was washed three times with brine solution (30 ml each). It was dried over MgSO_4 and concentrated by vacuum. Glucal grafted Ge NPs were purified by GPC column packed with Bio-beads S-X1 using methylene chloride as a eluting solvent. Yield of solid yellow product: 34 mg (68% by weight).

3.6 Analytical Method

3.6.1 Infrared spectroscopy.

Fourier Transform Infrared (FT-IR) Spectroscopy was performed using a Thermo Nicolet NEXUS 670 FT-IR. Sample preparation consisted of the formation of thin film of functionalized Ge NPs by depositing dichloromethane solution of Ge NPs on a KBr plate. FT-IR sample chamber was flushed with dry nitrogen before collecting any data. FT-IR spectra were recorded with 512 scans at 1 cm^{-1} resolution.

3.6.2 Nuclear magnetic resonance spectroscopy.

Nuclear magnetic resonance spectroscopy was performed using chloroform- d , methylene chloride- d_2 and benzene- d_6 , as solvents, with a Bruker Avance 300 MHz high resolution NMR spectrometer. Ge NPs were dissolved in the nmr solvent and the solution was transferred into a clean NMR tube.

3.6.3 Transmission electron microscopy.

Transmission electron microscopy (TEM) images were taken with a JOEL 2011 transmission electron microscope using an accelerating voltage of 200 kV. A droplet of a dilute solution of nanoparticles in toluene was deposited on the carbon coated copper grid placed on filter paper. The filter paper soaked the excess solution before inserting in grid in the TEM sample holder. Energy dispersive spectroscopic (EDS) data were obtained in the TEM using an Oxford Inca attachment with a 3 nm beam spot on a copper grid.

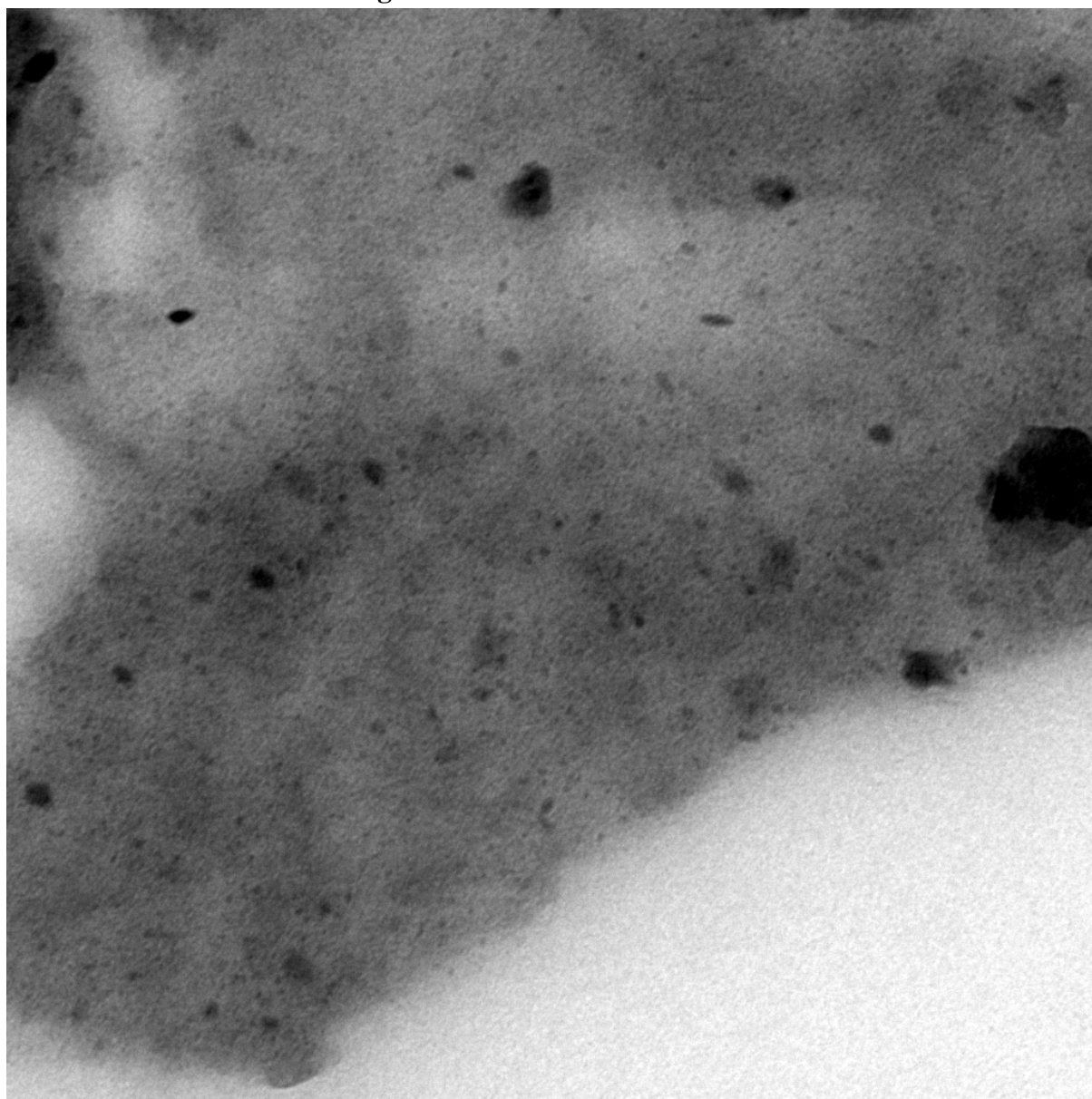
3.6.4 *UV-vis Absorption and Photoluminescence spectroscopy.*

UV-Vis absorbance spectra were obtained with a Cary 50 spectrophotometer in dichloromethane. Maximum absorbance was kept below 0.5. The photoluminescence emission characteristics from the Ge nanoparticles in dichloromethane were acquired using a Varian Cary Eclipse spectrofluorimeter and the emission spectra were recorded with excitation wavelength between 300 nm to 450 nm with slow scanning speed in a 1 cm quartz cuvette.

3.6.5 *GC-MS.*

Various molecular precursors (bromides and azides) were confirmed by GC-MS (Varian 450 GC, Varian 300 MS) using a VF5-MS capillary column.

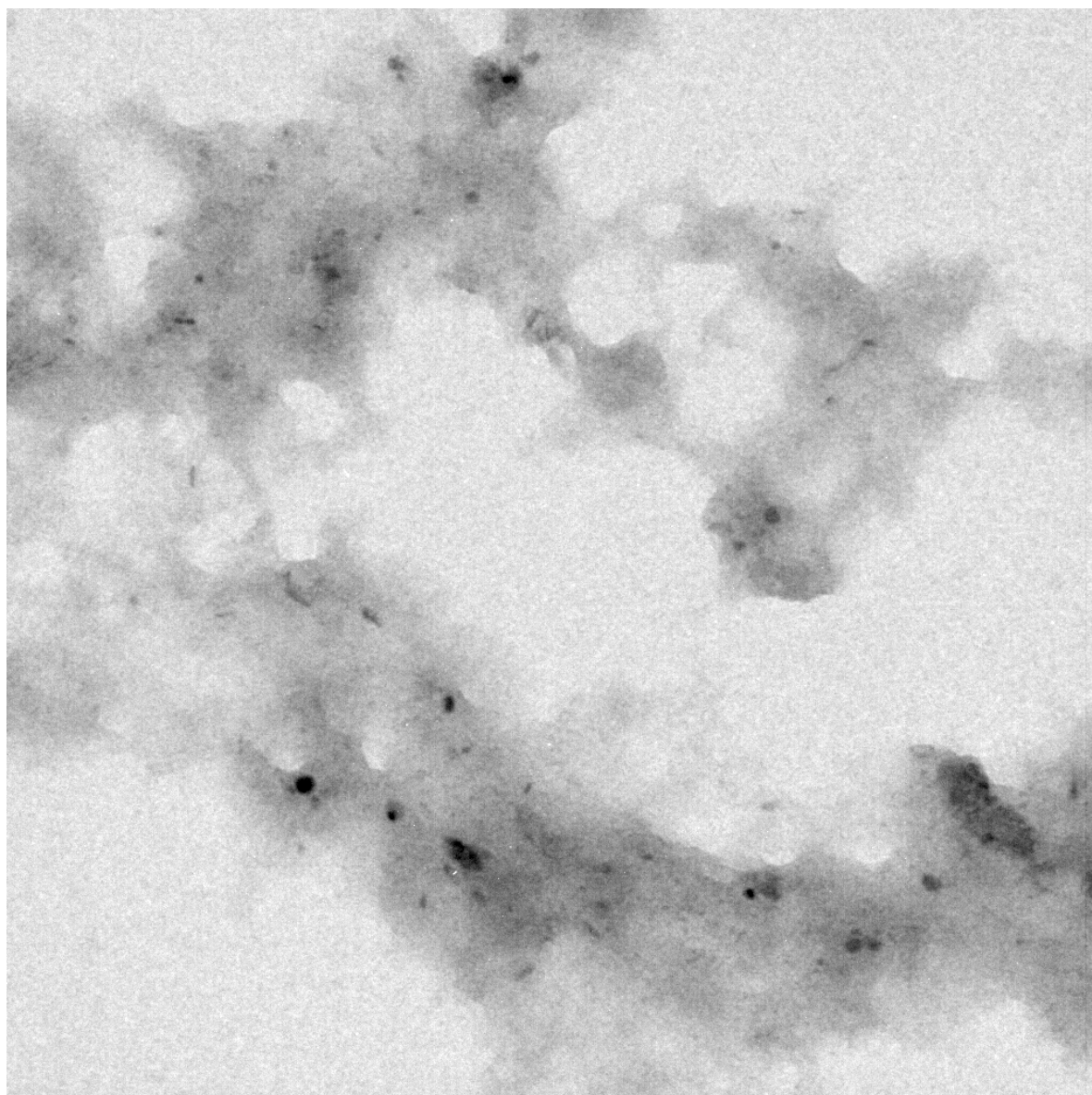
3.7 APPENDIX: TEM images



05.tif
GeHexDiyne50 C ppt

100 nm

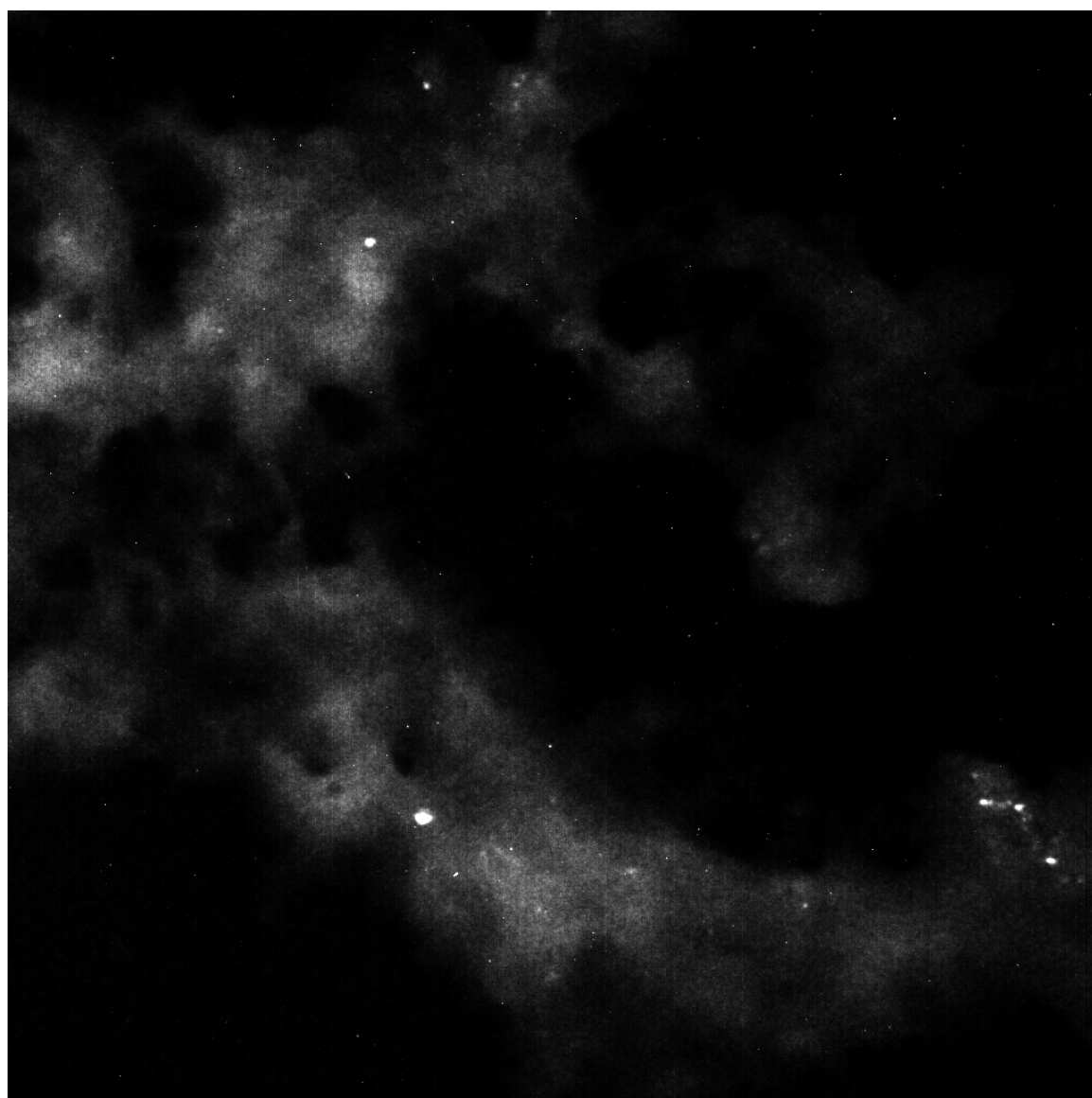
Figure 3.25: TEM image of toluene dispersed residue of Ge-alkyne50% NPs (which show cross-linking of 1,7-octadiyne resulting precipitation of nanoparticles).



02.tif
BM51
BM51-ppt part

100 nm
HV= 200kV

Figure 3.26: TEM image of ω -alkynyloctenyl (20%) Ge NPs after dispersion from the toluene solution.



02-dark.tif

BM51

BM51-ppt part

Print Mag = 142461x @ 2.5 in

100 nm

HV= 200kV

Discont Mag = 15000x

Figure 3.27: Dark field TEM image of Ge-alkyne20% NPs after dispersion from the toluene solution.

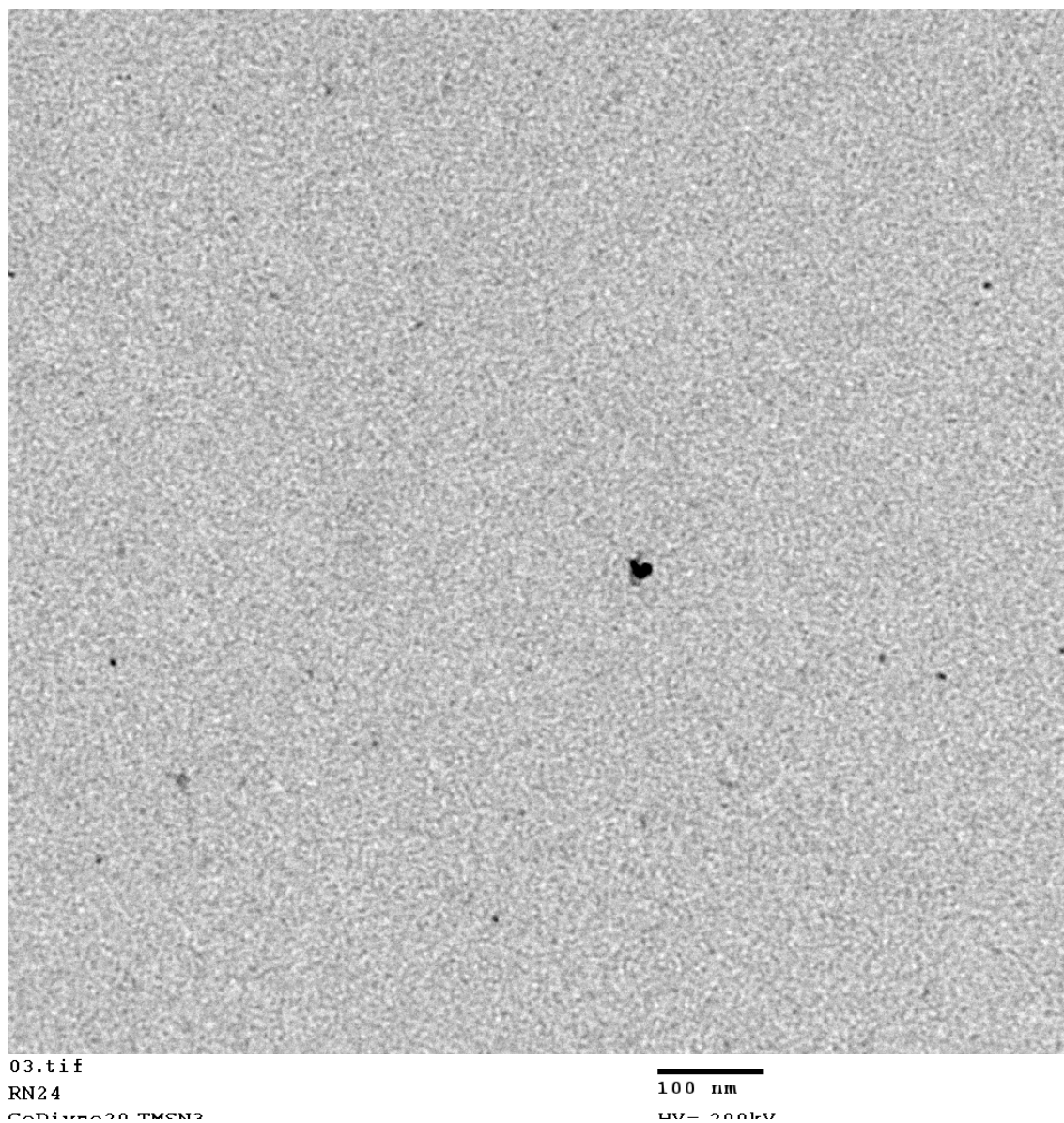


Figure 3.28: TEM image of TMS-azide grafted Ge NPs

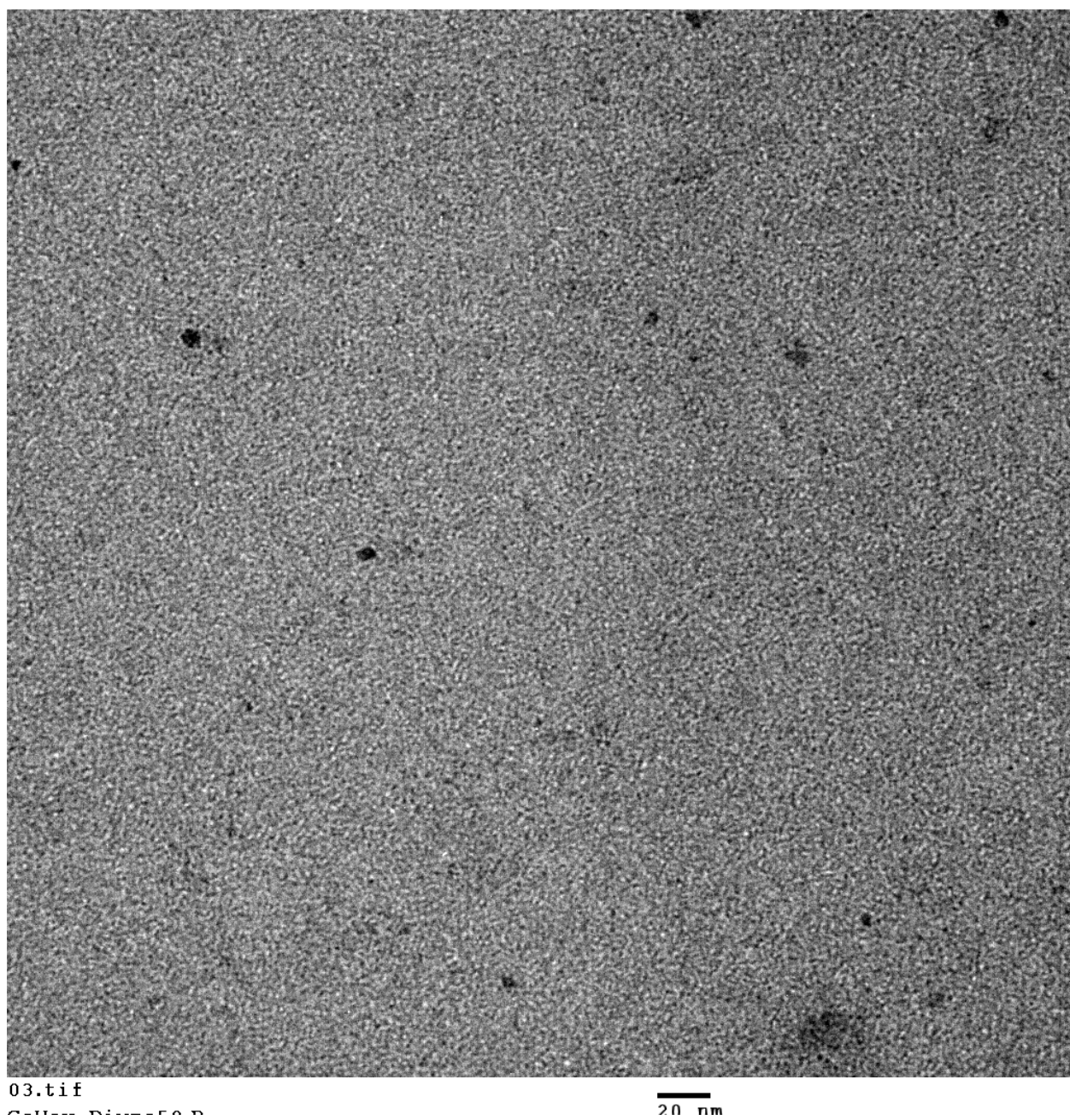


Figure 3.29: TEM images of ferrocene grafted Ge NPs

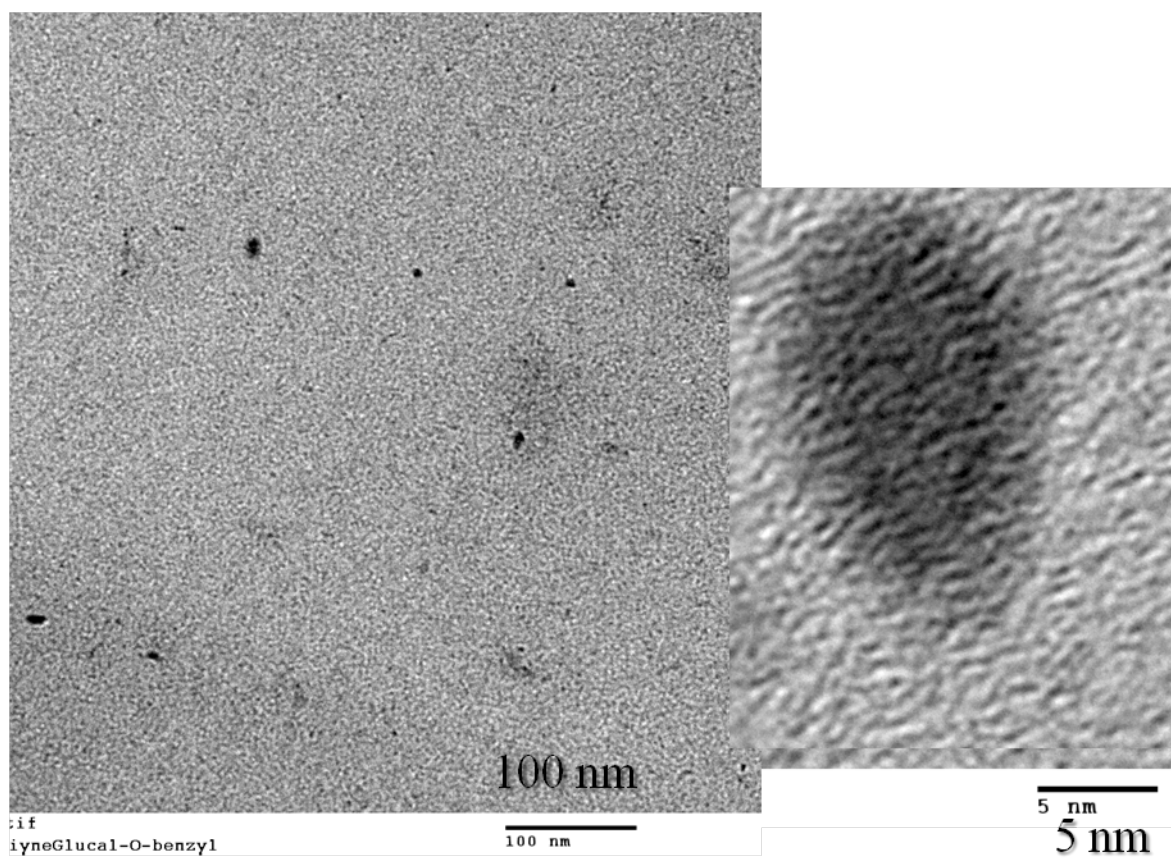


Figure 3.30: TEM image of tri-O-benzylglucal-grafted Ge NPs.

3.8 References

1. Veinot, J., Surface Passivation and Functionalization of Si Nanocrystals. In *Silicon Nanocrystals*, Wiley-VCH Verlag GmbH & Co. KGaA: 2010; pp 155-172.
2. Fan, J.; Chu, P. K., Group IV Nanoparticles: synthesis, Properties, and Biological Applications. *Small* **2010**, 6, (19), 2080-2098.
3. Hartmuth, C. K.; Finn, M. G.; Sharpless, K. B., Click Chemistry: Diverse Chemical Function from a Few Good Reactions. *Angew. Chem. Int. Ed.* **2001**, 40, (11), 2004-2021.
4. Liang, L.; Astruc, D., The copper(I)-catalyzed alkyne-azide cycloaddition (CuAAC) "click" reaction and its applications. An overview. *Coordination Chemistry Reviews* 255, 2933-2945.
5. Astruc, D.; Liang, L.; Rapakousiou, A.; Ruiz, J., Click Dendrimers and Triazole-Related Aspects: Catalysts, Mechanism, Synthesis, and Functions. A Bridge between Dendritic Architectures and Nanomaterials. *Accounts of Chemical Research* **ASAP**.
6. Nebhani, L.; Barner-Kowollik, C., Orthogonal Transformations on Solid Substrates: Efficient Avenues to Surface Modification. *Advanced Materials* **2009**, 21, (34), 3442-3468.
7. Evans, R. A., The Rise of Azide-Alkyne 1,3-Dipolar 'Click' Cycloaddition and its Application to Polymer Science and Surface Modification. *Aust. J. Chem.* **2007**, 60, (6), 384-395.
8. Binder, W. H.; Kluger, C., Azide/Alkyne-"Click" Reactions: Applications in Material Science and Organic Synthesis. *Current Organic Chemistry* **2006**, 10, (14), 1791-1815.
9. Hawker, C. J.; Wooley, K. L., The Convergence of Synthetic Organic and Polymer Chemistries. *Science* **2005**, 309, (5738), 1200-1205.
10. Kolb, H. C.; Sharpless, K. B., The growing impact of click chemistry on drug discovery. *Drug Discovery Today* **2003**, 8, (24), 1128-1137.
11. Zhang, T.; Zheng, Z.; Ding, X.; Peng, Y., Smart Surface of Gold Nanoparticles Fabricated by Combination of RAFT and Click Chemistry. *Macromol. Rapid Commun.* **2008**, 29, (21), 1716-1720.
12. Voliani, V.; Ricci, F.; Signore, G.; Nifosi, R.; Luin, S.; Beltram, F., Multiphoton Molecular Photorelease in Click-Chemistry-Functionalized Gold Nanoparticles. *Small* **2011**, 7, (23), 3271-3275.

13. Cardiel, A. C.; Benson, M. C.; Bishop, L. M.; Louis, K. M.; Yeager, J. C.; Tan, Y.; Hamers, R. J., Chemically Directed Assembly of Photoactive Metal Oxide Nanoparticle Heterojunctions via the Copper-Catalyzed Azide-Alkyne Cycloaddition "Click" Reaction. *ACS Nano* **2012**, 6, (1), 310-318.
14. Hu, J.; Qian, Y.; Wang, X.; Liu, T.; Liu, S., Drug-Loaded and Superparamagnetic Iron Oxide Nanoparticle Surface-Embedded Amphiphilic Block Copolymer Micelles for Integrated Chemotherapeutic Drug Delivery and MR Imaging. *Langmuir* **2012**, 28, (4), 2073-2082.
15. Moitra, N.; Trens, P.; Raehm, L.; Durand, J.-O.; Cattoen, X.; Man, M. W. C., Facile route to functionalized mesoporous silica nanoparticles by click chemistry. *J. Mater. Chem.* **2011**, 21, (35), 13476-13482.
16. Kai, H.; et al., Ferrocene and Porphyrin Monolayers on Si(100) Surfaces: Preparation and Effect of Linker Length on Electron Transfer. *ChemPhysChem* **2009**, NA.
17. Marrani, A. G.; Dalchiele, E. A.; Zanoni, R.; Decker, F.; Cattaruzza, F.; Bonifazi, D.; Prato, M., Functionalization of Si(1 0 0) with ferrocene derivatives via "click" chemistry. *Electrochimica Acta* **2008**, 53, (11), 3903-3909.
18. Devaraj, N. K.; Collman, J. P., Copper catalyzed azide-alkyne cycloadditions on solid surfaces: applications and future directions. *QSAR Comb. Sci.* **2007**, 26, (11-12), 1253-1260.
19. Sato, S.; Swihart, M. T., Propionic-Acid-Terminated Silicon Nanoparticles: Synthesis and Optical Characterization. *Chemistry of Materials* **2006**, 18, (17), 4083-4088.
20. Warner, J. H.; Rubinsztein-Dunlop, H.; Tilley, R. D., Surface Morphology Dependent Photoluminescence from Colloidal Silicon Nanocrystals. *J. Phys. Chem. B* **2005**, 109, (41), 19064-19067.
21. Tanke, R. S.; Kauzlarich, S. M.; Patten, T. E.; Pettigrew, K. A.; Murphy, D. L.; Thompson, M. E.; Lee, H. W. H., Synthesis of Germanium Nanoclusters with Irreversibly Attached Functional Groups: Acetals, Alcohols, Esters, and Polymers. *Chemistry of Materials* **2003**, 15, (8), 1682-1689.
22. Heintz, A. S.; Fink, M. J.; Mitchell, B. S., Mechanochemical Synthesis of Blue Luminescent Alkyl/Alkenyl-Passivated Silicon Nanoparticles. *Adv. Mater.* **2007**, 19, (22), 3984-3988.
23. Shimanouchi, T.; Nsrd, N. B. S. *Tables of molecular vibrational frequencies consolidated. I*; Univ. Tokyo: 1972; p 164 pp.

24. Ma, X.; Wu, F.; Kauzlarich, S. M., Alkyl-terminated crystalline Ge nanoparticles prepared from NaGe: Synthesis, functionalization and optical properties. *J. Solid State Chem.* **2008**, 181, (7), 1628-1633.
25. Taylor, B. R.; Fox, G. A.; Hope-Weeks, L. J.; Maxwell, R. S.; Kauzlarich, S. M.; Lee, H. W. H., Solution preparation of Ge nanoparticles with chemically tailored surfaces. *Materials Science and Engineering B* **2002**, 96, (2), 90-93.
26. Lee, D. C.; Pietryga, J. M.; Robel, I.; Werder, D. J.; Schaller, R. D.; Klimov, V. I., Colloidal Synthesis of Infrared-Emitting Germanium Nanocrystals. *Journal of the American Chemical Society* **2009**, 131, (10), 3436-3437.
27. Holzer, W., On the application of NOE difference spectroscopy for spectral and structural assignments with substituted 1,2,3-triazoles. *Tetrahedron* **1991**, 47, (47), 9783-9792.
28. Nagel, B.; Warsinke, A.; Katterle, M., Enzyme Activity Control by Responsive Redoxpolymers. *Langmuir* **2007**, 23, (12), 6807-6811.
29. Zhou, N.; Zhang, Z.; Zhu, J.; Cheng, Z.; Zhu, X., RAFT Polymerization of Styrene Mediated by Ferrocenyl-Containing RAFT Agent and Properties of the Polymer Derived from Ferrocene. *Macromolecules* **2009**, 42, (12), 3898-3905.
30. Landis, E. C.; Hamers, R. J., Covalent Grafting of Redox-Active Molecules to Vertically Aligned Carbon Nanofiber Arrays via "Click" Chemistry. *Chemistry of Materials* **2009**, 21, (4), 724-730.
31. Ciampi, S.; Le Saux, G.; Harper, J. B.; Gooding, J. J., Optimization of Click Chemistry of Ferrocene Derivatives on Acetylene-Functionalized Silicon(100) Surfaces. *Electroanalysis* **2008**, 20, (14), 1513-1519.
32. Ferrier, R. J., Unsaturated sugars. *Adv Carbohydr Chem Biochem* **1965**, 20, 67-137.
33. Wieczorek, E., GLYCALs: Extensive, interesting and inexpensive starting materials for building blocks synthesis. *Acros Organics Acta* **2003**, 10, 13.
34. Ferrier, R. J., Unsaturated carbohydrates. Part 21. A carbocyclic ring closure of a hex-5-enopyranoside derivative. *Journal of the Chemical Society, Perkin Transactions 1* **1979**, 1455-1458.
35. Ferrier, R. J.; Zubkov, O. A., Transformation of Glycals into 2,3-Unsaturated Glycosyl Derivatives. In *Organic Reactions*, John Wiley & Sons, Inc.: 2004.

36. Yadav, J. S.; Reddy, B. V. S.; Chary, D. N.; Reddy, C. S., A tandem Ferrier and Click reaction: a facile synthesis of triazolyl-2,3-dideoxypyranosides. *Tetrahedron Letters* **2008**, 49, (16), 2649-2652.
37. Alvarez, S. G.; Alvarez, M. T., A practical procedure for the synthesis of alkyl azides at ambient temperature in dimethyl sulfoxide in high purity and yield. *Synthesis* **1997**, (4), 413-414.
38. Campbell-Verduyn, L.; Elsinga, P. H.; Mirfeizi, L.; Dierckx, R. A.; Feringa, B. L., Copper-free click: 1,3-dipolar cycloaddition of azides and arynes. *Org. Biomol. Chem.* **2008**, 6, (19), 3461-3463.
39. Barral, K.; Moorhouse, A. D.; Moses, J. E., Efficient Conversion of Aromatic Amines into Azides: A One-Pot Synthesis of Triazole Linkages. *Organic Letters* **2007**, 9, (9), 1809-1811.
40. Sanders, R.; Mueller-Westerhoff, U. T., The lithiation of ferrocene and ruthenocene: a retraction and an improvement. *Journal of Organometallic Chemistry* **1996**, 512, (1-2), 219-224.
41. Herberhold, M.; Ayazi, A.; Milius, W.; Wrackmeyer, B., Silyl derivatives of ferrocene with pending indenyl or fluorenyl substituents at silicon. *Journal of Organometallic Chemistry* **2002**, 656, (1-2), 71-80.

CHAPTER 4

4 Synthesis of PEGylated Germanium Nanoparticles and Nanoparticle Arrays for Biological Application

4.1 Introduction

Fluorescent semiconductor nanoparticles, such as Si and Ge nanoparticles, are highly attractive to the field of bioimaging since they can be detected *in vivo* by their size tunable visible PL in the nanoparticle regime.¹⁻⁴ Unlike organic dyes, semiconductor nanoparticles are resistant to photo-bleaching. Also, compound semiconductors such as CdSe, CdS, ZnS, etc. show a significant amount of cytotoxicity and they are not suitable for biological application.⁵ In contrast to these cytotoxic compound semiconductor nanoparticles, germanium nanoparticles (Ge NPs) exhibit a very low toxicity *in vivo* and *in vitro*.⁶⁻⁸

Proper functionalization could lead to water soluble biocompatible Ge nanoparticles and nanoparticle arrays for biological application; nanoparticle arrays also could lead to nanoparticle-based devices through inter-particle coupling. To date, an insignificant amount of work has been reported on water soluble biocompatible germanium nanoparticles. Amine-terminated blue luminescent Ge NPs functionalized by hydrogermylation with allylamine, were used in biological imaging.^{6, 7} These Ge NPs show very low cytotoxicity according to the mitochondrial activity of the cells. However, another amine-terminated water soluble Ge NPs showed high toxicity to cells. These

amine terminated cationic surfaces might increase the level of intracellular calcium and reactive oxygen species (ROS) causing cytotoxicity.⁹

Germanium nanoparticles (Ge NPs) can be made water soluble and biocompatible with appropriate surface functionalization. Polyethylene glycol (PEG) derivatives are widely used as biocompatible and biodegradable polymers to make water soluble functionalized nanomaterials for biological application. Grafting of hydrophilic PEG on a nanomaterial surface is called PEGylation; which not only makes water soluble or biocompatible materials, it also increases the hydrodynamic radius of PEGylated nanoparticles.^{10, 11} These nanoparticles with larger hydrodynamic radius (up to 20 nm) can escape premature clearance via reticulo-endothelial system (RES).^{10, 11} PEGylated Ge NPs can also be used for bioimaging. On the other hand, PEGylated nanoparticle arrays can be used as vehicles for drug delivery. Silicon nanoparticle clusters terminated with carboxylic acid group and PEGylated silicon nanoparticles for biological application were reported recently.^{1, 12, 13} However there is no report on PEGylation of Ge NPs with covalent bond or the synthesis of PEGylated globular Ge nanoparticle arrays.

This chapter presents copper(I) catalyzed alkyne azide "click" reaction either with alkyne-terminated Ge NPs or with azido-terminated Ge NPs; to the synthesis of PEGylated Ge NPs and NP arrays from chloroalkyl-terminated surface. Ge NPs with chloroalkyl-termination are prepared by high energy ball-milling (HEBM) of various ratios of 5-chloro-1-pentyne and 1-pentyne with germanium pieces. Previously, α,ω -chloro-alkyne was used to make chloro-terminated Si NPs by high energy ball-milling and it was proposed that the alkyne group of α,ω -chloro-alkyne reacts quickly with the

reactive silicon sites during the milling process, whereas the chloro group is non-reactive and therefore remains at the periphery.

4.2 PEGylated germanium nanoparticles and their aggregates from alkyne terminated Ge NPs

Alkyne-terminated (ω -alkynyloctenyl) Ge NPs and their use in alkyne-azide “click” chemistry were described in the previous chapter. Here, Ge alkyne nanoparticles were used to synthesize PEGylated Ge NPs by alkyne-azide “click” reaction using mono-azido PEG or α, ω -bisazido PEG derivatives. PEGylated Ge NPs with 15% surface coverage were synthesized from Ge NPs with 15% alkyne-terminated surface (ω -alkynyloctenyl(15%)-Ge NPs) as prepared by HEBM using 15% (v/v) 1, 7-octadiyne and 1-octyne. The Ge-alkyne NPs were purified by gel-permeation chromatography (GPC) to remove molecular impurities before using them for alkyne azide "click" reaction. TEM images of these particles show a polydispersed sample with sizes from 3 nm to 20 nm and an average size of 5-7 nm. The high resolution TEM shows lattice fringes from the crystalline particles from the Ge(111) surface which have a d-spacing of 3.3 Å.¹⁴

The PEGylated Ge NPs were purified by GPC and can be redispersed in dichloromethane. The PEGylated Ge NPs with low surface coverage are not soluble in water. FT-IR spectrum of the PEGylated Ge NPs show peaks mostly from the PEG ligand. The $\nu(\text{CH}_2)$ stretching from the PEG appeared as a broad peak centered at 2888 cm^{-1} . Peaks, at 3300 cm^{-1} and 2038 cm^{-1} for as $\nu(\equiv\text{C}-\text{H})$ and $\nu(\text{C}\equiv\text{C})$, were absent in the FT-IR spectrum. A couple of new sharp peaks appeared at 1110 cm^{-1} and 844 cm^{-1} are

assigned to the asymmetric $\nu(\text{C-O-C})$ and symmetric $\nu(\text{C-O-C})$ stretching. A couple of peaks at 1450 and 1350 cm^{-1} are due to C-H bending.

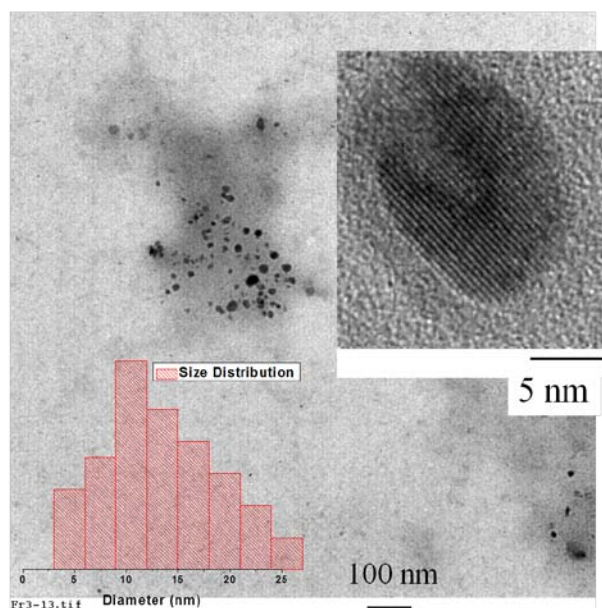


Figure 4.1: TEM images of alkyne-terminated Ge NPs.

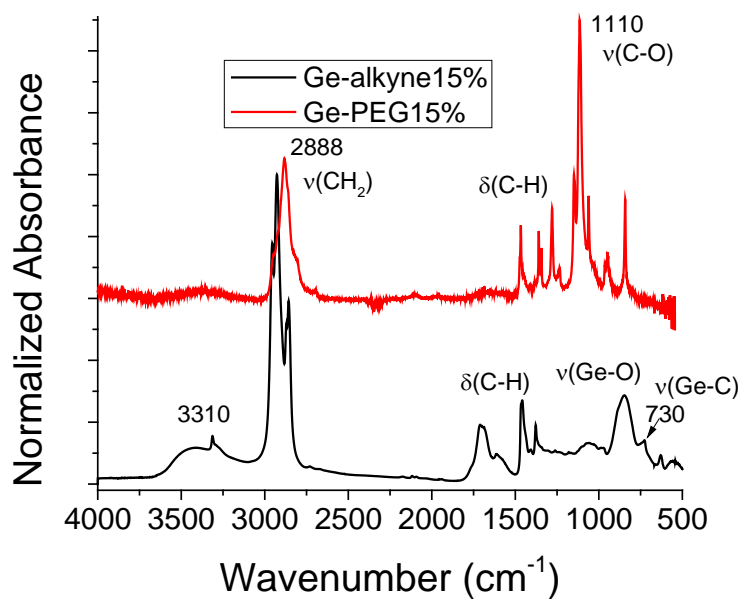


Figure 4.2: FT-IR spectra of alkyne-terminated and PEGylated Ge NPs

The optical properties of PEGylated Ge NPs are shown by UV-Vis absorption spectra and The PL emission spectra of various excitation wavelengths (**Figure 4.3**). The UV-vis absorption spectrum shows a single absorption with a tail up to 500 nm. The PL emission peak at lower excitation wavelengths (especially at 300 nm) was found to be a red shifted (by ~40 nm) compared to the starting ω -alkynyloctenyl-Ge NPs. This difference decreases with increasing excitation wavelength. This red shift in PL emission might be due to removing smaller particles by successive GPC separations – one before “click” reaction and another after the “click” reaction to remove excess PEG from the nanoparticles.

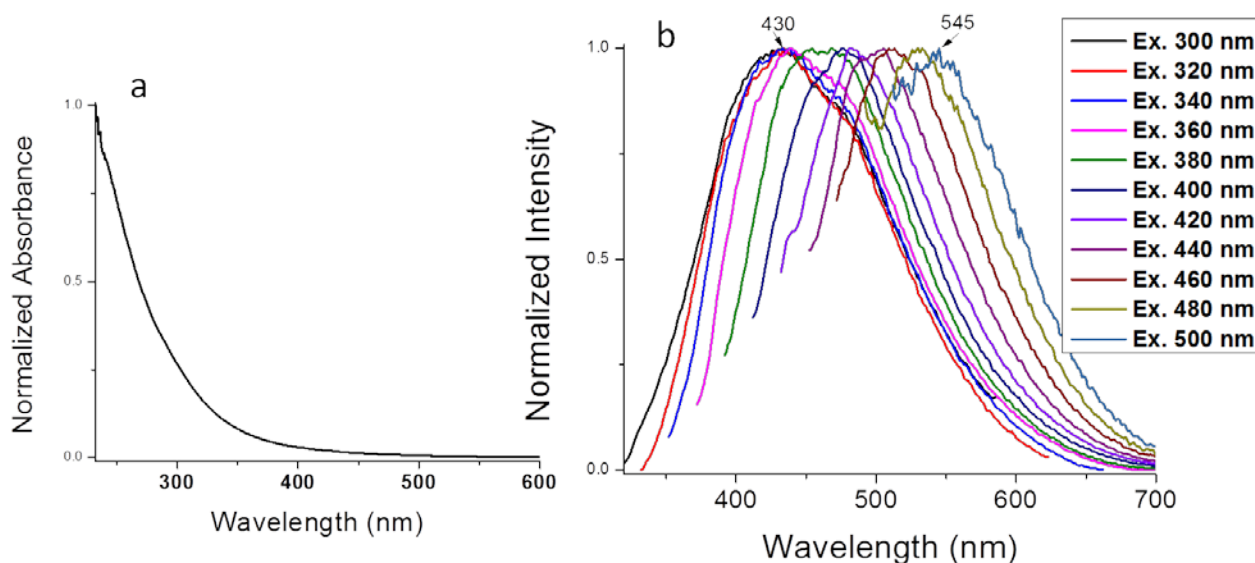
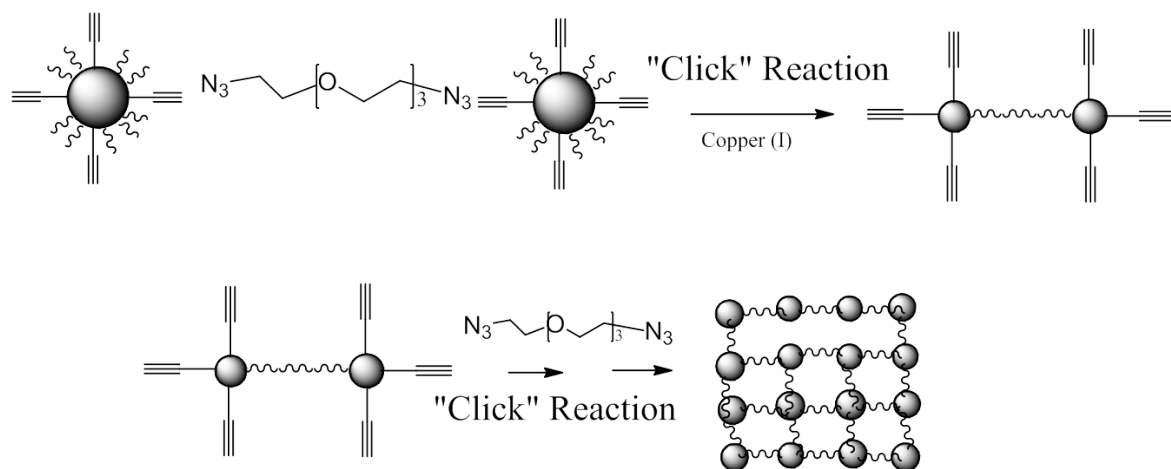


Figure 4.3: UV-vis absorption (a) and PL emission spectra (b) of PEGylated Ge NPs in dichloromethane

4.2.1 PEGylated Ge NP Clusters by "click" reactions using diazido-TEG.

Diazido tetraethylene glycol (1,11-diazido-3,6,9-trioxaundecane) was used to make Ge NP clusters through inter-particle covalent linking of ω -alkynyloctenyl(15%)-Ge NPs by copper(I) catalyzed alkyne-azide "click" reaction (**Scheme 4.1**). Products were purified by precipitation by adding 50% aqueous ethanol into the reaction mixture and washing several times using 95% ethanol. The product can be barely dispersed in toluene, as the solubility of NP clusters made from small spacer such as TEG is very poor. The FT-IR spectrum (**Figure 4.4**) confirmed the formation of triazole ring showing a tiny peak at 3143 cm^{-1} . Peaks at 3300 cm^{-1} were absent after the "click" reaction. A broader peak at $\sim 3400\text{ cm}^{-1}$ is due to some water in the sample, which could not be removed by vacuum. The C-H stretching and bending were seen similar as starting alkyne terminated Ge at $2850\text{-}3000\text{ cm}^{-1}$ respectively. A new peak at 1110 cm^{-1} is due to $\nu(\text{C-O})$

The Ge NP clusters were dispersed in toluene and sonicated for few minutes before taking on the TEM grid. TEM images of the Ge-TEG NP cluster (in **Figure 4.5**) show globular structure consisting of individual particles. The average size of the globular NP cluster is 40-80 nm. In the high-resolution TEM, individual particles were seen with average size $\sim 5\text{ nm}$ and an inter-particle distance of $\sim 3\text{-}4\text{ nm}$ (which is consistent with the length of the spacer TEG). Globular nanoparticle clusters, consisting of Ge NPs, were confirmed by EDX spectrum, which shows peaks at 1.3 keV, 10 keV and at 11 keV.



Scheme 4.1: Nanoparticle array synthesis from alkyne-terminated Ge NPs

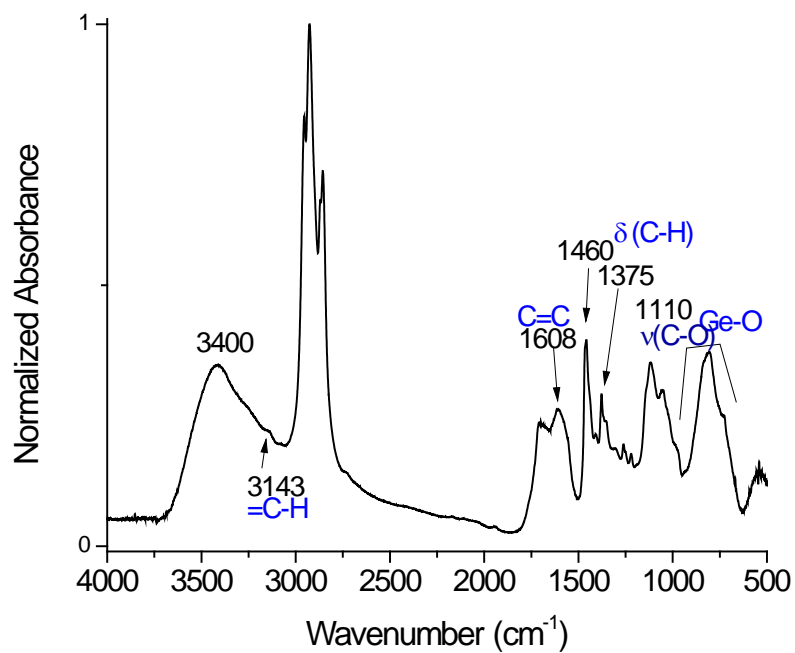


Figure 4.4: FT-IR spectrum of globular nanoparticle arrays using bis-azido-TEG.

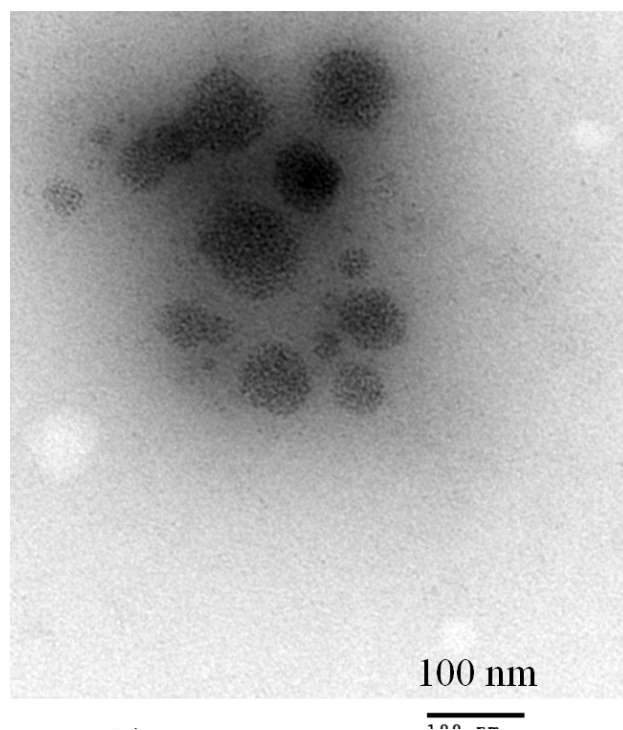


Figure 4.5a: TEM and HRTEM of globular nanoparticle arrays using bis-azido-TEG.

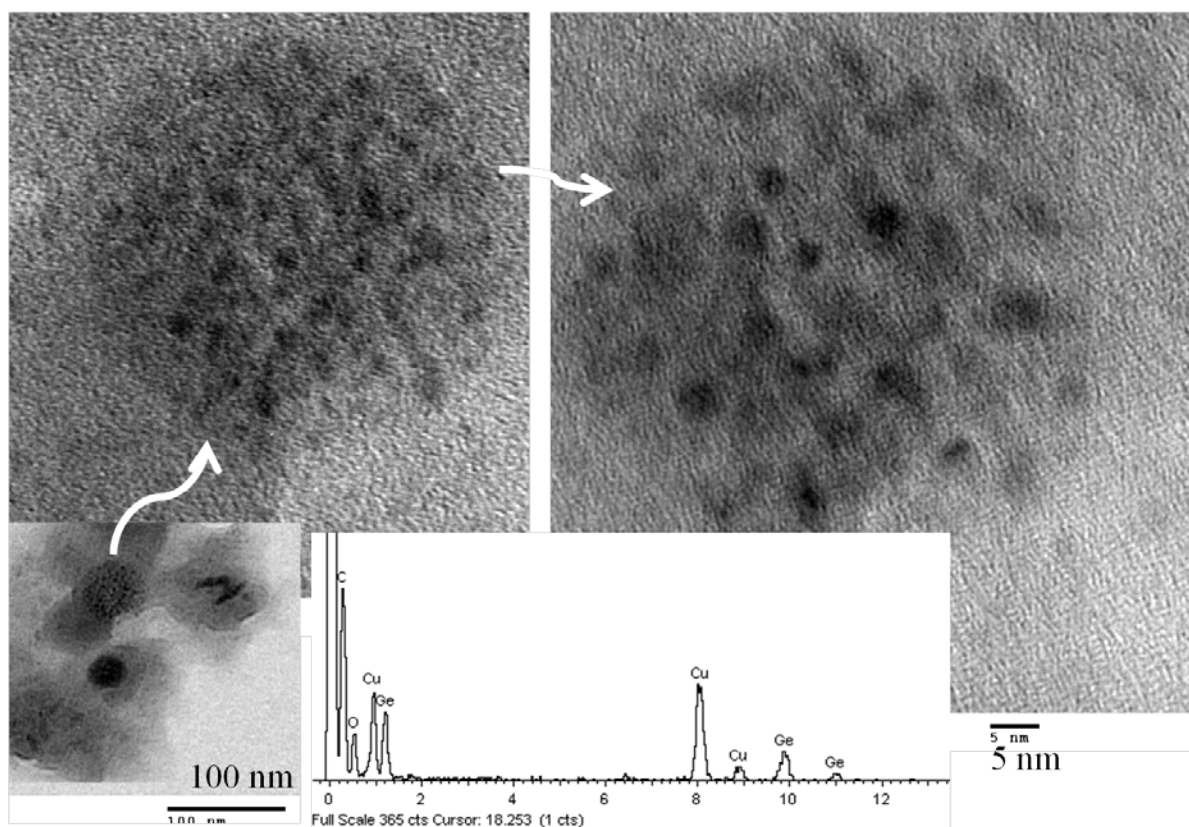


Figure 4.5b: TEM and HRTEM of globular nanoparticle arrays using diazido-TEG.

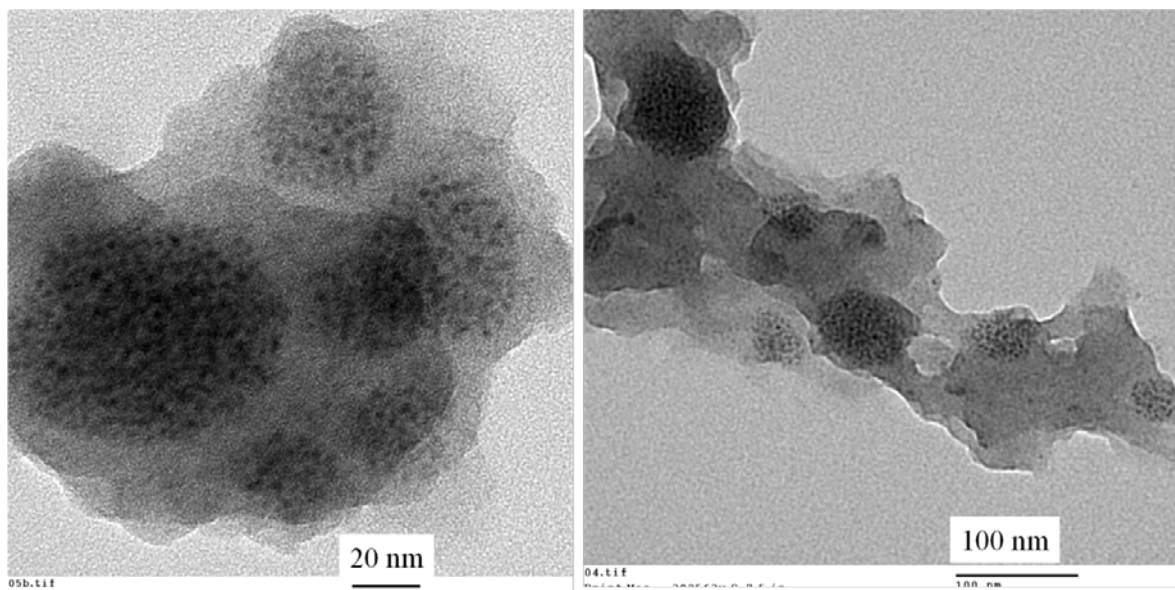
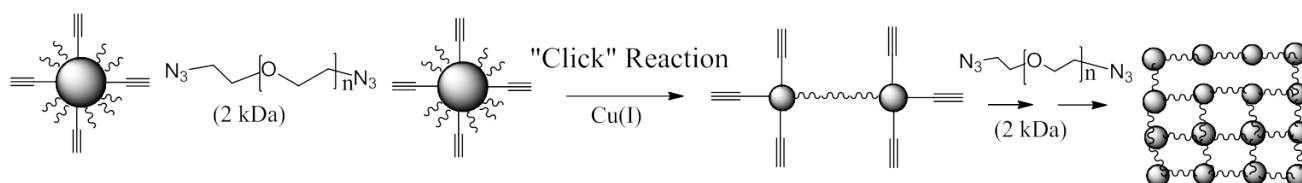


Figure 4.5c: TEM images of globular nanoparticle arrays using diazido-TEG.

4.2.2 PEGylated Ge NP Clusters by a "click" reaction using diazido-PEG (2Kda).

Diazido PEG (2kDa) was used as longer spacer to make Ge NP cluster using ω -alkynyloctenyl(15%)-Ge NPs (**Scheme 4.2**). The product was separated from the reaction mixture by precipitation using 50% ethanol followed by centrifugation. The Ge NP clusters can be slightly dispersed in common organic solvents such as toluene, ethanol. FT-IR spectrum of the purified product (in **Figure 4.6**) shows a sharp peak for $\nu(\text{C-O})$ stretching at 1110 cm^{-1} for polymeric PEG derivative. A tiny peak appeared at 3143 cm^{-1} due to the triazole C-H stretching.



Scheme 4.2: Synthesis of Ge-PEG NP Clusters

TEM images of Ge NP cluster (**Figure 4.7**) do not show uniform size or shape of the cluster. However, with diazido PEG as a longer spacer (13 nm), the interparticle distance is increased and individual particles can be seen by high resolution TEM. The size of the clusters varies from 80 nm to 150 nm. The size of individual particle, observed in HRTEM, was approximately 5 nm. The size and shape of the cluster might depend on the amount of surface coverage and amount of available linker in the solution.

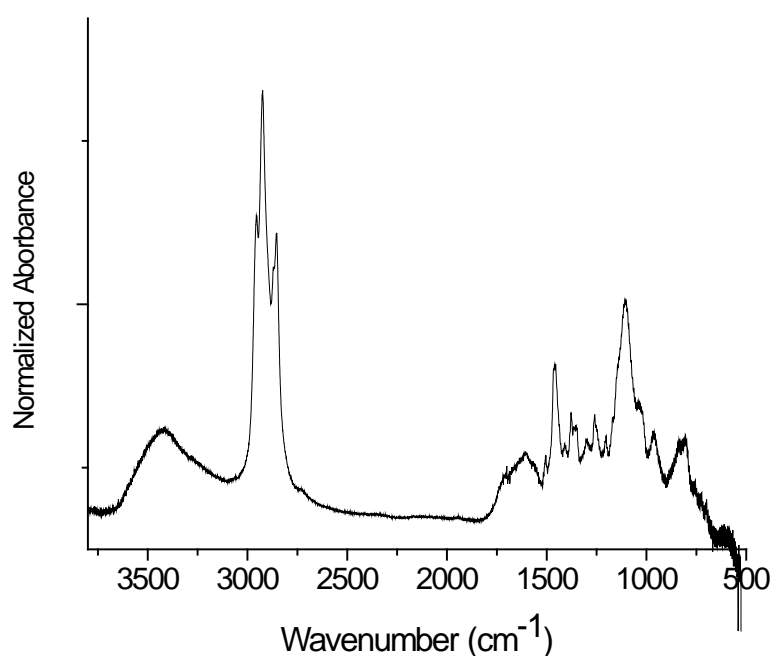


Figure 4.6: FT-IR spectrum of globular nanoparticle arrays using diazido-PEG (2kDa).

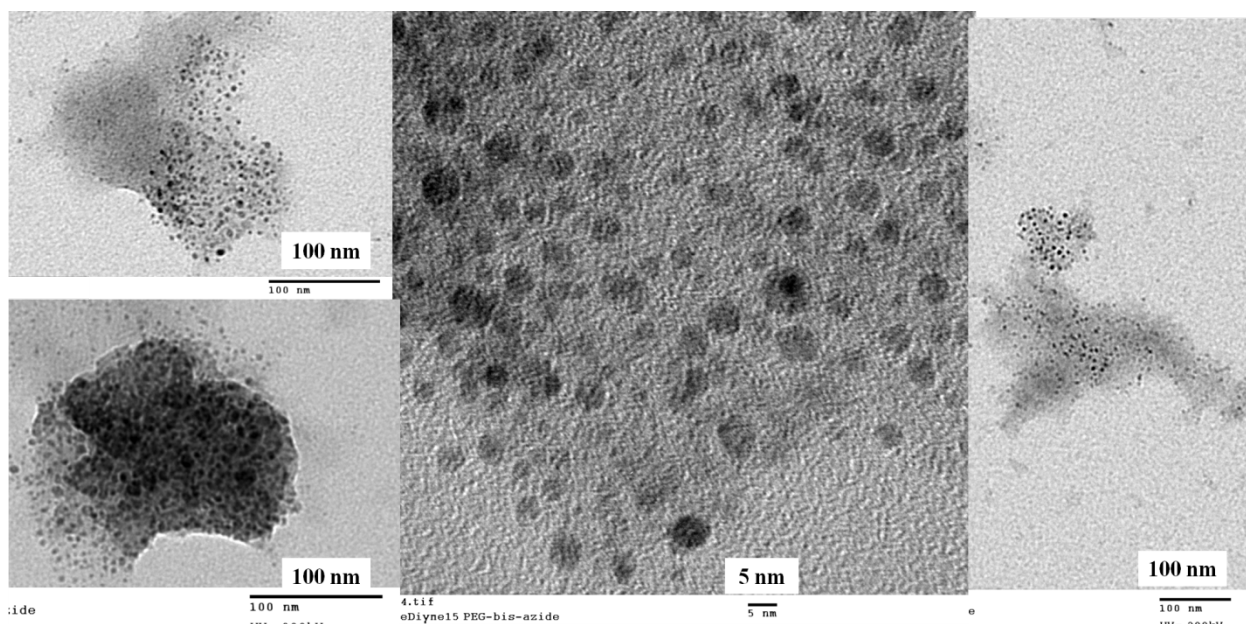


Figure 4.7: TEM images of globular nanoparticle arrays using diazido-PEG (2 kDa).

4.3 PEGylated Ge NPs and their aggregates from azido terminated germanium nanoparticles

4.3.1 *Synthesis of ω -chloropentenyl Ge NPs*

Germanium nanoparticles (Ge NPs) with various surface coverages of chloro-termination were prepared by high energy ball-milling (HEBM) using 5-chloro-1-pentyne and 1-pentyne. Surface coverage (20% to 50%) of ω -chloro pentenyl Ge NPs was achieved by using various ratio of 5-chloro-1-pentyne to 1-pentyne. Nanoparticle solutions were separated by centrifugation after HEBM and about 15% (150 mg) solid residue was recovered after distillation of the starting alkynes. The crude ω -chloropentenyl Ge NPs were purified by gel-permeation chromatography. Purified product can be redispersed by dichloromethane, toluene or THF.

The ω -chloropentenyl-Ge NPs were characterized by their ^1H NMR spectrum (in **Figure 4.9**); which can be compared with previous ω -chloroalkyl-terminated Si

NPs.¹⁵ A broad peak in the ^1H NMR spectrum at 3.5 ppm is due to the methylene group neighboring to Cl. Methyl protons from the chain pentenyl group were seen at 0.9 ppm. Other methylene peaks from the pentenyl group appeared at 1.2–1.5 ppm. The methylene protons adjacent to CH_2Cl were appeared as broad peaks at 2 ppm. The FT-IR spectrum of ω -chloropentenyl(20%)-Ge NPs (**Figure 4.8**) shows peaks from ~ 2850 to 3000 cm^{-1} and at 1375 and 1465 cm^{-1} due to $\nu(\text{C-H})$ and $\delta(\text{C-H})$ respectively. A sharp peak appeared at 700 cm^{-1} due to $\nu(\text{C-Cl})$ and weak peak at 740 cm^{-1} is due to $\nu(\text{Ge-O})$.

Azido-terminated Ge-NPs were synthesized from the ω -chloropentenyl-Ge NPs by azidation using sodium azide at 65°C . The ω -azidopentenyl Ge NPs were extracted in dichloromethane after extraction three times with brine solution. They were further purified by GPC. A new peak appeared in the FT-IR spectra (in **Figure 4.8**) due to the azide (N_3) asymmetric stretching. A weak broad peak at 1260 cm^{-1} is due to $\nu(\text{C-N})$. The peak for $\nu(\text{C-Cl})$ at 700 cm^{-1} is absent in the spectra and the $\nu(\text{Ge-C})$ peak at 740 cm^{-1} appears as a prominent peak.

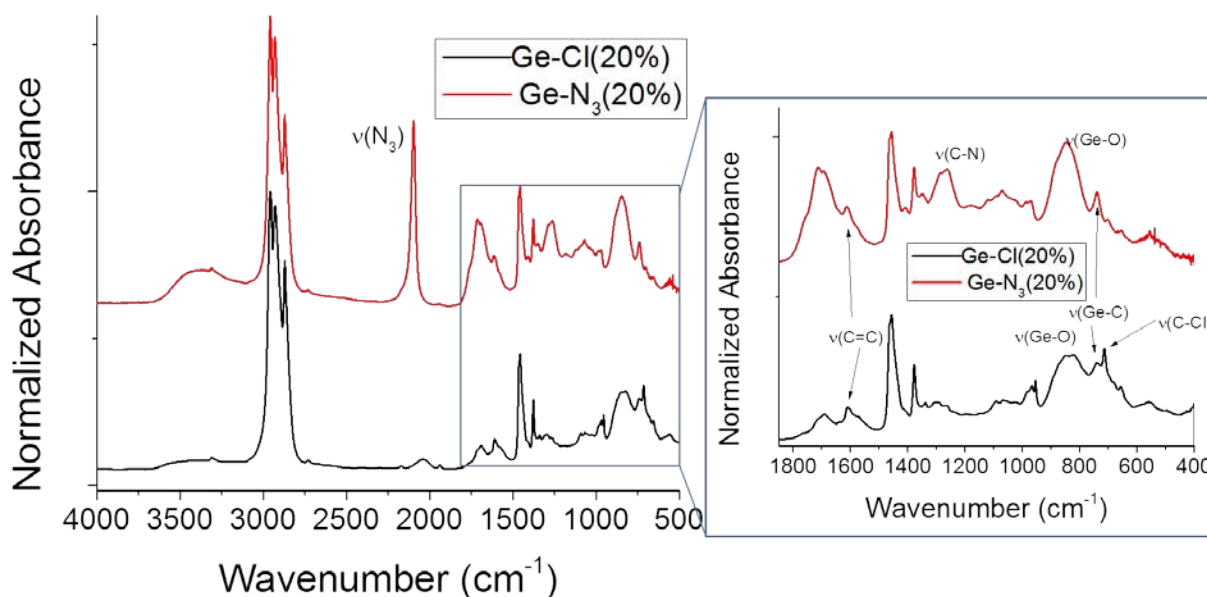


Figure 4.8: FT-IR spectra of chloro-terminated and azido-terminated Ge NPs.

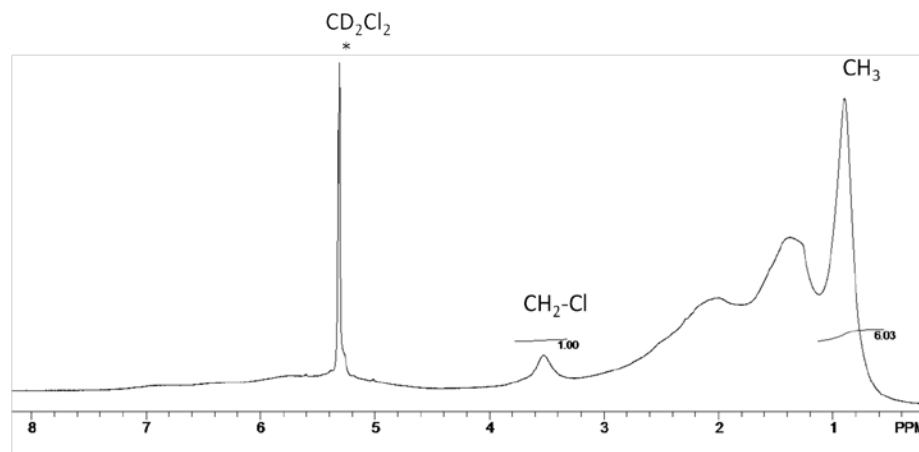


Figure 4.9: ^1H NMR spectrum of ω -chloropentenyl(20%) Ge NPs in CD_2Cl_2 .

4.3.2 PEGylated water soluble germanium nanoparticles

Water soluble PEGylated Ge NPs were synthesized from azido-terminated Ge NPs by alkyne-azido “click” reaction using mono-alkyne polyethylene glycol (alkyne PEG), 2KDa (scheme 4.2). It was found that PEGylated Ge NPs with 50% surface coverage are highly soluble in water (10mg/1ml).

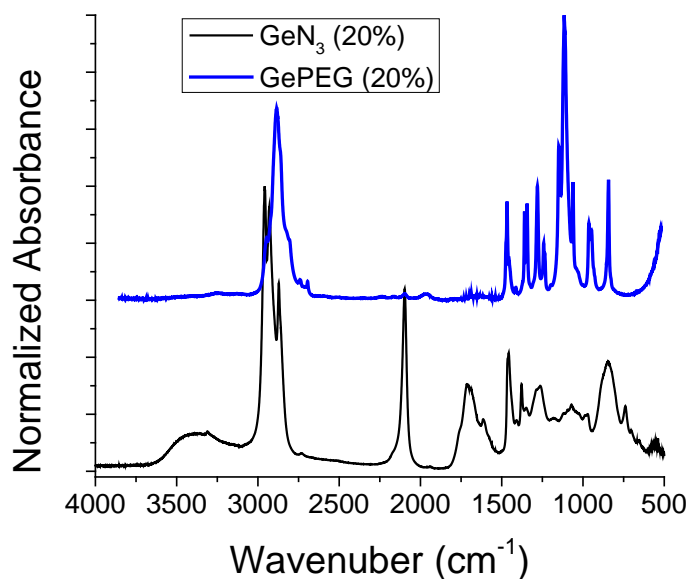
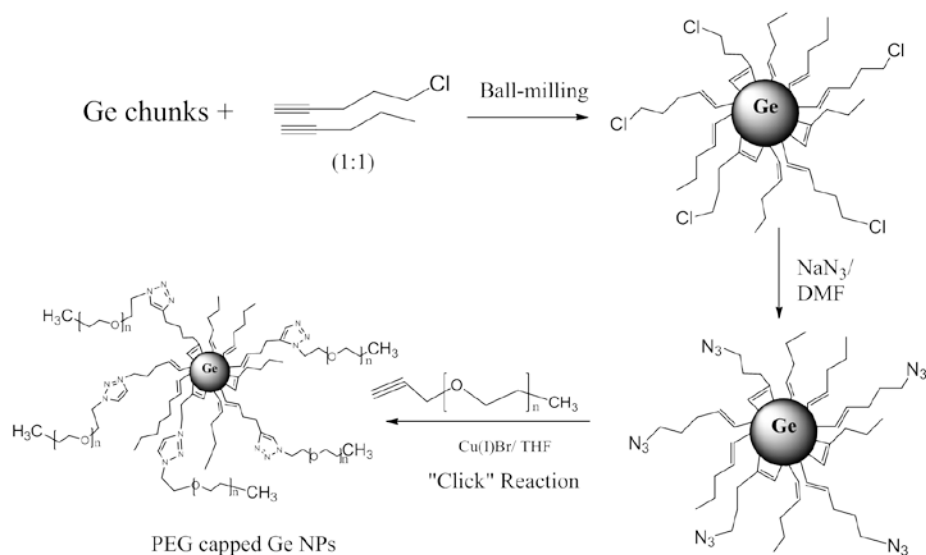


Figure 4.10: FT-IR spectra of azido-terminated and PEGylated Ge NPs

The FT-IR spectrum (in **Figure 4.10**) shows a broad peak centered at 2888 cm^{-1} and is due to methylene $\nu(\text{C-H})$ stretching from the PEG. A couple of new sharp peaks appeared at 1110 cm^{-1} and 844 cm^{-1} which are due to asymmetric $\nu(\text{C-O-C})$ and symmetric $\nu(\text{C-O-C})$ stretching. A couple of peaks at 1450 and 1350 cm^{-1} are due to C-H bending stretching. The azide stretching peak at 2100 cm^{-1} was not seen in the FT-IR spectrum of the PEGylated Ge NPs.

In the ^1H NMR spectra in CD_2Cl_2 (**Figure 4.11a**), a sharp peak was seen at 3.6 ppm due to methylene protons of PEG. Resonances from the NPs surface peak can be seen once the spectrum is vertically expanded. In the vertically expanded ^1H NMR spectrum (**Figure 4.11b**) triazole proton appeared at 7.6 ppm as a tiny broad peak. Methyl protons from the pentenyl group on Ge surface were seen exactly at same position at 0.9 ppm. Other methylene protons from the nanoparticles appeared as broad peak from 1.2 to 2.2 ppm.



Scheme 4.3: Synthesis of PEGylated Ge NPs

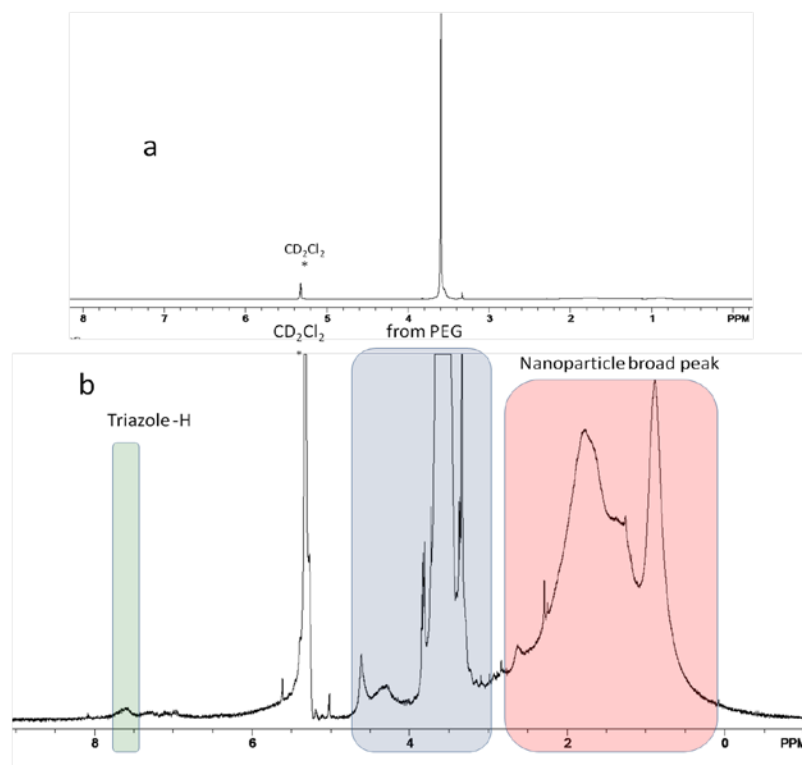


Figure 4.11: ^1H NMR spectra of PEGylated Ge NPs synthesized from ω -azido pentenyl (50%) Ge NPs.

The optical properties of the blue luminescent PEGylated Ge NPs were characterized in both water and dichloromethane by UV-vis absorption and PL-emission spectra (**Figure 4.12**). The UV-vis absorption spectrum shows a single absorption with a tail extended upto 500 nm. The PL emission spectra (**Figure 4.12**) show a red shifted emission peaks compared to the starting ω -chloropentenyl-Ge NPs. At an excitation wavelength 300 nm, the spectrum shows a much broader emission showing a peak at 500 nm and a shoulder at 440 nm. At an excitation wavelength of 340 nm, a peak at 440 nm was observed. The emission peaks move towards 500 nm upon increasing excitation wavelength from 380 nm to 420 nm. The red shift of PL may be due to polar PEG group on the nanoparticle surface and not due to solvent polarity. This effect is consistent with our dimethylaminopropenyl-Ge NPs and trimethylammonium-terminated Ge NPs (Chapter 2.3), as well as previously reported amine-terminated Si NPs.¹⁶ TEM images of PEGylated water soluble Ge NPs (**Figure 4.13**) show a larger average size particle of 15-20 nm due to aggregation of particles.

A cytotoxicity study was performed by Zuihof *et al* with these PEGylated Ge NPs along with other Si and Ge NPs on human colonic adenocarcinoma Caco-2 and rat alveolar macrophage NR8383 cells and it was found that water soluble PEGylated Ge nanoparticles did not show any cytotoxicity.⁹ On the other hand, amine-terminated cationic Ge NPs show a significant cytotoxicity through reactive oxygen species (ROS) generation in the cell. PEGylated Ge NPs are therefore biocompatible and biodegradable materials for potential biological application.⁹

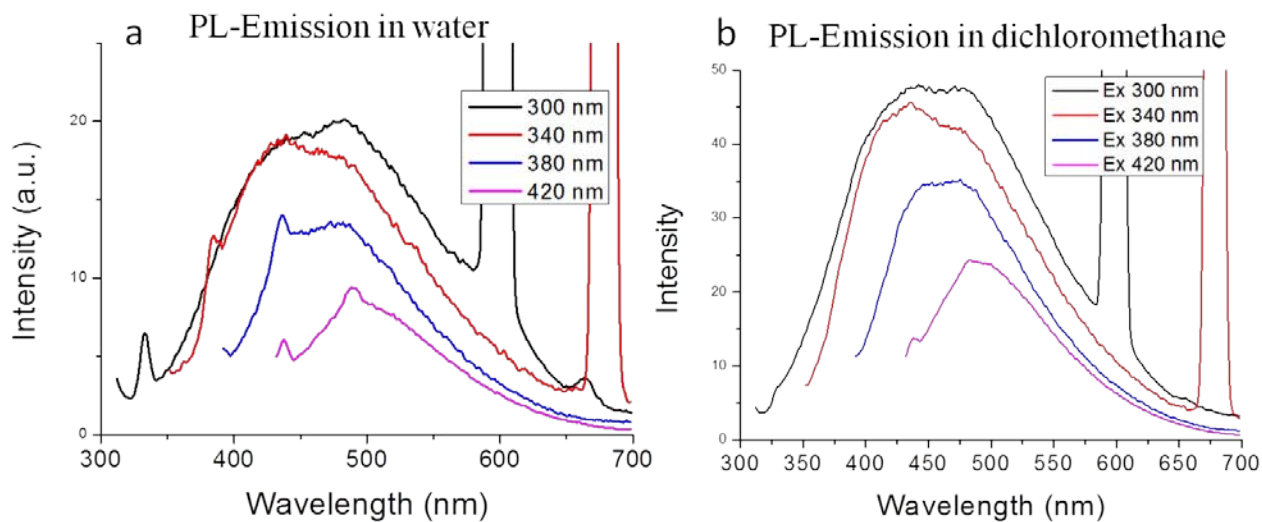


Figure 4.12: PL emission spectra of PEGylated Ge NPs in water and in dichloromethane.

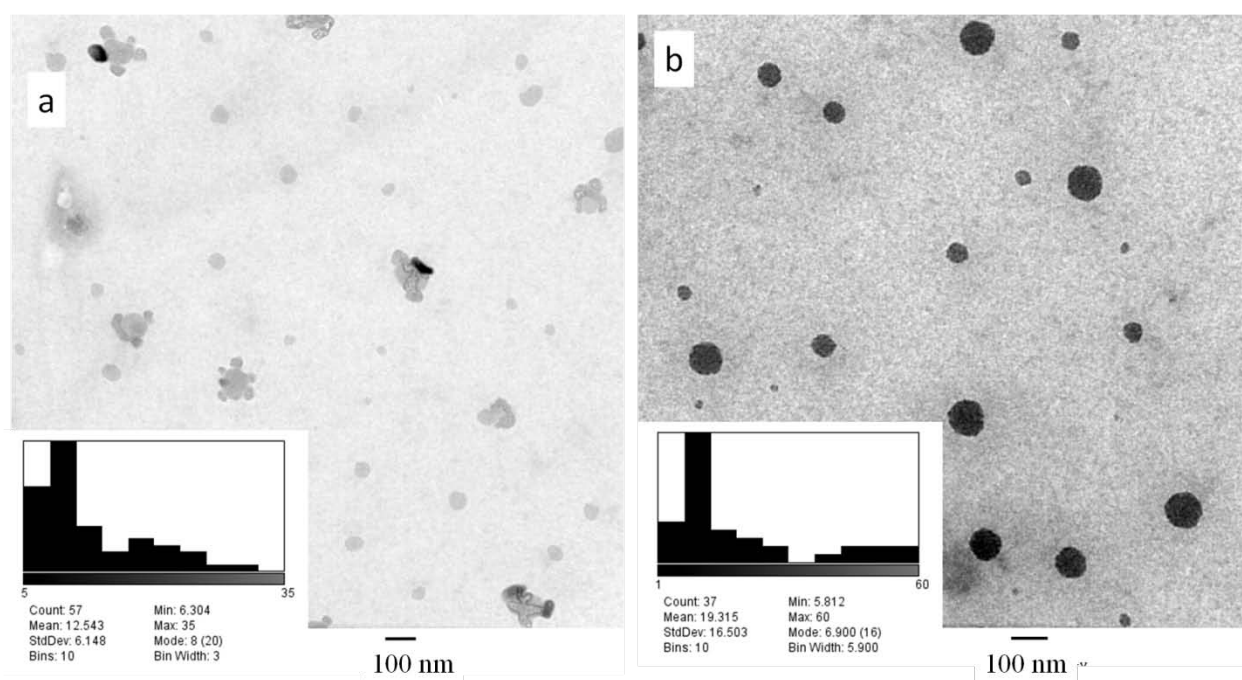
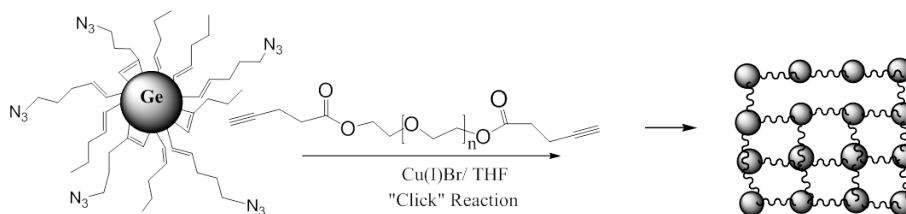


Figure 4.13: TEM images of PEGylated water soluble Ge NPs.

4.3.3 PEGylated Ge NP Clusters by a "click" reaction using bis-alkynyl PEG

Azido-terminated Ge NPs with various surface-coverage had undergone alkyne azide “click” reaction with various α,ω -bis-alkynyl PEG derivatives to form PEGylated Ge NP clusters (**Scheme 4.4**). For smaller spacers (like bis-alkyne TEG etc) Ge NP clusters were not identified by TEM, as they aggregated to form insoluble product and therefore cannot be redispersed in any solution before putting on a TEM grid. On the other hand, for bis-alkyne PEG (1KDa) there is some aggregation in the TEM (**Figure 4.14**) and individual particles cannot be seen from the clusters.



Scheme 4.4: Synthesis of PEGylated Ge NP Clusters using bis-alkynyl PEG

However, α,ω -bis-alkynyl PEG (2KDa) produced globular NP clusters with significant interparticle separation (in **Figure 4.16**). These clusters were made from 20% surface coverage of an azido-terminated surface. The product can be redispersed in dichloromethane or toluene and it was purified by GPC.

The FT-IR spectrum of Ge-PEG (2kDa) NP clusters (in **Figure 4.15**) shows a couple of new sharp peaks appeared at 1110 cm^{-1} and 844 cm^{-1} are due to asymmetric $\nu(C-O-C)$ and symmetric $\nu(C-O-C)$ stretching. A broad peak centered at 2888 cm^{-1} is due to the methylene $\nu(C-H)$ stretching from the PEG. A couple of peaks at 1450 and 1350 cm^{-1} are due to C-H bending stretching.

Similarly NP clusters were made from bis-alkyno PEG (10kDa); which are highly soluble in CH_2Cl_2 , methanol and water. However, the shape and size of the NP clusters, shown in the TEM images (in **Figure 4.18**) are not uniform.

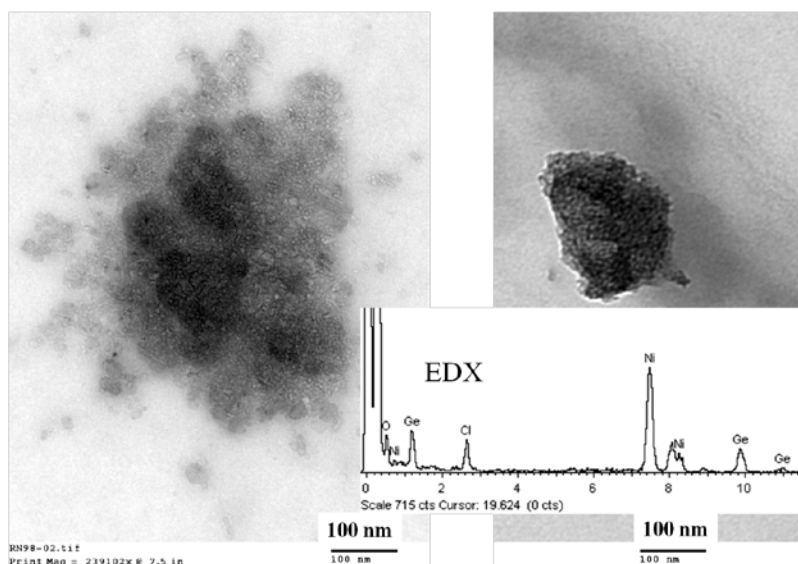


Figure 4.14: NP clusters with bis alkyno PEG (1kDa)

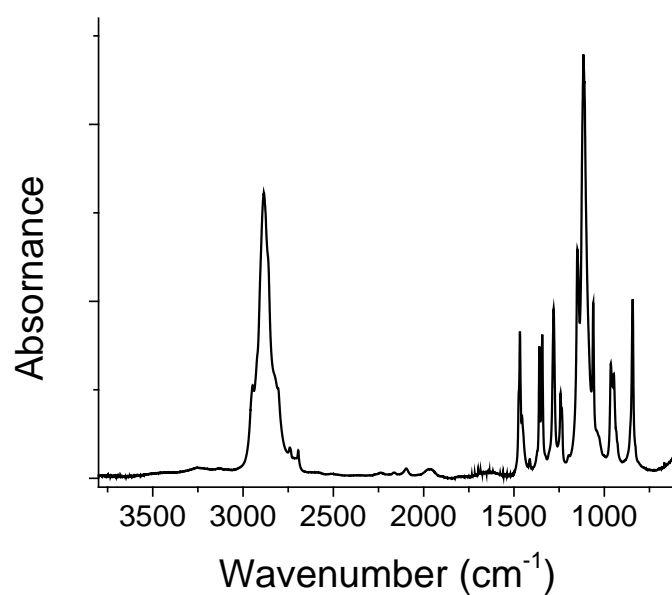


Figure 4. 15: FT-IR spectrum of NP clusters using bis alkyno-PEG (2kDa).

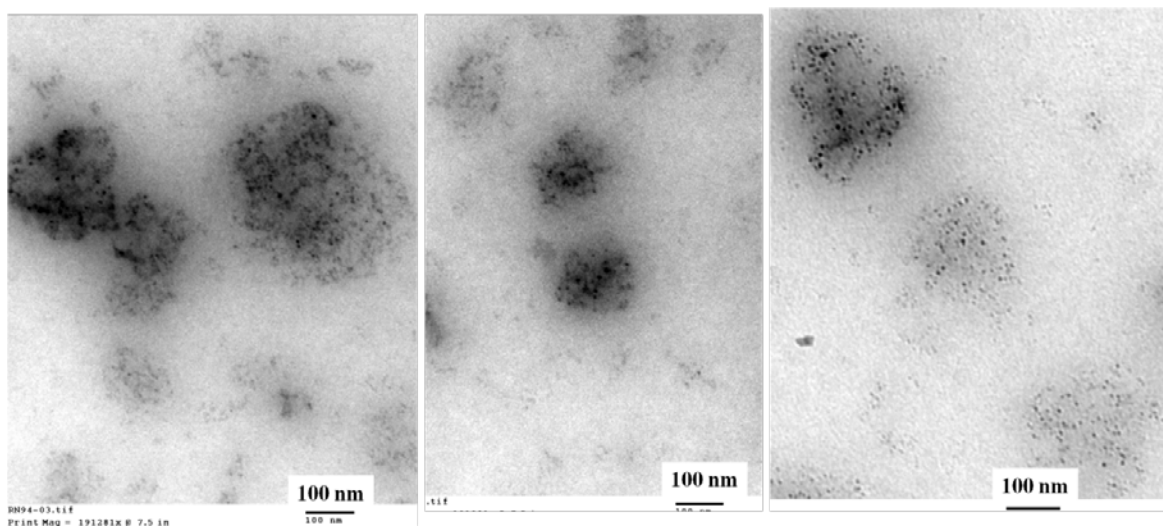


Figure 4.16: TEM images of NP clusters using bis alkynoPEG (2 kDa)

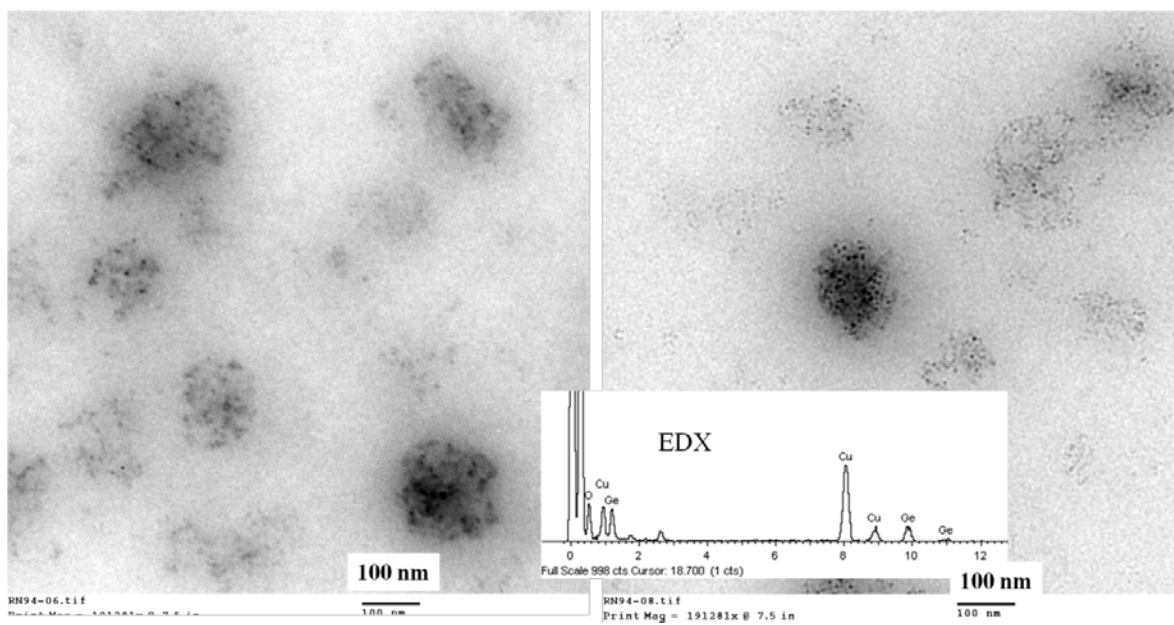


Figure 4.17: TEM images and EDX of NP clusters using bis alkynoPEG (2 kDa)

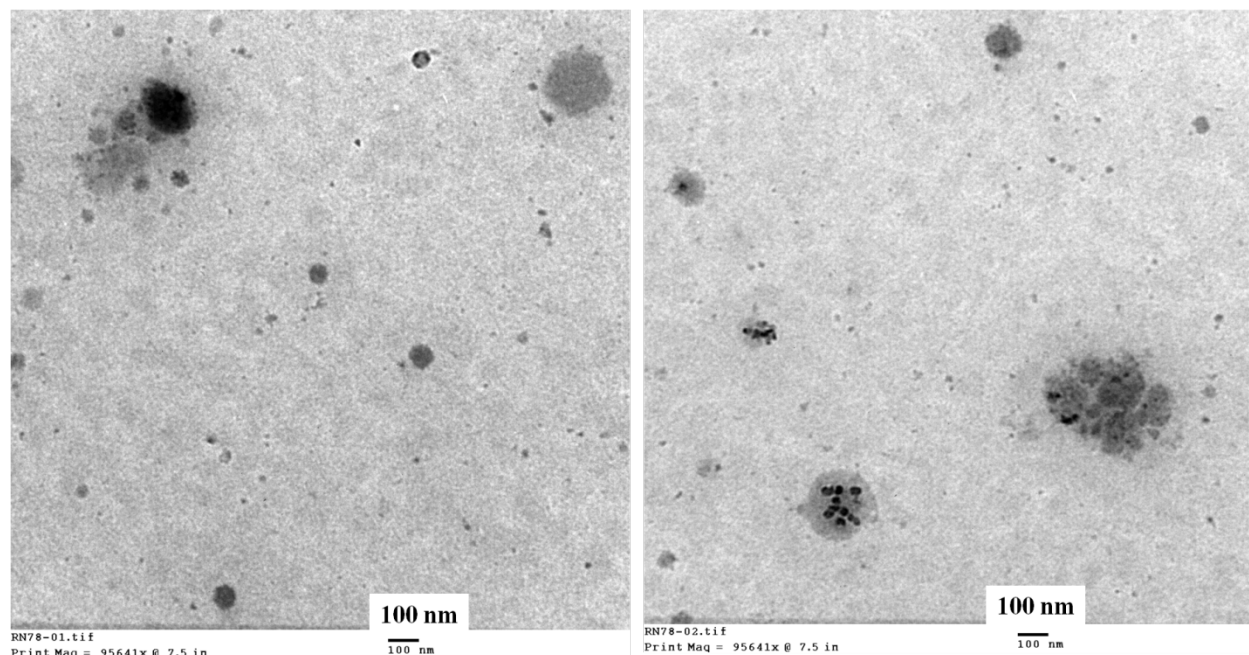


Figure 4.18: TEM images of NP clusters using bis alkynoPEG (10 kDa)

4.3.4 *Ge NP Clusters using conjugated spacer*

3D semiconductor nanoparticle arrays with shorter interparticle distance or with conjugated spacer could lead to nanoparticle based devices through inter particle coupling.^{17, 18} A simple conjugated spacer, which can be used for alkyne azide "click" reaction, is 1,4-diazido benzene. The conjugated spacer was synthesized from p-phenylenediamine.¹⁹ Ge NP clusters were prepared by a copper (I) catalyzed alkyne azide "click" reaction using ω -alkynyloctenyl(20%) Ge NPs and 1,4-diazidobenzene in THF. The product was separated by precipitation using aqueous ethanol solution. The solubility of the Ge NP clusters is very low in common organic solvents. TEM image (**Figure 4.19**) of the Ge NP clusters shows aggregated clusters. This may not be due to large cluster formation during the "click" reaction; rather low solubility of these clusters show the aggregated structure on TEM.

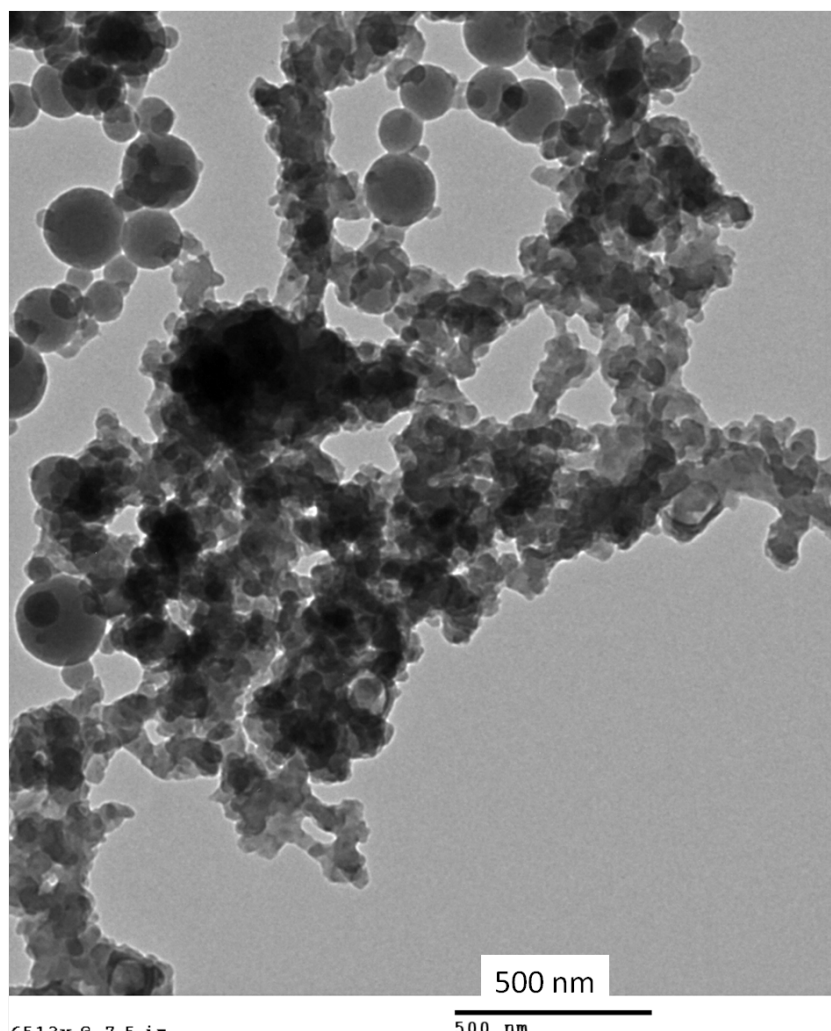


Figure 4.19: TEM image of Ge NP clusters synthesized by "click" reaction using conjugated spacer.

4.4 Nanoparticle Assembly by "Host-Guest" Chemistry

The assembly of three-dimensional semiconductor nanomaterials may be interesting in the field of biology or microelectronics due to their special optical and electrical properties.²⁰⁻²⁴ Host-guest chemistry which includes interactions through noncovalent bonding (hydrogen bonds, ionic bonds, van der Waals forces, and hydrophobic interactions), play an important role in the assembly of nanomaterials.^{25, 26} Macrocyclic hosts are molecular receptors that are arranged as a cavity, in which the guest, or substrate, may bind in the interior of the cavity.²⁵ Among various macrocyclic host molecules β -cyclodextrin, a cyclic oligosaccharide, is a biologically important molecule and it is used extensively as a host in supramolecular chemistry for biological applications.^{25, 27}

β -Cyclodextrin grafted Ge NPs were synthesized by copper(I) catalyzed alkyne-azide "click" reaction. Globular nanoparticle clusters were prepared from the functionalized Ge NPs through interparticle assembly using "host-guest" chemistry.

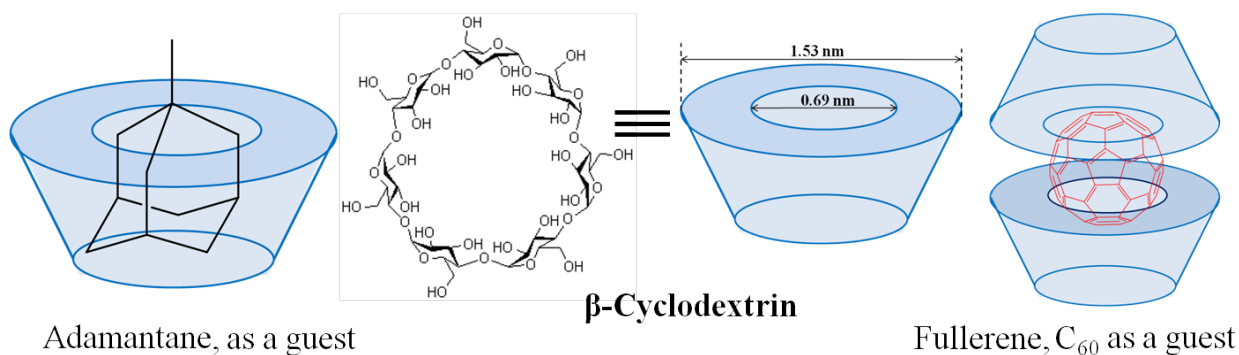


Figure 4.20: Structure of β -cyclodextrin, adamantane, fullerene and their inclusion complexes.

Adamantane, consisting of four fused cyclohexane rings in chair conformation, is the simplest diamondoid and widely used in a guest in supramolecular chemistry. Adamantane (which has a ring size ~ 6.9 Å) forms a strong (1:1) inclusion complex with β -cyclodextrin, as its outer ring size is 6.9 Å and inner ring size is about 0.5 Å.²³ On the other hand, fullerene C₆₀, a spherical fullerene, which consists of 60 C atoms with π -conjugation similar to graphite, plays an important role in the fields of nanotechnology, supramolecular chemistry and materials chemistry.²⁸ When fullerene C₆₀ is used as a guest it forms (2:1) inclusion complex with β -cyclodextrin (**Figure 4.20**).^{20, 29}

4.4.1 *β -Cyclodextrin-grafted germanium nanoparticles*

The β -cyclodextrin-grafted germanium nanoparticles were synthesized from alkyne terminated (ω -alkynyloctenyl(30%)) Ge NPs by copper catalyzed “click” reaction using mono-azido cyclodextrin in DMF/THF. The later was synthesized from mono-tosylated β -cyclodextrin by azidation. The CD 30% NPs were purified by dialysis using dialysis membrane (MWCO 1KDa) for three days in aqueous alcohol. The product can be re-dispersed in aqueous alcohol (50%) and DMSO.

The ¹H NMR spectrum of ω - β CD octenyl(30%)-Ge NPs (in **Figure 4.21**) confirms a triazole proton peak at 7.8ppm, as well as peaks from β -cyclodextrin and alkyl protons from the nanoparticle surface. A broad peak at 5.8ppm is due to O-H protons from the β -cyclodextrin. Other protons from the β -cyclodextrin appeared at 4.8ppm, 3.6ppm and 3.3 ppm. Methyl protons and methylene protons from nanoparticle surface appeared at 0.9 ppm and 1.2-1.5 ppm respectively. Integration of triazole protons to the

nanoparticles' methyl proton (1:18) gives an estimated surface coverage of β -CD of about 14-15%.

The FT-IR spectrum of ω - β CD octenyl (30%) Ge NPs (in **Figure 4.22**) shows clear evidence of β -cyclodextrin moiety on the surface as shown by a broad peak at $\sim 3400\text{ cm}^{-1}$ and a sharp peak at 1110 cm^{-1} due to $\nu(\text{O-H})$ and $\nu(\text{C-O})$ respectively. Saturated $\nu(\text{C-H})$ and $\delta(\text{C-H})$ appeared at $2850\text{--}3000\text{ cm}^{-1}$ and $1375\text{--}1460\text{ cm}^{-1}$ respectively. A bending O-H vibration was seen at $\sim 1650\text{ cm}^{-1}$.

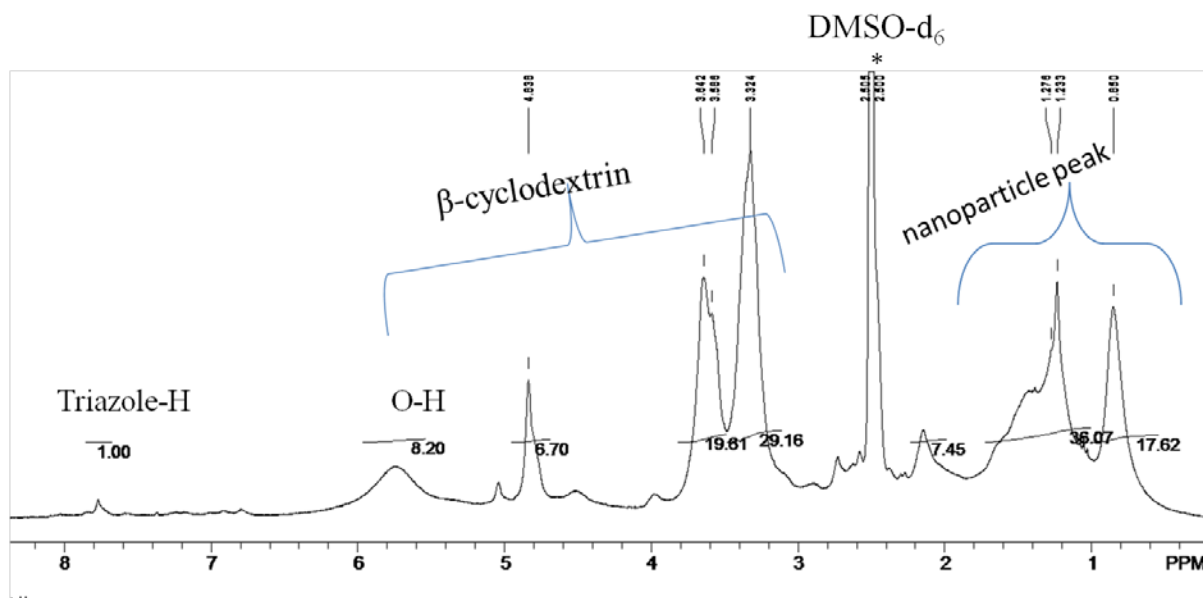


Figure 4.21: ^1H NMR of ω - β CD octenyl (30%) Ge NPs in DMSO-d_6 .

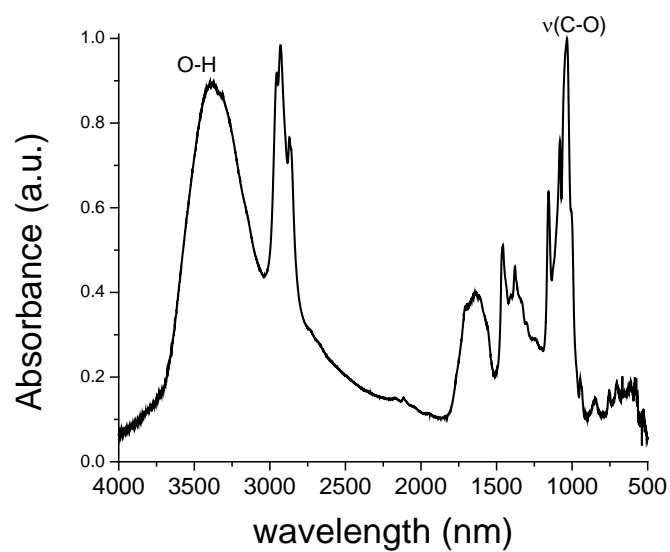


Figure 4.22: FT-IR spectrum of ω - β CD-octenyl (30%) Ge NPs.

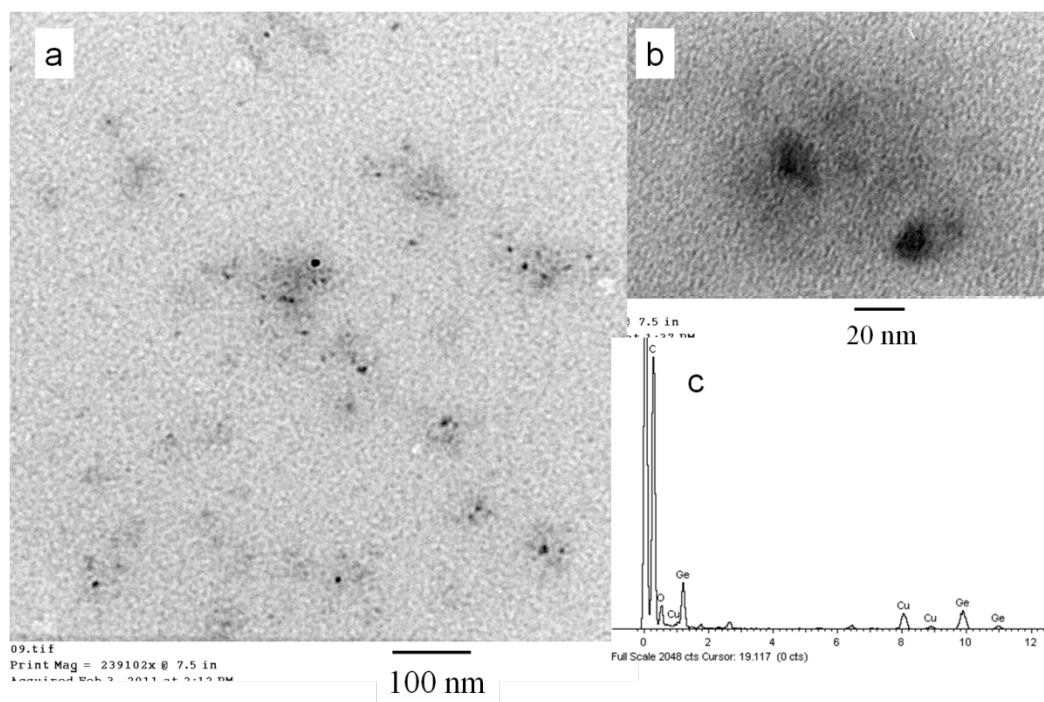


Figure 4.23: TEM image and EDX of ω - β CD octenyl (30%) Ge NPs.

4.4.2 Adamantane-grafted Ge nanoparticles

The ω -adamantanyloctenyl(20%)-Ge NPs were synthesized from ω -alkynyloctenyl(20%)-Ge NPs by copper(I) catalyzed “click” reaction using mono-azido adamantane in THF. Product was purified by GPC using Bio-beads S-X1 as a stationary phase and dichloromethane as an elutant. Assembly of nanoparticles were made by host-guest interaction of CD-terminated Ge NPs with either ω -adamantanyloctenyl(20%) Ge NPs or ω -adamantanyloctenyl(20%) Si NPs which were synthesized by a similar method.

The ^1H NMR spectrum of ω -adamantanyloctenyl(20%)-Ge NPs in CD_2Cl_2 is shown in **Figure 4.24**. A couple of sharp peaks at 2.2 ppm and at 1.6-1.8 ppm appeared due to CH and CH_2 peaks from adamantane moiety. The triazole proton peak was seen at 7.4-7.6 ppm. The methyl protons from octenyl group appeared at 0.8 ppm and a broad peak from 1.1 to 1.4 ppm due to chain methylene protons. The ratio of the integration over triazole proton, adamantane peaks and the chain CH_3 peak is 1:13:12; therefore, the coverage of adamantane moiety is about 20%. However, adamantane's peak appeared same position (at 2.2 ppm) as the alkyne proton's peak.

In the FT-IR spectra of ω -adamantanyloctenyl(20%)-Ge NPs (**Figure 2.25**) alkyne C-H stretching at 3300 cm^{-1} and $\nu(\text{C}\equiv\text{C})$ at 2050 cm^{-1} were absent and a new weak peak appeared at 3140 cm^{-1} due to triazole $\nu(\text{C-H})$. Saturated C-H stretching comes from $2850\text{-}3000\text{ cm}^{-1}$ and peaks at 1375 and 1475 cm^{-1} for C-H bending vibration. A enhanced peak at $1600\text{-}1650\text{ cm}^{-1}$ is $\nu(\text{C}=\text{C})$ and $\nu(\text{C}=\text{N})$ from the triazole. A peak at 750 cm^{-1} is due to $\nu(\text{Ge-C})$.

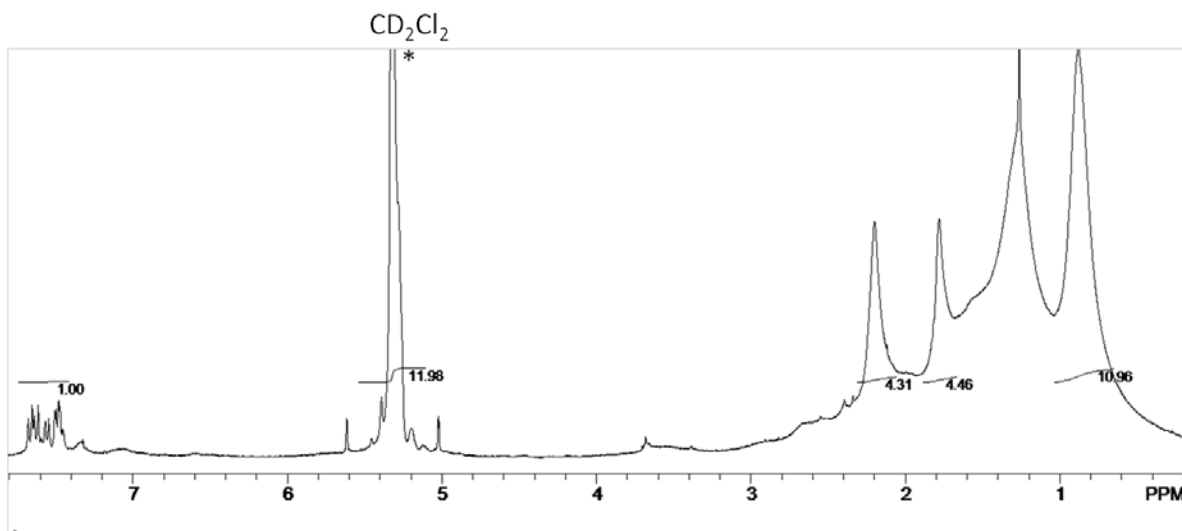


Figure 4.24: 1H NMR spectrum of ω -adamantanyloctenyl(20%) Ge NPs.

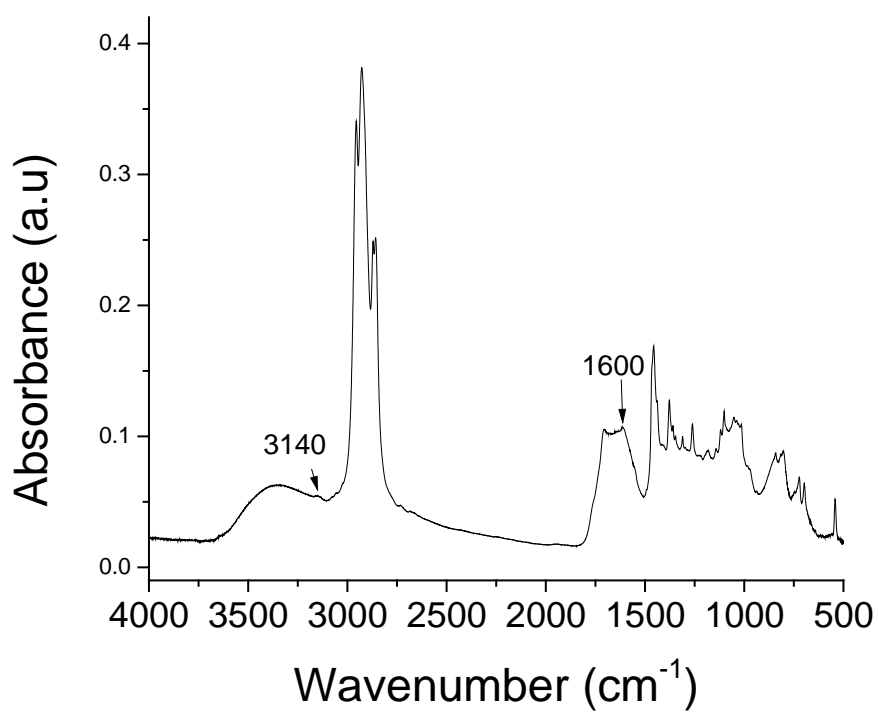


Figure 4.25: FT-IR spectrum of ω -adamantanyloctenyl(20%) Ge NPs.

4.4.3 Ge-C₆₀-Ge Nanoparticle Assembly

Interparticle 3D assembly of Ge NPs was made incorporating fullerene, C₆₀, in between the hydrophobic cores of two β -CD from different Ge-CD NPs. The toluene solution β -CD (30%)-terminated Ge-CD NPs and fullerene, C₆₀, were stirred for a week to prepare the Ge NP assembly. Unreacted fullerene can be precipitated out by adding excess methanol in the solution.

FT-IR spectrum of Ge-C₆₀-Ge clusters (**Figure 2.26**) should show a couple of peaks at 1186 cm⁻¹ and 1430 cm⁻¹ for fullerene, C₆₀.^{30, 31} A strong peak was seen at 1110 cm⁻¹ due to ν (C-O) from β -CD; which might overlap the fullerene peak. Another peak (at 1430 cm⁻¹) might overlap with δ (C-H) which appeared at 1460 cm⁻¹ and 1370 cm⁻¹. Saturated C-H stretching was seen from 3000 cm⁻¹ to 2850 cm⁻¹.

UV-vis spectra of Ge-C₆₀-Ge NP (**Figure 2.27**) clusters show featureless absorption with a couple of weak shoulders at ~252 nm and at 326 nm. UV-vis spectra of pure fullerene, C₆₀ show two peaks at 257 nm and 329 nm. The PL emission spectra of the Ge NP clusters show a very broad emission at 300 nm excitation wavelength showing a couple of peaks at 400 nm and 340 nm. Narrower emission peaks move to higher wavelength upon increasing excitation wavelengths from 320 nm to 420 nm. The broad emission at lower excitation wavelength may be due to partial energy transfer from G NPs to fullerene.

TEM images of Ge-C₆₀-Ge NP clusters (**Figure 2.28**) show that the average NP cluster size is 40-80 nm. EDX from HRTEM confirms Ge showing peaks at 1.2, 10 and 11 keV.

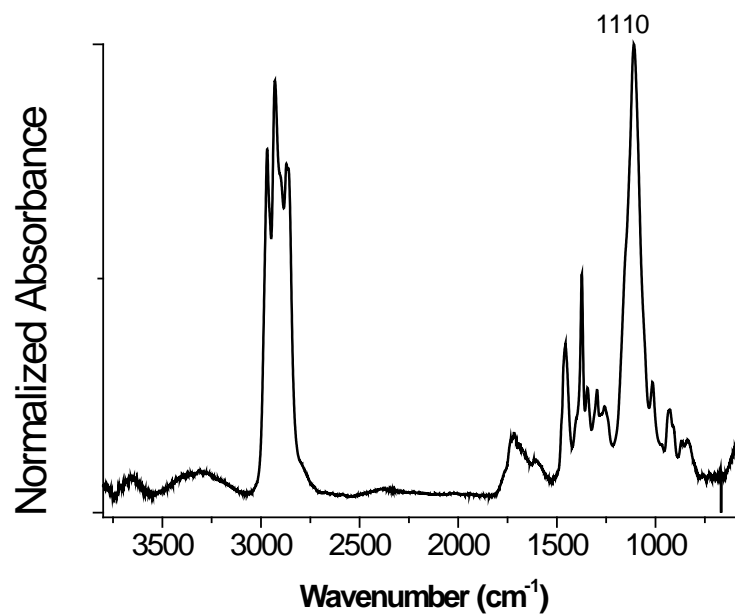


Figure 2.26 : FT-IR spectrum of Ge-C₆₀-Ge NP clusters

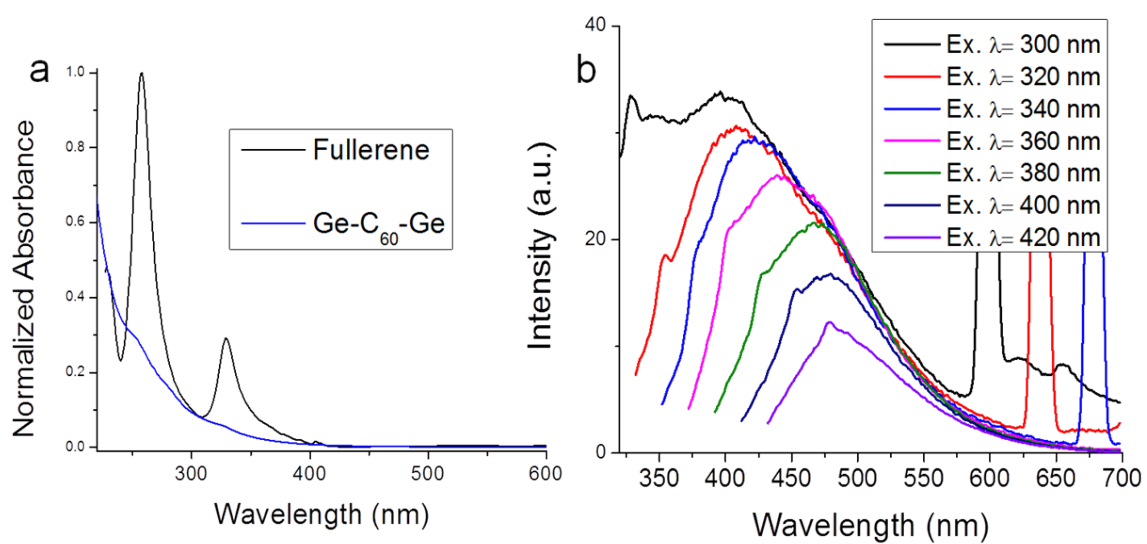


Figure 4.27: UV-vis absorption (a) and PL emission spectra (b) of Ge-C₆₀-Ge NP clusters.

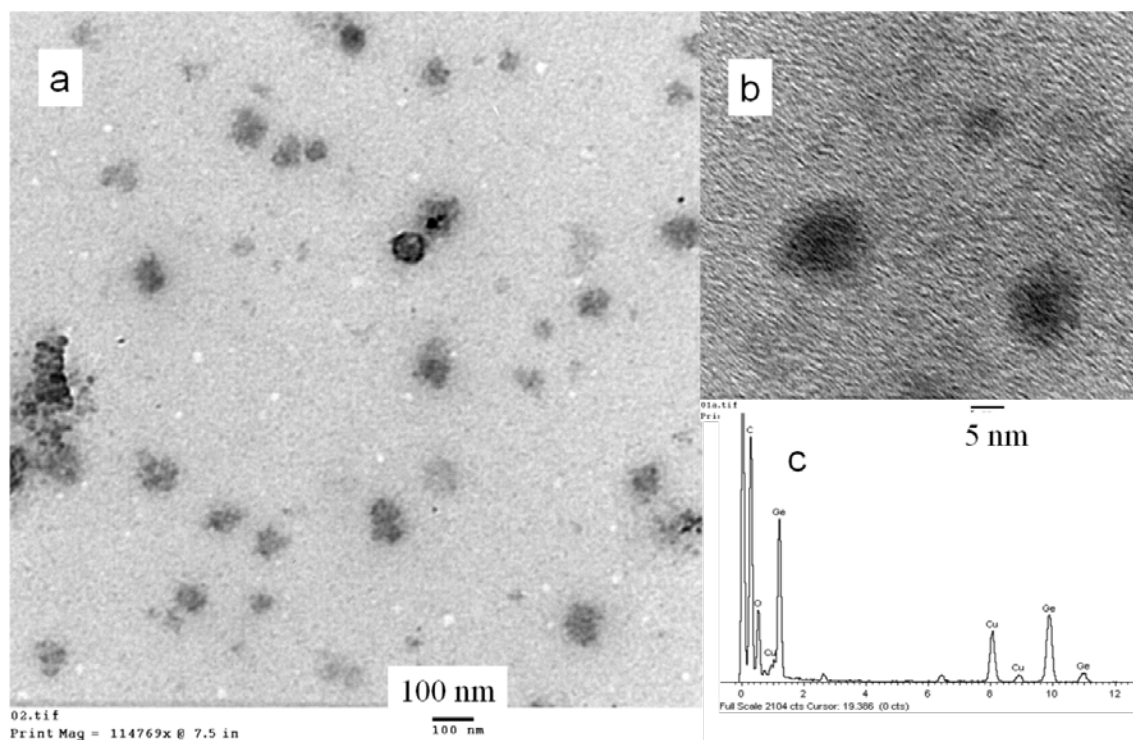
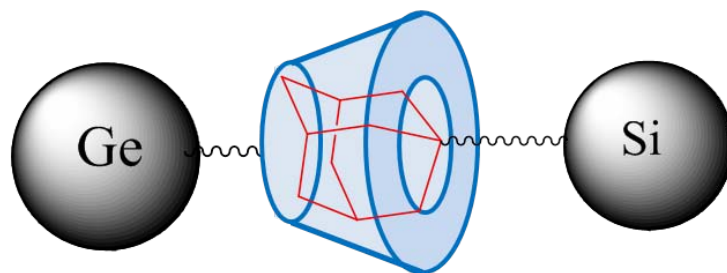


Figure 4.28: TEM (a) HRTEM (b) image and EDX (c) of Ge-C₆₀-Ge NP clusters.

4.4.4 Ge-Si Nanocluster by assembly of Ge and Si NPs using host-guest interaction

Ge and Si 3D nanostructures were prepared from ω - β CD octenyl(30%) Ge NPS and ω -adamantanyloctenyl(20%)-Si NPs by host-guest interaction in DMF. Ge-Si NP clusters were separated as precipitate by centrifugation after stirring for 3 days in DMF.

TEM images of the Ge-Si NP (**Figure 4.29**) clusters show very large aggregated NP cluster with average size from 100 nm-700 nm. EDX spectrum (**Figure 4.30**) confirm the Ge peaks at 1.2 kev, 10 kev and 11 kev. It also confirms Si showing a peak at 1.8 kev. Dynamic light scattering (DLC) data show average hydrodynamic radius of these clusters is ~700 nm.



Scheme 4.5: A noncovalent bonding between Ge and Si NPs through host-guest interaction of β -CD and adamantane in the NP Clusters.

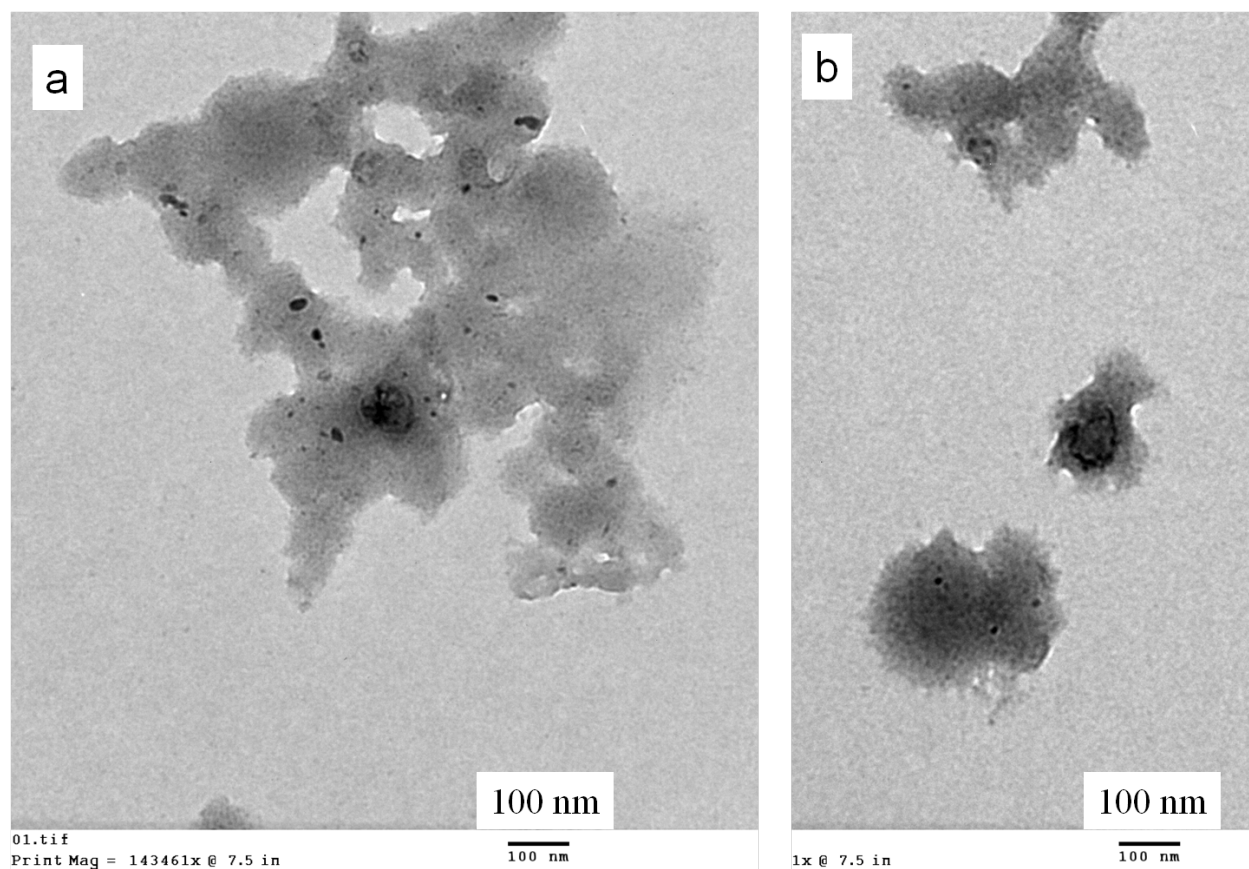


Figure 4. 29: TEM images of Ge-Si NP clusters.

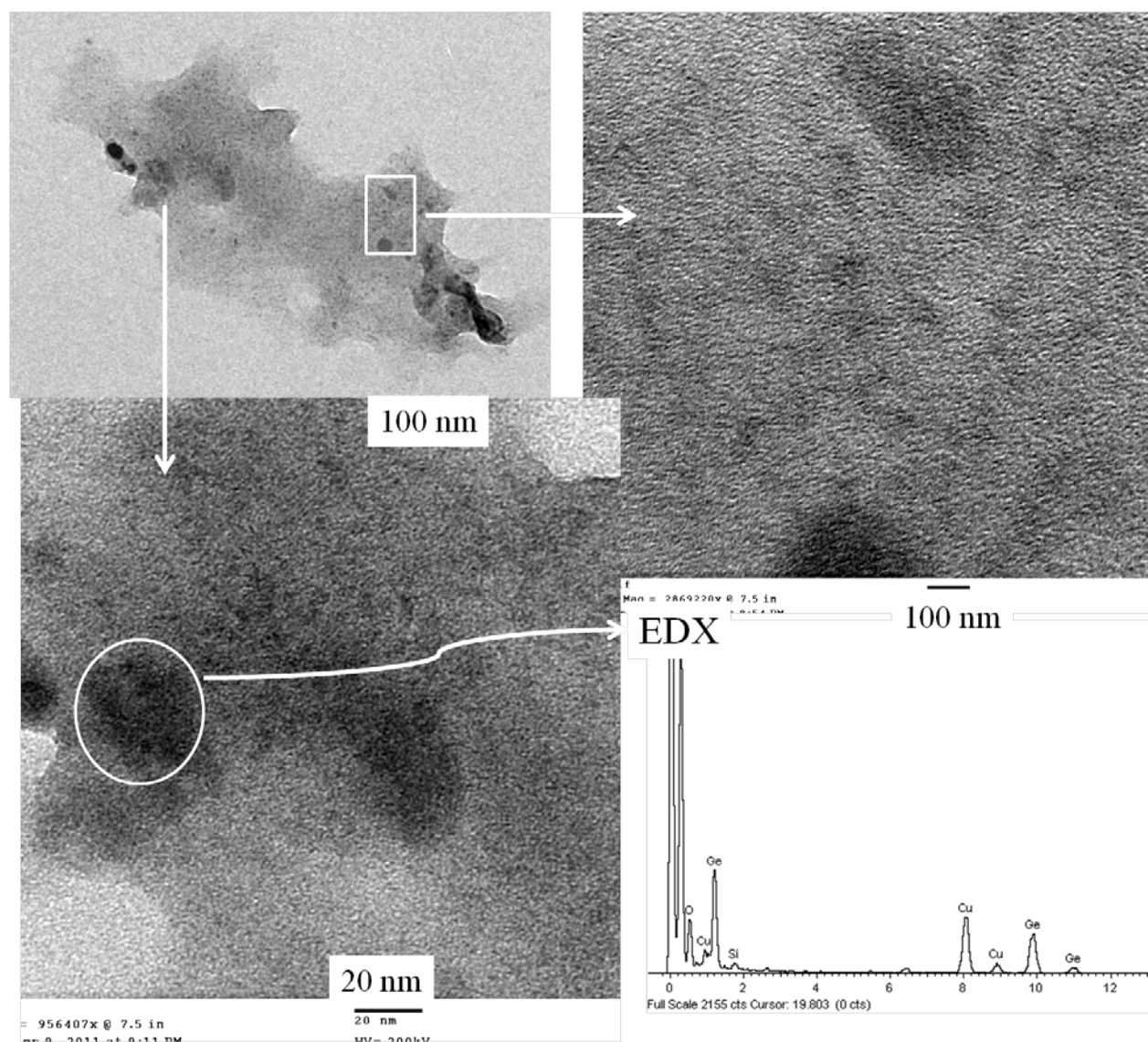


Figure 4. 30: HRTEM images and EDX of Ge-Si NP clusters.

4.5 Experimental

4.5.1 Method and materials

Germanium (~2mm pieces), 99.999% purity, purchased either from Sigma-Aldrich or from Alfa Aesar. 1-Octyne (98%), 1,7-octadiyne (98%), 1-pentyne (98%) and 5-chloro-1-pentyne were purchased from Alfa-Aesar and used after distillation under nitrogen. Tetraethylene glycol (TEG, 99%), sodium azide (99%), copper(I)bromide, dimethyl sulfide (99.9%) and N,N,N',N',N''-pentamethyldiethylenetriamine (PMDTA, 98%) were purchased from Sigma Aldrich. *mono*-alkynyl-polyethylene glycol (PEG, 2 kDa), bis-alkynyl PEG (2 kDa, 4.6 kDa, 10 kDa) and *bis*-azido PEG (2 kDa) were synthesized in Dr. Graysen's Group. For host-guest chemistry, *mono*-azido-adamantane (98%) was purchased from Sigma Aldrich and used without further purification.

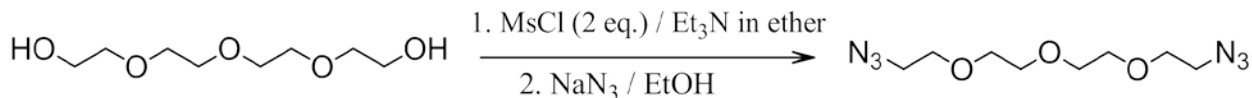
4.5.2 Synthesis of ω -alkynyloctenyl-Ge NPs.

Germanium (0.75g) was placed in a stainless steel milling vial along with stainless steel milling balls, each with a diameter of 1.2 cm and weighing 8.1 g. In a nitrogen filled glovebox, the milling vial was filled with 25ml of reactive alkynes having various ratios of 1-octyne and 1,7-octadiyne (with 10%, 15%, 20%, 30% and 50% (v/v) of diyne) and then tightly sealed. The milling vial was placed in a SPEX 8000-D Dual Mixer/Mill, and high energy ball-milling was performed for 24 hours. After milling, the reaction mixture was centrifuged, and soluble nanoparticles were separated from the residue of bigger particles. The synthesized nanoparticle was dried and starting alkynes (i.e. 1-octyne and 1,7-octadiyne) were recovered by vacuum distillation. Crude yield: 140 mg. The crude Ge NPs can be purified and fractionated by particle size in to various fractions by gel permeation chromatography (GPC) using a Bio-beads S-X1 beads as

stationary phase and dichloromethane as elutant. $^1\text{H NMR}$ (300 MHz, CDCl_3): δ 5.4-6 ppm (broad and weak), 2.2(broad), 1.8 (broad), 1.2-1.5 (m), 0.8 (s). **FT-IR** (thin film on KBr plate): 3300, 2850-3000, 2100, \sim 1600, 1465, 1375, 750-900, 750 cm^{-1} .

4.5.3 Synthesis of 1,11-diazido-3,6,9-trioxaundecane (diazido-TEG)

1,11-diazido-3,6,9-trioxaundecane (diazido tetraethyleneglycol (TEG) was synthesized by a modified reported method (**Scheme 4.5**).³² Tetraethylene glycol (11.5 ml, 0.065 mol) was taken in a two neck flask equipped with an addition funnel and magnetic stir bar. It was degased under vacuum at room temperature for an hour. Dry ether (50 ml) and followed by dry $\text{N}(\text{CH}_3)_3$ (12.5 ml) was added under nitrogen and the solution was cooled to 0 $^\circ\text{C}$. Methaneaulfonyl chloride (15.0 g, 0.130 mol) was added through additional funnel and the solution was allowed to warm slowly to room temperature and stirred for few hours. The reaction mixture with yellow-white precipitate was concentrated by rotary evaporation. 95% ethanol (125 ml) and 9.75 g (0.15 mol) of sodium azide were added and the reaction mixture was heated at reflux for 12 hours. It was cooled to room temperature, and concentrated by rotary evaporation. The product was extracted in ether (150 ml) after washing it with brine solution (60 ml), dried by rotary evaporation and then by vacuum to obtain a yellowish viscous oil. Yield: 11 g (70%). **FT-IR** (thin film on KBr): 2880, 2106, 1460, 1350, 1300, 1110, 936, 887, 851 cm^{-1} . $^1\text{H NMR}$ (300 MHz, CD_2Cl_2): δ 3.34 (t, 4H), 3.6 (m, 12H) ppm.



Scheme 4.5: Synthesis of 1,11-diaddo-3,6,9-trioxaundecane.

4.5.4 Synthesis of Ge NP clusters using ω -alkynyloctenyl(15%)-Ge NPs and diazido

TEG by "Click" Reaction:

In most cases Ge NP clusters were synthesized using size separated fraction to have nearly monodispersed nanoparticles in the clusters. 30 mg of 1,11-diazido-3,6,9-trioxaundecane (diazido TEG) was added to the GPC separated (Fraction 3) ω -alkynyloctenyl(15%) Ge NPs solution (24 mg Ge NPs in 50 ml THF). PMDTA (0.5 ml) was added to the flask. The reaction mixture was degassed in three pump-thaw-degas-cycles. The catalyst, Cu(I)Br. \cdot S(CH₃)₂ (13 mg) was added in the degassed solution and the reaction mixture was stirred for overnight at room temperature under N₂ flow. The reaction mixture was concentrated and 50% aqueous ethanol was added to get precipitate of NP clusters. The precipitate. was separated by centrifugation and washed three times with 50% aqueous ethanol. TEM was taken in toluene dispersion of these clusters. Weight of the white solid product: 12 mg (yield: 50% by weight). **FT-IR** (KBr pellet was made from solid sample and KBr powder mixture): 3140, 2850-3000, ~1600, 1465, 1375, 1110, 900-750 cm⁻¹.

4.5.5 Synthesis of Ge NP cluster using ω -alkynyloctenyl(15%)-Ge NPs and diazido

PEG by "Click" Reaction:

Diazido PEG (2kDa, 40 mg), synthesized in Dr. Grayson's group, was added to the GPC separated (Fraction 3) ω -alkynyloctenyl(15%) Ge NPs solution (30 mg of Ge NPs in 50 ml THF). PMDTA (0.5 ml) was added to the flask. The reaction mixture was degassed in three pump-thaw-degas-cycles. The catalyst, Cu(I)Br. \cdot S(CH₃)₂ (20 mg) was added in the degassed solution and the reaction mixture was stirred for overnight at

room temperature under N₂ flow. The reaction mixture was concentrated and 50% aqueous ethanol was added to get precipitate of NP clusters. The precipitate. was separated by centrifugation and washed three times with 50% aqueous ethanol to remove all copper. TEM was taken in Toluene dispersion of these clusters. Weight of white solid product: 18 mg and yield: 60% (by weight). **FT-IR** (KBr pellet was made from solid sample and KBr powder mixture): 3140, 2850-3000, ~1600, 1465, 1375, 1110, 900-750 cm⁻¹.

4.5.6 Synthesis of ω -PEGylactenyl(20%) Ge NPs from ω -alkynylactenyl(20%)-Ge NPs

ω -alkynylactenyl(20%) Ge NPs (50 mg) were dissolved in 10 ml of THF in a 100 ml Schlenk flask. Azido-PEG (2kDa) (50 mg) and 0.5 ml of PMDTA were then added to the solution. The solution was degassed three pump-thaw-degas cycles. Copper(I)bromide.dimethylsulfate (~20-30 mg) was added To the degassed mixture under N₂ flow. The reaction flask was stirred overnight under nitrogen to complete the reaction. The reaction mixture then was concentrated by rotary evaporation and the particles redispersed in 40 ml dichloromethane. The dichloromethane solution was washed three times with 40 ml brine/ ethylene diamine solution. The nanoparticle solution was dried over anhydrous MgSO₄, filtered and concentrated by rotary-evaporation. The crude NPs were further purified by gel permeation chromatography (GPC) using Bio-beads S-X1, as stationary, and dichloromethane, as eluting solvent, to remove unreacted PEG. The PEGylated Ge NPs can be redispersed in common organic solvents including toluene, dichloromethane and alcohols. **FT-IR** (thin film on KBr):

3140 (weak), 3000-2850, 1470, 1353, 1278, 1110, 954, 846 cm^{-1} . **^1H NMR** (300 MHz, CD_2Cl_2): δ (ppm) 0.8 (weak), 1.2-2 (broad, weak), 3.6 (m), 7.6 (weak).

4.5.7 Synthesis of ω -chloropentenyl Ge NPs by HEBM.

Germanium (0.75g) was placed in a stainless steel milling vial along with stainless steel milling balls, each with a diameter of 1.2 cm and weighing 8.1 g. In a nitrogen filled glovebox, the milling vial was filled with 25 ml of reactive alkynes taking various ratios of 1-pentyne and 5-chloro-1-pentyne (with 10%, 15%, 20%, 30% and 50% chloropentyne) and then tightly sealed. The milling vial was placed in a SPEX 8000-D Dual Mixer/Mill, and high energy ball-milling (HEBM) was performed for 24 hours. After milling, the reaction mixture was centrifuged, and soluble nanoparticles were separated from the residue of bigger particles. The synthesized nanoparticle was dried and the starting alkynes (i.e. 1-pentyne and 5-chloro-1-pentyne) were recovered by vacuum distillation. The crude yield: 160 mg. The crude NPs were purified by gel permeation chromatography (GPC) using a Bio-beads S-X1 beads packed column (40 cm height and 1.2 cm width), as stationary phase and dichloromethane, as mobile phase. **^1H NMR** (300 MHz, CD_2Cl_2): δ 5.5-6 ppm (broad and weak), 3.5 ppm (s), 1.2-2.5 ppm (m, broad), 0.9 ppm (s). **FT-IR** (thin film on KBr plate): 2850-3000, ~1600, 1465, 1375, 900-750, 730 cm^{-1} .

4.5.8 Synthesis of ω -azidopentenyl (50%) Ge NPs.

Chloro-terminated (ω -chloropentenyl(50%)) Ge NPs (100 mg) were dissolved in 30 ml N,N-dimethyl formamide (DMF) and placed in a 100 ml reaction flask, equipped

with a stirr bar. Sodium azide (100 mg, in excess) was then added to the reaction flask. The reaction mixture was stirred overnight at 70 °C. The reaction mixture was concentrated by rotary evaporation and the product was extracted in dichloromethane (50 ml) after washing three times with brine solution (50 ml). It was dried over anhydrous MgSO_4 and concentrated by rotary evaporation. The product was purified by gel permeation chromatography (GPC) using a Bio-beads S-X1 beads (GPC technique was described in Chapter 2). Yield: 78 mg (78% by weight). **^1H NMR** (300 MHz, CD_2Cl_2): δ 5.5-6 ppm (broad and weak), 4.23 ppm (s), 1.2-2.5 ppm (m, broad), 0.9 ppm (s). **FT-IR** (thin film on KBr plate): 2850-3000, 2100, ~1600, 1465, 1375, 900-750, 730 cm^{-1} .

4.5.9 Synthesis of ω -PEGylpentenyl Ge NPs from ω -azidopentenyl Ge NPs.

ω -Azidopentenyl Ge NPs with 20% and 50 % surface coverage were used to synthesize PEGylated Ge NPs. The ω -Azidopentenyl Ge NPs solution (50 mg in 40 ml THF), azido-PEG (2kDa), (50 mg) and a 0.5 ml of PMDTA were taken in a 100 ml Schlenk flask.. The solution was degassed three pump-thaw-degas cycles. Copper(I)bromide.dimethylsulfate (~20-30 mg) was added To the degassed mixture under N_2 flow. The reaction flask was stirred overnight under nitrogen to complete the reaction. The reaction mixture then was concentrated by rotary evaporation and the particles redispersed in 40 ml dichloromethane. The dichloromethane solution was washed three times with 40 ml brine/ ethylene diamine solution. The nanoparticle solution was dried over anhydrous MgSO_4 , filtered and concentrated by rotary-evaporation. The crude NPs were further purified by gel permeation chromatography (GPC) using Bio-beads S-X1, as stationary, and dichloromethane, as eluting solvent, to

remove unreacted PEG. The PEGylpentenyl(20%) Ge NPs can be redispersed in common organic solvents including toluene, dichloromethane and alcohols. The PEGylpentenyl(50%) Ge NPs can be redispersed in common organic solvents and water (water solubility: 5 mg/ 1ml). **FT-IR** (thin film on KBr): 3140 (weak), 3000-2850, 1470, 1353, 1278, 1110, 954, 846 cm^{-1} . **^1H NMR** (300 MHz, CD_2Cl_2): δ (ppm) 0.8 (weak), 1.2-2 (broad, weak), 3.6 (m), 7.6 (weak).

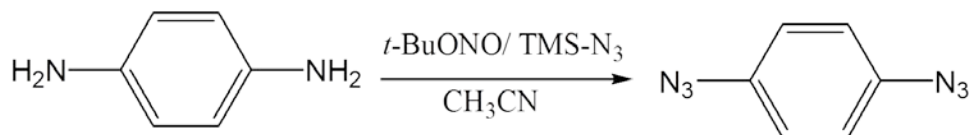
4.5.10 Synthesis of PEGylated Ge NP clusters using bisazido PEG.

ω -Azidopentenyl Ge NPs with various surface coverage undergo copper(I) catalyzed "click" reaction with α,ω -bisazido PEG derivatives (1 kDa, 2 kDa, 4.6 kDa and 10 kDa). In general "click" reaction, ω -azidopentenyl Ge NPs solution (40 mg in 30 ml THF), bisazido-PEG (30 mg) and a 0.5 ml of PMDTA were taken in a 100 ml Schlenk flask.. The solution was degassed three pump-thaw-degas cycles. Copper(I)bromide.dimethylsulfate (~20-30 mg) was added to the degassed mixture under N_2 flow. The reaction flask was stirred overnight under nitrogen to complete the reaction. The reaction mixture then was concentrated by rotary evaporation and the particles redispersed in 40 ml dichloromethane. The dichloromethane solution was washed three times with 40 ml brine/ ethylene diamine solution. The nanoparticle solution was dried over anhydrous MgSO_4 , filtered and concentrated by rotary-evaporation. The crude NPs were further purified by GPC using Bio-beads S-X1, as stationary, and dichloromethane, as eluting solvent, to remove unreacted PEG. The Ge NP clusters synthesized from longer spacer (2 kDa and higher molecular weight PEG) can be redispersed in common organic solvents including toluene, dichloromethane and

alcohols. **FT-IR** (thin film on KBr): 3140 (weak), 3000-2850, 1470, 1353, 1278, 1110, 954, 846 cm^{-1} .

4.5.11 Synthesis of 1,4-Diazidobenzene from *p*-phenylenediamine

1,4-diazidobenzene was synthesized using a reported procedure starting from *p*-phenylenediamine (or 1,4-diaminobenzene) using **Scheme 4.6**.^{19, 33} In a 100 ml Schlenk flask, 1,4-diaminobenzene (1.62 gm, 15 mmol) was cooled to 0°C in an ice bath. To this stirred reaction mixture, *t*-BuONO (4.64gm, 5.36 ml, 45 mmol) followed by TMSN_3 (4.14 gm, 4.78 ml, 36 mmol) was added drop-wise. The resulting solution was stirred for 24 hours at room temperature. The reaction mixture was concentrated by rotary evaporation, and the crude product was purified by silica gel chromatography (hexane) to give brown solid 1,4-diazidobenzene (1.2 g, 50%). ^1H NMR (300 MHz, CD_2Cl_2): δ (ppm) 7.01 (s, 4 H). FT-IR (thin film on KBr): 3100, 3050, 2108, 1625, 1510, 1272, 824.



Scheme 4.6: Synthesis of 1,4-diazidobenzene as a conjugate spacer.

4.5.12 Synthesis of Ge NP arrays using 1,4-diazidobenzene as a spacer via "click"

reaction

PMDTA (0.5 ml) and 1,4-diazidobenzene (20 mg) were added to the Ge NP nanoparticle solution (50 mg in 20 ml THF) in a 50 ml Schlenk flask. The solution was degassed in three pump-thaw-degas cycles and Cu(I) catalyst, $(\text{Cu(I)BrS}(\text{CH}_3)_2)$, (10 mg), was added under nitrogen. The solution was degassed one more time and back filled

nitrogen. Then the reaction mixture was stirred for overnight at room temperature under nitrogen. The reaction mixture was concentrated by rotary evaporation and a reddish precipitate of Ge NP clusters was formed, when aq. NH_4Cl solution (50 ml) was added in to the concentrated reaction mixture. The precipitate was washed twice with 75% ethanol (20 ml) and once with methanol (20 ml). The precipitate was further washed twice with CH_2Cl_2 / methanol (3:2) solution (15 ml each) to remove any unreacted starting azido-compound. Weight of reddish brown solid product is 38 mg (yield: 76% by weight). Solubility: slightly soluble in toluene

"Host-guest" Chemistry

4.5.13 Synthesis of mono-6-O-(p-tolylsulfonyl)- β -cyclodextrin

Mono-6-O-(p-tolylsulfonyl)- β -cyclodextrin (mono-azido- β -cyclodextrin) was synthesized by azidation of *mono*-tosyl- β -cyclodextrin following a modified reported method.³⁴ *Mono*-tosyl- β -cyclodextrin (1 g, 0.776 mmol) and sodium azide (165 mg, 2.5 mmol) were added to a 40 ml of aqueous 50% ethanol in flask equipped with a reflux condenser. The solution was allowed to reflux for overnight. It was then concentrated by rotary evaporation. Product was precipitated by adding acetone and dried by vacuum for overnight. to yield 0.72 g (80%) of white solid powder. **FT-IR** (KBr pellet): 3600-3100 (broad), 300-2850, 2100, ~1650, 1460-1360, 1153, 1035 cm^{-1} . **^1H NMR** (300 MHz, DMSO-d_6): δ (ppm) 3.3 (m, 14H), 3.6 (m, 28H), 4.5 (broad, 6H), 4.8 (s, 7H), 5.7 (broad, 14H).

4.5.14 Synthesis of β -CD grafted Ge NPs

Mono-azido β -CD (100 mg) was added to a solution of ω -alkynyloctenyl(30%) Ge nanoparticle (50 mg in 20 ml 1:1 DMF/ THF) in a Schlenk flask. The solution was degassed in three pump-thaw-degas cycles and Cu(I)Br.S(CH₃)₂ (20 mg) and Cu(0) wire (50 mg) were added under N₂. The solution was degassed again and it was heated up to 50°C and allowed to stir overnight under N₂. The reaction mixture was then concentrated by rotary-evaporator and 50 ml CH₂Cl₂ was added to the solution which was sonicated for 30 min. The CH₂Cl₂ solution was washed with aqueous NH₄Cl (50ml). The separation of layers was not clear. The organic solution was concentrated and dialyzed for four days using 1 kDa dialysis membrane, first with 50% aqueous ethanol (for 2 days), 95% ethanol (for 1 day), then with methanol (for 1 day). ω - β CD-octenyl Ge NPs as a yellowish powder were obtained by concentrating dialyzed solution using rotary evaporation. Yield: 36 mg (72%, by weight). **FT-IR** (KBr pellet): 3600-3100 (broad), 300-2850, ~1650, 1460-1360, 1153, 1035 cm⁻¹. **¹H NMR** (300 MHz, DMSO-d₆): δ (ppm) 0.8 (s, 18H), 1.2-1.6 (broad, m, 3H), 2.1 (s, 7H), 3.3 (m, 29H), 3.6 (m, 20H), 4.8 (s, 7H), 5.7 (broad, 8H), 7.8 (broad, 1H).

4.5.15 Synthesis of ω -adamantanyloctenyl(20%)-Ge NPs from ω -alkynyloctenyl(20%)-Ge NPs

A THF solution of ω -alkynyloctenyl(20%)-Ge NPs (50 mg NPs in 50 ml THF), azido-adamantane (30 mg), PMDTA (0.5 ml) was added to a Schlenk flask equipped with a stir bar. The catalyst, Cu(I)Br.S(CH₃)₂, (20 mg) was added to the reaction mixture under high N₂ flow after degassing it in three pump-thaw-degas cycles. The temperature

of reaction mixture was brought up to 60°C and the solution was stirred for overnight. The reaction mixture was concentrated by rotary evaporation and approximately 50 ml CH₂Cl₂ was added to the product mixture which was sonicated for 5 min. The dichloromethane solution was then washed three times with brine solution (30ml) dried over anhydrous MgSO₄ and the clear CH₂Cl₂ solution was then separated by centrifugation. The product was concentrated, first by rotary evaporation and then by vacuum. The crude product was purified by GPC using Bio-beads S-X1. Weight of yellow-red solid ω-adamantanyloctenyl(20%)-Ge NPs is 35 mg (70% yield by weight). **¹H NMR** (300 MHz, CD₂Cl₂): δ 0.8 (s); 1.2-1.4 (broad, m); 1.7 (m); 2.2; 7.4-7.6 (m) ppm. **FT-IR** (thin film on KBr plate): 3140, 2850-3000, ~1600, 1465, 1375, 740 cm⁻¹.

4.5.16 Synthesis of Ge-C₆₀-Ge Assembly by host-guest interaction

ω-βCD octenyl (30%) Ge NPs (12 mg) were dissolved in 10 ml distilled toluene. Fullerene (C₆₀) (3 mg) was added to the solution and the solution was allowed to stirred for one week. The unreacted fullerene was precipitated by adding excess methanol to the toluene solution. The methanol layer was concentrated and dried, to yield 6 mg (50% by weight) of Ge-C₆₀-Ge NP cluster as a reddish solid. **FT-IR** (thin film on KBr plate): 2850-3000, ~1600, 1465, 1375, 1110, 740 cm⁻¹.

4.6 Analytical Methods

4.6.1 Infrared spectroscopy.

Fourier Transformed Infrared (FT-IR) Spectroscopy was performed using a Thermo Nicolet NEXUS 670 FT-IR. Samples were prepared either as a thin film of functionalized Ge NPs, prepared by depositing dichloromethane solution of Ge NPs on

KBr plate, or as KBr palette, prepared by mixing solid sample and KBr power. FT-IR sample chamber was purged with dry nitrogen before collecting any data. FT-IR spectra were recorded after 512 scan with 1 cm^{-1} resolution.

4.6.2 *Nuclear magnetic resonance spectroscopy.*

Nuclear magnetic resonance spectra were obtained using a Bruker Avance 300 MHz high resolution NMR spectrometer. Ge NPs were dissolved in nmr solvents, such as, in chloroform-*d*, methylene chloride-*d*₂ and DMSO-*d*₆ and the solution was transferred into a clean NMR tube.

4.6.3 *Transmission electron microscopy.*

Transmission electron microscopy (TEM) images were taken with a JOEL 2011 TEM using an accelerating voltage of 200 kV. A droplet of diluted nanoparticle solution in toluene was deposited on the carbon coated copper grid placed on a filter paper. The filter paper soaked up the excess solution before inserting in grid in the TEM sample holder. Energy dispersive spectroscopic (EDS) data were obtained in the TEM using an Oxford Inca attachment with a 3 nm beam spot on a copper grid.

4.6.4 *UV-vis Absorption and Photoluminescence spectroscopy.*

UV-Vis absorbance spectra were obtained with a Cary 50 spectrophotometer in dichloromethane. The photoluminescence emission characteristics from the Ge nanoparticles either in dichloromethane or in water were acquired using a Varian Cary Eclipse spectrofluorimeter. The emission spectra were recorded with excitation wavelengths between 300 nm to 450 nm with slow scanning speed (120 nm/ min) using a 1 cm quartz cuvette.

4.7 References

1. He, Y.; Kang, Z.-H.; Li, Q.-S.; Tsang, C. H. A.; Fam, C.-H.; Lee, S.-T., Ultrastable, highly fluorescent, and water-dispersed silicon-based nanospheres as cellular probes. *Angew. Chem., Int. Ed.* **2009**, 48, (1), 128-132.
2. Dubertret, B.; Skourides, P.; Norris, D. J.; Noireaux, V.; Brivanlou, A. H.; Libchaber, A., In vivo imaging of quantum dots encapsulated in phospholipid micelles. *Science (Washington, DC, U. S.)* **2002**, 298, (5599), 1759-1762.
3. Gao, X.; Yang, L.; Petros, J. A.; Marshall, F. F.; Simons, J. W.; Nie, S., In vivo molecular and cellular imaging with quantum dots. *Curr. Opin. Biotechnol.* **2005**, 16, (1), 63-72.
4. Nayfeh, M. H.; L. Mitas, V. K., Silicon nanoparticles: New photonic and electronic material at the transition between solid and molecule. In *Nanosilicon*, Nayfeh, M. H., Ed. Elsevir: 2007; p 1.
5. Bottrill, M.; Green, M., Some aspects of quantum dot toxicity. *Chem. Commun. (Cambridge, U. K.)* **2011**, 47, (25), 7039-7050.
6. Lambert, T. N.; Andrews, N. L.; Gerung, H.; Boyle, T. J.; Oliver, J. M.; Wilson, B. S.; Han, S. M., Water-soluble germanium(0) nanocrystals: cell recognition and near-infrared photothermal conversion properties. *Small* **2007**, 3, (4), 691-699.
7. Ma, Y.-H.; Huang, C.-P.; Tsai, J.-S.; Shen, M.-Y.; Li, Y.-K.; Lin, L.-Y., Water-soluble germanium nanoparticles cause necrotic cell death and the damage can be attenuated by blocking the transduction of necrotic signaling pathway. *Toxicol. Lett.* **2011**, 207, (3), 258-269.
8. Prabakar, S.; Shiohara, A.; Hanada, S.; Fujioka, K.; Yamamoto, K.; Tilley, R. D., Size Controlled Synthesis of Germanium Nanocrystals by Hydride Reducing Agents and Their Biological Applications. *Chem. Mater.* **2010**, 22, (2), 482-486.
9. Bhattacharjee, S.; Rietjens, I.; Alink, G.; Antonius, M.; Purkait, T. K.; Xu, Z.; Singh, M.; Atkins, T.; Regli, S.; Clark, R.; Shukaliak, A.; Mitchell, B.; Fink, M. J.; Veinot, J. G.; Kauzlarich, S.; Zuilhof, H., Cytotoxicity of Surface-functionalized Silicon and Germanium Nanoparticles: The Dominant Role of Surface Charges. *Particle and Fibre Toxicology* **2012**, submitted.
10. Gao, W.; Liu, W.; Christensen, T.; Zalutsky, M. R.; Chilkoti, A., In situ growth of a PEG-like polymer from the C terminus of an intein fusion protein improves pharmacokinetics and tumor accumulation. *Proc. Natl. Acad. Sci. U. S. A.* **2010**, 107, (38), 16432-16437, S16432/1-S16432/5.

11. Hubbell, J. A.; Chilkoti, A., Chemistry. Nanomaterials for drug delivery. *Science* **2012**, 337, (6092), 303-5.
12. Erogbogbo, F.; Yong, K.-T.; Roy, I.; Hu, R.; Law, W.-C.; Zhao, W.; Ding, H.; Wu, F.; Kumar, R.; Swihart, M. T.; Prasad, P. N., In Vivo Targeted Cancer Imaging, Sentinel Lymph Node Mapping and Multi-Channel Imaging with Biocompatible Silicon Nanocrystals. *ACS Nano* **2011**, 5, (1), 413-423.
13. Erogbogbo, F.; Yong, K.-T.; Roy, I.; Xu, G.; Prasad, P. N.; Swihart, M. T., Biocompatible Luminescent Silicon Quantum Dots for Imaging of Cancer Cells. *ACS Nano* **2008**, 2, (5), 873-878.
14. Taylor, B. R.; Kauzlarich, S. M.; Lee, H. W. H.; Delgado, G. R., Solution Synthesis of Germanium Nanocrystals Demonstrating Quantum Confinement. *Chem. Mater.* **1998**, 10, (1), 22-24.
15. Hallmann, S.; Fink, M. J.; Mitchell, B. S., Mechanochemical synthesis of functionalized silicon nanoparticles with terminal chlorine groups. *J. Mater. Res.* **2011**, 26, (8), 1052-1060.
16. Rosso-Vasic, M.; Spruijt, E.; Popovic, Z.; Overgaag, K.; van, L. B.; Grandidier, B.; Vanmaekelbergh, D.; Dominguez-Gutierrez, D.; De, C. L.; Zuilhof, H., Amine-terminated silicon nanoparticles: synthesis, optical properties and their use in bioimaging. *J. Mater. Chem.* **2009**, 19, (33), 5926-5933.
17. Lei, Y.; Chim, W.-K., Shape and size control of regularly arrayed nanodots fabricated using ultrathin alumina masks. *Chem. Mater.* **2005**, 17, (3), 580-585.
18. Grutmacher, D.; Fromherz, T.; Dais, C.; Stangl, J.; M¹ller, E.; Ekinci, Y.; Solak, H. H.; Sigg, H.; Lechner, R. T.; Wintersberger, E.; Birner, S.; Hol¹/₂, V. c.; Bauer, G. n., Three-Dimensional Si/Ge Quantum Dot Crystals. *Nano Letters* **2007**, 7, (10), 3150-3156.
19. Miyake, J.; Chujo, Y., The Aza-Wittig Polymerization: An Efficient Method for the Construction of Carbon-Nitrogen Double Bonds-Containing Polymers. *Macromolecules (Washington, DC, U. S.)* **2008**, 41, (15), 5671-5673.
20. Fathalla, M.; Li, S.-C.; Diebold, U.; Alb, A.; Jayawickramarajah, J., Water-soluble nanorods self-assembled via pristine C60 and porphyrin moieties. *Chemical Communications* **2009**, (28), 4209-4211.
21. Isenb¹gel, K.; Ritter, H.; Branscheid, R.; Kolb, U., Nanoparticle Vesicles Through Self Assembly of Cyclodextrin- and Adamantyl-Modified Silica. *Macromolecular Rapid Communications* **2010**, 31, (24), 2121-2126.
22. Mark, S. S.; Bergkvist, M.; Yang, X.; Teixeira, L. M.; Bhatnagar, P.; Angert, E. R.; Batt, C. A., Bionanofabrication of Metallic and Semiconductor Nanoparticle Arrays

Using S-Layer Protein Lattices with Different Lateral Spacings and Geometries. *Langmuir* **2006**, 22, (8), 3763-3774.

23. Park, J. H.; Hwang, S.; Kwak, J., Nanosieving of Anions and Cavity-Size-Dependent Association of Cyclodextrins on a 1-Adamantanethiol Self-Assembled Monolayer. *ACS Nano* **2010**, 4, (7), 3949-3958.

24. Lopez, C., Materials aspects of photonic crystals. *Adv. Mater. (Weinheim, Ger.)* **2003**, 15, (20), 1679-1704.

25. Song, L. X.; Bai, L.; Xu, X. M.; He, J.; Pan, S. Z., Inclusion complexation, encapsulation interaction and inclusion number in cyclodextrin chemistry. *Coord. Chem. Rev.* **2009**, 253, (9+10), 1276-1284.

26. Wan, P.; Xing, Y.; Chen, Y.; Chi, L.; Zhang, X., Host-guest chemistry at interface for photoswitchable bioelectrocatalysis. *Chem. Commun. (Cambridge, U. K.)* **2011**, 47, (21), 5994-5996.

27. Del, V. E. M. M., Cyclodextrins and their uses: a review. *Process Biochem. (Oxford, U. K.)* **2004**, 39, (9), 1033-1046.

28. Langa, F.; Nierengarten, J. F.; Editors, *Fullerenes Principles And Applications, 2nd Edition. [In: RSC Nanosci. Nanotechnol., 2012; 20]*. Royal Society of Chemistry: 2012; p 634 pp.

29. Ikeda, A.; Hatano, T.; Konishi, T.; Kikuchi, J.-i.; Shinkai, S., Host-guest complexation effect of 2,3,6-tri-O-methyl-[beta]-cyclodextrin on a C60-porphyrin light-to-photocurrent conversion system. *Tetrahedron* **2003**, 59, (19), 3537-3540.

30. Ma, B.; Milton, A. M.; Sun, Y.-P., Infrared spectroscopy of all-carbon poly[60]fullerene polymer and [60]fullerene dimer model. *Chemical Physics Letters* **1998**, 288, (5-6), 854-860.

31. Hare, J. P.; Dennis, T. J.; Kroto, H. W.; Taylor, R.; Allaf, A. W.; Balm, S.; Walton, D. R. M., The IR spectra of fullerene-60 and -70. *Journal of the Chemical Society, Chemical Communications* **1991**, (6), 412-413.

32. Bertozzi, C. R.; Bednarski, M. D., The synthesis of heterobifunctional linkers for the conjugation of ligands to molecular probes. *J. Org. Chem.* **1991**, 56, (13), 4326-9.

33. Barral, K.; Moorhouse, A. D.; Moses, J. E., Efficient Conversion of Aromatic Amines into Azides: A One-Pot Synthesis of Triazole Linkages. *Organic Letters* **2007**, 9, (9), 1809-1811.

34. Hamasaki, K.; Ikeda, H.; Nakamura, A.; Ueno, A.; Toda, F.; Suzuki, I.; Osa, T., Fluorescent sensors of molecular recognition. Modified cyclodextrins capable of

exhibiting guest-responsive twisted intramolecular charge transfer fluorescence. *J. Am. Chem. Soc.* **1993**, 115, (12), 5035-40.

Chapter 5

5 Conclusion and Future Direction

5.1 Conclusion

A novel top-down method has been demonstrated for the synthesis of organic-passivated germanium nanoparticles using high-energy ball-milling (HEBM). This green process does not use corrosive solvent and the starting materials can be recycled. Alkynes may undergo cyclotrimerization to form substituted benzene as molecular impurities during HEBM. Crude passivated Ge NPs were purified from molecular impurities by various purification process, such as gel permeation chromatography (GPC), Soxhlet dialysis etc. GPC was found to be an effective method to purify the crude nanoparticles and at the same it separates polydispersed Ge NPs by size.

For a GPC separated fraction, SAXS size distribution shows a smaller particle size compare to TEM size distribution. As SAXS is a better technique for pore morphology materials and nanoparticles, it gave better size distribution of size separated Ge NPs. The efficiency of the size separation can be improved by using a preparative column in a HPLC machine. Though the origin of PL of indirect band-gap semiconductor in debate, the blue PL of Ge NPs might originate from the defects in the oxide or other surface defects. However, size dependent blue PL was observed from TMSA-passivated Ge NPs. In this case, a surface defect state is fixed in energy and it remains higher in energy compared to the lowest level of conduction band (specially for larger NPs). The observed size dependent blue PL of TMSA-passivated Ge NPs is due to the

recombination of an electron from the defect state with a hole from the valence band whose energy is size dependent.

Copper(I) catalyzed alkyne-azide “click” chemistry was explored as an alternative efficient method compare to hydrogermylation or other organometallic methods to modify Ge surfaces for surface functionalization. Various organic, organometallic and biomolecularazide were used to functionalize passivated Ge NPs by copper (I) catalyzed alkyne-azide “click” chemistry. Further functionalization provides enhance solubility and stability against air oxidation and nanoparticle aggregation. Surface of the functionalized Ge NPs were confirmed by ^1H NMR and FT-IR spectra. The surface coverage of functional moieties was calculated by integrating ^1H NMR peaks. Optical properties of the functionalized Ge NPs with low surface coverage do not differ with starting passivated Ge NPs.

Water soluble of trimethylammonium propenyl Ge NPs were synthesized from direct top-down method using HEBM followed by N-methylation. Cytotoxicity study of these water soluble Ge NPs was performed *in vitro*. Compare to other amine-terminated cationic Si and Ge nanoparticles, these particles show very low cytotoxicity due to steric hindered positive charge by three bulky methyl group on the N.

Water soluble, luminescent Ge nanoparticles were also synthesized by grafting polyethylene glycol (PEG) derivatives using copper(I) catalyzed alkyne-azide "click" reaction. These nanoparticles are biocompatibles and did not show any cytotoxicity when studied *in vitro*. PEGylated Ge NP clusters have been successfully synthesized by the "click" reaction using bis azido or bis alkyno PEG derivaties as spacers. These biocompatible materials could be used for potential biological application.

Additionally β -cyclodextrin grafted Ge NPs were prepared by copper (I) catalyzed "click" reaction for biological application. Ge-Si NP assembly were made by "host-guest" chemistry. Fullerene, C₆₀, was incorporated in the β -cyclodextrin grafted Ge NPs to make a new class of materials.

5.2 Future Direction

There are numerous open questions remaining to be answered concerning of germanium nanoparticles. There are several recommendations related to our research for future study that could clarify our understanding of photoluminescence, surface chemistry and functionalization of germanium nanoparticles. More investigation is required to get full control of defect free PL from Ge nanoparticles and to find the origin of PL from indirect band gap semiconductor.

One of the recommendation is to prepare passivated defect free Ge NPs with predictable properties by high energy ball-milling using small reactive molecules such as ethylene, acetylene or hydrogen gas. In this advanced ball-milling process we need high pressure capable milling vials containing reactive gases. In this case small reactive molecules can eventually passivate the germanium surfaces without leaving any surface defect.

Potential biological application of Ge NPs was not explored much due to lack of functionalization techniques. The future study would focus on mechanochemical synthesis of germanium NPs with various functional groups for multimodal functionalization; which would deal with water solubility, biocompatibility as well as

binding of biomolecules. Biocompatible PEGylated Ge NPs can be attached with some biomolecules through -NH, -SH, or -COOH functional group for biological application. In another recommendation conjugated spacers, organic dyes or fullerene can be attached in the three dimension Ge NP clusters for optoelectronic application.

BIOGRAPHY

Tapas K Purkait was born and raised in a remote village in West Bengal, India. He received his B.Sc. in Chemistry from Presidency College, Kolkata, India. He did master in Chemistry from Indian Institute of Technology (IIT)-Bombay, Mumbai, India. In spring 2007, he joined Tulane University in New Orleans for his doctoral degree. He received the Hans Jonassen Memorial Scholarship for the year 2009-2010 from the Department of Chemistry, Tulane University. He attended several national and international seminars including 16th International Symposium on Silicon Chemistry.